

STRATEGIES TO MODEL AND CIRCUMVENT ACQUIRED
RESISTANCE TO THERAPEUTICS IN SMALL CELL LUNG
CANCER

by
Eric Edison Gardner, PharmD

A dissertation submitted to Johns Hopkins University in conformity with the requirements
for the degree of Doctor of Philosophy

Baltimore, Maryland

October 2016

Abstract

Small cell lung cancer (SCLC) is an extremely aggressive, pulmonary malignancy linked to lifetime smoking of cigarette tobacco. Most SCLC is diagnosed in the metastatic setting and surgical resection is rarely performed. However, SCLC is one of the most chemosensitive tumors, with >50% objective responses observed in *de novo* disease. These responses are impressive, but brief. Median progression free survival remains less than 5 months in current clinical trials. Recent studies have characterized the genome and epigenome of primary, untreated SCLC tumors. These studies have revealed near universal inactivation of the tumor suppressors *TP53* and *RB1*, with frequent alterations in chromatin modifying enzymes, Notch signaling and amplification of *MYC* family members. Little is known about what factors permit acquired resistance and enable such a rapid shift in chemosensitive to chemorefractory disease within the same patient. No studies to date have comprehensively characterized paired sensitive and resistant disease states.

The research presented below describes three studies aimed at determining how acquired resistance to chemotherapy is generated *in vivo* and targeted therapeutic approaches to chemoresistant disease. The first study details the discovery of genetic and epigenetic mediators of acquired chemoresistance *in vivo* through the development and characterization of paired chemosensitive and chemoresistant patient derived xenograft (PDX) models of SCLC. This work establishes a central role for EZH2 in promoting resistance to DNA damaging agents by silencing the gene *SLFN11* and is highlighted by the impressive efficacy of EZH2 inhibition with first or second line standard of care chemotherapy. The second study describes a targeted approach to overcoming resistance to programmed cell death (apoptosis) by chemically inhibiting a protein-protein interaction between BCL-2 family members in SCLC. This study relied on

the small molecule ABT-263 and attempts to explain disappointingly transient responses in SCLC patients observed in clinical testing. Finally, the third study builds on the second study, highlighting the importance of combinatorial strategies to improve the efficacy of this targeted agent *in vivo*, with a focus on potential mechanisms of acquired resistance, notably genomic loss of *BAX*. Research presented in these studies is directly informing the design of proposed clinical trials in SCLC.

Advisor: Charles M. Rudin, MD, PhD

Thesis Reader: Christine L. Hann, MD, PhD

Acknowledgements

I need to thank my thesis mentor Charlie Rudin, for taking a risk on me and allowing me to join his lab with minimal experience at the bench. Charlie's approach to mentorship was one that I immediately identified with, where his mentees are given the freedom to pursue questions they find stimulating while clinically relevant to patients with lung cancer. I've learned a great deal in watching your group and career continue to thrive. I greatly appreciate your willingness to get me involved in team projects early and often; I feel I benefitted from these interactions through the years, shaping my own mentorship style and increasing my breadth of knowledge within the lung cancer community. Thank you for challenging me, knowing when to step in and edit, and permit my own self-editing.

I would next like to thank Christine Hann and members of her laboratory, especially Nick Connis and Shekhar Kamat. Christine, your mentorship and guidance were a critical part of my development as a student. I have learned a great deal under your guidance, especially on how to think clinically about a therapeutic approach.

Linde Miles and JT Poirier, you were both mentors to me early in the lab at Hopkins and continued when we transitioned to MSKCC. Linde, thank you for listening to me complain about life in and out of the lab. I appreciate you taking the time to train me and volunteering to take the role of the lab matriarch. JT, thank you for being available for conversations both long and short, coming up with fresh ideas when my projects were stuck, and always adding strict, statistical thinking for the data at hand. The final push of my thesis work would not have been possible without your guidance, mentorship and ability to secure project funding. I've appreciated every critique and I think it has made me a better student and scientist.

I would also like to thank patient AD and her family for allowing me to be part of her care team during my final year of pharmacy school, learning from her clinical experience. Together with her husband, she convinced me that the world needed more people focused on difficult clinical problems in cancer care.

My partner in life, Jenn Walker, you make the struggle worth it. Thank you for picking me up when experiments had me down. We met each other at a perfectly coincidental time in our lives and I've loved every moment since. I can see how we've grown together even after just two years and I can't wait for our future together.

At the top of the list, yet bottom of the page, are my parents and sister. To my parents, Peg and Fred, I am forever grateful for the life you have provided me with and the opportunities presented throughout my childhood into adulthood. I was never directed to one career path or another – I would like to think that the directions I have chosen are leaving, or will leave, the world a little brighter and more informed. To my sister Kirsten, thank you for always putting the pressure on me to be “the professional” sibling, but reminding me how to have fun and live a full life. I know we're across the country, but if I ever needed it, you were there for me. I also understand that what follows in this text may not make a whole lot of sense – abbreviations used, terminology, etc. Know that my time at Hopkins and MSKCC was well spent, full of personal and professional growth.

Table of Contents

Abstract.....	ii
Acknowledgements.....	iv
List of Tables.....	viii
List of Figures.....	ix
Introduction.....	1
Small Cell Lung Cancer (SCLC).....	1
Genetic and Epigenetic Hallmarks of SCLC.....	3
Mechanisms of Cell Death.....	8
Chapter 1. Modeling Human Cancer in a Mouse Host: Applications of Patient-Derived Xenograft (PDX) Models.....	11
Chapter 1 <i>Brevis</i>	11
Maintaining Genetic and Epigenetic Integrity.....	12
Tumor Microenvironment Differences and Limitations.....	15
Considerations in Preclinical Experimental Design – Case Study of Sunitinib....	19
Chapter 2. Epigenetic Silencing of <i>SLFN11</i> Defines a Recurrent Mechanism of Acquired Resistance to Chemotherapy in SCLC.....	27
Chapter 2 <i>Brevis</i>	27
Study Introduction.....	29
Materials and Methods.....	32
Results.....	50
Discussion.....	92
Chapter 3. Targeted Inhibition of BCL-2 Has Limited Utility in SCLC and Combined Inhibition of mTOR Shows Preclinical Synergy.....	97
Chapter 3 <i>Brevis</i>	97
Study Introduction.....	100

Materials and Methods.....	103
Results.....	108
Discussion.....	131
Chapter 4. Allosteric or Kinase Inhibition of mTOR is Therapeutically Non-inferior When Combined with BCL-2/xL Inhibition in SCLC.....	134
Chapter 4 <i>Brevis</i>	134
The Mechanistic Target of Rapamycin (mTOR) Pathway and Therapeutic Targeting.....	136
Results.....	142
Discussion.....	167
Conclusions.....	170
References.....	174
Curriculum Vitae.....	196

Intended to be blank

List of Tables

Table 1.	Preclinical reporting metrics for studies examining tumor volume responses in animals.....	24
Table 2.	Validity threats to preclinical research efficacy.....	25
Table 3.	PDX model characteristics used throughout studies.....	33
Table 4.	List of shRNA sequences tested and used within Chapter 2.....	38
Table 5.	List of antibodies and dilutions used throughout Chapter 2.....	42
Table 6.	Description of ABT-737 treatment collection time points in PDXs.....	112
Table 7.	Top 20 differentially expressed genes in ABT-737 treated tumors.....	113
Table 8.	Gene Set Enrichment Analysis (GSEA) in ABT-737 treated tumors.....	114
Table 9.	Top 20 connectivity map hits for ABT-737 treatment signature.....	117

List of Figures

Fig. 1.	Spectrum of reported genomic mutations reported in primary SCLC.....	6
Fig. 2.	High level RNA expression of EZH2 is a defining feature of SCLC.....	7
Fig. 3.	Impact of murine cellular components on human mutational calling by next-generation sequencing.....	18
Fig. 4.	Chapter 2 <i>Brevis</i>	28
Fig. 5.	Modeling acquired resistance to standard of care chemotherapy in patient-derived xenograft (PDX) models of small cell lung cancer.....	52
Fig. 6.	Complete response criteria of remaining 8 of 10 PDX models.....	54
Fig. 7.	Credentialing exome sequencing data from paired PDX models.....	58
Fig. 8.	Genomic characterization of paired chemonaïve and chemoresistant SCLC PDX models.....	59
Fig. 9.	Paired RNA sequencing identifies conserved changes <i>SLFN11</i> and <i>TWIST1</i> across multiple models.....	63
Fig. 10.	<i>TWIST1</i> is recurrently up regulated in the chemoresistant setting but does not drive acquired resistance to cisplatin/etoposide in SCLC.....	64
Fig. 11.	<i>SLFN11</i> is down regulated at the transcript and protein level in SCLC following exposure to chemotherapy.....	69
Fig. 12.	<i>SLFN11</i> is rapidly down regulated <i>in vivo</i> and expression by IHC H-score does not correlate with survival.....	71
Fig. 13.	Chemical EZH2 inhibition rescues <i>SLFN11</i> expression and sensitizes SCLC to DNA damage.....	75
Fig. 14.	EZH2 chemical inhibition shows dose-dependent re-expression of <i>SLFN11</i> and the re-expression is suppressible by shRNA.....	77
Fig. 15.	EZH2 inhibition by EPZ011989 has limited single agent activity in PDX models of SCLC and EZH2 directly targets <i>SLFN11</i> for silencing.....	81
Fig. 16.	Epigenetic changes acquired in chemoresistance are reversible with chemical EZH2 inhibition <i>in vivo</i>	83
Fig. 17.	H3K27me3 is increased following DNA damage and is an actionable target in combination with first or second line	

	chemotherapy in SLFN11+ SCLC.....	88
Fig. 18.	Combining EPZ01989 with first or second line chemotherapy is well tolerated <i>in vivo</i>	90
Fig. 19.	Chapter 3 <i>Brevis</i>	98
Fig. 20.	Responses to ABT-737 in PDX models of SCLC are short-lived and progression is preceded by a decrease in HIF-1 α transcripts.....	110
Fig. 21.	Combining ABT-737 with etoposide is not well tolerated <i>in vivo</i>	111
Fig. 22.	Rapamycin has potent <i>in vitro</i> synergy with ABT-737.....	118
Fig. 23.	Rapamycin displays non-monotonic efficacy across a broad range of SCLC cell lines.....	119
Fig. 24.	Combining rapamycin with ABT-737 (R+ABT) <i>in vivo</i> is well tolerated..	122
Fig. 25.	Combining rapamycin with ABT-737 (R+ABT) provides durable responses in SCLC PDXs that express BCL-2.....	123
Fig. 26.	R+ABT differentially affects HIF-1 α regulated genes and the mTOR pathway in LX33 and LX47.....	126
Fig. 27.	Rapamycin increases levels of BAX protein <i>in vitro</i> and <i>in vivo</i> in SCLC.....	129
Fig. 28.	ABT-737 treatment <i>in vivo</i> leads to destruction of ARNT.....	130
Fig. 29.	Allosteric versus kinase domain mTOR inhibitory small molecules.....	135
Fig. 30.	Expression of core anti-apoptotic BCL-2 family members does not correlate with response to cisplatin and etoposide.....	143
Fig. 31.	Genes involved in programmed cell death are not frequently mutated in primary SCLC.....	144
Fig. 32.	Combined inhibition of BCL-2/xL with ABT-263 is superior to ABT-199 in multiple <i>in vitro</i> models of SCLC.....	147
Fig. 33.	Inhibition of mTOR with an allosteric or kinase inhibitor is superior in combination with ABT-263 versus ABT-199 <i>in vitro</i>	148
Fig. 34.	Acquired resistance to ABT-263/737 proceeds through the loss of BAX in SCLC.....	151
Fig. 35.	Suppression of BAX – but not BAK – is sufficient to confer resistance to BCL-2/xL inhibition, but not cisplatin+etoposide.....	152

Fig. 36.	mTOR kinase inhibition by MLN0128 is variable across independent PDX models of SCLC.....	156
Fig. 37.	Acute conditioning of SCLC with different classes of mTOR inhibitors does not “prime” tumors for apoptosis with ABT-263.....	160
Fig. 38.	Acquired resistance to cisplatin/etoposide does not confer cross-resistance to ABT-263/MLN0128 <i>in vivo</i>	161
Fig. 39.	The combinations of ABT-263 with an mTOR allosteric or kinase domain inhibitor are non-inferior <i>in vivo</i> and ineffective in certain SCLC models.....	165
Fig. 40.	Approaches to studying mechanisms of acquired resistance <i>in vivo</i> using PDX models of SCLC.....	172

Intended to be blank

Introduction

Small Cell Lung Cancer (SCLC)

Lung cancer is the most common cause of cancer death in both men and women, responsible for more deaths than colon cancer, breast cancer and prostate cancer combined (Siegel et al., 2013). Small cell lung cancer (SCLC) represents approximately 15% of all lung cancers, or about 25,000 cases annually in the United States. SCLC is strongly associated with tobacco usage and exposure, and is anticipated to be a global public health concern over the next several decades, particularly in the developing world, mirroring smoking trends. Globally, more than 200,000 people die from SCLC every year.

Median survival for limited stage SCLC (disease confined to one hemi-thorax) is approximately 18 months from the time of diagnosis and upwards of 20% of patients are curable with a combination of chemotherapy and radiation (Slotman and Senan, 2011). However, the majority (>70%) of SCLC patients present with metastatic disease, limiting the clinical benefit of gross surgical resection. Median survival for extensive stage disease is less than one year. First line systemic therapy for extensive stage SCLC, consisting of platinum and etoposide chemotherapy, yields objective responses in >50% of patients, placing this cancer among the most chemotherapy-sensitive solid tumors. However, chemotherapy-resistant relapse is universal following treatment, resulting in uniformly fatal outcomes.

The only FDA-approved therapy for second line treatment in SCLC is the topoisomerase I poison topotecan (Hycamtin®), where response rates in the relapsed setting vary between 10-25%, depending on whether the relapse was initially chemosensitive (>3mo progression free interval) or chemoresistant (<3mo) (Horita et al., 2015). Further, while various classes of chemotherapies have activity in the third line

setting and beyond versus best supportive care, they provide little in the way survival benefit (Behera et al., 2016; Pelayo Alvarez et al., 2013). Indeed, no progress had been made within the last 40 years on extending the survival of patients with extensive stage disease (Oze et al., 2009). With several new classes of therapeutics on the horizon for clinical testing in SCLC, the time is now appropriate to define the hallmarks of SCLC and work to uncover why it is so exceptionally resistant to cytotoxic chemotherapy upon relapse (Bunn et al., 2016; Tan et al., 2016; Thomas and Pommier, 2016).

Genetic and Epigenetic Hallmarks of SCLC

Recent genomic characterization of SCLC has revealed near universal, bi-allelic inactivation of the tumor suppressors *RB1* and *TP53* (George et al., 2015; Peifer et al., 2012; Rudin et al., 2012a) (**Figure 1**). The tight link between diagnosis of SCLC and lifetime tobacco smoking also places SCLC among one of the mostly highly mutated cancers, with an average of >10 non-synonymous (coding) mutations per megabase of tumor genome (George et al., 2015; Lawrence et al., 2013). SCLC is also characterized by a high frequency of genomic amplifications of MYC family members, usually in a mutually-exclusive fashion, including *MYC*, *MYCN* and *MYCL1* and certain *MYCL1* fusions (Little et al., 1983; Makela et al., 1992; Nau et al., 1985; Nau et al., 1986; Rudin et al., 2012a; Takahashi et al., 1989). Inhibition of MYC function is thought to be a potential therapeutic approach in SCLC, possibly by targeting a long-term proliferative population of cells (Fiorentino et al., 2016; Jahchan et al., 2016).

The first description of spontaneous SCLC in a genetically engineered mouse models (GEMMs) was pioneered by Anton Bern's group in the Netherlands, where conditional inactivation of *Trp53* and *Rb1* in mouse lung epithelial cells produced histologically similar disease to human SCLC, with predilection for metastases to the liver and bone (Meuwissen et al., 2003). It was later shown that murine SCLC can arise from multiple lung cell progenitor lineages and are composed of both neuroendocrine and mesenchymal components (Calbo et al., 2011; Semenova et al., 2015; Sutherland et al., 2011), without a clear necessity for initiation in type II alveolar cells, as had been hypothesized by other groups. Additional genetic alterations are known to decrease the relatively long incubation period for tumor formation in these murine models (median survival time ~200d for *Trp53/Rb1* KO), including: loss of *PTEN* (Cui et al., 2014; McFadden et al., 2014), gain of *MYCL1* (Huijbers et al., 2014), and amplification of *NFIB*

(Denny et al., 2016; Dooley et al., 2011; Semenova et al., 2016; Wu et al., 2016), inhibition of Notch1 signaling (George et al., 2015), and activation of Hedgehog signaling (Park et al., 2011b).

Recently, the critical role of the developmental transcription factor *ASCL1* has been demonstrated in murine tumorigenesis, where a similarly related transcription factor *NEUROD1* played more of a role in driving metastatic spread through the activation of *MYC*; however, unlike *ASCL1*, genetic removal of *NEUROD1* did not limit spontaneous tumor formation in animals (Borromeo et al., 2016). Both transcription factors are believed to be responsible for driving gene expression of key neuroendocrine markers in SCLC, including synaptophysin, *CD56/NCAM* and *CHGA* (Chen et al., 1997; Jiang et al., 2009; Kosari et al., 2014; Nascashio et al., 2011; Westerman et al., 2002). The relative roles of *Ascl1* and *NeuroD1* in defining molecularly distinct subsets of SCLC have been suggested previously by others, and may correlate with both gene expression and DNA methylation patterns in primary tumors (Kalari et al., 2013; Osborne et al., 2014; Poirier et al., 2013; Poirier et al., 2015). One key difference outside of mutational frequency/tobacco signature between human and murine SCLC may lie in the epigenetic regulation of tumorigenesis and metastasis. Upwards of 25% of human SCLC cases harbor inactivating mutations in *CREBBP/CBP*, *EP300*, or *MLL2/KMT2D*, which at first glance in a limited dataset, appear mutually exclusive. It is not clear whether inactivation of these genes affects tumorigenesis, metastasis or sensitivity to chemotherapy in murine or human models.

A DNA hypomethylation signature has been recently reported as a potential biomarker of sensitivity to small molecular inhibition of lysine demethylase 1 (LSD1) in SCLC (Mohammad et al., 2015). LSD1 is a histone-modifying enzyme responsible for de-methylating histone H3 lysine 4 (H3K4) and regulates gene expression. One distinct

feature of both human and murine SCLC is high-level expression of *EZH2*, a histone methyltransferase enzyme within the Polycomb Repressive Complex 2 (PRC2) responsible for catalyzing the conversion of histone H3K27 to the trimethylated state and gene silencing (Vire et al., 2006). Dysregulation through either activating somatic mutations or overexpression in cancers can confer a DNA hypermethylation phenotype observed in aggressive cancers with poor outcomes, including SCLC (Knutson et al., 2012; McCabe et al., 2012; Morin et al., 2010; Souroullas et al., 2016; Yap et al., 2011). In cases of SCLC the near universal loss of *RB1* relieves E2F-dependent transcription, driving high levels of *EZH2* (Bracken et al., 2003). In primary SCLC, levels of *EZH2* transcript are among the highest of all tumor types surveyed within the TCGA, as well as some of the highest in cancer cell lines included in the CCLE (Barretina et al., 2012; Poirier et al., 2015) (**Figure 2**). Taken together, these data suggest that while core losses in tumor suppressor genes define a hallmark of SCLC, currently mutational data does not suggest the presence of additional driver genes, in stark contrast to NSCLC where *KRAS* and *EGFR* driving alterations broadly classify more than 45% of histologic disease and are used to inform therapeutic treatment. What emerges is the presence of distinct subsets of SCLC via transcriptional and epigenetic profiling of cell lines and primary tumors that may be differentially susceptible to emerging classes of therapeutic agents targeting transcription/translation and epigenetic modifying enzymes.

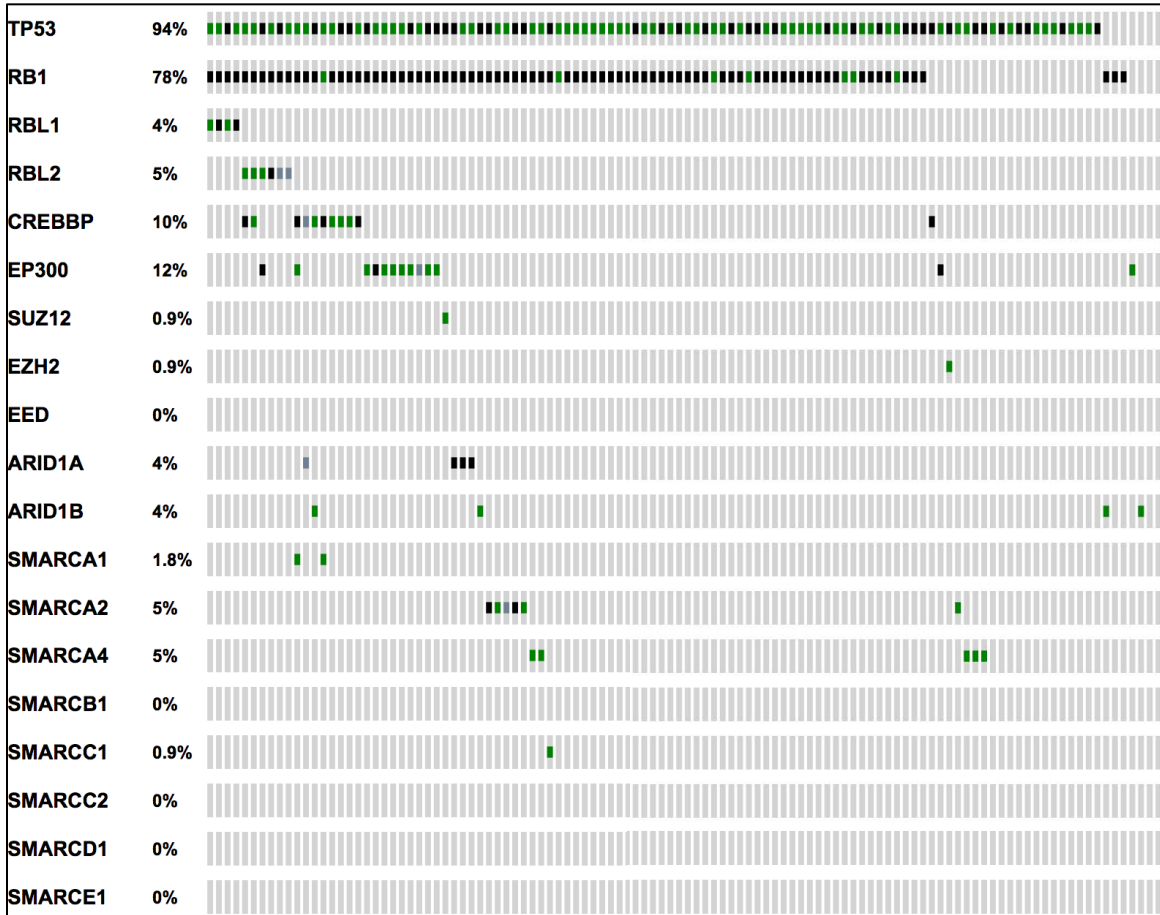


Figure 1. Spectrum of reported genomic mutations reported in primary SCLC. Oncoprint figure shown for 110 primary SCLC cases (George et al., 2015), highlighting missense (green) and truncating mutations (black) detected in tumor samples, with a focus on specific histone methyltransferases and components of the SWI/SNF complex. Frequency of detected alterations shown along left near gene name.

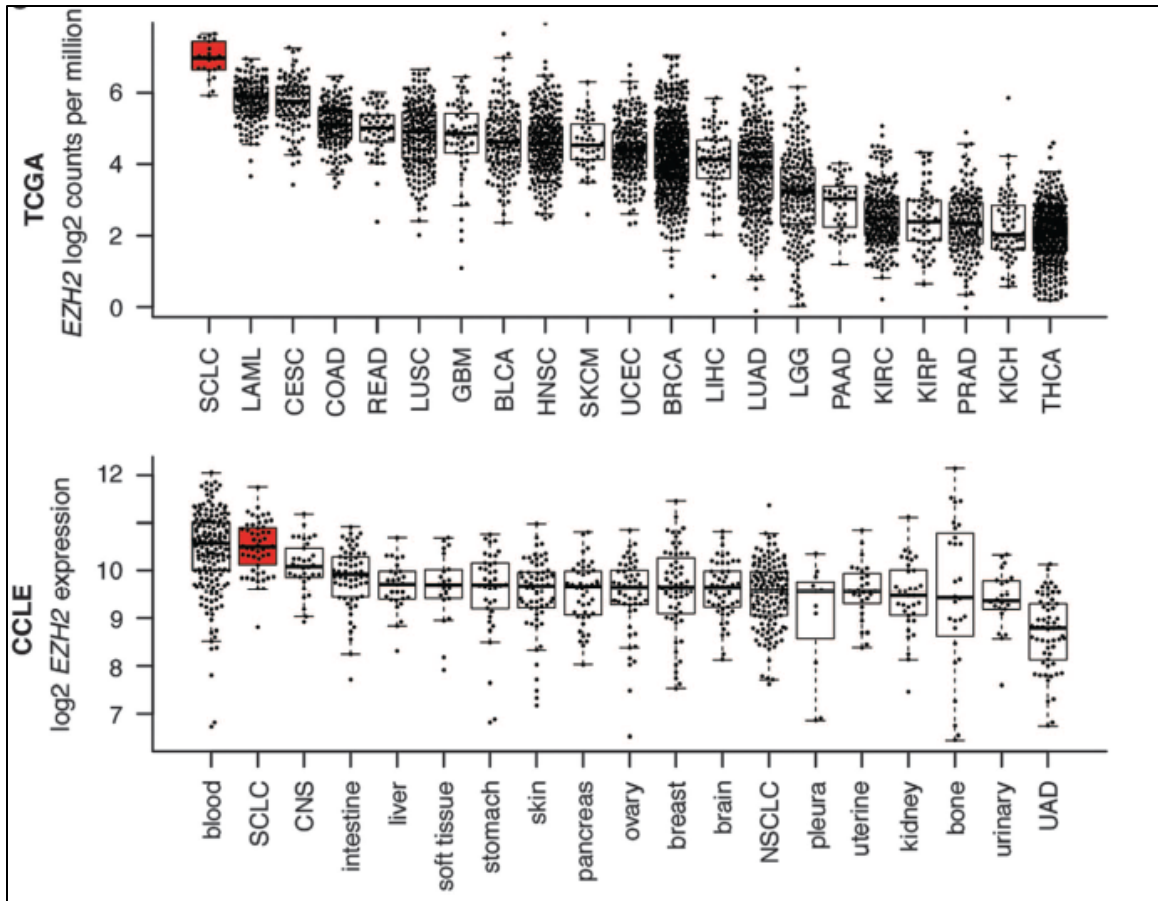


Figure 2. High level RNA expression of EZH2 is a defining feature of SCLC
 Above: RNAseq expression of *EZH2* in a cohort of SCLC (Rudin et al., 2012a) as compared to other histologies included in the TCGA
 Below: Microarray expression of *EZH2* from CCLE datasets; SCLC subsets called out in red for both panels.

Mechanisms of Cell Death

Disciplines focused on cell death have progressed over the years to identify unique definitions of both programmed pathways and relatively disjointed pathways by which a cell can die. In reality, these processes occur together, involving the turnover of billions of cells in unique compartments of the human body each day. Traditional cytotoxic chemotherapy that damages DNA, directly or indirectly, is a good example of a therapeutic process where both programmed and disjointed cell death occur. Whereas immunogenic cell death involves the release of materials processed by the body to antigenic peptides from dying cells and activation of cellular pathways downstream of pattern recognition receptors, programmed cell death, or apoptosis, is thought to be a relatively compartmentalized process that triggers a minimal immune response, at best (Galluzzi et al., 2015; Krysko et al., 2013).

Apoptosis is activated in a committed process triggered by at least two broad classes of cues, termed the extrinsic pathway and intrinsic pathway. Where the extrinsic pathway involves signaling through various classes of death and TNF- α / TNF- α -related classes of receptors leading to an intracellular cascade that ultimately activates pro-caspase 8, intrinsic cell death is regulated at the level of the mitochondria where the B-cell lymphoma 2 (BCL2) family of pro-/anti-apoptotic proteins interact on the mitochondrial outer membrane to regulate mitochondrial health/function, while preserving integrity. Abundant displacement of pro-apoptotic effectors from various binding partners can lead to oligomerization of pro-apoptotic proteins BAX and BAK, leading to channel formation and permeabilization of the mitochondrial outer membrane. This then leads to release of both cytochrome c and second mitochondria-derived activator of caspases (SMACs) from mitochondria into the cytosol, the former being critical for pro-caspase activation leading to an effector caspase cascade, and the latter

being important in inhibiting proteins that normally function to inhibit apoptosis (IAPs). Together, both pathways converge on phenotypic observations critical to apoptosis of nuclei condensation, cytosolic blebbing and coordinated destruction of protein/DNA components contained within apoptotic bodies (Green, 2016).

New mechanisms continue to emerge, but to date, have been broadly characterized by qualitative differences in cell or sub-cellular membrane composition during the execution of the given process, drawing comparisons or specifying differences between apoptosis (non-lytic), necroptosis (lytic) and/or autophagy (lysosomal; non-lytic). For example, necroptosis is a relatively recent description of a process thought for decades to be passive cellular lysis, releasing/lysing cellular components into intercellular space, and indeed, is currently not distinguishable from passive destruction/crush artifact in samples examined by electron microscopy. However, at the molecular levels, it is becoming established that necroptosis has at least two defined cellular paths activating either the downstream pseudokinase mixed lineage kinase domain like protein (MLKL) or gasdermin-D (pyroptosis; activation of inflammatory non-apoptotic caspases). Although these two components represent a divergence in signaling pathways between the two necrotic programs, it is unclear whether they represent terminal events. Another distinguishing feature of pyroptosis is the conversion and release of proinflammatory IL-18 and IL-1 β , conversion from the zymogen state by the “inflammatory” caspases 1, 4, 5 and 11 (human/mouse). While the intracellular effectors are still being discovered, it has been shown that TNF family members can drive classic necroptosis, where pathogen derived agents such as LPS or nucleic acids may preferentially activate pyroptosis in cell line models (Wallach et al., 2016); however, it should be made clear that much is still to be discovered and uncovered in the field of programmed cell death and its impact on cancer and inflammatory disease.

Intended to be blank

Chapter 1. Modeling Human Cancer in a Mouse Host: Applications of Patient-Derived Xenograft (PDX) Models

Brevis

Historically, studies investigating human cancers have relied on repositories of banked clinical samples embedded in paraffin or kept in a freezer. Successful generation of immortalized cell lines from primary tumor tissue is still a challenge and plagued with clonal bottlenecks. Application of genetically engineered mouse models of cancers have rapidly advanced and taught the community much about disease development and dependencies, but murine systems may represent only a fraction of the heterogeneity seen within a single human cancer. All of these scenarios present limitations in one way or another to the problem – studying and manipulating human cancer as it lives: within a human host, with a functional immune system and supportive tumor microenvironment. The chapter that follows is intended to briefly introduce PDX model systems and serve as an application note when using PDX models to study human cancer.

Maintaining Genetic and Epigenetic Integrity

Several large PDX-focused consortia have recently established the utility of PDX generation and screening *en masse*, including the EuroPDX working group and the Novartis Institute for Biomedical Research (Gao et al., 2015; Hidalgo et al., 2014). Research teams have approached the task of screening *in vivo* tumor sensitivity to experimental therapeutics using small numbers of animals per group(s) as well as large numbers per treatment, to determine the extent of response heterogeneity in a given model system (Gao et al., 2015; Tentler et al., 2012; Townsend et al., 2016). In addition to engraftment and propagation in murine hosts, other groups have explored the development of tumor organoids from primary tumor tissue or from successfully engrafted PDX models, most notably in prostate, lung and colorectal cancers (Crystal et al., 2014; Gao et al., 2014; Karthaus et al., 2014). What consistently emerges from these efforts are the attempts of research teams to generate models systems that more closely resemble that of an actual tumor and preservation of the intratumoral heterogeneity over multiple *in vivo* passages. These degrees of similarity are usually lost in cell line xenograft (CLX) models where the relationship between the primary tumor of origin and resulting immortalized cell lines can be highly divergent due to clonal bottlenecks *in vitro*.

Our research team was one of the first groups to suggest that establishing cell lines from PDX models caused irreversible gene expression changes that did not revert to the “parental” signature (Daniel et al., 2009). These data suggested that in order for a PDX system to truly emulate the parental tumor of origin, it must be maintained in the murine host, and not placed into cell culture where irreversible changes, perhaps in adaptation to *in vitro* growth conditions, can occur. Other groups have gone on to establish the importance of passage number *in vivo*, where the Novartis Institute has

conclusively shown using several hundred PDXs of various histology that >6 rounds of *in vivo* passage, new single nucleotide polymorphisms (SNPs) are gained in the tumor that were not present in the principal, or primary, engrafted tumor tissue (Gao et al., 2015). This did not appear to be a function of limited sequencing depth where certain low presence sub-clones were below the limit of detection, but rather the acquisition of new mutations in the PDX due to unstable genome maintenances across models, collectively. While it is unclear whether the changes in gene expression patterns and gaining of new SNPs yield models that are less useful to discovery efforts, the fact that they occur and can be quantitated has led other groups to establish hard cutoffs for passage numbers of given tumors, where most report “low passage” numbers below 8-10 *in vivo* rounds of passaging (Hidalgo et al., 2014; Tentler et al., 2012).

Scaling up the propagation of a given PDX can impose some technical restraints on their utility, as several rounds of *in vivo* passage may be required to expand tumor material to the point that it can be used to engraft 100s of animals for a large screening effort. Therefore, an alternative strategy has been to use PDX-derived materials in short-term *ex vivo* culture, so called patient-derived tumor cells (PDTC). Recently, several groups have shown that screening drug sensitivity in short term culture can largely recapitulate *in vivo* drug response, although these assays are largely limited to agents that have quick onsets or are grossly cytotoxic, such as receptor tyrosine kinase inhibitors (RTKi) and DNA damaging agents, respectively (Bruna et al., 2016; Crystal et al., 2014; Witkiewicz et al., 2016). Part of the reason PDX models are more representative of patient tumor biology versus traditional cell line xenografts may stem from a preservation of the epigenetic integrity of the primary tumor during direct transplantation into the murine host. Our group has shown PDXs to more closely resemble and cluster with primary, unmatched tumors than tumor cell lines or even cell

lines derived directly from paired PDXs (Poirier et al., 2015). Using CpG methylation arrays, these data strongly suggest that at the level of epigenetic similarity, only PDX systems approach the epigenetic landscape maintained in primary tissue of origin. The defining characteristics of PDX models versus other systems begin to highlight the advantages to using PDX models to understand the likely clinical response of a patient to an investigational therapy using a patient-derived “avatar” model (Hidalgo et al., 2011; Izumchenko et al., 2016), as well as the likely prevalence of certain subclones, whether they are genetically or epigenetically defined, within a tumor bulk population to drive therapeutic resistance or metastasize (Bertotti et al., 2015; DeRose et al., 2011; Forsheew et al., 2012; Kreso et al., 2013; Murtaza et al., 2013).

Tumor Microenvironment Differences and Limitations

Approaches towards reconstructing the human tumor microenvironment in a murine host have largely taken one of two routes: co-engraftment of human tumor component with matched/paired immune tissues into a highly immunocompromised mouse strain (e.g. NSG) or humanization of genomic loci on the current background of an otherwise highly immunocompromised mouse strain. The former strategy requires the isolation of CD34+ stem cells via the bone marrow or circulating in the periphery, gross isolation of peripheral blood mononuclear cells from whole blood (PBMCs) or the most intense approach being to biopsy the thymus/liver and bone marrow compartment to completely repopulate the irradiated immunocompromised host (Morton et al., 2016; Shultz et al., 2012). The later strategy involves “knocking-in” humanized loci for specific cell lineage defining receptors or growth factors on the background of a highly immunodeficient mouse strain.

Recently, the Falvell group had demonstrated the utility of humanizing components of the innate immune system, developing the MITRG/MISTRG strains on the background of $Rag2^{-/-}Il2rg^{-/-}$ mice knocking in genes for human M-CSF, IL-3/GM-CSF and TPO into their respective murine loci (Rongvaux et al., 2014). Engraftment of human tumor xenografts into these animals produced human macrophage infiltration into the xenograft, matching the polarization phenotype observed in primary samples. Moreover, it's logical to envision a combination of approaches for both genetically-engineered and co-engrafted murine models, where specific lineages can be interrogated for their impact on disease state or xenograft growth, while receiving the necessary growth signals and support from the humanized cytokine loci. Taken together, approaches utilizing PDX models are focusing on ways to better recapitulate the immune infiltrate and supportive

environment that have traditionally been neglected when engrafting human tissue into highly immunocompromised animals.

Another limitation that most current PDX models do not address deals with the contribution of stromal components to tumor response and growth *in vivo*. It is well established that many solid tumors have a large fibroblast component to them, the cancer associated fibroblast (CAFs), and these fibroblasts play a role in remodeling extracellular matrix of the tumor, and perhaps even contribute to therapeutic resistance and response via tumor cell-stroma paracrine loops (Augsten, 2014; Kalluri, 2016; Straussman et al., 2012; Wilson et al., 2012). What is also clear is that these human stromal components are gradually phased out of the tumor through multiple *in vivo* passages and effectively replaced by murine stroma (Schneeberger et al., 2016). The presence of a murine component/contaminant within a human tumor population can also lead to technical challenges down the road when interrogating genomic differences between the primary/archival tissue and that which successfully engrafted into murine host. The high degree of variability of stromal components in a given PDX model has the potential to cause error rates in mutation calling algorithms if the user is not aligning sequencing data against a human/mouse hybrid genome or not taking some steps to ensure the majority of mouse tissue has been removed prior to DNA extraction (**Figure 3**). However, it is less clear whether the murine stroma contributes the same degree of functionality and tumor support as that of the human origin, leading some groups to attempt co-engraftment of paired/matched tumor and stromal components from primary surgical samples. Taken together, this first Chapter introduces the utility of the PDX models as a highly concordant model system to that of the primary tissue in terms of genomic and epigenomic architecture. The inability to completely recapitulate the human microenvironment and immunologic infiltrate should be taken into consideration when

choosing how to apply findings from experiments using PDX models as a tool for discovery science.

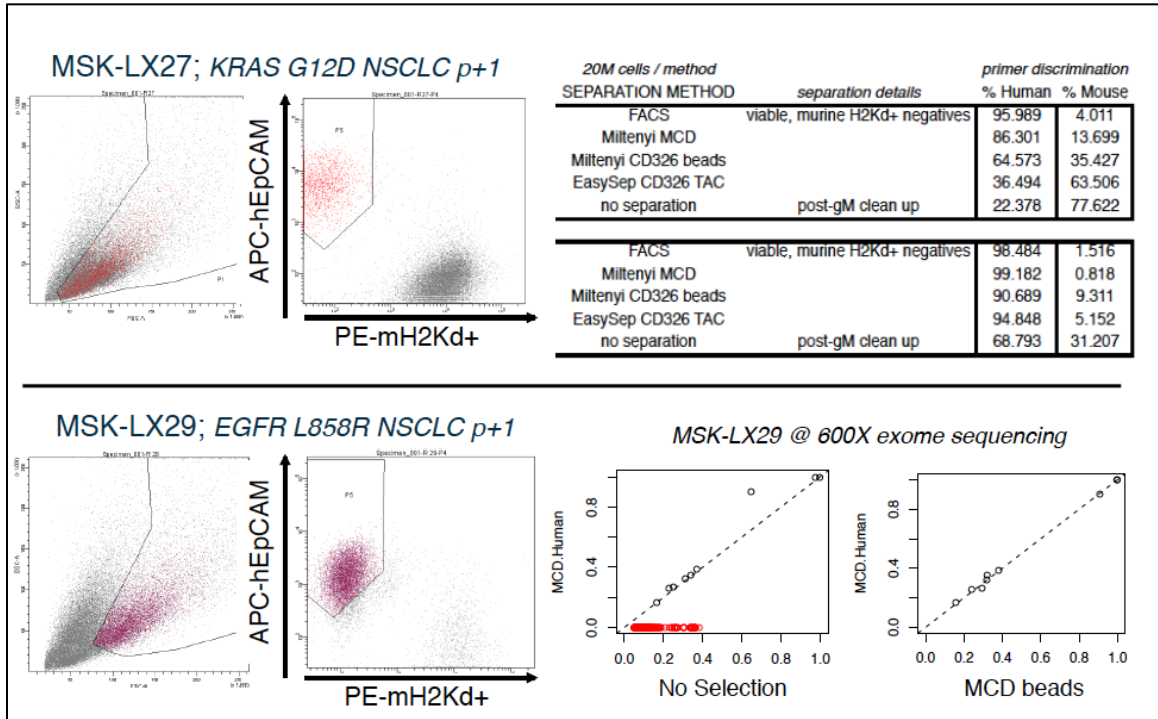


Figure 3. Impact of murine cellular components on human mutational calling by next-generation sequencing.

Example flow cytometry data of human tumor cells and mouse stromal components from two human non-small cell lung cancer (NSCLC) PDX models – MSK-LX27, a G12D Kras mutant tumor, and MSK-LX29, an L858R EGFR mutant tumor. Established hind flank tumors of indicated early passage (p+1) were enzymatically dissociated with a Miltenyi human tumor dissociation kit on an octoMACS dissociator before staining ~20M viable cells with limiting dilutions of antibodies against human CD326 (APC-hEpCAM; y-axis) and mouse H2kd (PE-mH2Kd; x-axis). Both models contain varying degrees of stroma, which our group has shown to negatively influence downstream sequencing approaches by increasing the rate of false mutation calls, even when compared to human-murine hybrid genomes (Schneeberger et al., 2016). Inset table comparing murine and human DNA contribution from extractions of bulk and sorted/purified populations of cells using species-specific primers. MCD=mouse cell depletion beads (cited in *Materials and Methods* within Chapter 2).

Considerations in Preclinical Experimental Design – Case Study of Sunitinib

Oncologists are all too familiar with the challenges of translating findings from animal models into patients. In a previous study, Henderson and colleagues (Henderson et al., 2013) identified what they believed to be the most-common threats to preclinical experimental validity, which were classified as internal, construct and external threats (**Table 1**). In a recent meta-analysis, this group takes as an informative case study the preclinical testing of sunitinib, an oral multitargeted tyrosine kinase inhibitor that is licensed as a monotherapy for advanced-stage renal-cell carcinoma, gastrointestinal stromal (GIST) and pancreatic neuroendocrine tumors (Henderson et al., 2015). Using sunitinib as an example, these authors describe how underpowered or poorly designed experiments in animals, together with reporting biases, can conspire to construct misleading results. The interpretation of these results can lead scientists and clinicians to overestimate the preclinical therapeutic efficacy of sunitinib. This wrong judgment might be partially to blame for the disappointing activity sunitinib has shown in early stage clinical trials across multiple malignancies (Henderson et al., 2015). For example, the authors note the disappointing results of a phase II study in relapsed or refractory small cell lung cancer (Han et al., 2013) where the observed efficacy was minimal and responses were partial at best, yet the preclinical evidence – again, albeit minimal – suggested modest tumor growth inhibition. However, one should note that a recent study has also shown sunitinib to be clinically beneficial in SCLC for chemosensitive relapse (Abdelraouf et al., 2016) as well as reports in specific scenarios, one of these scenarios possibly following prophylactic cranial irradiation (Salama et al., 2016). Nonetheless, both studies were early phase trials in limited numbers of patients, and the benefit conferred has been called into the question of practicality by others (Di Maio et al., 2016).

Not surprisingly, when interrogating the published literature on preclinical studies examining the efficacy of sunitinib as a single agent, Henderson *et al.* found that most studies fell short on taking—or disclosing—appropriate measures to reduce threats to internal and construct validity, such as blinded outcome assessment and using more than one model system, respectively. The ability of this meta-analysis to compare multiple, divergent study types relied on inferring effect sizes as standardized mean differences (SMDs) using Hedges’ *g* score. In total, 74 studies, describing 332 experiments in animals in which tumor volumes or volume responses were indicated, were included in the capture step. The dataset was further reduced to 158 experiments by selecting only those that met the criteria for data extraction applicable to a *g*-score calculation. The authors then summarized all of the experimental data with respect to identified threats to internal, external and construct validity. The internal validity of a study pertains to the efforts taken to reduce experimental/experimenter bias, such as blinded outcome assessment, whereas the external validity of a study is scored based on numbers of models and species tested (Henderson et al., 2015). Finally, construct validity metrics help shed light on the relevance a given model system has to the end application – e.g. predictive power of a model. The majority of studies contained threats that might, across or within certain malignancies, lead to an overestimation of sunitinib efficacy. They further demonstrated that all of the preclinical studies that explored the dose–response relationships between tumor volume and sunitinib dose failed to show associations comparable to those observed in the cited clinical studies (Faivre et al., 2006)—albeit this was a difficult comparison to perform owing to the limited number of studies. Finally, by comparing the effect size calculated per study using a trim and fill method, Henderson and colleagues showed that, in specific malignancies with results from >20 preclinical studies available for analysis, their data fitting indicated an overall

publication bias, as compared with the reported effect from studies for renal-cell carcinoma (the indicated positive control).

The authors have subsequently called for an overhaul of the way *in vivo* preclinical oncology experiments are designed and reported, making note of the ARRIVE guidelines (Kilkenny et al., 2010) and suggesting immediate, actionable changes. These and other (Landis et al., 2012) recommendations in the preclinical arenas comprise useful standard operating procedures for optimizing preclinical study design. For certain preclinical questions, conducting limited analyses in a single species or not exploring a wide range of doses is appropriate. For example, proof of principle studies focused on a single disease, using a drug for which doses and schedules have been previously explored, may opt for a previously validated regimen in the model of choice, rather than repeat an extensive dose-finding experiment. Depending on the context in which the work is being performed, however, researchers should at least consider these recommendations when planning, conducting, analyzing and reporting preclinical experimental data. An important consideration that might ultimately drive this field forward would be the adoption of good practice standards by all peer-reviewed publication outlets.

So, how can we translate the findings of this meta-analysis of sunitinib to our current work? The predictive value attributable to a given animal model system must be taken into account before actively researching experimentally which model is optimal for each study, because each system is both limited and complex (Day et al., 2015). What should be recognized is that no model system is ideal, nor can any model be completely predictive across and within therapeutic categories in oncology (Gould et al., 2015). Because of these limitations, there is a real need to utilize multiple nonhuman models, reflective of the complex biology of the conditions that clinicians aim to treat. The

standard models based on human cell-line xenografts that grow easily in immunocompromised mice do not need to be abandoned, but should be used with acknowledgement of the limitations of the system, and a realization that complementary genetically-engineered mouse models (GEMM) and patient-derived xenografts (PDX) exist; certain models are more appropriate for discovery applications whereas others are suitable for prediction of clinical efficacy. Make no mistake; underpowered studies that use single models will be an old habit that dies hard in the research community.

Henderson and colleagues should be commended for acknowledging the limitations of any potential recommendations based on the results of their own study. Indeed, the authors note that they were limited only to studies that reported data in a manner useful for calculating standardized mean differences. They further note that implementing more rigorous preclinical standards such as testing therapeutic agents in multiple model systems or blinded outcome assessment would certainly come at a greater monetary and time cost to those who adopt such practices. However, the benefit of implementing more-rigorous standards upfront becomes evident when considering the already staggering levels of clinical trial attrition in oncology (Begley and Ellis, 2012). The results of a follow-up analysis from the same group demonstrated that performing additional clinical testing of sunitinib in other tumor types was of minimal benefit, and further investigation beyond the original, approved indication worsened the risk–benefit ratio (Carlisle et al., 2016) of this therapy across all examined malignancies, when viewed in aggregate. This analysis of data for sunitinib is one specific and dated example of the preclinical and clinical legacy of an approved therapeutic agent. However, similar conclusions would likely result from examination of the past and current threats to clinical inference across preclinical studies examining the efficacy of small molecules, biologic agents and radiotherapeutic regimens. Looking forward, the need for

appropriately powered and diversified preclinical animal studies becomes even more relevant in an age when investigators seek to combine multiple targeted therapies to combat resistance mechanisms in genetically-annotated tumor types—including contexts in which agents that might have minimal efficacy as monotherapies are given in combination.

For future analyses of preclinical efficacy in oncology drug development to be appropriately powered and to avoid overestimating the magnitude of the effect of a given therapeutic agent, researchers should adhere, whenever possible, to recommended best practices for *in vivo* preclinical oncology research (**Table 2**). Whether such recommendations become adopted as requirements for the publication of preclinical therapeutic findings will likely depend on the active engagement of journal peer-reviewers and editors to hold our feet to the fire.

Table 1. Preclinical Reporting Metrics for Studies Examining Tumor Volume Responses in Animals

Pre-specified metrics	Active metrics
Sample size calculation	Blinded assessment
Power calculation	Blinded treatment allocation
Inclusion criteria	Statistical comparisons
Exclusions criteria (e.g. outliers)	Study replication
Definition(s) of significance	

Table 2. Validity Threats to Preclinical Research Efficacy

Threat Category	<i>application</i>	<i>example</i>
Internal	reduce experimental bias	random allocation
External	transfer of a cause-and-effect relationship across systems	# of model systems used
Construct Validity	relevance of model system(s) to end application	predictive power of model

Intended to be blank

Chapter 2. Epigenetic Silencing of *SLFN11* Defines a Recurrent Mechanism of Acquired Resistance to Chemotherapy in SCLC

Brevis

Small cell lung cancer is among the most lethal human malignancies. Typical progression of this disease is characterized by a rapid shift between initial chemoresponsive and subsequent chemoresistant states. The mechanisms responsible for acquired therapeutic resistance in small cell lung cancer have not been defined. Using patient-derived tumor xenografts to closely model clinical acquired resistance, this work: (1) defines a mechanism of chemoresistance operant across multiple, independent small cell lung cancers, (2) identifies an epigenetic regulator controlling the mechanism of acquired resistance, and (3) establishes a novel therapeutic strategy to both prevent and treat acquired resistance *in vivo* (**Figure 4**). These observations have immediate clinical implications, describing an approach that may lead to a durable and effective treatment for patients with this disease.

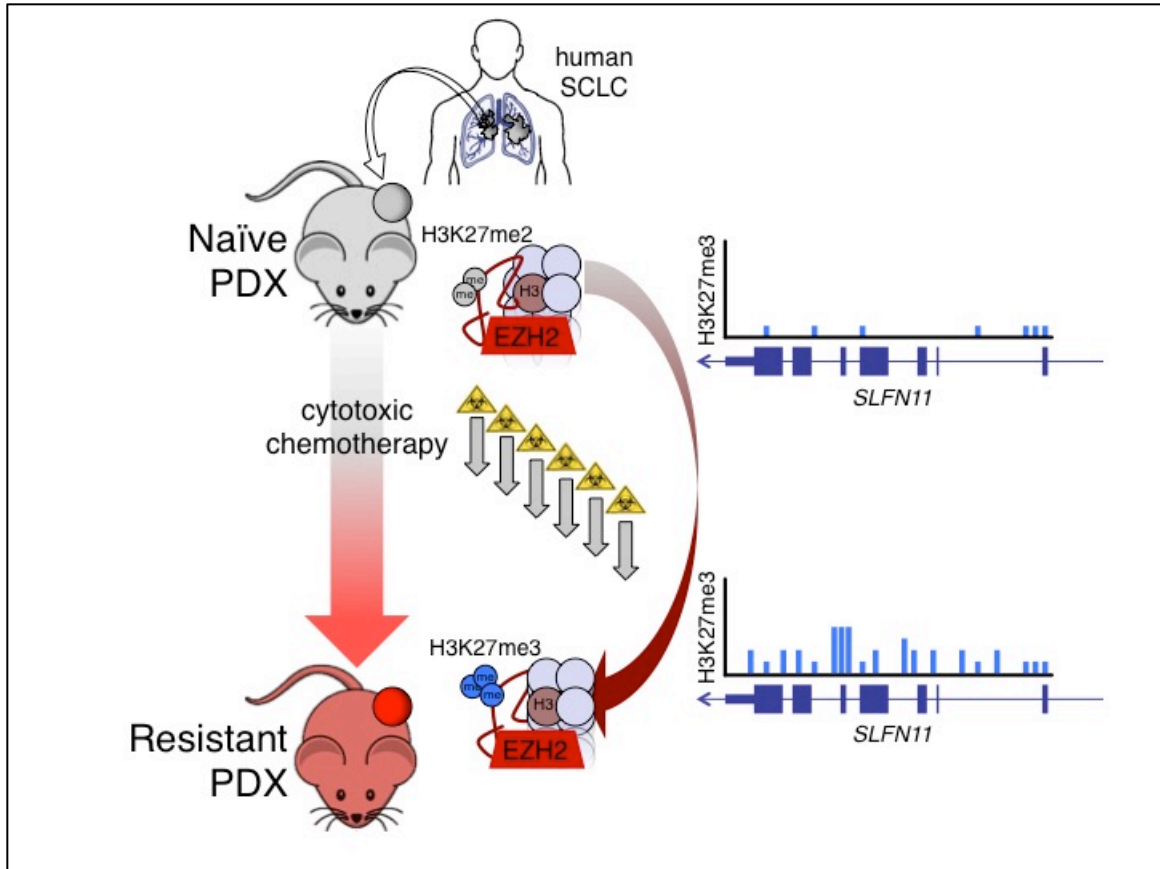


Figure 4. Chapter 2 Brevis.

PDX models are generated by directly engrafting human tumor cells into immunocompromised mice, without any intervening cell culture (e.g. *ex vivo*). Once stably established and passage in animals, groups of chemonaïve tumor-bearing animals were challenged with a schedule of chemotherapy used as first line in patients, until their tumors were robustly chemoresistant. Comparing conserved gene expression changes between multiple chemonaïve and chemoresistant models revealed down regulation of *SLFN11*, a gene implicated in sensitivity to DNA damaging agents, particularly topoisomerase I poisons. Herein we show that the histone methyltransferase EZH2 is responsible for this silencing event *in vivo*, depositing H3K27me3 throughout the gene body of *SLFN11*, and this can be reversed by inhibition EZH2's catalytic activity with the clinical stage EZH2 inhibitor EPZ011989.

Study Introduction

Small cell lung cancer (SCLC) affects an estimated 270,000 individuals per year worldwide, and is metastatic at the time of diagnosis in approximately two thirds of cases (Shepherd et al., 2007; Torre et al., 2015). Metastatic SCLC is exceptionally lethal, associated with a median survival from the time of diagnosis of 9 to 10 months, and a 5-year survival of less than 2% (Shepherd et al., 2007). Even when detected prior to metastasis, most patients with localized disease will suffer disease recurrence and death within the first 2 years. More effective treatment approaches to SCLC are desperately needed.

The standard first line treatment for metastatic SCLC consists of a platinum doublet, cisplatin or carboplatin, generally paired with the topoisomerase II inhibitor etoposide (Kalemkerian et al., 2013). Standard approaches to recurrent SCLC include treatment with a topoisomerase I inhibitor, topotecan or irinotecan. There are no approved therapies for SCLC after progression on a second line regimen. *De novo* SCLC is remarkably sensitive to first line platinum doublet chemotherapy, with objective response rates of over 50% in patients without substantial co-morbid conditions. These impressive responses are also disappointingly transient: median progression-free survival in current trials remains less than 5 months (Belani et al., 2016). The response rates to second line topoisomerase I inhibitor therapy are substantially lower, below 20% overall (Horita et al., 2015).

The molecular mechanisms responsible for the remarkable shift between *de novo* chemosensitive disease and rapidly emergent chemoresistant disease in SCLC have not been defined. Recurrent SCLC is rarely biopsied: recurrence is expected and repeat biopsy is not known to be useful in guiding decisions regarding second line therapy. Defining these mechanisms would both provide novel insights into the biology of SCLC

and inform clinical strategies to prevent or delay therapeutic resistance. More broadly, characterizing mechanisms of acquired resistance in this cancer that undergoes a dramatic shift between chemosensitivity and chemoresistance could have implications for understanding acquired resistance to DNA damaging cytotoxic therapy in other malignancies.

We and others have characterized the mutational landscape of SCLC (George et al., 2015; Rudin et al., 2012a). This disease is tightly linked to heavy tobacco smoking. Chronic mutagenic exposure, coupled with essentially universal loss of tumor suppressor genes *RB1* (*RB transcriptional corepressor 1*) and *TP53* (*tumor protein 53*), translates into an exceptionally high burden of mutations and genomic rearrangements. A simple comparison of disparate models representing *de novo* and recurrent SCLC could limit sensitivity to detect causal alterations due to the high background mutational load and inter-tumoral genomic heterogeneity of SCLC. We hypothesized that a more informative approach would be to conduct a pair-wise comparison of changes in individual tumor models prior to, and following, acquired chemotherapy resistance.

We sought to characterize mechanisms of acquired resistance to first line cisplatin and etoposide therapy in SCLC by mimicking clinical practice as closely as possible through *in vivo* treatment of a set of chemosensitive SCLC patient-derived xenograft (PDX) models. Over the past decade, our research group has established and characterized a library of lung cancer PDX models, including tumors from both chemonaïve and previously treated SCLC patients (Daniel et al., 2009). We have demonstrated that these SCLC models more closely resemble the human disease than do cell line-based xenografts, in global gene expression and genome-wide methylation profiles (Poirier et al., 2015). In this study we selected ten SCLC PDX demonstrating initial *in vivo* chemosensitivity to cisplatin and etoposide. Through repeated cycles of

cisplatin and etoposide in tumor-bearing mice, we derived tumors that progressed through treatment. Progressing tumors were disaggregated, transplanted into second and third generations of mice, and retreated to verify that these tumors in fact represented acquired, intrinsic chemotherapeutic resistance. Here we describe the results of detailed genomic analyses of these chemosensitive and subsequent chemoresistant pairs. We discovered that epigenetic silencing of *SLFN11*, a gene involved in DNA damage repair sensitivity, was a recurrent event in acquired chemoresistance. Chemically inhibiting EZH2 prevented *in vivo* acquired resistance and sensitized resistant tumors and cell lines to DNA damaging agents. These observations put forth an epigenetic mechanism to explain the dramatic change in chemosensitivity observed in primary SCLC.

Materials and Methods

PDX model use and characterization

All animal experiments were approved by the Memorial Sloan Kettering Cancer Center (MSKCC) Animal Care and Use Committee. All primary tumors and whole blood samples collected for generation of patient-derived xenograft (PDX) models were obtained under protocols approved by the MSKCC Institutional Review Board (IRB). Subcutaneous flank tumors were generated as previously described (Daniel et al., 2009), engrafting $\sim 1 \times 10^6$ viable cells in a 50% Matrigel (BD; 356231) mixture per 8-10 week old female NSG mouse (Jackson Labs; #005557 NOD.Cg-Prkdc^{scid} Il2rg^{tm1Wjl}/SzJ). All animal experiments using PDX models were performed in female NSG animals that did not exceed 8 months in age at any point on study. When tumors reached volumetric or toxicity/exposure limits on study, tumors were resected and tissue was enzymatically dissociated using a gentleMACS tissue dissociator and a human tumor dissociation kit (Miltenyi; 130-095-929). Animal weights and tumor volumes were monitored 2-3 times per week, with volumes calculated from manual caliper measures using a modified ellipsoid formula: tumor volume = $(Length \times Width^2) / 2$. A list of PDX model treatment history can be found in (**Table 3**).

Table 3. PDX model characteristics used throughout studies.

Text ID	Source	Patient Diagnosis	PDX Diagnosis	Treatment	Site	Reference
JHU-LX22	John Hopkins University	SCLC	SCLC	none	pleura	(Hann et al., 2008)
JHU-LX33	John Hopkins University	SCLC	SCLC	none	transbronchial	(Hann et al., 2008)
JHU-LX44	John Hopkins University	SCLC	SCLC	unknown	unknown	(Poirier et al., 2013)
JHU-LX48	John Hopkins University	SCLC	SCLC	platinum based therapy	unknown	(Poirier et al., 2013)
JHU-LX101	John Hopkins University	SCLC	SCLC	none	transbronchial	(Leong et al., 2014)
JHU-LX102	John Hopkins University	SCLC	SCLC	none	transbronchial	(Leong et al., 2014)
JHU-LX108	John Hopkins University	SCLC	SCLC	carboplatin, radiation	transbronchial	(Leong et al., 2014)
JHU-LX110	John Hopkins University	SCLC	SCLC	none	transbronchial	(Leong et al., 2014)
SCRX-Lu149	StemcentRx, Inc.	SCLC	SCLC	none	lung	(Saunders et al., 2015)
MSK-LX40	Memorial Sloan Kettering Cancer Center	SCLC	SCLC	cisplatin + etoposide	lung	<i>unpublished</i>
MSK-LX95	Memorial Sloan Kettering Cancer Center	SCLC	SCLC	cisplatin + etoposide	lung	<i>unpublished</i>

In vitro and in vivo generation of acquired resistance to cisplatin/etoposide

Mouse DKO and TKO cells were cultured under increasing concentrations of etoposide, refreshing media and drug twice weekly, until stable cultures were capable of proliferating in the presence of 1 μ M etoposide. Parental and resistant versions of the DKO and TKO cell lines were confirmed by STR, as lines were in continuous culture for ~6 months. *In vivo*, cohorts of tumor-bearing animals were challenged weekly with cycles of cisplatin (5 mg/kg IP d1) and etoposide (8 mg/kg IP d1-3) as long as the following conditions were met: 1) tumor volumes were greater than 100mm³ and actively progressing and 2) animals did not lose >20% body weight when compared to the point of randomization (starting weights). The morning of d1 of each cycle, animals were given 0.8-1.0cc of normal saline subcutaneously to facilitate renal clearance of the cisplatin, as cumulative dehydration from platinum was the dose-limiting toxicity. Where toxicity (usually uniform within a treatment cohort) was encountered, animals were given a one-week holiday from treatment to allow recovery of weight. All animals were maintained on Sulfatrim diet throughout the period of study.

Use of mSCLC (TKO) allograft model

All *in vivo* mSCLC experiments were performed using an allograft of the triple (*Rb/p53/p130*) knockout mouse model of SCLC (Park et al., 2011a; Schaffer et al., 2010), maintained in female, 2-3 month old athymic nude mice (Envigo; Hsd:Athymic Nude-*Foxn1^{nu}*). Flank tumors were engrafted and maintained as described for PDX models with the exception of using a mouse tumor dissociation kit to process these tumors into single cell suspensions (Miltenyi; 130-096-730) for engraftment.

In vivo irradiation

Once tumor volumes reached approximately 150mm³, mice were randomized to control and treatment arms. Flank irradiation was administered at 2Gy/fraction to anesthetized mice for 4 consecutive days delivered by an X-Ray irradiator (XRAD 320, Precision X-Ray) with secondary collimation by custom lead cut-outs.

Tumor Micro Array (TMA) construction and immunohistochemistry

Tumor cores were obtained from embedded PDX tumors tissue in donor blocks using a 1mm biopsy punch needle (IHC World; W-125-0) then embedded/inserted into paraffin recipient block/negative mold (IHC World; 10*17 Quick Ray mold IW-UM01-1). Empty slots were filled with blank paraffin cores. All cores were gently tamped down using biopsy punch needle then the entire block was placed face down on a glass slides and heated to 50°C for 2hrs to merge donor cores with the recipient block. Block and glass slide were then placed on ice for 30 minutes before sectioning. Two tissue microarrays (TMAs) made of primary and metastatic SCLC specimens were prepared from formalin-fixed paraffin-embedded (FFPE) tissue blocks following previously reported methods (Kononen et al., 1998; Ocak et al., 2010). Pathology blocks were retrieved from the archives of the Department of Pathology at Vanderbilt University Medical Center, Nashville VA Medical Center and St-Thomas Hospital in Nashville, Tennessee. They were obtained between 1996 and 2008 from patients who had surgery or bronchoscopy prior to medical treatment. SCLC diagnosis was confirmed on hematoxylin and eosin-stained (H&E) sections by an experienced lung cancer pathologist. Treatment was administered on an individualized basis according to disease stage and patient performance status (PS) as per standard of care therapy (chemotherapy and radiotherapy). All patients were followed through chart review until death or until data analysis of this manuscript. Clinical data were obtained from tumor registry and hospital

charts. The study was approved by Institutional Review Boards at each medical center. Staining and H-score calculations, a weighed score that ranges from 0 - 300 and integrates IHC staining intensity and area, was performed as previously described (Lok et al., 2016).

Cell culture, in vitro viability assays and chemical inhibitors

All cell lines were obtained from the American Type Culture Collection (ATCC), were confirmed by STR (DDC Medical) and tested negative for mycoplasma (Lonza MycoAlert PLUS; LT07-710) within 6 months of use. All cell lines were maintained in RPMI-1640 supplemented with 10% FBS, 2mM L-glutamine and 1x penicillin/streptomycin. *Ex vivo* cell culture of PDX tumors was performed as previously described (Poirier et al., 2015). EPZ011989 was provided by Epizyme and formulated as previously described (Campbell et al., 2015). Cisplatin (APP), etoposide (Teva) and irinotecan (Hospira) for *in vivo* use were obtained from the MSKCC hospital pharmacy and formulated in normal saline immediately before use. Topotecan (Selleck Chem), GSK126 (Selleck Chem) and 5-azacitidine (Sigma) were purchased commercially and formulated in DMSO. Cell viability experiments were performed at 72hrs post-dosing, where $1-5 \times 10^4$ viable cells were seeded in 100 μ L/well of fresh media in black 96-well plates and drugs added to a final volume of 200 μ L one day after seeding plates (Corning; 3916). Cell viability experiments were monitored using AlamarBlue (Life Technologies), allowing the reagent to develop overnight (~16hrs) before reading plates on a compatible plate reader (BioTek; Synergy Neo). Throughout the text DMSO is used as the vehicle control for *in vitro* or *ex vivo* experiments.

Plasmids and generation of lentiviral supernatants

SLFN11 (HsCD00082389) and human *TWIST1* (HsCD00042456) cDNAs in pDONR vectors were purchased from DNASU plasmid repository. Mouse *Twist1* cDNA was purchased from Origene (MR227370). Polymerase chain reactions (PCRs) were performed using a GeneAmp PCR System 9700 Thermocycler (Applied Biosystems). Competent Stbl3 cells were purchased from Invitrogen. Plasmids were isolated and purified from bacteria using QIAquick Spin Miniprep Kit (Qiagen). *SLFN11* was cloned into plasmid pDONR 221 (Life Technologies). Using primers with the following sequences 5'- TGATGATAATGATACCCAGCTTTCTTGTACAAAGTGGGCATT-3' and 5'- TCATTATCATCAATGGCCACCCCACGGAAAAATATACAGGTG-3', the pDONR201-*SLFN11* plasmid was used as a PCR template to add 4 tandem stop codons between the C-terminal end of *SLFN11* cDNA and the Myc-DDK tag sequence to ensure termination after the *SLFN11* cDNA translation. Site-directed mutagenesis of mouse *Twist1* cDNA to the DNA-binding mutant K145E (Maia et al., 2012) was performed using a QuikChange Site-Directed Mutagenesis Kit (Agilent) and the following primers: forward 5'-GGACAAGCTGAGCGAGATTCAGACCC-3' and reverse 5'-GGGTCTGAATCTCGCTCAGCTTGTCC-3'. Gateway® cloning was performed according to manufacturer's recommendations (BP/LR clonase enzyme mixes; Life Technologies). The plasmid pLIX_402 was a gift from David Root (Addgene plasmid # 41394) and pLT3GEPIR (Fellmann et al., 2013) was obtained from the MSKCC RNAi core facility. A list of tested shRNA sequences is available in **Table 4**. Lentiviral supernatants in HEK-293T/17 cells were generated as previously described (Lok et al., 2016; Moffat et al., 2006). Sanger sequencing of plasmids was performed by Genewiz, Inc. Nucleotide and protein sequence alignments were performed in Geneious Pro 4.7.6.

Table 4. List of shRNA sequences tested and used within Chapter 2.

Target	Species	Library ID	Text ID	97mer sequence (5'-3')
<i>TWIST1</i>	human	TWIST1.503	-	TGCTGTTGACAGTGAGCGACA GGTACATCGACTTCCTCTATAG TGAAGCCACAGATGTATAGAG GAAGTCGATGTACCTGGTGCC TACTGCCTCGGA
<i>TWIST1</i>	human	TWIST1.533	-	TGCTGTTGACAGTGAGCGCGA GCAAGATTCAGACCCTCAATA GTGAAGCCACAGATGTATTGA GGGTCTGAATCTTGCTCATGC CTACTGCCTCGGA
<i>TWIST1</i>	human	TWIST1.540	-	TGCTGTTGACAGTGAGCGAAC AAGCTGAGCAAGATTCAGATA GTGAAGCCACAGATGTATCTG AATCTTGCTCAGCTTGTCTGCC TACTGCCTCGGA
<i>TWIST1</i>	human	TWIST1.548	shTWIST1.1	TGCTGTTGACAGTGAGCGCGC CCTCGGACAAGCTGAGCAATA GTGAAGCCACAGATGTATTGC TCAGCTTGTCCGAGGGCATGC CTACTGCCTCGGA
<i>TWIST1</i>	human	TWIST1.674	-	TGCTGTTGACAGTGAGCGACG GCGGGAGTCCGCAGTCTTATA GTGAAGCCACAGATGTATAAG ACTGCGGACTCCCGCCGCTGC CTACTGCCTCGGA
<i>TWIST1</i>	human	TWIST1.752	shTWIST1.2	TGCTGTTGACAGTGAGCGACC AGGGCAAGCGCGCAAGAATA GTGAAGCCACAGATGTATTCTT GCCGCGTTGCCCTGGGTGCC TACTGCCTCGGA
Renilla luciferase	sea pansy	Renilla.713	shRen.713	TGCTGTTGACAGTGAGCGCAG GAATTATAATGCTTATCTATAG TGAAGCCACAGATGTATAGATA AGCATTATAATTCCTATGCCTA CTGCCTCGGA
<i>Twist1</i>	mouse	mTWIST1.671	-	TGCTGTTGACAGTGAGCGACC AGCGCACGCAGTCGCTGAATA GTGAAGCCACAGATGTATTCA GCGACTGCGTGCGCTGGCTGC CTACTGCCTCGGA
<i>Twist1</i>	mouse	mTWIST1.731	shTWIST1.1	TGCTGTTGACAGTGAGCGCGC CCTCGGACAAGCTGAGCAATA GTGAAGCCACAGATGTATTGC TCAGCTTGTCCGAGGGCATGC CTACTGCCTCGGA
<i>Twist1</i>	mouse	mTWIST1.739	shTWIST1.2	TGCTGTTGACAGTGAGCGAAC AAGCTGAGCAAGATTCAGATA GTGAAGCCACAGATGTATCTG AATCTTGCTCAGCTTGTCTGCC TACTGCCTCGGA

<i>Twist1</i>	mouse	mTWIST1.746	-	TGCTGTTGACAGTGAGCGCGA GCAAGATTCAGACCCTCAATA GTGAAGCCACAGATGTATTGA GGGTCTGAATCTTGCTCATGC CTACTGCCTCGGA
<i>Twist1</i>	mouse	mTWIST1.747	-	TGCTGTTGACAGTGAGCGAAG CAAGATTCAGACCCTCAAATAG TGAAGCCACAGATGTATTTGAG GGTCTGAATCTTGCTCTGCCTA CTGCCTCGGA
<i>Twist1</i>	mouse	mTWIST1.776	-	TGCTGTTGACAGTGAGCGACA GGTACATCGACTTCCTGTATAG TGAAGCCACAGATGTATACAG GAAGTCGATGTACCTGGTGCC TACTGCCTCGGA
<i>SLFN11</i>	human	SLFN11.464	-	TGCTGTTGACAGTGAGCGCTA GAAGTAATCCTTCATTTAATAG TGAAGCCACAGATGTATTAAT GAAGGATTACTTCTAATGCCTA CTGCCTCGGA
<i>SLFN11</i>	human	SLFN11.553	-	TGCTGTTGACAGTGAGCGATC AGACCAATATCCAAGAGAATAG TGAAGCCACAGATGTATTCTCT TGGATATTGGTCTGAGTGCCTA CTGCCTCGGA
<i>SLFN11</i>	human	SLFN11.3552	-	TGCTGTTGACAGTGAGCGACA CCAGGATATTTGCGATATATAG TGAAGCCACAGATGTATATATC GCAAATATCCTGGTGGTGCCT ACTGCCTCGGA
<i>SLFN11</i>	human	SLFN11.3676	shSLFN11.1	TGCTGTTGACAGTGAGCGCCA GTTGTCTGAAGATTTTGAATAG TGAAGCCACAGATGTATTCAA ATCTTCAGACAACCTGTTGCCTA CTGCCTCGGA
<i>SLFN11</i>	human	SLFN11.4390	shSLFN11.2	TGCTGTTGACAGTGAGCGATC AGTTCTTCATTATACCGTATAG TGAAGCCACAGATGTATACGG TATAATGAAGAACTGAGTGCCT ACTGCCTCGGA
<i>SLFN11</i>	human	SLFN11.4395	-	TGCTGTTGACAGTGAGCGACA GCCTCAGTTCTTCATTATATAG TGAAGCCACAGATGTATATAAT GAAGAACTGAGGCTGCTGCCT ACTGCCTCGGA
<i>EZH2</i>	human	EZH2.61	-	TGCTGTTGACAGTGAGCGCAC CAGTGAATTTTTGCAATAATAG TGAAGCCACAGATGTATTATTG CAAAAATTCAGTGGTATGCCTA CTGCCTCGGA

<i>EZH2</i>	human	EZH2.536	shEZH2.1	TGCTGTTGACAGTGAGCGAAA GAGGGAAAGTGTATGATAATA GTGAAGCCACAGATGTATTATC ATACACTTTCCCTCTTCTGCCT ACTGCCTCGGA
<i>EZH2</i>	human	EZH2.1948	-	TGCTGTTGACAGTGAGCGCCA GGATGGTACTTTTCATTGAATAG TGAAGCCACAGATGTATTCAAT GAAAGTACCATCCTGATGCCTA CTGCCTCGGA
<i>EZH2</i>	human	EZH2.1723	-	TGCTGTTGACAGTGAGCGCCG GAAATTTCCCTTCTGATAAATAG TGAAGCCACAGATGTATTTATC AGAAGGAAATTTCCGATGCCTA CTGCCTCGGA
<i>EZH2</i>	human	EZH2.136	-	TGCTGTTGACAGTGAGCGATG TAAGAATAATTTATAGTAATAG TGAAGCCACAGATGTATTACTA TAAATTATTCTTACAGTGCCTA CTGCCTCGGA

Antibodies

A detailed list of antibodies and dilutions used in this Chapter is available in **Table 5**.

Table 5. List of antibodies and dilutions used throughout Chapter 2.

Target	Source	Product#	Application	Fold Dilution
EZH2	Cell Signaling	5246	WB	1000
EZH2	Active Motif	39901	ChIP	5ug/reaction
H3K27me1	Active Motif	61015	WB	1000
H3K27me2	Cell Signaling	9728	WB	2500
H3K27me3	Active Motif	39155	WB	2500
H3K27me3	Millipore	07-449	ChIP	4ug/reaction
H3K36me3	Cell Signaling	4909	WB	1000
H3K4me3	Cell Signaling	9751	WB	1000
H3K27Ac	Active Motif	39685	WB	1000
H3K27Ac	Active Motif	39133	ChIP	4ug/reaction
actin (mouse)	Cell Signaling	3700	WB	5000
actin (rabbit)	Cell Signaling	8457	WB	5000
H3 (mouse)	Cell Signaling	14269	WB	5000
H3 (rabbit)	Cell Signaling	4499	WB	5000
vinculin	Cell Signaling	13901	WB	1000
TWIST1	Abcam	ab50887	WB	1000
SLFN11	Santa Cruz	sc-374339	WB	250
cleaved-PARP	Cell Signaling	5625	WB	1000
γ H2A.X (phospho-S139)	Cell Signaling	9718	WB	1000
H2A.X	Cell Signaling	2595	WB	1000
GFP	Cell Signaling	2956	WB	5000
donkey anti-rabbit IRDye 800CW	LI-COR	926-32213	WB	25000
donkey anti-mouse IRDye 680LT	LI-COR	926-68022	WB	25000
donkey anti-mouse IRDye 800CW	LI-COR	926-32212	WB	25000
donkey anti-rabbit IRDye 680LT	LI-COR	926-68023	WB	25000
SLFN11	Santa Cruz	sc-374339	IHC	2ug/mL

Protein extraction, near-infrared Western blotting and protein quantitation

Whole cell lysates were prepared from frozen cell pellets or flash frozen tissue using RIPA lysis and extraction buffer (Thermo; 89901) supplemented with Halt protease and phosphatase inhibitor cocktail (Thermo; 78440). For extraction from frozen tissue, 50-100mg of tissue was placed into gentleMACS M tube (Miltenyi; 130-094-392) in ~2mL of ice-cold extraction buffer and processed using a pre-specified protein extraction cycle, followed by a 10 sec. sonication setup using 200V microtip sonicator set to 40% amplitude (QSonica; CL18). Crude lysates were clarified at 14,000rpm for 10 minutes in a refrigerated bench top centrifuge (Eppendorf; 5340 R). Protein lysates were quantified using a micro BCA protein assay kit (Pierce; 23235) and then diluted with extraction buffer, NuPAGE® LDS sample buffer and reducing reagent (Life Technologies) prior to resolving on 4-12% Bis-Tris gradient gels. Gels were wet-transferred to 0.45µm Immobilon-FL PVDF membrane (Millipore; IPFL00010, lot#R5GA0255H for all blots reported). All primary antibodies were incubated overnight with membranes in TBS Odyssey blocking buffer supplemented with 0.1% Tween-20 (LI-COR; 927-50000), while secondary antibodies were incubated at room temperature with agitation for 1 hour in primary blocking buffer supplemented with 0.01% SDS. Membranes were dried at 37C and protected from light before imaging (LI-COR; Odyssey Sa). The same instrument gain settings were used for all targets examined (3.0 for 700nm channel; 6.0 for 800nm channel), with normalization of the 800nm channel against the 700nm channel, where indicated in the text. Images were analyzed in ImageStudio (LI-COR; version 3.1.4) Recombinant GST-SLFN11 (Abnova; H00091607-P01) was used to determine the limit of detection for SLFN11 in cell lines and PDX tissue. 5µg of total, clarified cell lysate was determined to be optimal for detection of 4 logs of dynamic range of for SLFN11 from *in vivo* sources (SCRX-Lu149 chemo-naïve tumor used to benchmark).

DNA/RNA extraction and sequencing

DNA and RNA were extracted from flash frozen tissue using AllPrep DNA/RNA mini kits (Qiagen; 80204), homogenizing tissue using a gentleMACS M tube containing ~2mL of RLT Plus buffer (Qiagen; 1053393) supplemented with 2-mercaptoethanol (Fisher) and processing samples on a pre-specified RNA extraction cycle. Samples were passed through QIAshredder columns (Qiagen; 79656) and DNA and RNA components were eluted in water before storing DNA at -20C and RNA at -80C for future analyses. RNA library preparation (w/ polyA selection), multiplexing and sequencing on an Illumina HiSeq2500 in RapidRun mode (50bp single end reads) was performed by Genewiz. SureSelect Human All Exon V4 and SureSelect Mouse All Exon enrichment kits (Agilent) were used for whole exome library preparation. MSK-IMPACT (Cheng et al., 2015; Wagle et al., 2012) and whole exome sequencing were performed by the MSKCC integrated genomics operation (iGO) core facility.

Mutation and copy number analysis

Raw reads were aligned to a custom hybrid reference genome using BWA 0.7.12-r1039 with default settings (Li and Durbin, 2009). The hybrid index was generated using a FASTA file consisting of all human GRCh38 and mouse GRCm38.p3 reference contigs. Mapped reads were piped to SAMBLASTER 0.1.22 and samtools 1.2 for on-the-fly duplicate removal and sorting, respectively. Sorted reads were processed through the Genome Analysis Toolkit (GATK) 3.6, according to standard practices, including generation of depth of coverage analysis statistics (DePristo et al., 2011; McKenna et al., 2010). Each sample was genotyped at >1,000 common SNP sites using HaplotypeCaller to generate a fingerprint. SNP concordance was confirmed by bcftools 1.2. Mutations were called using MuTect2 the subset of common SNPs in dbSNP 147

found in >1% of the population. Variants that did not pass a MuTect2 filter, had a variant frequency <10%, or were a common SNP were excluded. Filtered mutations were annotated with snpEff. Final mutations and their annotations were loaded into the R statistical computing environment for final analysis. For novel mutation discovery, genes were rank ordered by the number of models in which a gene was mutated in the chemoresistant setting, but not the chemo-naïve setting. Copy number plots were generated using the copy number package for R (Nilsen et al., 2012).

Gene expression analysis

Raw reads were aligned to a custom hybrid reference genome using STAR 2.4.1b (Dobin et al., 2013). The hybrid index was generated using a FASTA file consisting of all human GRCh38 and mouse GRCm38.p3 reference contigs and the human GENCODE gene set (release 20) transcript model. Mapped reads were assigned to GENCODE 20 genes using Subread 1.5.0-p2 to generate a raw counts table (Liao et al., 2014). Raw counts were read into the R statistical computing environment for further analysis (R Core Team (2016). R: A language and environment for statistical computing. R Foundation for Statistical Computing, Vienna, Austria. URL: <https://www.R-project.org/>). Downstream analysis was performed with the limma package for R (Ritchie et al., 2015). Genes with ≥ 5 counts per million in ≥ 3 samples were considered for analysis. Counts were normalized to library size and transformed to log₂ counts per million with upper quartile normalization. Weights were calculated based on a combination of observational-level weights determined from an estimate of the mean-variance relationship within all samples and sample-level weights reflecting the degree to which each sample follows the linear model (Ritchie et al., 2006). A linear model was fit for each contrast and standard errors were moderated using an empirical Bayes method. T

statistics B statistics and *p*-values were generated for each gene. *P*-values were corrected for multiple testing by the method of Benjamini and Hochberg. To identify genes with biologically significant effect sizes, statistically significant *p*-values, and recurrent alterations, we chose to highlight genes with a fold change of ≥ 2 that were significant in ≥ 3 models.

Robust Multi-array Average (RMA) and quantile normalized gene expression microarray data for 1,037 cancer cell lines was downloaded from the Cancer Cell Line Encyclopedia (Barretina et al., 2012). The gene expression signal distribution of *SLFN11* is distinctly bimodal. The minor mode comprises cell lines in which the gene is not expressed while the major mode, having a greater standard deviation, comprises cell lines in which *SLFN11* is expressed at varying levels. To discriminate between cell lines based on *SLFN11* expression, a gene expression cutoff was established using two independent approaches: the method of Zilliox et al. (Zilliox and Irizarry, 2007), which estimates a gene expression cutoff based on the standard deviation of the minor mode based on the left side of the mean, and by fitting a finite mixture of 2 Gaussian components. Both approaches were in agreement in establishing a cutoff of 5.

ChIP-seq and ChIP-qPCR

Tumor tissue was submersed 1% formaldehyde in PBS, cut into small pieces and incubated at room temperature for 15 minutes. Fixation was stopped by the addition of 0.125M glycine (final concentration). The tissue pieces were then treated with a TissueTearer and finally spun down and washed twice in PBS. Chromatin was isolated by the addition of lysis buffer, followed by disruption with a Dounce homogenizer. NCI-H446 cells were fixed with 1% formaldehyde for 15 min and quenched with 0.125 M glycine. Chromatin was isolated by the addition of lysis buffer, followed by disruption with

a Dounce homogenizer. Lysates were sonicated and the DNA sheared to an average length of 300-500 bp. Genomic DNA (Input) was prepared by treating aliquots of chromatin with RNase, proteinase K and heat for de-crosslinking, followed by ethanol precipitation. Pellets were re-suspended and the resulting DNA was quantified on a NanoDrop spectrophotometer. Extrapolation to the original chromatin volume allowed quantitation of the total chromatin yield.

Aliquots of chromatin (20-30 μ g) were pre-cleared with protein A agarose beads (Invitrogen). Genomic DNA regions of interest were isolated using 5 μ l antibody against EZH2 (Active Motif; 39901), or 4 μ g of antibody against H3K27Ac (Active Motif; 39133) and H3K27me3 (Millipore; 07-449). Complexes were washed, eluted from the beads with SDS buffer, and subjected to RNase and proteinase K treatment. Crosslinks were reversed by incubation overnight at 65C, and ChIP DNA was purified by phenol-chloroform extraction and ethanol precipitation.

Quantitative PCR (qPCR) reactions were carried out by Active Motif in triplicate using SYBR Green Supermix (Bio-Rad; 170-8882) on a CFX Connect™ Real Time PCR system. The *SLFN11* primer pair targeting upstream of the first exon are as follows: forward 5'-CGAGCCAGAGTGGGATTTAAC-3' and reverse 5' TTTTCATATCACTAGCAGCGTGAC3'. The resulting signals were normalized for primer efficiency by carrying out qPCR for each primer pair using Input DNA (pooled unprecipitated DNA from cells or tissues). Test sites were run alongside the positive control sites targeted to the *ACTB* promoter (Active Motif; 71023) and *CCND2* gene (Active Motif; 71008) and a negative control primer pair that amplifies a region in a gene desert on chromosome 12 (Active Motif; 71001). Data are reported as "binding events per 1000 cells" which considers chromatin input, ChIP volumes and primer pair efficiencies.

Illumina sequencing libraries were prepared from the CHIP and Input DNAs by the standard consecutive enzymatic steps of end-polishing, dA-addition, and adaptor ligation. After a final PCR amplification step, the resulting DNA libraries were quantified and sequenced on Illumina's NextSeq 500 (75nt reads, single end). Reads were aligned to the human genome (hg19) using the BWA (Li and Durbin, 2009) algorithm (default settings). Duplicate reads were removed and only uniquely mapped reads (mapping quality ≥ 25) were used for further analysis. Alignments were extended *in silico* at their 3'-ends to a length of 200bp, which is the average genomic fragment length in the size-selected library, and assigned to 32nt bins along the genome. The resulting histograms (genomic "signal maps") were stored in bigWig files. CHIP target enriched regions were identified using the SICER (Zang et al., 2009) algorithm (FDR $1E^{-10}$, gap = 600bp). Drosophila genome spike-in was used to downsample and normalize tag counts for comparisons across treated and untreated samples (Active Motif; CHIP Normalization Strategy) (Orlando et al., 2014). For the spike-in adjusted analysis, the downscaling of H3K27me3 in the EPZ011989-treated samples was >5 -fold, compared to the vehicle controls. In addition, the resistant vehicle H3K27Ac data was downscaled by ~ 2.5 -fold as compared to all other samples. The EZH2 data was only normalized by <1.5 -fold across all samples based on the spike-in tag counts. All plots were generated using the R statistical computing environment

Statistics

Sample sizes per *in vivo* groups were at a minimum of 5 per condition, unless specified within the text for purposes of target analysis/pharmacodynamics. Power calculations and sample size estimates were not performed. Student's *t*-tests, one-way ANOVA, Pearson's correlation and log-rank tests were performed using GraphPad Prism version

6.00 for Mac, GraphPad Software, La Jolla California USA, www.graphpad.com. Where indicated, degrees of p -value significance are as follows: $<0.05^*$, $<0.005^{**}$, $<0.0005^{***}$, and $<0.0001^{****}$.

Results

Modeling acquired resistance in vivo

Patients with SCLC are typically treated with a regimen of up to 6 cycles of chemotherapy, each cycle consisting of cisplatin on day 1, and etoposide on days 1, 2, and 3, at near maximally tolerated doses. To study mechanisms that may govern acquired chemoresistance *in vivo*, we adopted an analogous approach of repeated chemotherapy cycles in tumor bearing animals in order to select populations of tumor cells that could effectively grow through chemotherapy (**Figure 5A**). We determined that we could safely administer 6-8 cycles of a schedule of cisplatin day 1 and etoposide days 1, 2, and 3 (C/E) on a weekly schedule in tumor-bearing NSG mice, achieving major tumor regression without dose-limiting toxicity. We applied this approach to ten independent PDX models of SCLC, the majority of which were derived from treatment-naïve patients (**Table 3**). We observed a spectrum of response across models, with 2/10 models achieving complete responses (complete regression of flank tumor), and 8/10 showing a broad index of partial responses, ranging from 65% to 95% tumor growth inhibition (**Figure 5B** and **Figures 6A-C**). To ensure that tumors progressing through multiple cycles of chemotherapy would develop intrinsic chemoresistance, these tumors were harvested, disaggregated, and re-implanted into a second generation of mice, and selected again through multiple cycles of chemotherapy (**Figure 5C**). To assess the extent of acquired chemoresistance, progressing tumors re-implanted in a third generation of mice were again randomized to chemotherapy or vehicle control arms. Comparing the chemonaïve to the chemoresistant state across all models, we observed a significant ($p=0.0008$) difference in the median survival time, defined herein as time to reach a volumetric endpoint of $1,000\text{mm}^3$ (**Figure 5D**). Further, we observed a clear

difference between the total cycles of C/E administered to naïve versus resistant models ($p=0.026^*$, **Figure 5E**); this was not due to a change in the time to randomization of these models (**Figure 5F**), or mitotic index as measured by Ki-67 staining (**Figure 5G**), but rather reflects the ability of the chemoresistant derivative tumors to grow through the selective pressure (**Figure 5C** and **Figure 6**).

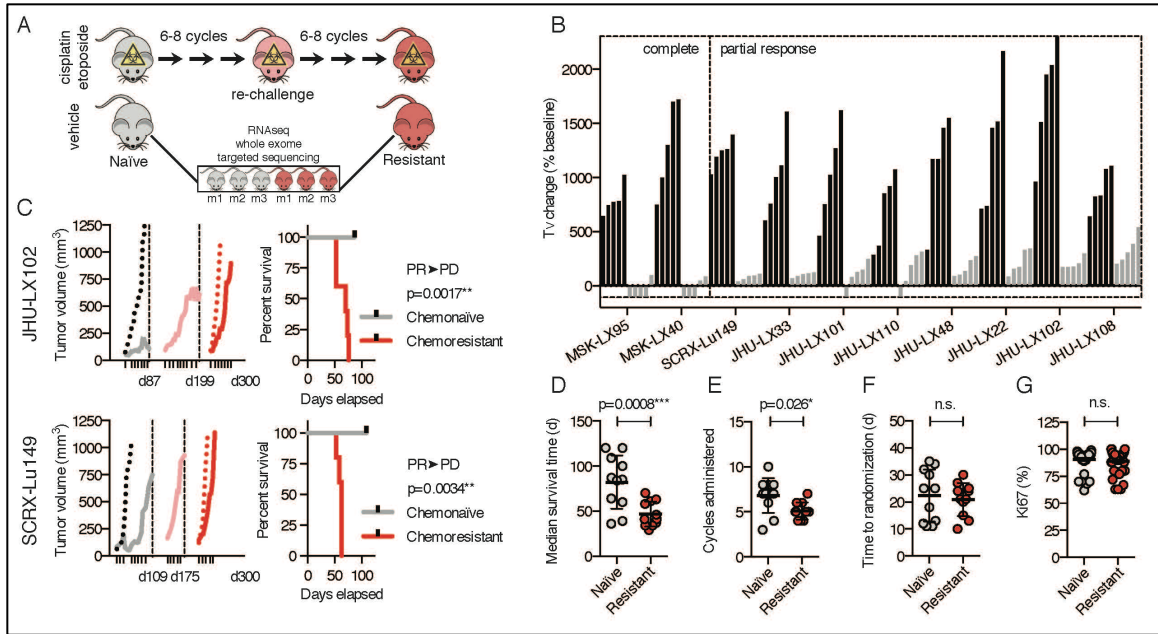


Figure 5. Modeling acquired resistance to standard of care chemotherapy in patient-derived xenograft (PDX) models of small cell lung cancer.

(A) Graphical depiction of model generation and workflow. Cohorts of 5 tumor-bearing animals were administered weekly cycles of cisplatin/etoposide (C/E) or vehicle, randomizing animals as tumor volumes approached 150mm³. Treatment continued weekly, as tolerated, for a total of 6-8 cycles. Surviving tumor cells were pooled and re-implanted into a secondary cohort of 5 animals to be challenged with C/E as before, enriching for a resistance phenotype. As tumors grew through treatment in the secondary cohort, tumor cells were pooled and re-implanted into a tertiary cohort of 10 animals, 5 to be challenged with C/E and 5 serving as vehicle controls. Vehicle-treated tumors in the primary (naïve) and tertiary (resistant) cohorts were compared using the indicated next generation sequencing approaches.

(B) Indices of observed responses to C/E across 10 SCLC PDX models. Comparisons per animals (5 per cohort) are shown as individual bars for vehicle (black) and C/E-treated (grey) at the last comparable day on study for both arms. Where the majority (≥ 3 of 5) of mice showed complete regressions of flank tumors, we considered these models complete responses, whereas all others with any measurable residual tumor mass were considered partial responses.

(C) Average tumor growth kinetics of representative PDX models JHU-LX102 and SCRXLu149 while on study. Average traces for tumor-bearing animals during the initial C/E challenge, vehicle (black dotted line) and treated (grey solid line). Vertical ticks along the x-axis indicate d1 of a weekly C/E cycle. Dashed vertical lines with corresponding x-axis values indicate the time on study treated tumors were collected, pooled and re-implanted into either secondary (pink solid line) or tertiary (red; vehicle-dotted, C/E-solid line) cohorts. Total time on study between primary and tertiary engraftments did not exceed 300d for any model. Survival events for each model are reported as the time to reach 1000mm³ in volume, or where a volumetric endpoint was not obtained, the last day on study prior to re-implantation (censored point). Statistical comparisons between survival of chemo-naïve and chemo-resistant cohorts were

performed using a log-rank (Mantle-Cox) test. Model chemosensitivity conversion status is indicated above p-value; CR=complete response, PR=partial response, PD=progressive disease, SD=stable disease, NR=no response. See Figure 6 A-C for more details

(D) Median survival time in days for chemonaïve and chemoresistant settings. Median survival times were calculated from survival curves of treated chemonaïve (naïve-grey) or chemoresistant (resistant-red) cohorts. *P*-values are reported for paired *t*-tests for all naïve versus resistant comparisons.

(E) Cycle of C/E administered to the chemonaïve and chemoresistant cohorts.

(F) Time to randomization (e.g. time post-engraftment to treatment) in the chemonaïve and chemoresistant settings.

(G). Ki67 IHC positivity of tumors in the chemonaïve and chemoresistant setting. Three independent tumor cores were evaluated per model, per setting. The pathologist scoring staining intensity was blinded to sample identification.

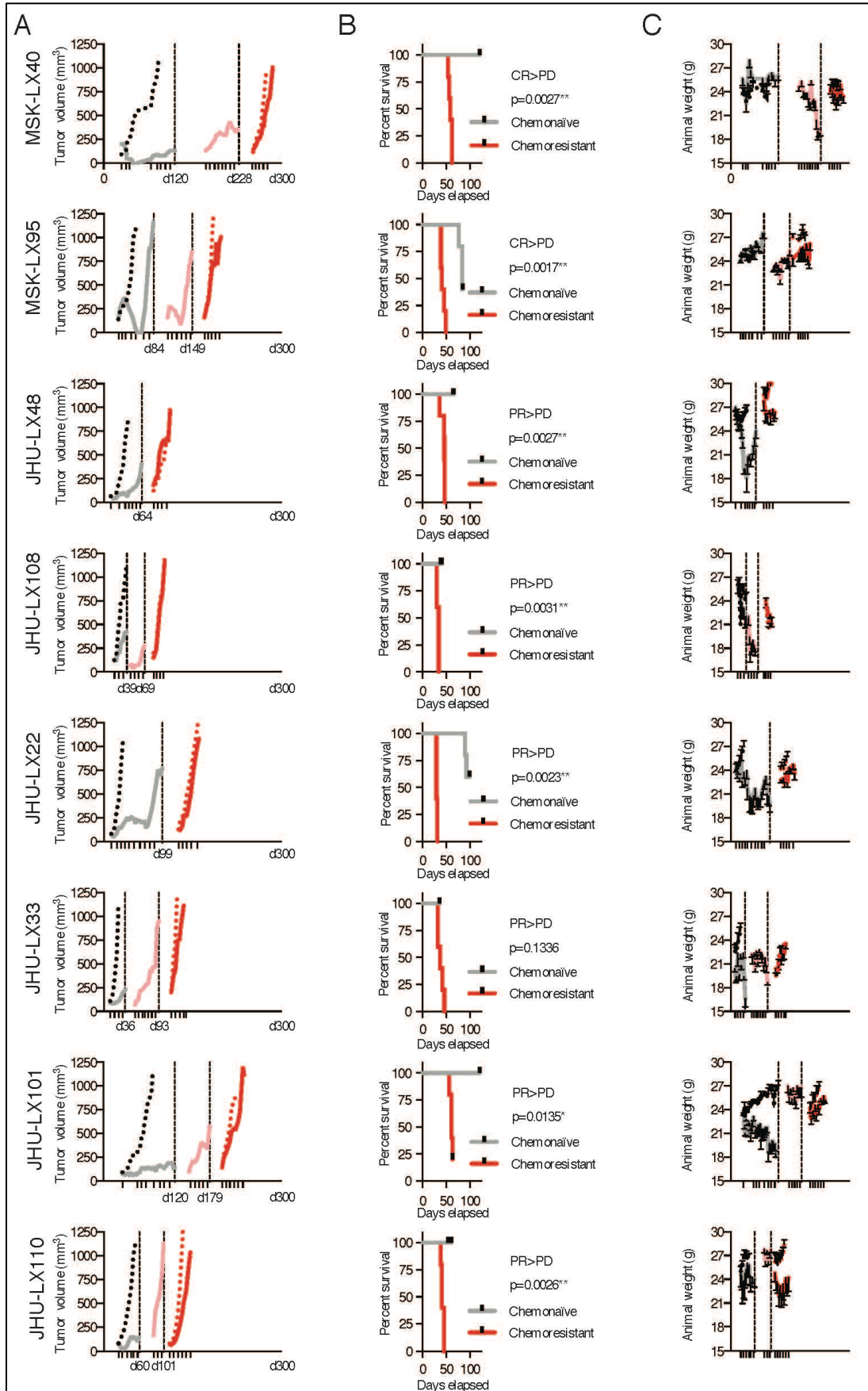


Figure 6. Complete response criteria of remaining 8 of 10 PDX models.

(A) Average tumor volume trace curves for all ten models included in study. Five animals per treatment group, per PDX model. JHU-LX102 and SCRX-Lu149 were included in Figure 1C, thus are omitted in these data.

(B) Survival for chemo-naïve and chemoresistant versions of models on C/E treatment. Model chemosensitivity conversion status (>) indicated above *p*-values for Log-rank (Mantle-Cox) tests; CR=complete response, PR=partial response, PD=progressive disease, SD=stable disease, NR=no response

(C) Animal weight on study. Data are reported as averages +/- SEM.

Acquired chemoresistance is not associated with emergence of novel, recurrent mutations

We hypothesized that the development of acquired resistance to chemotherapy in these models could be caused by changes in their genetic landscapes. To investigate this possibility, we performed whole exome sequencing in 8 paired models. We first confirmed by examining more than 1,000 common single nucleotide polymorphisms (SNPs) that the acquired resistance models were from the same individuals as the parental models and did not arise from cross-contamination with other cell lines, PDX, or spontaneous murine malignancies (**Figure 7A**). In all cases, >90% of bases could be called based on a read depth of ≥ 15 (**Figure 7B**). We observed the expected pattern of genetic alterations consistent with SCLC, including frequent alterations in *TP53* and *RB1* (**Figure 8A**), as well as frequent mutations in CREB binding protein (*CREBBP*). Importantly, in each case the key genetic alterations identified in the chemonaïve model were maintained through acquisition of chemoresistance. We next sought to determine to what extent the total mutational burden was shared between the chemonaïve and chemoresistant models. In all cases, a majority of called mutations were shared, while only a minority of mutations was private to either the chemonaïve or chemoresistant setting (**Figure 7B**). The number of private mutations was consistently greater in the chemoresistant setting, suggesting that additional mutations were acquired during treatment. However, we were not able to identify recurrent acquired mutations across independent tumor models: no putative causal mutations of acquired resistance were found, leading us to conclude that private mutations in the chemoresistant setting are passengers, not directly driving resistance (**Figure 7C**). Consistent with apparent stability of key mutations, we found copy number alterations to be concordant between chemonaïve and chemoresistant models and failed to identify any significant focal copy

number alterations (**Figure 8C**). Without clear evidence of a genetic basis for the chemoresistance phenotype, we chose to focus subsequent analyses on potential epigenetic mechanisms of acquired chemoresistance.

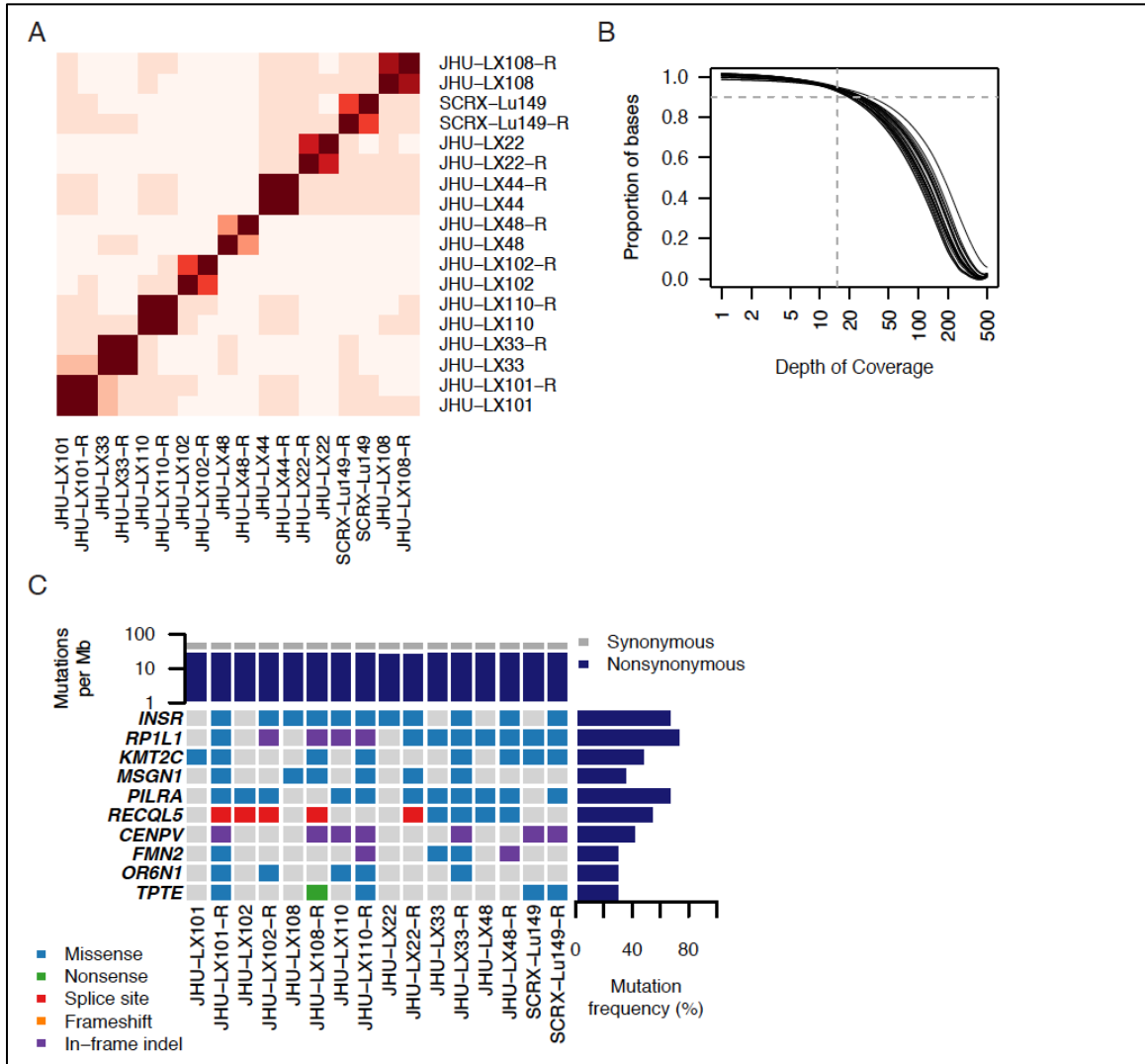


Figure 7. Credentialing exome sequencing data from paired PDX models.

(A) Concordance of genotypes for >1,000 common SNPs confirm that sample identity was maintained throughout the experiment.

(B) The proportion of bases in the exome capture region covered to a given depth. The intersection of the horizontal (90%) and the vertical lines (15) indicate that for all samples >90% of bases were covered to the minimum depth for mutation calling using MuTect2.

(C) A mutation plot indicating the most common mutations occurring in the chemoresistant setting.

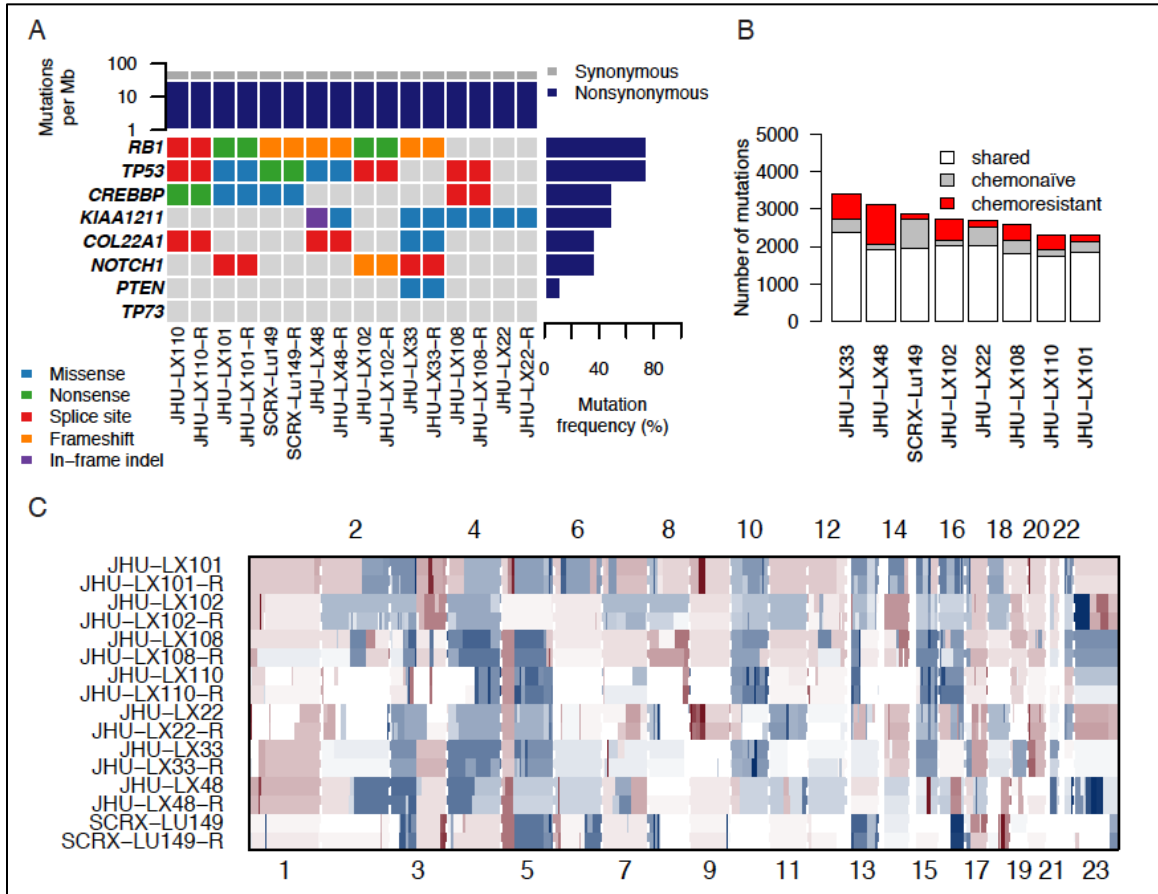


Figure 8. Genomic characterization of paired chemo-naïve and chemo-resistant SCLC PDX models

(A) Mutational analysis of paired naïve and resistant PDX models by whole exome sequencing. Shown are identifiable mutations by class with respect to several of the most frequently mutated genes in primary SCLC (George et al., 2015). Top panel shows mutation density per Mb of mapped reads. Right panel shows frequency of mutations for each gene in the cohort.

(B) Private versus shared mutations between paired naïve and resistant PDX models by whole exome sequencing. Colors indicate mutations called as unique to the naïve (grey) or resistant (red) tumor, with shared mutations in white.

(C) Copy number variation in somatic chromosomes for paired chemo-naïve and chemo-resistant models.

SLFN11 suppression and *TWIST1* induction characterize distinct subsets of chemoresistant disease

We hypothesized that there could be epigenetically driven recurrent changes in gene expression in the setting of acquired chemoresistance. To pursue this hypothesis, we performed RNA-sequencing (RNAseq) on 3 biological replicates for each of the 10 paired models. Principal component analysis suggested that gene expression patterns were remarkably consistent between the chemonaïve and chemoresistant setting and could easily discriminate between PDX models derived from different patients (**Figure 9A** and **Figure 10A**). Due to the high degree of similarity between paired models, we hypothesized that changes in the expression of a minority of genes, as opposed to broad transcriptional changes, could drive the chemoresistance phenotype we observed. We therefore performed differential gene expression analysis on all paired samples to identify significantly differentially expressed genes. To identify recurrently differentially expressed genes, we generated a meta *p*-value for each gene based on the degree of differential expression in each of the individual models. The empirical cumulative distribution function (ECDF) of the *p*-value of each gene was then plotted, highlighting the top 10 genes significantly differentially expressed in at least 3 independent models (**Figure 9B**). Schlafen family member 11 (*SLFN11*), a gene that we and others (Barretina et al., 2012; Lok et al., 2016; Sousa et al., 2015; Stewart et al., 2014; Tang et al., 2015; Zoppoli et al., 2012) have reported as being critical to sensitivity to DNA damaging agents, was among the most significantly down-regulated genes. Cancer-testis antigens, a family of genes that are highly sensitive to epigenetic perturbation (De Smet et al., 1999), were significantly up-regulated, as well as twist family bHLH transcription factor 1 (*TWIST1*), a gene previously described to play an important role in acquired resistance to a variety of chemotherapies *in vivo* (Fischer et al., 2015; Zheng et

al., 2015). In addition to its role in therapeutic resistance, *TWIST1* is also a well-known mediator of epithelial-mesenchymal transition (EMT), metastasis, and stemness (Beck et al., 2015; Schmidt et al., 2015; Yang et al., 2004; Yang et al., 2012) (**Figures 9C-E**). The potential mechanisms identified are mutually exclusive and together are represented in 7 of 10 chemoresistance models.

We extended these results by modeling acquired resistance to C/E in murine models of SCLC (mSCLC), including two cell lines (*Rb1/Trp53* null, DKO and *Rb1/p130/Trp53* null, TKO) previously generated by others (Jahchan et al., 2013; Park et al., 2011b) and one chemonaïve allograft directly isolated from a tumor and passaged exclusively in NSG mice (*Rb1/p130/Trp53* null, TKO-A). Robust *in vitro* acquired resistance to etoposide was associated with a strong change in phenotype, converting from primarily suspension, floating spheroid cultures to exclusively adherent culture (**Figure 10B**). *In vivo*, acquired resistance to the same schedule to C/E used in PDXs was strongly associated with a decrease in survival of hind flank tumor bearing animals on treatment when comparing the naïve to the resistant models ($p=0.0026$, **Figures 10C-E**). Principal component and differential gene expression analysis suggested conserved EMT-like changes in all three models tested, with the first principal component strongly separating parental and resistant versions of the models (**Figures 8F-H**).

Given the consistent up-regulation of *TWIST1* in both human and mouse models of SCLC upon acquired resistance, we assessed whether directly gaining or losing *TWIST1* could affect chemosensitivity in both model systems. We infected the parental and resistant versions of the allograft *ex vivo* with lentiviruses expressing doxycycline-inducible murine *Twist1* constructs and generated stable cell lines in culture. Notably, conditional gain of wild type or the DNA-binding mutant K145E of mouse *Twist1* (Maia et

al., 2012) did not robustly change the sensitivity to etoposide, in contrast to the shift we observed *ex vivo* between the naïve and resistant allograft lines (IC₅₀ naïve TKO-A ~0.15µM, versus IC₅₀ resistant TKO-AR ~3.0µM; **Figure 10I**). Moreover, conditional suppression of *Twist1* by shRNA could neither rescue chemosensitivity in mouse or TWIST1^{High} human SCLC cell lines or influence other features of EMT observed in the resistant mSCLC cell lines, such as down regulation of E-cadherin (**Figures 10J,K**). Taken together, these results suggest that while increases in TWIST1 may be associated with acquired resistance to cytotoxic therapy in multiple models of SCLC, this gene does not appear to directly promote the acquired resistance observed in our models.

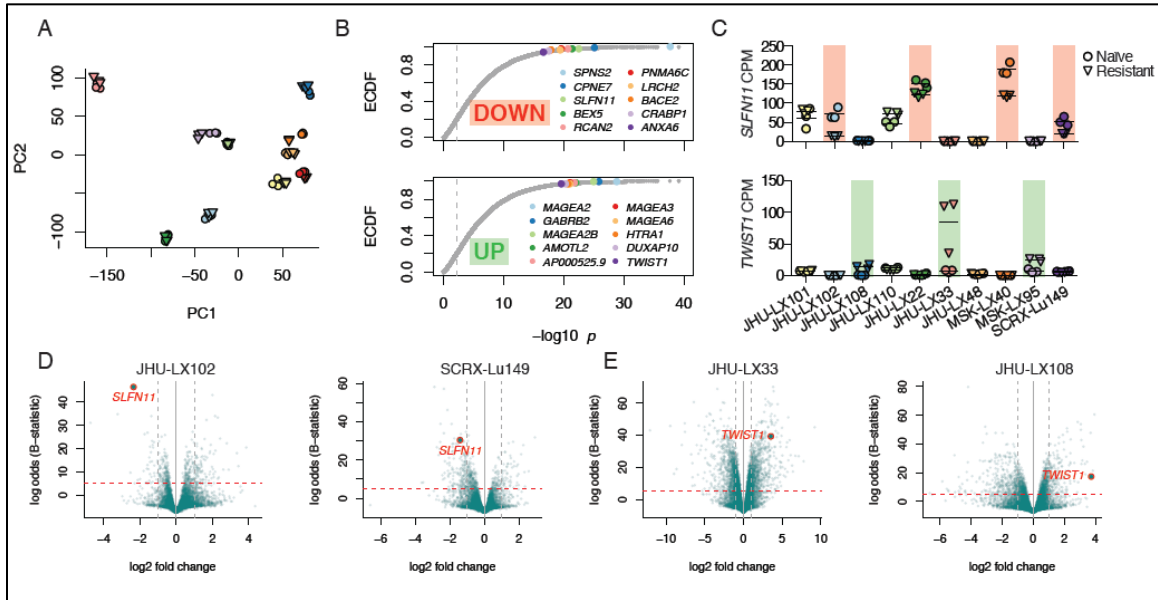


Figure 9. Paired RNA sequencing identifies conserved changes *SLFN11* and *TWIST1* across multiple models.

(A) Principal Component Analysis (PCA) of RNA sequencing (RNAseq) data from chemonaïve (circles) and chemoresistant (downward triangles) replicate samples from the 10 paired PDX models included in this study. For color legend, see Figure 6C or Figure 7A.

(B) Empirical cumulative distribution function (ECDF) of combined p -values of differentially down- or up-regulated genes. The top ten significantly down-regulated (top panel) or up-regulated (bottom panel) genes that occur in at least 3 of 10 models with a \log_2 change >1.5 -fold are highlighted.

(C) Individual gene expression changes in each model for *SLFN11* (top panel) and *TWIST1* (bottom panel) by RNAseq. Models with down-regulated *SLFN11* and up-regulated *TWIST1* are indicated by red and green backlighting, respectively.

(D) Volcano plots demonstrating down-regulation of *SLFN11* in the chemoresistant setting, JHU-LX102 (left) and SCR-X-Lu149 (right)

(E) Volcano plots demonstrating up-regulation of *TWIST1* in the resistant setting, JHU-LX33 (left) and JHU-LX108 (right).

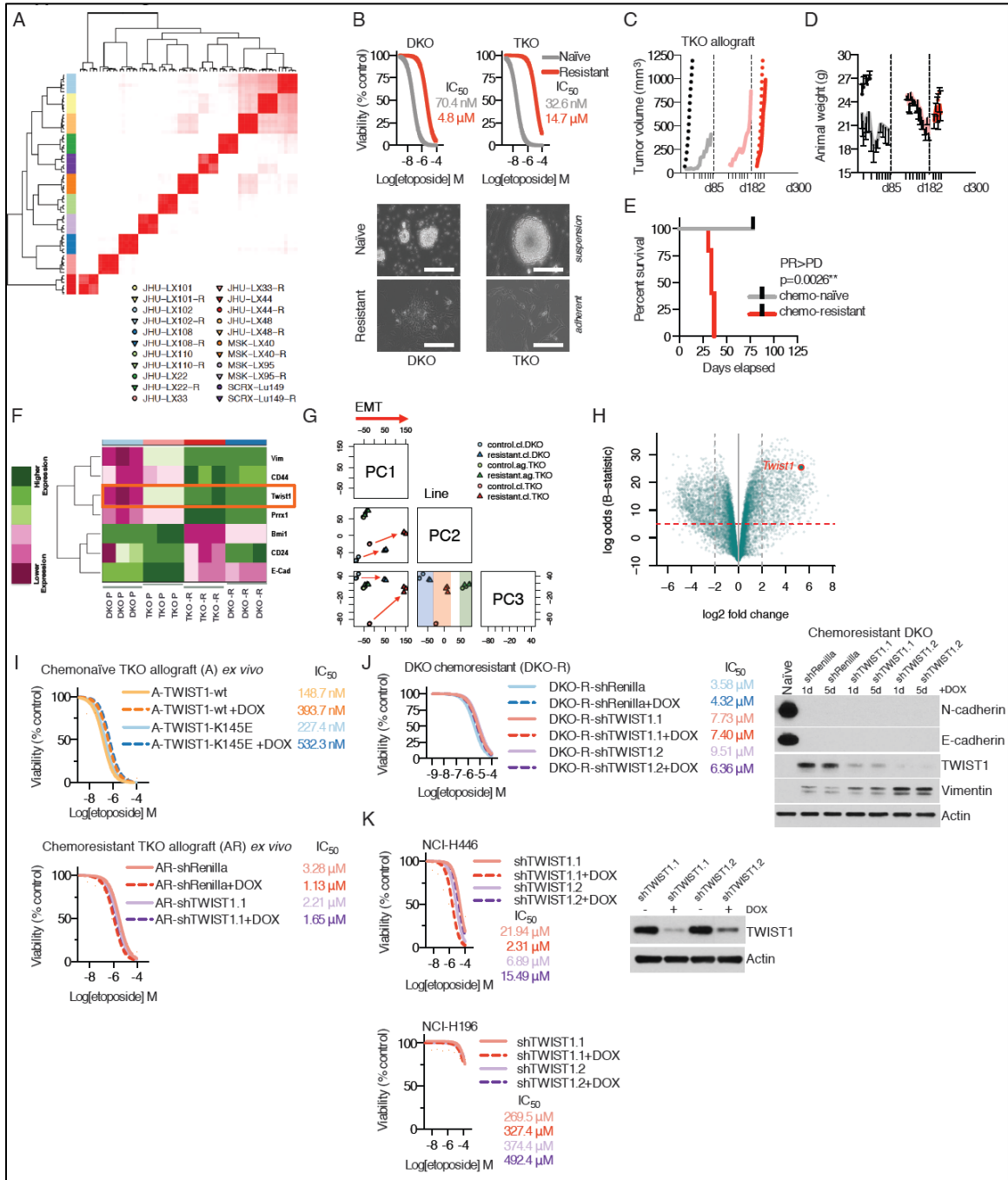


Figure 10. TWIST1 is recurrently up regulated in the chemoresistant setting but does not drive acquired resistance to cisplatin/etoposide in SCLC.

(A) Hierarchical clustering of correlation coefficients of RNAseq data from triplicates of chemonaïve and chemoresistant paired PDX samples. Samples clearly cluster by model. (B) Shift in etoposide sensitivity from *in vitro* acquired resistance modeling in DKO and TKO mSCLC cell lines. Change in morphologic appearance and culture conditions of chemonaïve (suspension/spheroid) and chemoresistant (adherent) cell lines Images

collected using 40x objective lens; scale bar 200 μ m. Experimental results are shown for 72hrs post-dose of etoposide.

(C) Average tumor volume progression plot for TKO allograft mSCLC model, when engrafted as a hind flank tumor – naïve-vehicle (black dotted line), naïve-C/E (grey solid line), C/E re-challenge (pink solid line), resistant-vehicle (red dotted line), resistant-C/E (red solid line). Points of re-transplant are indicated along the x-axis with vertical dashed lines. Day 1 of C/E cycles are indicated as vertical ticks along the x-axis.

(D) Average animal (n=5 per group) weights on study reported in grams +/- SEM

(E) Survival of naïve versus resistant C/E-treated cohorts of mSCLC TKO allograft (TKO-A) models. Model conversion from partial response (PR) to progressive disease (PD) indicated in margin. Difference in survival reported as a p-value from log-rank (Mantle-Cox) test.

(F) Relative expression for select genes involved in EMT between naïve or parental (P) and resistant (R) cell lines, calling out *Twist1* (red circle).

(G) Principal component analysis for naïve and resistant versions of mSCLC models broken down by component. The first component of epithelial-mesenchymal transition (EMT) strongly separates model, with the second component separating parental and resistant cell lines, but to a lesser extent the allograft. Legend colors and shapes shown for cell lines (cl) and allograft (ag).

(H) Volcano plot for differential gene expression across all mSCLC paired naïve/parental as compared to resistant models (*pooled analysis*). *TWIST1* called out in red.

(I) Conditional gain of TWIST1 or the K145E DNA-binding mutant of TWIST1 in the naïve setting or conditional suppression of TWIST1 in the resistant setting of the TKO allograft model does not change *ex vivo* sensitivity to etoposide. *Ex vivo* resistance did not separate as strongly as *in vitro* resistance (compare 7B or 7L IC₅₀ values), but nonetheless produced > 1 log difference in IC₅₀ to etoposide (LogEC₅₀; one-way ANOVA $p < 0.0001$). Doxycycline (1 μ g/mL) was added to the culture media every other day for 5d before plating for experiments. Experimental results are shown for 72hrs post-dose of etoposide.

(J) Conditional suppression of TWIST1 in the resistant DKO cell lines (DKO-R) does not change sensitivity to etoposide. Experimental results are shown for 72hrs post-dose of etoposide. Conditional suppression of TWIST1 does not rescue EMT-associated changes in E-cadherin, N-cadherin or vimentin expression. Shown are western blot results for resistant DKO cells on doxycycline (1 μ g/mL) for 1d or 5d.

(K) Conditional suppression of TWIST1 in the TWIST1^{High} human SCLC cell lines NCI-H446 and NCI-H196 does not change sensitivity to etoposide. Doxycycline (1 μ g/mL) was added to the culture media every other day for 5d before plating for experiments. Experimental results are shown for 72hrs post-dose of etoposide. Both shRNAs tested against human TWIST1 show modest suppression at 72hrs after a single dose (1 μ g/mL) of doxycycline in NCI-H446.

SLFN11 expression is decreased in cell lines and clinical samples from previously treated patients

We further interrogated the role of *SLFN11* in the context of acquired chemoresistance, as it had been previously implicated as a factor regulating DNA damage repair (Mu et al., 2016), was shown to correlate with responses to DNA damaging agents in cell lines (Barretina et al., 2012; Sousa et al., 2015) and patients (Tang et al., 2015), and may have unique biology in human cancer as there is no murine ortholog (Li et al., 2012). To further test the relevance of our model system, we assessed whether the observed suppression of *SLFN11* from *in vivo*-selected chemoresistant PDXs was reflected in cell lines and tumors derived from previously treated versus untreated patients. *SLFN11* is bi-modally expressed when examined across cancer cell lines within the CCLE, as well as within SCLC in both primary tumor (Lok et al., 2016) and cell line samples (**Figure 11A**). Many SCLC cell lines have been established and annotated with regards to their primary source (Carney et al., 1985). If suppression of *SLFN11* is associated with chemoresistance, we might expect cell lines generated from treated patients to have lower levels of *SLFN11* expression relative to cell lines generated from patients that were untreated. Indeed, we observed this difference ($p=0.031$; **Figure 11B**), which also held true when comparing all chemonaïve PDX models with all derivative chemoresistant models ($p=0.003$; **Figure 11C**). We observed similar results when examining *SLFN11* protein expression by IHC using an H-score as the comparative metric, including either all models or only model with detectable *SLFN11* at baseline (**Figures 12D,E**). In 2 models where chemoresistance was associated with a substantial decrease in *SLFN11* expression by immunohistochemistry (**Figure 11F**), we confirmed quantitative decreases in *SLFN11* expression at both the transcript level by RNAseq and protein level by quantitative Western blotting (**Figure 11G & Figures 12A-**

C). Interestingly, an endpoint analysis of the vehicle and C/E treatment groups of both the chemo-naïve and chemoresistant cohorts in one model revealed a rapid decrease in SLFN11 protein expression in progressing tumors ($p=0.029$; **Figure 12D**).

To assess whether SLFN11 expression was correlated with clinical response to C/E in patients with SCLC, SLFN11 immunohistochemistry was performed on clinically annotated tumor microarrays including both untreated (Vanderbilt Medical Center; VMC) and previously treated (Case Western Reserve University; CWRU) SCLC patients, with H-scores for each intact core determined by a pathologist blinded to the sample identity/source (**Figure 11H**). Immunostaining for SLFN11 was low to nearly absent in lung squamous cell carcinoma and adenocarcinoma in contrast to SCLC (**Figure 11I**). SLFN11 expression was modestly associated with stage of disease when viewed in aggregate, with SLFN11 intensity being greater in limited stage versus extensive stage patients ($p=0.0397$; **Figure 11J**). Consistent with a role in determining chemosensitivity, among all treated patients, SLFN11 expression was higher in tumors from patients who responded to therapy, versus those who did not ($p=0.0192$; **Figure 11K**). When evaluating SLFN11 as a pretreatment predictor of response in untreated patients (**Figure 11L**) and as a post-treatment correlate of response (**Figure 11M**), we found that SLFN11 expression was greater in patients categorized as treatment responsive; however, the test was underpowered to demonstrate a statistically significant difference in these subsets. Notably, among untreated patients, 83% (10/12) of patients with a SLFN11 H-score >75 responded to treatment: using the same threshold among previously treated patients, all 6 patients with an H-score >75 responded to treatment. Applying a dichotomized H-score of 68.8 using Youden's index (Youden, 1950) demonstrated greater overall response rate (ORR) in patients with an H-score >68.8 ($p=0.023$, Fisher's exact test), but did not show a difference in overall survival ($p=0.884$,

Log-rank test; **Figure 12E**). Taken together, these data suggest that high SLFN11 expression in SCLC confers greater sensitivity to chemotherapy, but does not confer an overall survival benefit in this clinical cohort.

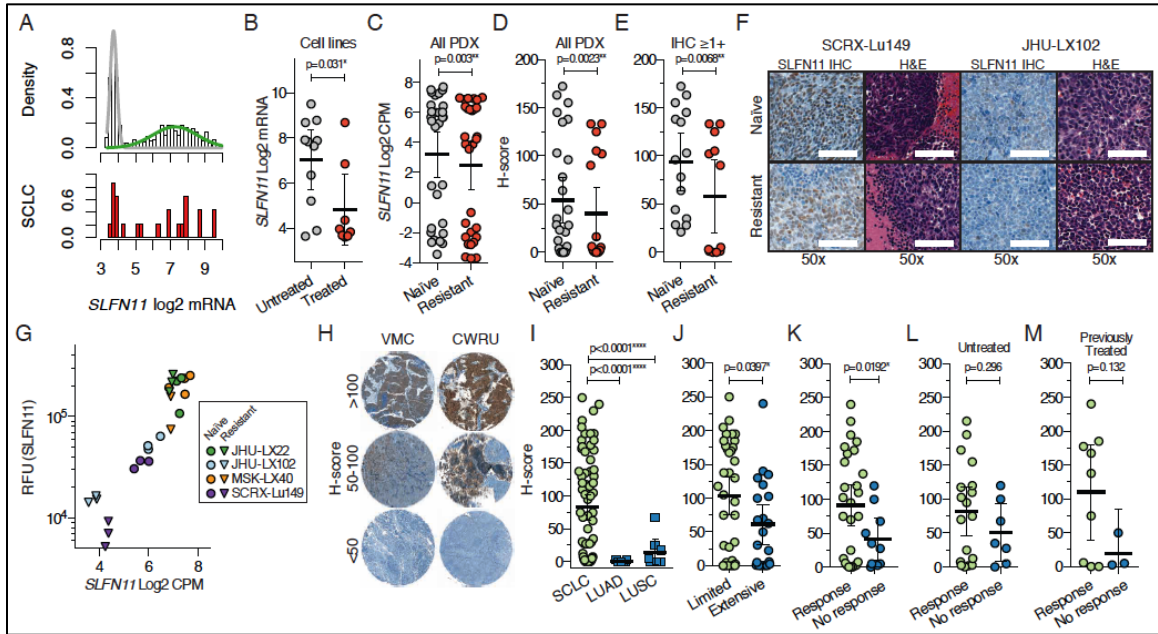


Figure 11. SLFN11 is down regulated at the transcript and protein level in SCLC following exposure to chemotherapy.

(A) *SLFN11* gene expression across the CCLE dataset as compared to SCLC cell lines. Cell lines within the CCLE are shown as density distributions of those that express little to no *SLFN11* (grey distribution) versus the broad distribution of *SLFN11* levels in other lines (green distribution). SCLC cell lines are shown in red (lower panel).

(B) Comparison of *SLFN11* expression in SCLC cell lines derived from patients that had never been treated or who had received at least one prior therapy before the sample for cell line generation was collected (Polley et al., 2016) ($p=.031$, Fisher's exact test).

(C) *SLFN11* gene expression compared between all chemonaïve and chemoresistant PDX models. Three independent samples per model, per condition are plotted. P -values shown for two-tailed paired Student's t -test.

(D) *SLFN11* IHC scoring metric (H-score) compared between all chemonaïve and chemoresistant PDX models. Three independent core samples per model, per condition are plotted. Exact p -values are reported from a Mann-Whitney test for PDX *SLFN11* IHC staining comparisons.

(E) H-score comparison including only models with detectable *SLFN11* IHC reactivity at baseline (IHC positivity $\geq 1+$ and at least one of three core samples with an H-score >20)

(F) Representative *SLFN11* IHC and H&E stained tumors for two models (SCRXLu149 and JHULX102) demonstrating strong reduction in *SLFN11* expression in the chemoresistant, relative to the chemonaïve, setting. All images shown are at 50x resolution of cores punches from constructed TMAs. Scale bars 100 μ m.

(G) Concordance between *SLFN11* gene expression by RNAseq and *SLFN11* protein expression by actin-normalized quantitative Western blot. Symbols are color-coded by model and plotting symbols represent the in the chemonaïve (circles) or chemoresistant (downward triangle) setting.

(H) Representative IHC staining for SLFN11 in two independent, clinically-annotated SCLC TMAs. VMC=Vanderbilt Medical Center, CWRU=Case Western Reserve University.

(I) SLFN11 expression by IHC in SCLC as compared to lung adenocarcinoma (LUAD) and squamous cell carcinoma (LUSC). 60/215 untreated VMC and 12/22 previously treated CWRU cores were evaluable for analysis and pooled for comparison. Primary and metastatic samples were included. *P*-values shown for unpaired two-tailed *t*-tests.

(J) Comparison of SLFN11 H-score by clinical stage of patient from pooled analysis of VMC and CWRU TMAs.

(K) Comparison of SLFN11 H-score by clinical response of patients from both cohorts. Responses include CR and PR, where no response includes PD and SD.

(L) Comparison of SLFN11 H-score by clinical response of patients from untreated cohort; *p*-value not significant.

(M) Comparison of SLFN11 H-score by clinical response of patients from previously treated cohort; *p*-value not significant.

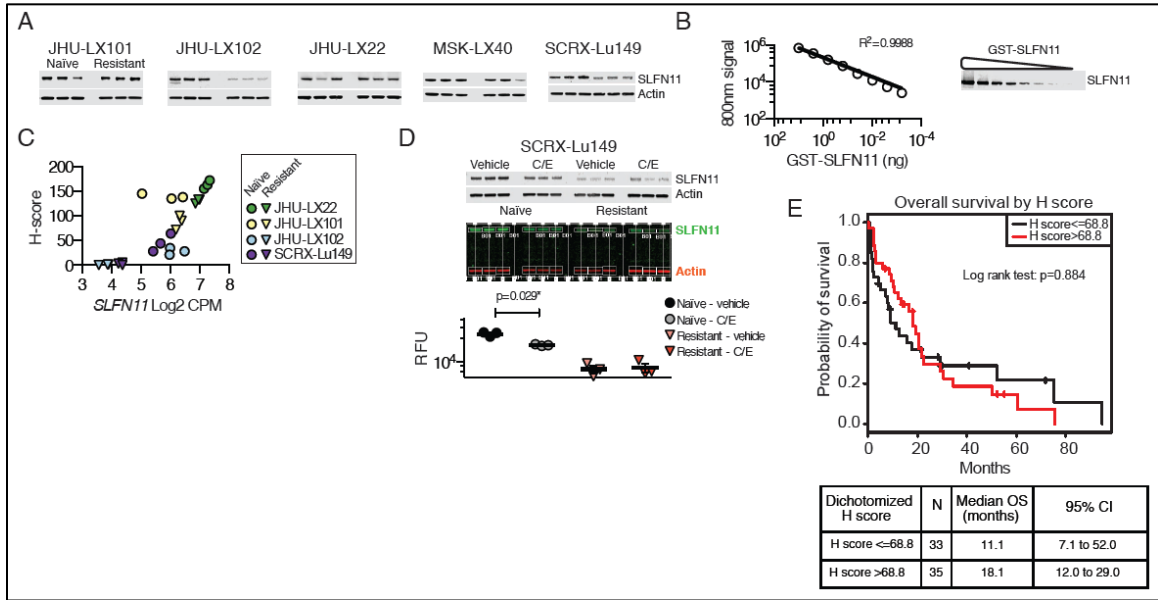


Figure 12. SLFN11 is rapidly down regulated *in vivo* and expression by IHC H score does not correlate with survival.

(A) Western blot images from triplicate chemo-naïve and resistant PDX tumor samples used for calculating data included in Figure 9, normalizing SLFN11 signal (800nm channel) to actin (700nm channel).

(B) Standard curve for detection of recombinant SLFN11 establishes conservative upper (ULD) and lower limits of detection (LLD) in pure versus crude experimental samples under the assumption <1:10,000-fold natural abundance in RIPA-extracted proteomes; GST-SLFN11 ULD was ~10ng, whereas the LLD was ~10pg with an R^2 value of 0.9988.

(C) RNAseq versus SLFN11 H-score for available PDX naïve and resistant tumors. Paired triplicates are color-coded in the naïve (*circles*) or resistant (*downward triangle*) and correspond to the color grid used above.

(D) Example of LI-COR image readout for triplicate tumors from vehicle or C/E-treated arms of chemo-naïve or resistant SCR-X-Lu149 model in color and gray scale. 800nm channel for SLFN11 signal in green; 700nm channel for actin in red. Relative near-infrared fluorescence units (RFU; abbreviation used hereon within text, unless normalized in time course samples) as a function on time on treatment in PDX model SCR-X-Lu149. *P*-values shown for paired *t*-tests.

(E) Survival of SCLC by dichotomized H-score. The best cutoff of H score for predicting ORR is 68.8 based on maximizing the Youden's J index ($J = \text{sensitivity} + \text{specificity} - 1$). H score is then dichotomized at >68.8 and associated with OS. Table below shows usable clinical cases from H-score on TMAs analyzed in aggregate.

EZH2 inhibition restores SLFN11 expression and chemosensitivity in vitro

A recent report suggested that *SLFN11* expression is partly regulated by an epigenetic silencing mechanism, which could be reversed by broad DNA methylation inhibitors such as 5-Azacytidine (5-Aza) (Nogales et al., 2016). We chose to examine whether EZH2 (*Enhancer of zeste homology 2*) could have a similar role in silencing *SLFN11* in SCLC for several reasons: 1) there is evidence for an EZH2 binding site upstream of the first exon of *SLFN11* from human cell line data reported by the ENCODE project (Gerstein et al., 2012; Wang et al., 2013), 2) our group has shown *EZH2* levels to be higher in SCLC than in any of the tumor types included in TCGA, with expression correlating with high level promoter methylation patterns in SCLC (Poirier et al., 2015), and 3) other groups have shown that PRC2 target gene repression correlates with shorter survival in primary SCLC (Sato et al., 2013). Overall, these lines of evidence prompted us to examine whether chemical inhibitors targeting DNA or histone methyltransferase enzymes, specifically DNMTs and EZH2, could play a role in regulating *SLFN11* expression.

Using short term *ex vivo* culture, we exposed chemonaïve and chemoresistant versions of select PDX models that had demonstrated the most striking down-regulation of *SLFN11* in the chemoresistant setting to 1 μ M of either 5-Aza or the EZH2 inhibitor EPZ011989 (abbreviated EPZ in Figures). After 7 days of continuous daily exposure, we noted striking increases in *SLFN11* expression in the EPZ011989-treated cells versus DMSO-treated controls, whereas 5-Aza treatment appeared to have minimal effect, suggesting that *SLFN11* expression may be regulated at the level of histone methylation, rather than DNA methylation, in SCLC (**Figure 13A**). Moreover, treatment with EPZ011989, but not 5-Aza, effectively restored *ex vivo* etoposide sensitivity of the chemoresistant model to that of the chemonaïve model (IC_{50} reduced from 4.65 μ M to

0.59 μ M in chemoresistant versus 0.51 μ M in chemonaïve; **Figures 13B,C**). We next interrogated the kinetics of SLFN11 re-expression in the SCLC cell line NCI-H82, which was derived from a previously treated patient and shows minimal expression of SLFN11 protein. We monitored the re-expression of SLFN11 over a 21d period in suspension culture, during which time cells were treated daily with 1 μ M EPZ011989 for 10d and then cultured in fresh media without compound for an additional 10d to monitor target dynamics. We noted striking re-expression of SLFN11 after ~7-10d of drug exposure, with concomitant suppression of H3K27me2/3, consistent with on-target activity of EPZ011989 inhibiting EZH2's repressive methylation in a global fashion (**Figure 13D**). Re-expression of SLFN11 was dose-dependent and stable under acute DNA damage (**Figure 14A**). This re-expression was sustained even as global H3K27me2/3 levels returned to baseline levels during a 10d washout period. In 7d treatment assays, we noted a dramatic increase in SLFN11 protein expression in cell lines with little to no detectable SLFN11 at baseline. This was in contrast to cell lines with high *de novo* expression of SLFN11, such as NCI-H526, in which no further increase above baseline was observed, suggesting a threshold effect (**Figure 13E**). The extent to which SLFN11 protein levels were increased by EPZ011989 was strongly correlated to an increase in topotecan sensitivity across all cell lines tested (Pearson $r=0.916$; **Figure 13F & Figure 14B**). SLFN11 protein re-expression was suppressible with shRNAs targeting *SLFN11* and was observed with another distinct EZH2 inhibitor, although EPZ011989 did show greater potency for SLFN11 re-expression when compared to another EZH2 chemical inhibitor GSK126 (McCabe et al., 2012) (**Figures 14C,D**).

A shift in global repressive histone methylation will have pleiotropic effects on gene expression that manifest in a cell line specific manner (Jadhav et al., 2016). To directly address whether re-expression of SLFN11 was sufficient to sensitize SCLC cell

lines with low levels of SLFN11 to DNA damaging agents, such as topotecan, an agent approved for recurrent SCLC, we used a doxycycline-inducible expression vector to express SLFN11 or an empty vector control in NCI-H82 and NCI-H446. Both of these cell lines were derived from previously treated patients and are highly resistant to etoposide. Exogenous expression of SLFN11 was capable of sensitizing these cell lines to topotecan, relative to non-induced or empty vector controls, although this effect was less pronounced than that of the EPZ011989-mediated sensitization (**Figure 13G**). Consistent with this observation, shRNA-mediated suppression of *SLFN11* in NCI-H526, a cell line with high baseline SLFN11 expression, modestly decreased sensitivity of this line to topotecan, although we note that complete suppression of SLFN11 was not possible even with a highly potent shRNA (**Figure 14E**). Remarkably, while EPZ011989-treatment shifted the sensitivity of this cell line to topotecan by approximately one log, this shift was mostly reversed by concurrent shRNA suppression of SLFN11. While we did not note changes in markers of acute DNA damage response (γ H2A.X), we found that EPZ011989-treated cells showed increased markers of programmed cell death (cleaved-PARP), that were suppressed when co-targeting SLFN11 by shRNA. Taken together, these data strongly implicate SLFN11 as a determining factor in sensitivity to DNA damaging agents in SCLC (**Figure 13I**).

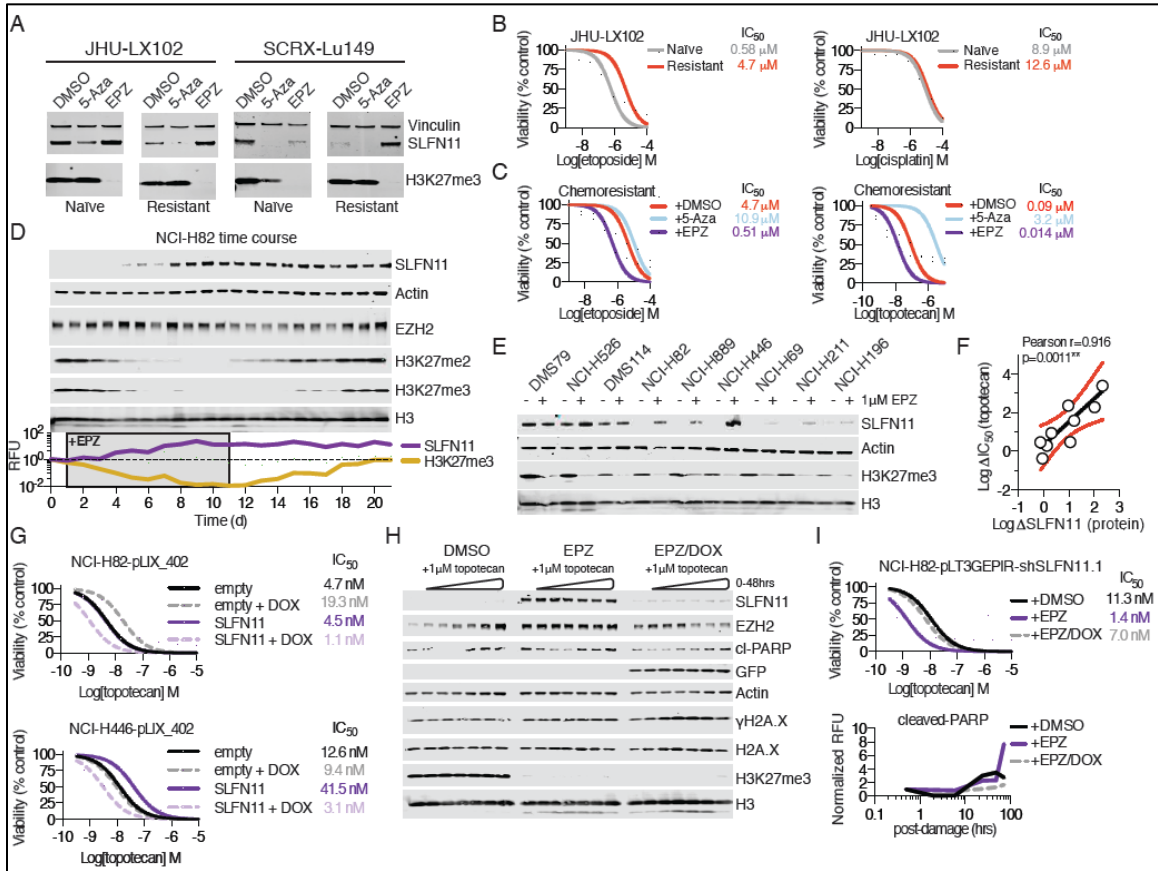


Figure 13. Chemical EZH2 inhibition rescues SLFN11 expression and sensitizes SCLC to DNA damage.

(A) Chemical inhibition of EZH2 rescues SLFN11 expression in chemoresistant PDX models *ex vivo*. Chemonaïve and chemoresistant PDX models JHU-LX102 and SCRX-Lu149 were cultured *ex vivo* for 7d and treated daily with 1 μ M of 5-azacitidine (5-Aza) or EZP011989 (EPZ) and then assayed for expression of SLFN11 by Western blot.

(B) *Ex vivo* differences in sensitivity to etoposide and cisplatin in chemonaïve and chemoresistant (acquired *in vivo*) versions of JHU-LX102. IC₅₀ values are colored accordingly throughout panels. Data traces are shown as normalized responses of nonlinear fits; data points and error bars removed for clarity of comparisons. n=4 data points per dose from 8-point dose series. All *ex vivo* experiments were in culture (*ex vivo*) for no more than 3 weeks and were not re-engrafted into mice.

(C) Chemical rescue of chemoresistant sensitivity to etoposide and topotecan, treated as in 2B. Cells were treated as above for 7d before re-plating and exposing to either etoposide or topotecan for 72hrs before assaying. Additional EPZ or 5-Aza was not added beyond the d7 time point.

(D) EZH2 chemical inhibition displays time-dependent rescue of SLFN11 and persists despite re-establishment of basal H3K27me3 levels in NCI-H82. Cells were treated daily for 10d with 1 μ M EPZ011989 before washing in media and releasing into fresh media for an additional 10d. Media was changed every other day. SLFN11 is normalized to actin; H3K27me3 is normalized to total H3; RFU data normalized to day 0 signal.

(E) Chemical inhibition of EZH2 rescues SLFN11 protein expression in SCLC cell lines lacking baseline protein expression. Cells were cultured in the presence of 1 μ M EPZ011989 for 7d, refreshing the compound everyday and the media every other day prior to collection of samples.

(F) Re-expression of SLFN11 under chemical EZH2 inhibition is correlated to a shift in sensitivity to topotecan. Pearson correlation $r=0.916$. Red lines represent 95% confidence intervals.

(G) Conditional re-expression of SLFN11 increases topotecan sensitivity in two SCLC cell lines. Doxycycline (DOX) at 1 μ g/mL was added to the media every other day for 4d before re-plating for 72hrs sensitivity to topotecan. IC₅₀ values are colored per arm.

(H) shRNA-mediated suppression of SLFN11 can partially reverse the sensitizing effects of chemical EZH2 inhibition on sensitivity to DNA damage. The SCLC cell line NCI-H82 was exposed to DMSO, 1 μ M EPZ011989 (EPZ) or a combination of 1 μ M EPZ and 1 μ g/mL DOX for 7d before exposure to topotecan. Times post-washout of the topotecan dose where cells were collected spanned 0.5-48hrs. Cells in suspension were released into fresh media after washing with serum free media following the 1hr exposure to topotecan.

(I) IC₅₀ shift in topotecan sensitivity for NCI-H82-pLT3GEPIR-shSLFN11.1 cell line after 7d of conditional run-in treatment with DMSO, 1 μ M EPZ011989 (EPZ) or 1 μ M EPZ011989 and doxycycline (EPZ/DOX). *Below*: normalized RFU for cleaved-PARP. Signals were normalized against un-damaged controls per 7d run-in condition (DMSO, EPZ, or EPZ/DOX) in far left lanes per the three conditions shown.

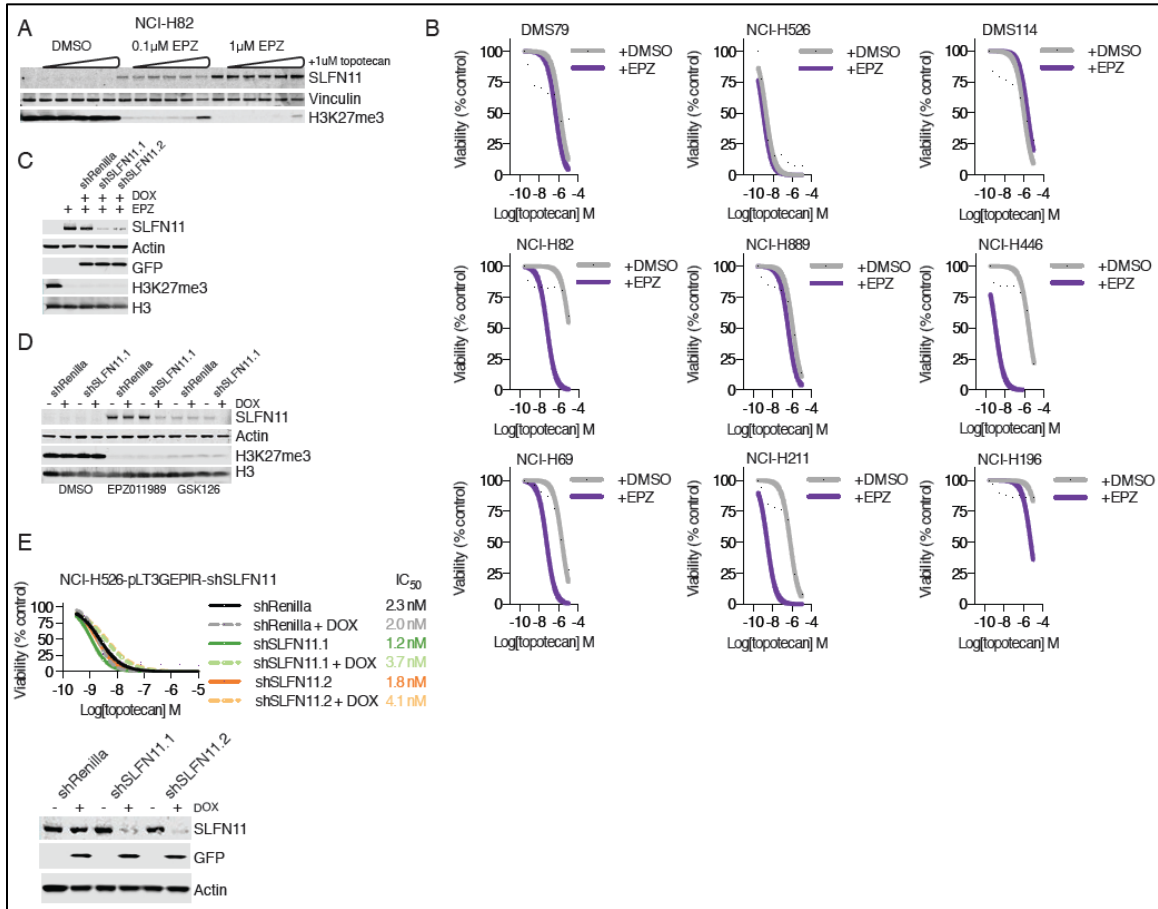


Figure 14. EZH2 chemical inhibition shows dose-dependent re-expression of SLFN11 and the re-expression is suppressible by shRNA.

(A) SLFN11 re-expression is dose-dependent. NCI-H82 cell lines was treated for 7d with DMSO, 100nM or 1µM EPZ011989 in culture, adding compound every day. Cells were then split, exposed to 1µM topotecan for 1hr, washed and then released into fresh media for a 48hr chase. Gradient bar indicates time post-release/washout.

(B) Individual IC₅₀ curve traces for the 9 human SCLC cell lines used for the construction of Figure 13G. Cells were split every 3d, adding 1µM EPZ011989 (EPZ) or vehicle (DMSO) every day for 7d, before plating 1-5x10⁴ cells in a black, opaque bottom plate as described in *Materials and Methods* for determining a 72hr kill curve for select agents. Average curve traces are shown from normalized data, restricting the Hill coefficient to 1.

(C) SLFN11 re-expression is suppressible by shRNA. NCI-H82 treated with 1µM EPZ011989 in culture for 7d with or without a 72hr co-treatment period with 1µg/mL doxycycline (DOX). Two independent shRNA's targeting SLFN11 are shown versus a non-targeting shRenilla control.

(D) SLFN11 re-expression under chemical EZH2 inhibition is not compound specific. Shown is NCI-H82 treated in culture for 7d with DMSO, 1µM EPZ011989 or 1µM GSK126 with or without a 72hr co-treatment period with 1µg/mL doxycycline (DOX) to suppress SLFN11.

(E) Conditional shRNA suppression of SLFN11 in the SLFN11^{High} SCLC cell line NCI-H526 modestly decreases sensitivity to topotecan. As in 13H, 1µg/mL doxycycline (DOX) was added to cell lines for 4d before re-plating for sensitivity assays. IC₅₀ values

are colored accordingly per arm. Extent of knockdown of SLFN11 indicated before for two independent SLFN11 targeting shRNAs (shSLFN11.1 and shSLFN11.2, respectively), as well as an shRNA targeting Renilla luciferase (shRenilla). GFP is co-expressed from an independent promoter upon exposure to doxycycline in the 3rd generation doxycycline inducible vector pLT3GEPiR (Fellmann et al., 2013).

EZH2 silences SLFN11 expression in SCLC

To further define the mechanistic relationship between EZH2 and *SLFN11* expression, we sought to explore the effects of EZH2 inhibition on local chromatin structure in the vicinity of the *SLFN11* locus. We examined the efficacy of EPZ011989 in 4 PDX models at two dose schedules over a treatment period of 3 weeks. As a single agent, EPZ011989 was well tolerated at 250 milligrams per kilogram body weight (mpk) administered orally, twice a day (PO bid) and slowed tumor growth rate to a modest extent in 3 of 4 models tested, including a chemorefractory model, JHU-LX44 (**Figures 15A-C**). Our ability to observe single agent efficacy *in vivo* may have been limited by the duration we were able to treat hind flank tumors, relative to the time required to remodel the epigenome with such agents, which is thought to require weeks to months (LaFave et al., 2015). We further assessed the contribution of time-dependence for efficacy *in vivo* by re-engrafting equivalent viable cell numbers from tumors that had previously been treated for 21d with or without 250mpk EPZ011989 and then re-treating tumors with vehicle or a secondary round of EPZ011989 as the tumors became palpable (**Figure 15D**). These results suggest that prolonged exposure of SCLC tumors to EZH2 inhibition may have a greater effect on decreasing proliferative capacity, not easily observed within the first few weeks of conventional pre-clinical efficacy experiments.

To demonstrate the ability of EPZ011989 to modulate the SCLC chemoresistant epigenome *in vivo*, we performed chromatin immunoprecipitation followed by sequencing (ChIP-seq) from flash frozen tissue obtained from chemonaïve or chemoresistant SCRX-Lu149 tumors treated for 21d with either vehicle or 250mpk EPZ011989. ChIP-seq was performed on three targets: EZH2, H3K27me3, and H3K27Ac (**Figure 16A**). While total EZH2 levels were not significantly altered in any condition (red), we observed increased global H3K27me3 in the chemoresistant setting that could be abolished by EPZ011989

(blue), as well as decreased global H3K27Ac in the chemoresistant setting that could be rescued by EPZ011989 (green). As expected, global H3K27Ac levels were increased by EPZ011989 in both the chemonaïve and chemoresistant settings with concomitant loss of H3K27me3. The global reduction of H3K27Ac in the chemoresistant setting prompted us to explore differential intensities within genomic regions termed “super-enhancers” (Loven et al., 2013; Pott and Lieb, 2015), thought to be critical for SCLC proliferation (Christensen et al., 2014; Lin et al., 2012). We observed differential signal intensities in such regions, consistent with global loss of H3K27Ac that could be restored by EPZ011989. However, selective loss or rescue of discrete super-enhancer regions was not observed (**Figure 16B**).

Focusing specifically on the *SLFN11* locus, these data demonstrate focally concentrated EZH2 and H3K27me3 in the immediate vicinity of the transcription start site (TSS) in vehicle-treated tumors, with spreading of H3K27me3 across the gene body in the context of acquired chemoresistance (**Figure 16C**). Coordinate with the increase in H3K27me3 across the gene body in the chemoresistant derivatives, there is almost complete loss of H3K27Ac, a mark associated with transcriptionally active chromatin, at the TSS of *SLFN11* that we confirmed by ChIP-qPCR ($p < 0.0001$; **Figure 15E**). Interestingly, EPZ011989 treatment appears to increase the density of EZH2 bound near the *SLFN11* TSS, and while EPZ011989 treatment was able to largely erase H3K27me3 throughout the gene body of *SLFN11*, levels of H3K27me3 near the TSS, presumably tightly bound by EZH2, were largely unchanged. However, EPZ011989 treatment also resulted in a concomitant increase in levels of H3K27Ac near the *SLFN11* TSS. While speculative, these data suggest that re-expression of this target gene via chemical EZH2 inhibition also requires cooperation with placement of histone modifications that promote gene expression.

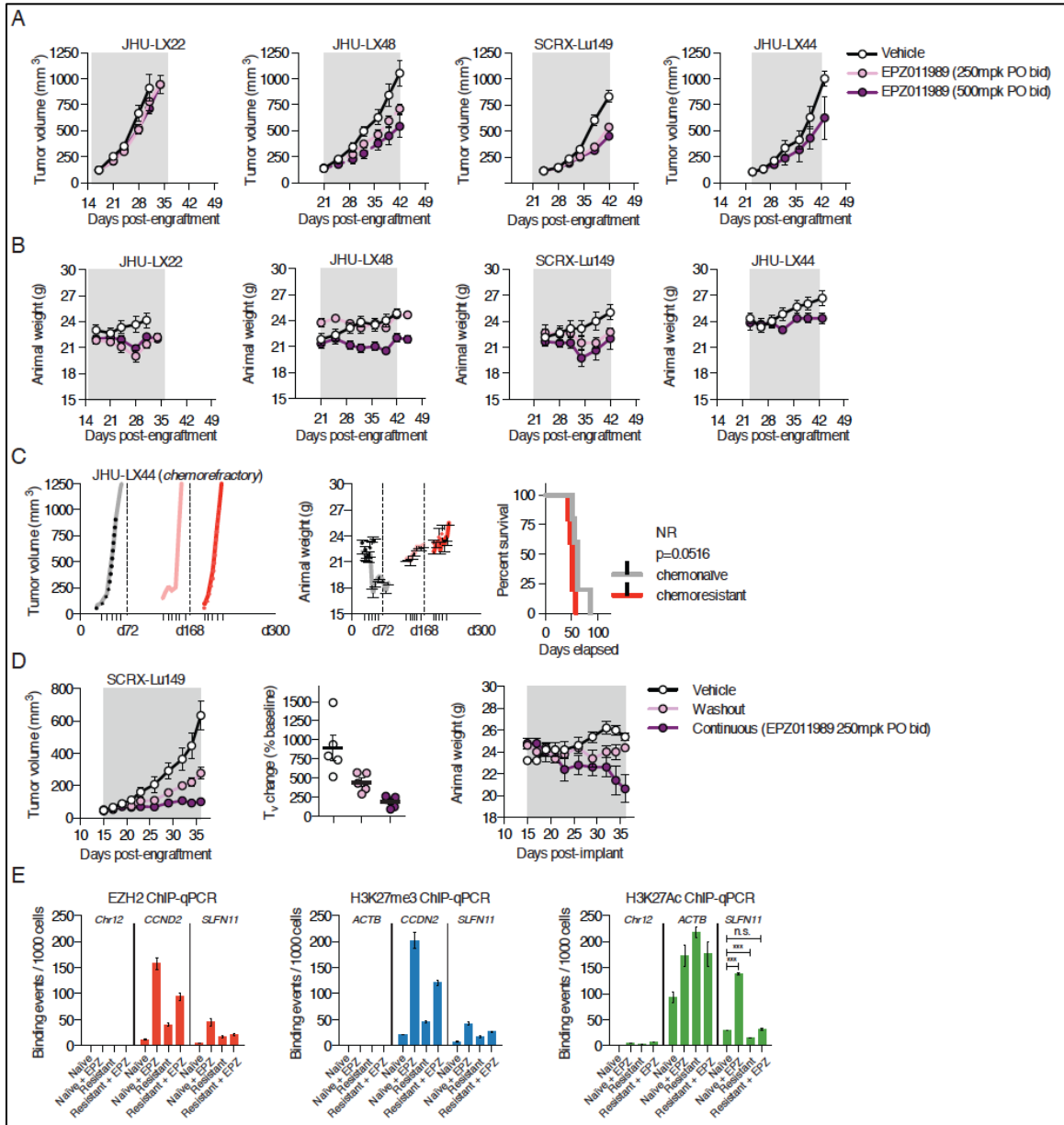


Figure 15. EZH2 inhibition by EPZ011989 has limited single agent activity in PDX models of SCLC and EZH2 directly targets *SLFN11* for silencing.

(A) Single agent activity of EPZ011989 across three independent chemo-naïve and one chemoresistant PDX models (JHU-LX44), using two separate dose schedules. Areas in grey represent the times on continuous treatment. EPZ011989 was administered on a 10AM/6PM schedule, 7 days a week for 14-21d, depending on tumor growth kinetics during treatment. Error bars shown +/- standard error of the mean (SEM); n=5-6 per arm. 250mpk arm for JHU-LX44 was not performed.

(B) Average animal weight on study above plots.

(C) Chemorefractory model JHU-LX44 does not respond to the schedule of C/E used to generate *in vivo* acquired resistance models. Shown are mean tumor volume curves, weights on study and survival as a function of time to 1,000mm³

(D) *Left*: Efficacy of continuous dosing through engraftment period. Tumors at the end of a three-week efficacy experiment for SCRX-Lu149 were engrafted from either vehicle or 250mpk treatment arms into mice and two weeks following engraftment, mice from previously treated tumors were either not treated with EPZ011989 (washout) or treated for 3 additional weeks. *Middle*: Comparison of tumor volume changes at week 3 on treatment versus baseline for 3 arms. Individual data points shown \pm SEM. *Right*: Average animal weight on study for left panel. Continuous arm approaches limits of protocol weight loss.

(E) ChIP-qPCR for SLFN11 (*upstream of first exon*) in various tumor samples used in Figure 16 (*follows*) as compared to positive and negative control primer pairs. ChIP target indicated in color: EZH2 (red), H3K27me3 (blue) and H3K27Ac (green). Each ChIP-qPCR series is shown for three targets in the order of negative control, positive control and SLFN11 (*left-to-right*): Chr12 refers to a gene desert region in chromosome 12, not known to bind any transcription factor (Active Motif; 71001). *P*-value indices (***) < 0.0001 reported for paired *t*-tests between groups within the H3K27Ac (green) sample set; n.s.=non-significant

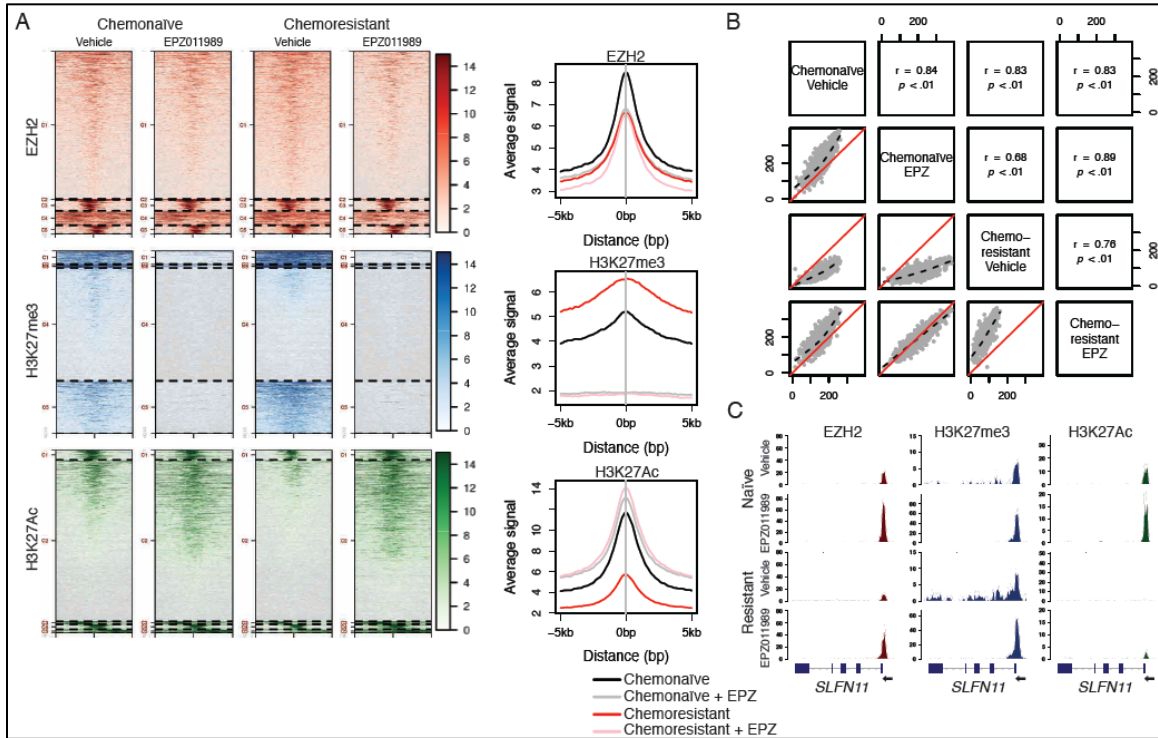


Figure 16. Epigenetic changes acquired in chemoresistance are reversible with chemical EZH2 inhibition *in vivo*.

(A) Cluster analysis of ChIP-4seq results from four SCRX-Lu149 tumor groups: chemo-naïve or chemoresistant, treated with either vehicle or 250mpk EPZ011989 PO bid for 21d. Chromatin was pooled from three independent tumor samples per arm prior to IP.

(B) Scatter plots of super-enhancer signal intensity demonstrate global loss of super-enhancer signal (spike-in normalized H3K27Ac binned region) in the chemoresistant setting.

(C) *SLFN11* ChIP-seq gene tracks for the indicated sample treatment arms. Y-axes limits are scaled to drosophila spike-in for each sample for peak height comparisons. The *SLFN11* gene model is oriented right-to-left along the x-axis as indicated.

Pharmacologic EZH2 inhibition prevents emergence of chemoresistance and augments chemoresponse in vivo

The down regulation of *SLFN11* in acquired chemoresistance, and its apparent regulation by EZH2, suggest a model in which EZH2, as part of the Polycomb Repressive Complex 2 (PRC2) is induced by cytotoxic chemotherapy. This induction yields *SLFN11* silencing, a decrease in SLFN11 protein expression and concomitant acquired chemoresistance. To test this hypothesis and evaluate time-dependent changes in EZH2 activity, we performed DNA damage time course experiments in NCI-H446, following exposure to topotecan, in the presence or absence of EPZ011989. Over the course of 48hrs following DNA damage, we noted a progressive increase in EZH2, as well as H3K27me3, that was suppressed by acute EPZ011989 treatment (**Figure 17A**). Further, we could demonstrate that the effect on H3K27me3 was a function of EZH2, as shRNA-mediated suppression of EZH2 during a similar DNA damage time course abolished any increase in H3K27me3, and the accompanying loss of H3K27me2 (**Figure 17B**). These data support a global methylation event in which di-methylated H3K27 is converted to the tri-methylated state. The effect of DNA damage increasing global H3K27me3 levels was not cell line specific (**Figure 18A**), demonstrated dose-dependence (**Figure 18B**), and was more pronounced for topoisomerase I poisons when compared to either cisplatin or etoposide on an equimolar basis (**Figure 18C**). These shifts in EZH2 activity and resultant H3K27me3 could also be observed *in vivo*, using a single dose-chase approach in tumor-bearing animals treated with irinotecan and quantitatively evaluating time-dependent changes in several H3 methyl marks, demonstrating specificity for the induction of H3K27me3, with contemporaneous decreases in H3K27me2 (**Figure 17C**).

These data support the hypothesis that EZH2 activity is an important determinant of acquired chemotherapy resistance in SCLC, in part through suppression of *SLFN11* and, conversely, that targeted EZH2 inhibition might prevent or reverse acquired resistance to cytotoxic chemotherapy. To examine the combinatorial activities of EPZ011989 with cytotoxic regimens *in vivo*, we chose to approach this in two clinically translatable scenarios: 1) combining EPZ011989 with standard of care in the first line setting for *SLFN11* expressing (*SLFN11+*) chemo-naïve models and, 2) combining EPZ011989 with a standard second line agent in the chemoresistant setting, in which the silencing of *SLFN11* has been established. Addition of EPZ011989 to 6 cycles of C/E strongly enhanced disease control in the chemo-naïve setting in both JHU-LX102 and SCRX-Lu149 relative to either EPZ011989 or C/E alone (**Figures 17D,E & Figures 18D,E**). To examine the benefit of EZH2 inhibition in tumors actively progressing on C/E, after three cycles we randomized 5 of 10 animals in the C/E arm to receive EPZ011989 in combination with three additional cycles of C/E. Remarkably, the addition of EPZ011989 potently induced tumor regression relative to C/E alone during the remaining 3 cycles, supporting the role of EZH2 in the development of chemorefractory disease (**Figures 17D,E orange group**).

We next assessed the efficacy of irinotecan, a topoisomerase I poison administered in the setting of relapsed SCLC, with or without EPZ011989 in two models that had acquired resistance to C/E, chemoresistant JHU-LX102 and SCRX-Lu149. Importantly, we observed strong cross-resistance to irinotecan, but not ionizing radiation (IR) in the chemoresistant setting, further supporting that the mechanism of acquired resistance operant in these models had specificity to the selection agents used (cisplatin and/or etoposide) (**Figures 18F,G**). The addition of EPZ011989 to irinotecan in the chemoresistant setting resulted in potent combinatorial activity that could control disease

to a greater extent than either agent alone through 6 weekly cycles of treatment (**Figures 17F,G & Figures 18H,I**).

To further assess active repression and de-repression of SLFN11 *in vivo*, we engrafted an additional cohort of animals bearing either chemonaïve or chemoresistant versions of JHU-LX102 and randomized these animals to the indicated treatment arms for 3 cycles of chemotherapy with or without EPZ011989. Strikingly, we noted quantitative suppression of SLFN11 protein levels in tumors after as few as 3 cycles of C/E in the chemonaïve setting and further suppression after 3 cycles of irinotecan in the chemoresistant setting (**Figure 17H**). Critically, EZH2 inhibition could rescue SLFN11 protein expression to baseline levels in the chemoresistant setting, even in the presence of concurrent chemotherapy (chemonaïve vehicle vs. chemoresistant 250mpk EPZ011989 + 3 cycles irinotecan).

We find that the greatest degree of chemosensitization by EZH2 inhibition in SCLC is with respect to topoisomerase I poisons. In the models tested *in vivo*, this effect was independent of CREBBP mutations, which are frequent events among all major forms of lung cancer (Campbell et al., 2016; George et al., 2015). Recent evidence suggests that loss of CREBBP function predisposes certain cancers to p300-HAT inhibition, in a synthetically lethal relationship (Ogiwara et al., 2016). Along a similar line, mutations in the SWI/SNF complex are known to define sensitivity to single agent EZH2 inhibition, and are currently being used as inclusion criteria in certain clinical trials (Kim et al., 2015b; Wilson et al., 2010). While we cannot definitively limit the combinatorial activity of EPZ011989 and irinotecan to a genetic subtype of SCLC, in the experiments performed, the combination appears to be potently active independent of detectable alteration in the SWI/SNF complex or CREBBP status. In combining EPZ011989 with irinotecan in the chemonaïve setting, we could completely ablate hind flank tumors

through 6 cycles of combination (5/5 animals with CRs). Moreover, the activity of the combination was greater, even when administered for a shorter duration of time (3 cycles), than the equivalent schedule of irinotecan when administered for a full 6 cycles (**Figures 17I,J**). However, we did not observe additional benefit when initiating adjuvant EPZ011989 as a single agent at the point of maximal consolidative effect of single agent irinotecan (post cycle 3), as this was inferior to 3 additional cycles of irinotecan at the point of comparison.

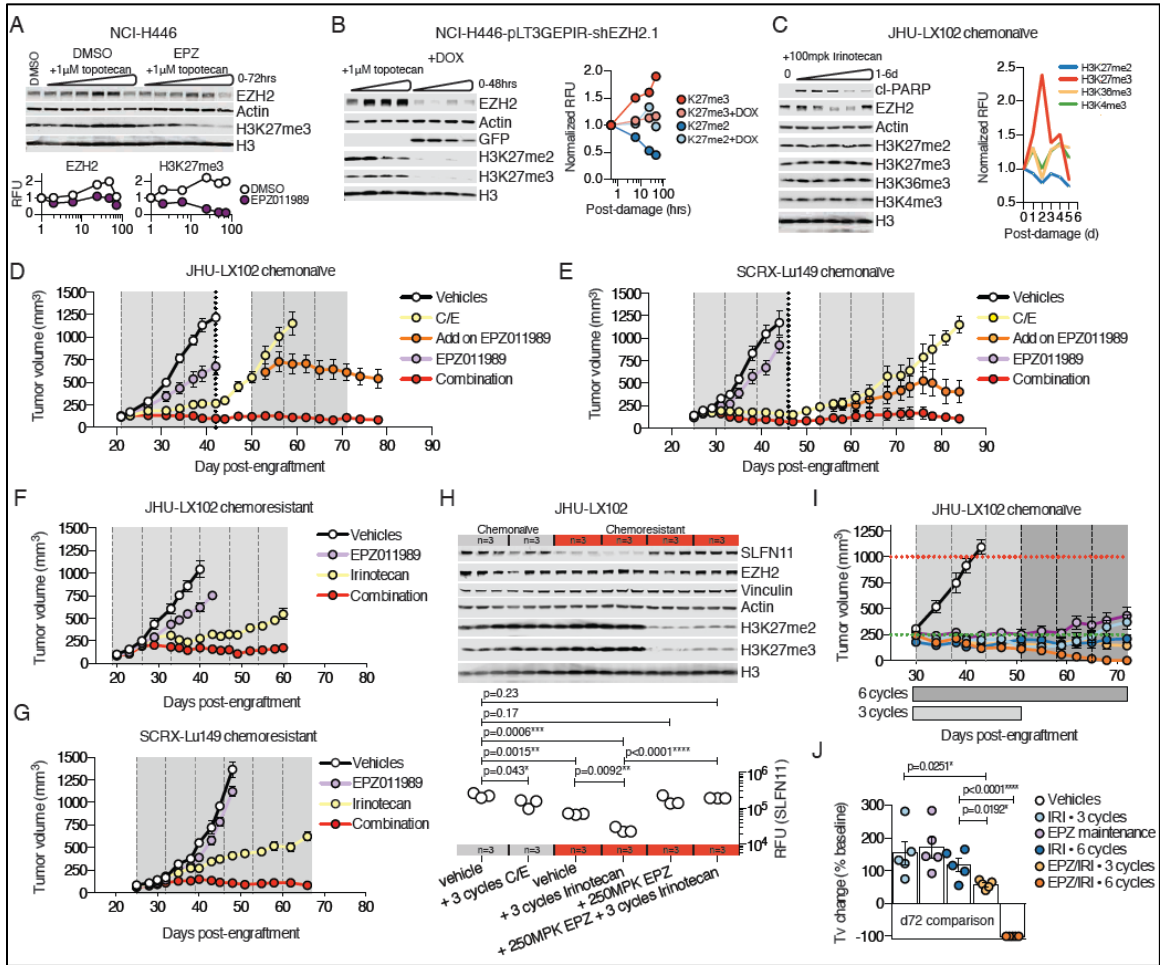


Figure 17. H3K27me3 is increased following DNA damage and is an actionable target in combination with first or second line chemotherapy in SLFN11+ SCLC.

(A) EZH2 and H3K27me3 are induced post-DNA damage and can be chemically inhibited with a single dose of EPZ011989. NCI-H446 was exposed to 1 μ M topotecan for 1hr in the presence or absence of 1 μ M EPZ011989, before washing out topotecan and collecting time points as indicated. EZH2 (normalized to actin) and H3K27me3 (normalized to H3) signal intensity (RFU) are normalized to the 72hrs DMSO control lane (far left sample).

(B) Genetic suppression of EZH2 can suppress the acute accumulation of global H3K27me3, and conversion of H3K27me2 to H3K27me3. NCI-H446-pLT3GEPiR-shEZH2.1 was treated with or without 1 μ g/mL doxycycline for 48hrs before damaging cells with 1 μ M topotecan, as before. On right, quantified H3K27me3 and H3K27me2 signal increases overtime (normalized to H3), normalized to the initial time point on the blot (0.5hrs).

(C) *In vivo* DNA damage of a SCLC PDX tumor displays acute H3K27me3 accumulation with coincident H3K27me2 decreases. The chemo-naïve JHU-LX102 model was engrafted and tumor-bearing mice were IP dosed with a single injection of 100mpk irinotecan and then tumors were collected at the indicated time points post-dose. All tumors were 400-500mm³ at the time of dosing to preserve tumor integrity and yield

enough tissue for downstream analyses. Quantitation of indicated histone H3 methyl marks normalized to total histone H3 from independent two-channel blots.

(D) Combining EPZ011989 with standard of care cisplatin/etoposide (C/E) provides durable disease control in SLFN11+ SCLC PDX models. Dashed vertical lines indicate d1 of a weekly C/E cycle (8mpk etoposide d1-3 + 5mpk cisplatin d1; all IP q7d). Dotted line at 4 weeks post-C/E 5 of the 10 animals within the C/E group were randomized to now receive EPZ011989 with 3 additional cycles of C/E. Grey areas indicate the dosing periods for EPZ011989 (250mpk; PO bid). n=5 animals per arm (n=10 in C/E arm through 3 cycles, before adding on EPZ)

(E) Results for chemonaïve SCRXLu149 as in D

(F) Combining EPZ011989 with a second line cytotoxic agent provides disease control in the chemoresistant setting. Dashed horizontal lines indicate d1 of a cycle. Six weekly cycles of irinotecan were administered with or without EPZ011989, as well as single agent EPZ011989.

(G) Results for chemoresistant SCRXLu149 as in I

(H) EPZ011989 rescues the expression of SLFN11 in chemoresistant PDXs and prevents down-regulation in the presence of chemotherapy. A separate pharmacodynamic (PD) cohort of animals was engrafted with either the chemonaïve (grey bar; n=6) or chemoresistant (red bar; n=12) versions of JHU-LX102. When tumors approached 400mm³ three animals were randomized to each treatment arm, collecting triplicate samples at week 4 on study (dosing weeks 1-3). Expression of SLFN11 is normalized to vinculin and plotted as RFU, as before. Paired *t*-tests were performed to compare differences between various groups indicated.

(I) Addition of EPZ011989 to a potent DNA damaging agent is superior to the DNA damaging agent alone and shows cumulative efficacy *in vivo*. Cohorts of chemonaïve JHU-LX102 were randomized to treatment arms (n=5 per arm) of either short periods – 3 weekly cycles – of 100mpk irinotecan (IRI) or in combination with EPZ011989 (EPZ/IRI), or full periods (6 cycles). Horizontal dashed lines indicate starting (green) and ending (red) tumor volume metrics per protocol with treatment period for 3 and 6 cycles shown along the x-axis. Vertical dashed lines indicate d1 of a weekly cycle of IRI.

(J) Changes in tumor volume from baseline as a measure of treatment and schedule. Comparisons were made at 6 weeks post-treatment initiation between cohorts (day 72). EPZ maintenance refers to single agent EPZ011989 being administered 250mpk PO bid for 21d after completion of 3 weekly cycles of irinotecan. All tumors in the EPZ/IRI 6 week treatment cohort were ablated at the final point of study shown (d72). *P*-values shown for paired *t*-tests.

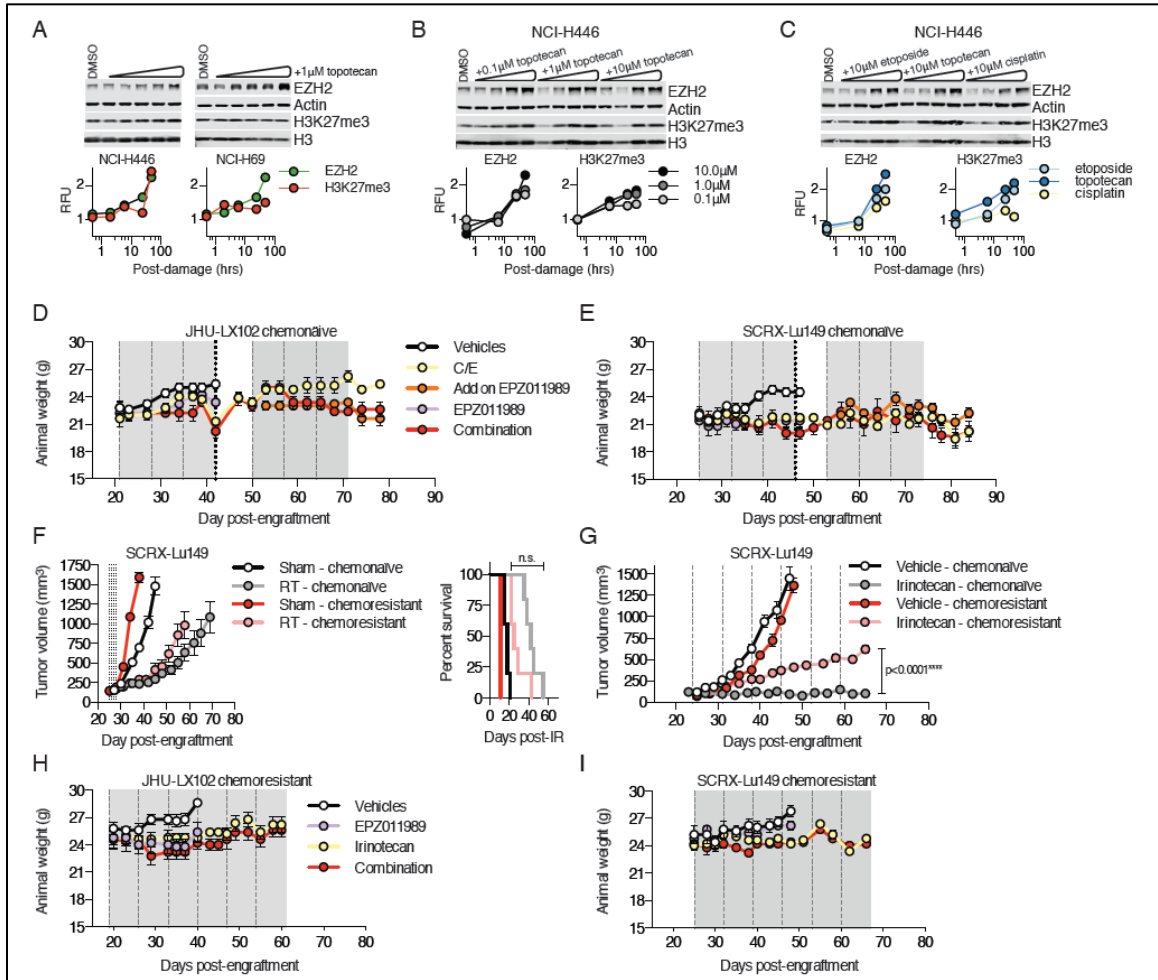


Figure 18. Combining EPZ011989 with first or second line chemotherapy is well tolerated *in vivo*

(A) EZH2 and H3K27me3 are induced following DNA damage in NCI-H446 and NCI-H69 cell lines. EZH2 signal normalized to actin and H3K27me3 normalized to H3. Data are plotted from 0.5-48hrs post-damage, normalizing to undamaged control (DMSO) at 48hrs.

(B) EZH2 and H3K27me3 are induced following dose-dependent DNA damage in NCI-H446. Time points shown post-damage are 0.5, 6, 24 and 48hrs. Data normalized to undamaged control at 48hrs.

(C) EZH2 and H3K27me3 are strongly induced by topoisomerase poisons in NCI-H446

(D) Average animal weights on study +/- SEM for each treatment arm indicated

(E) as in D

(F) Acquired resistance to C/E does not confer cross-resistance to radiation. As chemo-naïve and chemoresistant SCRX-Lu149 tumors approached 150mm³, treated groups (RT/IR) received 2Gy for 4 consecutive days and tumor outgrowth was recorded; n=5 animals per group. Survival reported as a measure of time post-IR to reach a volumetric endpoint of 1000mm³, as established before in the C/E resistance protocol. n.s.=non-significant by log-rank (Mantle-Cox) test.

(G) Acquired resistance to C/E confers cross-resistance to topoisomerase I poisons. As chemonaïve and chemoresistant SCR_X-Lu149 tumors approached 150mm³, treated groups received weekly cycles of irinotecan (100mpk; IP q7d) for 6 consecutive weeks and treated groups were then compared at one week after the final cycle. Dashed horizontal lines indicate d1 of a cycle. *P*-value shown for paired *t*-test.

(H) Average animal weights on study +/- SEM for each treatment arm indicated

(I) as in H

Discussion

SCLC has been singled out by the US National Cancer Institute (NCI) as one of two designated “recalcitrant” cancers (the other being pancreatic cancer) based on incidence rate, exceptionally high lethality, and the lack of substantial therapeutic progress made over several decades. The 2014 Scientific Framework for Small Cell Lung Cancer, an NCI report to Congress, outlined major research priorities in SCLC (National Cancer Institute, 2014). Three of the five priorities noted included developing better models reflecting phases of SCLC found in the clinic, characterization of mechanisms responsible for the rapid emergence of drug resistance, and the identification and targeting of novel therapeutic vulnerabilities in SCLC. The work described here addresses all three of these critical needs. By attempting to mimic as closely as possible the clinical experience of repeated cycles of cisplatin and etoposide exposure in PDXs, we have generated a set of novel paired SCLC models representing initial chemosensitive and subsequent chemoresistant disease. We have used these models to define two mutually exclusive mechanistic classes of acquired resistance, including an EMT shift associated with *TWIST1* up-regulation, and epigenetically mediated suppression of *SLFN11*. Finally, we have identified a novel and therapeutically tractable vulnerability of SCLC: dependence on EZH2 for development of acquired chemotherapeutic resistance *in vivo*.

In a cancer type with the high mutational load and resultant inter-patient heterogeneity of SCLC, it is not surprising that multiple mechanisms of acquired resistance are operant, and that different SCLCs may preferentially use different resistance pathways. What is perhaps more surprising, and encouraging, is that consistent gene expression and epigenetic changes, not mutations, are found to be associated with acquired chemoresistance across multiple independent SCLC models,

and indeed are reflected in primary human tumor samples. In the set of 10 PDX models examined here, *TWIST1* induction was observed in three; this pathway was additionally reflected in multiple murine models of SCLC. While initial data point to *TWIST1* as a biomarker rather than a driver of resistance *per se*, further exploration of therapeutic vulnerabilities associated with an EMT signature in this set of tumors is warranted. In 4 of the 10 PDX models, acquired resistance was associated with specific suppression of *SLFN11* expression. Most notably, our data point to *SLFN11* suppression as a primary contributor to acquired chemotherapy resistance in SCLC – one that can be prevented and/or actively remodeled through targeting of the key epigenetic regulator EZH2.

We recently reported that median *SLFN11* expression is higher in SCLC when compared to most other tumor types studied in the TCGA (Lok et al., 2016). Recent work has begun to focus on the molecular functions of the *SLFN11* protein (Mu et al., 2016). These emerging data offer insight into how high-level expression of *SLFN11* in SCLC might contribute to the initial exceptional chemosensitivity of this disease, and why *SLFN11* down-regulation would increase therapeutic resistance. Essentially all the therapeutic agents used to treat SCLC are DNA damaging agents that directly or indirectly result in double strand breaks (DSBs) – this list includes the platinum compounds, the topoisomerase inhibitors, alkylating agents such as temozolomide, and ionizing radiation. Resolution of DSBs is necessary for cell survival and occurs through two main DNA repair pathways: non-homologous end-joining (NHEJ) and homologous recombination (HR). HR is an important pathway as it is generally considered to be error-free. An important step in HR involves binding and protection of overhanging DNA by the single-strand binding protein replication protein A (RPA) to allow recruitment of HR mediators (i.e. BRCA2 and RAD51). *SLFN11* has been shown to localize to sites of DSBs and displace RPA from single strand overhangs: high levels of *SLFN11* thereby

result in HR deficiency, a state in some ways analogous to BRCA1/2 deficiency (Mu et al., 2016). Consistent with this framework, we found that *SLFN11* expression, as a surrogate biomarker of HR deficiency, was a particularly strong predictor of SCLC sensitivity to PARP inhibitors (Lok et al., 2016).

We have demonstrated here that *SLFN11* suppression during selection for acquired resistance in SCLC is associated with a global increase in H3K27me3 with modest reductions in global H3K27Ac, and that *SLFN11* gene expression can be restored and/or maintained by pharmacological inhibition of EZH2, even in the presence of DNA damaging agents. While we have shown that *SLFN11* is both necessary and sufficient for sensitivity to DNA damaging agents in SCLC, we fully recognize that EZH2 inhibition alters expression of many genes. We fully anticipate that factors beyond *SLFN11* will be identified that contribute to the ability of EZH2 inhibition to restore chemosensitivity in SCLC. Defining the relative contributions of *SLFN11* vs. other EZH2-modified factors remains an area for future investigation.

We find that the greatest degree of chemosensitization by EZH2 inhibition in SCLC is with respect to topoisomerase I poisons. From models tested *in vivo*, this effect was independent of CREBBP mutations, which are frequent events among all major forms of lung cancer, thought to remodel the epigenetic landscape of these cancers (Campbell et al., 2016; George et al., 2015). Recent evidence suggests that loss of CREBBP function predisposes certain cancers to chemical inhibition of p300's HAT domain, displaying a synthetically lethal relationship (Ogiwara et al., 2016). Along a similar line, mutations in the SWI/SNF complex are known to define sensitivity to single agent EZH2 inhibition, and are currently being used as inclusion criteria in certain clinical trials (Kim et al., 2015b; Wilson et al., 2010). While we cannot definitively limit the combinatorial activity of EPZ011989 and irinotecan to a genetic subtype of SCLC, in the experiments performed,

the combination appears to be potently active independent of detectable alteration in the SWI/SNF complex or CREBBP status. The remarkable combinatorial activity of an EZH2 inhibitor with standard first line chemotherapy for *de novo* disease, and with standard second line chemotherapy for recurrent, chemoresistant disease, has immediate translational relevance.

Several potent and selective EZH2 inhibitors are now in different stages of clinical development, including phase 2 (Epizyme) and phase 1 (Constellation, GSK) trials in multiple solid tumor and hematological indications. Epizyme recently updated the phase I experience and ongoing phase II experience (Ribrag et al. and, Morschhauser et al., ASH Lymphoma 2016) for their lead inhibitor tazemetostat (EPZ-6438, a closely related structural homolog of the tool compound inhibitor EPZ011989 described in this paper) (Fillmore et al., 2015). Clinical responses have been observed with tazemetostat in multiple patient populations, including diffuse large B-cell lymphoma (with and without EZH2 activating mutations), follicular lymphoma, malignant rhabdoid tumors, and small cell carcinoma of the ovary hypercalcaemic type (SCCOHT). The safety profile of tazemetostat in 82 patients with non-Hodgkin lymphoma on the ongoing phase II study was favorable, with the most frequent treatment-related adverse events being grade 1 or 2 nausea and asthenia. Myelosuppression was observed infrequently with only 11% and 6% of patients experiencing grade ≥ 3 thrombocytopenia and grade ≥ 3 neutropenia, respectively, suggesting tazemetostat may be safely combined with cytotoxic chemotherapy in SCLC. Importantly, the work presented here suggests that targeted EZH2 inhibitors should be anticipated to have minimal single agent activity in SCLC, and that evaluation of relevant combination therapies should be considered early in clinical development of these agents in SCLC. Clinical trials testing the therapeutic strategies defined here are now being designed with these considerations in mind.

Intended to be blank

Chapter 3. Targeted Inhibition of BCL-2 Has Limited Utility in SCLC and Combined Inhibition of mTOR Shows Preclinical Synergy

Brevis

Over-expression of the anti-apoptotic protein BCL-2 is observed in the majority of small cell lung cancer (SCLC) cases and is associated with resistance to chemotherapy. While targeting BCL-2 in hematologic malignancies continues to show signs of promise, translating the BH3 mimetic ABT-737 (or ABT-263; navitoclax) to the clinic for solid tumors has remained problematic, with limited single agent activity in early phase clinical trials. Here we used patient-derived xenograft (PDX) models of SCLC to study ABT-737 resistance and demonstrated that responses to ABT-737 are short-lived and coincide with decreases in HIF-1 α regulated transcripts. Combining the mTOR inhibitor rapamycin with ABT-737 rescued this resistance mechanism, was highly synergistic *in vitro*, and provided durable tumor regressions *in vivo* without notable hematologic suppression. In comparison, tumor regressions did not occur when ABT-737 was combined with etoposide, a gold standard cytotoxic for SCLC therapy. Rapamycin exposure was consistently associated with an increase in the pro-apoptotic protein BAX, whereas ABT-737 caused dose-dependent decreases in BAX. As ABT-737 triggers programmed cell death in a BAX/BAK-dependent manner, we provide pre-clinical evidence that the efficacy of ABT-737 as a single agent is self-limiting in SCLC, but the addition of rapamycin can maintain or increase levels of BAX protein and markedly enhance the anti-cancer efficacy of ABT-737 (**Figure 19**). These data have direct translational implications for SCLC clinical trials.

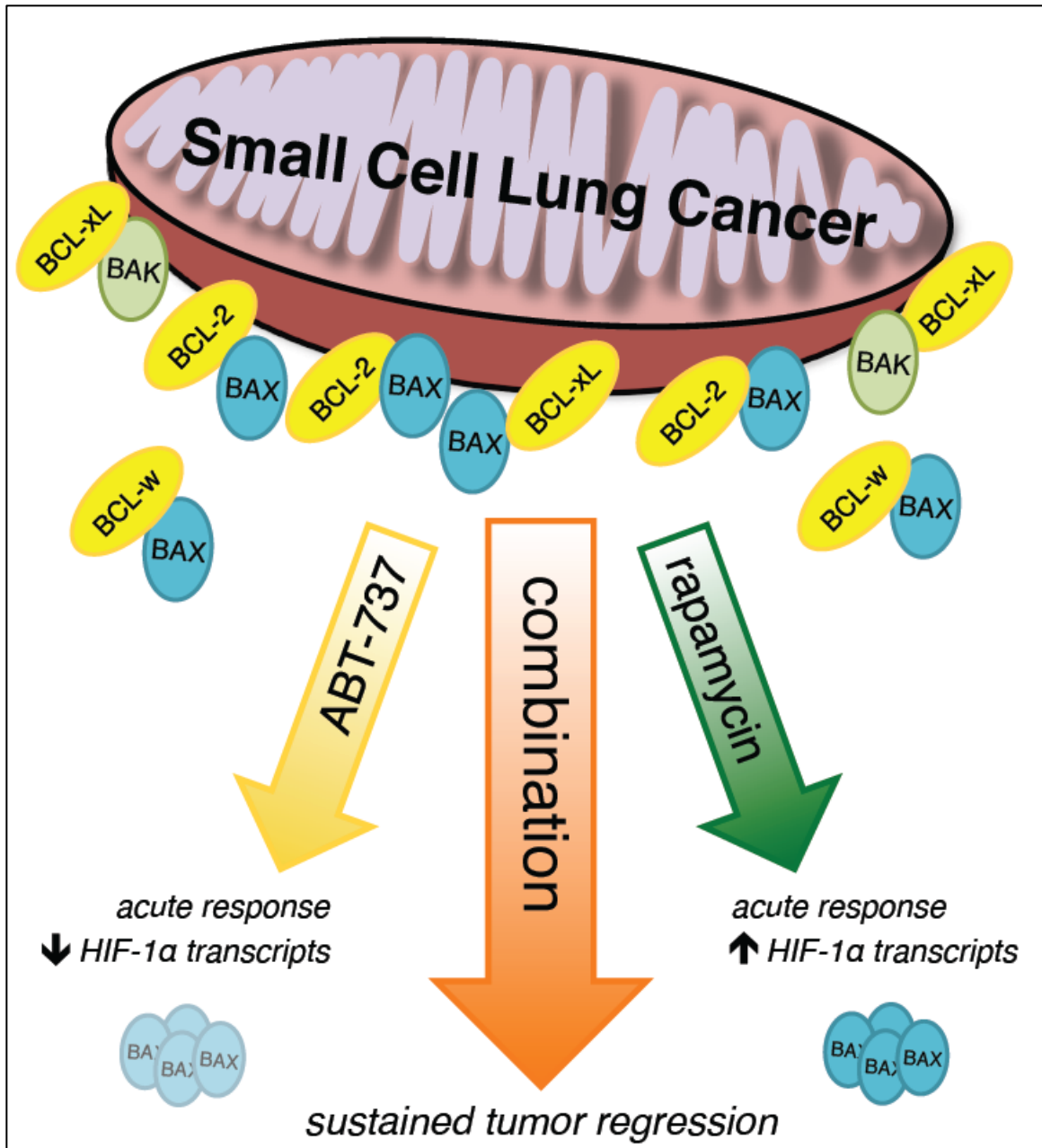


Figure 19. Chapter 3 Brevis

Single agent BCL2-/xL inhibitor ABT-737 has limited utility in SCLC. The BH3 mimetics ABT-737/263 were developed to trigger programmed cell death (apoptosis) in tumors that express high levels of the anti-apoptotic proteins BCL-2 and BCL-xL. Pre-clinical data in chronic lymphocytic leukemia (CLL) and small cell lung cancer (SCLC) warranted clinical investigation; however, single agent responses to ABT-263 in extensive-stage SCLC were minimal. Here, using patient-derived xenograft (PDX) models of SCLC, it was found that responses to single agent ABT-737 were acute in duration and accompanied by decreases in HIF-1α target genes. Using transcriptome signatures of ABT-737 responses, we identified that classes of PI3K/mTOR inhibitors were synergistic when combined with BH3 mimetics *in vitro* and provided durable tumor regressions in

BCL-2 expressing PDX models of SCLC *in vivo*. Interestingly, the mTOR inhibitor rapamycin preserved levels of BAX protein *in vivo*, a requisite gateway for programmed cell death by ABT-737. These data add a new light on acute resistance mechanisms to targeting anti-apoptotic proteins.

Study Introduction

Small cell lung cancer (SCLC) represents 12-15% of all lung cancers and accounts for nearly 30,000 deaths in the US annually (Siegel et al.). Etoposide plus cisplatin was established as the standard of care for SCLC in the 1980s and can confer high response rates (>60%) as initial therapy (Kalemkerian et al.). However, therapy-refractory recurrence is nearly universal and, as a consequence, SCLC has one of the highest case-fatality rates among cancer – a statistic that has not changed significantly over the past 30 years (Oze et al.). Since 2003, only one agent, topotecan, has received FDA approval for SCLC. New therapies are in critical need.

One targetable opportunity is in the over-expression of the anti-apoptotic protein BCL-2 where between 60-90% of SCLC cases have been reported to express high BCL-2 protein (Ikegaki et al., 1994; Jiang et al., 1995) and this is thought to be a mechanism by which SCLC resists programmed cell death. Through structure-guided medicinal chemistry efforts, the BCL-2 inhibitor ABT-737 emerged as the prototypic small molecule candidate to exploit over-expression of BCL-2 in cancer (Oltersdorf et al., 2005). ABT-737 most closely simulates the pro-apoptotic protein Bad from a functional standpoint and serves as a competitive BH3 mimetic with high affinity to the anti-apoptotic proteins BCL-2, Bcl-xL and Bcl-w. Thus, when targeting BCL-2 was possible with ABT-737 and the orally-bioavailable derivative ABT-263 (navitoclax), efforts were made to translate pre-clinical findings in SCLC to patients (Gandhi et al., 2011; Park et al., 2008).

However, early phase clinical trials investigating ABT-263 as a single agent in SCLC failed to show the dramatic responses that were observed in pre-clinical SCLC cell line xenograft models (Gandhi et al.; Rudin et al., 2012b; Shoemaker et al., 2008). In clinical studies of ABT-263, the inhibition of Bcl-xL in platelet populations yielded dose-dependent thrombocytopenia and has somewhat limited the utility of this high affinity

BCL-2/xL inhibitor. It is becoming increasingly evident that targeting certain BCL-2 family members in a tumor must be considered in the context of other lineage-specific dependencies to minimize toxicities (Juin et al., 2013). Moreover, while lead-in dosing strategies with ABT-263 could lessen the observed thrombocytopenia, inhibiting both BCL-2 and Bcl-xL with concurrent cytotoxic chemotherapy has added complexity to maximizing therapeutic combinations with ABT-263.

Strategies to model resistance to ABT-737/263 in SCLC and other tumor types have identified the anti-apoptotic protein MCL-1 as a major culprit, where MCL-1 can serve a functionally-redundant role in sequestering the pro-apoptotic proteins BAX and BAK and is not targeted by ABT-737. Efforts to increase the sensitivity of various cancers to ABT-737 have focused on mechanisms that impact MCL-1, either through direct targeting or exploiting the relatively short half-life of the MCL-1 protein (Inuzuka et al., 2011; Wei et al., 2012). Many compounds shown to synergize with ABT-737 in SCLC and other cancers are global transcriptional or translational repressors, such as anthracyclines (Chen et al., 2011; Xu and Krystal, 2010); however, combination of these agents in the clinic could prove challenging due to toxicity. While other anti-apoptotic proteins not targeted by ABT-737 have been implicated in resistance to ABT-737, the major anti-apoptotic players observed to be amplified across many cancer types are BCL-2, Bcl-xL and MCL-1 (Beroukhi et al., 2010). How these anti-apoptotic regulators govern the activity of pro-apoptotic BAX and BAK with other apoptotic effectors in the context of a given tumor help to define a cancer hallmark – resistance to programmed cell death (Hanahan and Weinberg, 2011).

We previously reported that ABT-737 could induce dramatic responses in SCLC cell lines, in agreement with what others have shown; however, ABT-737 alone failed to produce substantial tumor responses in SCLC patient-derived xenograft (PDX) models

that express low levels of BCL-2 (Hann et al., 2008). Here we show that BCL-2 expressing SCLC PDXs initially respond to ABT-737, but the responses are not durable and the addition of etoposide does not improve responses. We used these PDX models to investigate the transcriptional changes that occur during initial responses to ABT-737 in order to develop strategies to increase the efficacy of ABT-737. We found that the mTOR inhibitor rapamycin could enhance the antitumor activity of ABT-737 *in vitro* and *in vivo*, rescuing the self-limiting effects of single agent ABT-737. We further observed that this combinatorial activity correlated with an increase in pro-apoptotic BAX.

Materials and Methods

Cell lines and reagents

SCLC cell lines were purchased from American Type Culture Collection (ATCC) and maintained as recommended. All cell lines tested negative for *mycoplasma* (Lonza; MycoAlert™) and were STR verified at the Johns Hopkins Fragment Analysis Facility within 6 months of use. ABT-737 was obtained from Abbott Laboratories (*now Abbvie*) and purchased from Active Biochem (A-1002). For *in vivo* use, ABT-737 and etoposide (Accord Healthcare, Inc) were prepared as previously described (Hann et al., 2008). Rapamycin (LC Laboratories) was stored in 100% ethanol at 50 mg/ml. For *in vivo* use, rapamycin vehicle was 82% PBS/5% Tween-80/5% PEG 400/8% ethanol. AZD8055 (S1555), BEZ235 (S1009), everolimus (S1120), LY294002 (S1105) and wortmannin (S2758) were purchased from Selleck Chemicals. DMSO was used as a vehicle for all *in vitro* experiments.

Cell proliferation and viability assays

Cells were plated 24 h before treatments in 96-well plates at 1,000-5,000 cells/well. Proliferation (CellTiter 96® AQueous One; Promega) and viability (CellTiter-Glo®; Promega) assays were quantified on a compatible plate reader (SpectraMax M2®; Molecular Devices). All combination and drug synergy experiments were performed for 72hrs before assaying.

Assessment of drug synergy

Drug synergy was determined quantitatively using the combination index (CI) method of Chou and Talalay (Chou and Talalay, 1984). Viability was calculated across a wide range of doses for both ABT-737 and each compound of interest using a non-

constant ratio. CI was calculated as a function of response or fraction affected (Fa) using the formula $[CI = (D_1)/(D_x)_1 + (D_2)/(D_x)_2]$ where D_1 and D_2 are the doses used to achieve a specific response in combination and $(D_x)_1$ and $(D_x)_2$ are individual drug doses needed to achieve similar response. A CI >1 indicates antagonism, while a CI <1 indicates synergism.

Pimonidazole staining and immunohistochemistry

Mice were injected with Hypoxyprobe™-1 solution (Hypoxyprobe, Inc.) approximately 1 h before sacrifice. Tumors were fixed in formalin, embedded in paraffin, and sectioned at 5 μ m thickness. Sections were de-waxed and incubated in citrate, pH 6.0 (Vector Laboratories, H-3300) for 25 min. Sections were stained using the Dako EnVision Plus Detection System with rabbit PAb2627 (Hypoxyprobe, HP3-100Kit) for 45 min at 25 °C and were visualized with 3,3'-diaminobenzidine (DAB) reagent (Sigma, D423). H&E staining was performed with an automated slide stainer (Leica) with Modified Harris Hematoxylin (Richard-Allan Scientific).

Isolation of heavy membranes

Separation of crude mitochondria (“heavy membranes”) from cytosol in cell lines and tumor tissue was performed using a QProteome™ Mitochondrial Isolation Kit (Qiagen). Samples were lysed in RIPA buffer supplemented with protease/phosphatase inhibitor cocktails (Sigma-Aldrich) for 30 min on ice before clarification at 13,000 rpm for 10 min at 4 °C. Protein concentrations were determined using the BCA method (microBCA; Pierce).

Antibodies and Western Blot

The following primary antibodies were purchased from Cell Signaling Technology, Inc. (Danvers, MA) and used at a 1:1000 dilution according to manufacturer's instructions: BCL-2 (#4223), Bcl-xL (#2764), Bcl-w (#2724), Mcl-1 (#4572), Bim (#2933), Bad (#9239), Bid (#2006), β -actin (#4967), mTOR (#2972), p-mTOR S2448 (#2971), rictor (#2114), raptor (#2280), Akt (#4691), p-Akt S743 (#4060), p-Akt T308 (#9275), Puma (#12450), VEGF-B (#2463), S6 (#2217), p-S6 S235/6 (#4858), BAK (#6947), BAX (#2774), G β L (#3274), cytochrome c (#4272), VDAC (#4661), SDHA (#5839) cleaved-Parp (#9541), 4E-BP1 (#9452), p-4E-BP1 T37/46 (#9459), and eIF4E (#2067). Primary antibodies to NOXA (Imgenex; IMG-349A), VEGF-A (Abcam; ab51745), CXCR4 (ab58176), GAPDH (Santa Cruz; sc-25778) and FKBP8 (sc-166607) were used at a 1:500 dilution. Anti-mouse or anti-rabbit HRP-conjugated secondary antibodies (GE Healthcare) were used at a 1:5000 dilution. Blots were stripped and re-probed using standard techniques. All western blot film images were cropped to show adequate bandwidth above and below relevant bands; where western panels are shown, loading control bands were confirmed to be similar across multiple blots.

SCLC Patient-Derived Xenograft (PDX) models and dosing

All *in vivo* experiments were performed in accordance with protocols approved by the Johns Hopkins University Animal Care and Use Committee. The LX33 and LX48 PDXs were isolated and passaged as previously described (Daniel et al., 2009; Hann et al.; Poirier et al., 2013). LX47 PDXs were passaged as tumor tissue sections (~2-3 mm) coated in Matrigel™ and implanted via subcutaneous flap incisions. All treatment experiments were performed in female C.B-17 scid mice, 4-6 weeks old at time of PDX

injection/implantation (Taconic; C.B-*Igh-1^b/IcrTac-Prkdc^{scid}*). The LX33 and LX47 PDXs were derived from chemotherapy-naïve SCLC patients and the LX48 PDX from a patient previously treated with platinum plus etoposide. Tumor volumes were calculated from manual caliper measurements with an ellipsoid formula where volume (mm³) = (xy²)/2. Once tumor volumes reached ~150 mm³, mice were randomized to treatment arms and treated daily via intraperitoneal (IP) injections with vehicles, ABT-737 (100 mg/kg), rapamycin (20 mg/kg), etoposide (12 mg/kg on days 1, 4 and 9) or combinations of two agents.

RNA isolation and genome-wide transcriptional profiling

Total RNA was prepared using an RNeasy Mini Kit (Qiagen) with on-column DNase I digestion. RNA quality was assessed with a Nanodrop-1000 for OD260/280 and OD260/230 ratios and an Agilent 2100 Bioanalyzer. Total RNA (500 ng) from each sample was amplified and labeled using an Illumina® TotalPrep™ RNA amplification kit according to manufacturer's protocol (Ambion). Biotinylated RNA (750 ng) was combined with hybridization buffer and hybridized to HumanHT-12 v4 Expression BeadChip arrays (Illumina®) for 16-20 h at 58 °C. Arrays were washed at 55 °C and blocked at 25 °C. Bound biotinylated RNA was stained with streptavidin-Cy3 and washed. Dried arrays were protected from light until scanning with an iScan System. Data were extracted using the Gene Expression Module in GenomeStudio Software.

Gene expression analysis

Using the Bioconductor suite for R (Gentleman et al., 2004) and the limma package (Smyth, 2005), raw gene expression data were quantile normalized, then log-2 transformed. Differentially expressed genes were identified by fitting a linear model for

each feature. Standard errors of log-2 transformed changes were moderated using an empirical Bayesian approach. For each feature, moderated t statistics, B statistics, raw and adjusted p values (corrected for multiple testing by the Benjamini and Hochberg method) were calculated. Permutation based gene set enrichment was performed using GSEA, a sample permutation-based method, and CAMERA, a competitive gene set testing method that accounts for inter-gene correlation (Mootha et al., 2003; Wu and Smyth, 2012). The gene set database used was MSigDB 3.1 from the Broad Institute (Subramanian et al., 2005).

Hematology

Whole blood was collected immediately following cervical dislocation in C.B-17 scid mice via cardiac puncture using tuberculin syringes flushed with 1M EDTA, immediately transferred to K₂EDTA lavender tubes (BD microtainer®) and stored at 4 °C for less than 24 h before analysis. Complete blood count with differential parameters were measured on a Hemavet 950FS (Drew Scientific) at the Johns Hopkins Phenotyping Core

Statistical analysis of drug efficacy experiments

All animal data are reported as average tumor volumes +/- standard deviation (SD). Tumor volume comparisons between treatment groups utilized data from weekly time points using a two-sided Student's t test; throughout the text unless indicated: *, $p < 0.01$ and **, $p < 0.001$. All graphs in figures were created using GraphPad Prism 6.0c (GraphPad Software, Inc.). Figures for drug combination matrix outputs and drug synergy were created in R, as previously reported (Lehar et al., 2009).

Results

Treatment with ABT-737 results in short-lived tumor responses and is associated with a decrease in HIF-1 α transcripts.

We previously reported that ABT-737 had limited activity alone and in combination with etoposide in SCLC PDXs that express low levels of BCL-2 (Hann et al., 2008). To further assess the activity of ABT-737 in a more representative set of PDXs, we extended these studies to include three BCL-2 expressing SCLC PDX models - LX44, LX47 and LX48 – as well as a SCLC PDX model that does not express appreciable BCL-2 for historic control (LX33). Treatment with ABT-737 resulted in modest anti-tumor activity with statistically significant tumor growth inhibition (TGI) in LX47 and LX48, but minimal effects in LX44 and LX33 over a period of 3 weeks where ABT-737 was administered daily (**Figure 20A**). As shown in **Figure 20B**, all PDX models express other anti-apoptotic targets of ABT-737, as well as MCL-1. Treatment with ABT-737 was more effective than etoposide, a standard of care therapeutic agent for SCLC. Of great important to this study, the addition of etoposide to ABT-737 did not improve responses in a chemo-naïve/sensitive model (LX47) nor a chemo-resistant/treatment-experienced model (LX48). Further, this combination appeared to be poorly tolerated by mice as evidenced by weight loss while on treatment (**Figures 21A, B**). Notably, we observed that responses to ABT-737 in these PDXs were short-lived – minimal regressions during continuous treatment progressed at growth rates comparable to vehicle-treated tumors after treatment discontinuation.

To investigate potential acute resistance mechanisms to ABT-737 we selected LX47 and LX48 for further characterization of responses. We hypothesized that during tumor response, a sensitivity signature may exist and precede tumor outgrowth in such

models. Using whole genome transcriptional profiling, we compared the gene expression profiles of tumors from vehicle and ABT-737-treated mice collected at points of maximal response (**Table 6**). Transcriptional profiling results comparing ABT-737-treated to vehicle-treated tumors revealed that some of the most differentially expressed genes were well-established HIF-1 α transcriptional targets, such as *LDHA* and *BNIP3L* (**Figure 20D** and **Table 7**). Gene set enrichment analysis (GSEA) revealed that HIF-1 α gene sets comprised the majority of the most statistically significant gene sets down regulated in ABT-737-treated tumors (**Table 8**). To further illustrate the changes observed in HIF-1 α transcripts we generated an MA plot to visualize how genome-wide transcriptional profiling data from the ABT-737-treated PDX models compared to a benchmark HIF-1 α regulated gene set (Elvidge et al., 2006). Many transcripts that are normally up regulated by hypoxia (**Figure 20D** bottom; *green*) were decreased upon ABT-737 treatment, whereas transcripts down regulated by hypoxia (**Figure 1D** bottom; *magenta*) were unchanged. There are data supporting that ABT-737 is more effective under hypoxic conditions *in vitro* as well as *in vivo* and that hypoxia is a negative regulator of MCL-1 half-life (Harrison et al., 2011; Klymenko et al., 2011). We did not observe changes in MCL-1 transcript or protein levels during acute treatments with ABT-737 in LX47 or LX48. While transcriptional profiling data suggested that ABT-737-treated tumors lack expression of hypoxia induced genes, pimonidazole staining to assess regions of physiological hypoxia at time points within the window of maximal response to ABT-737 revealed no appreciable difference between treatment groups (**Figure 20E**).

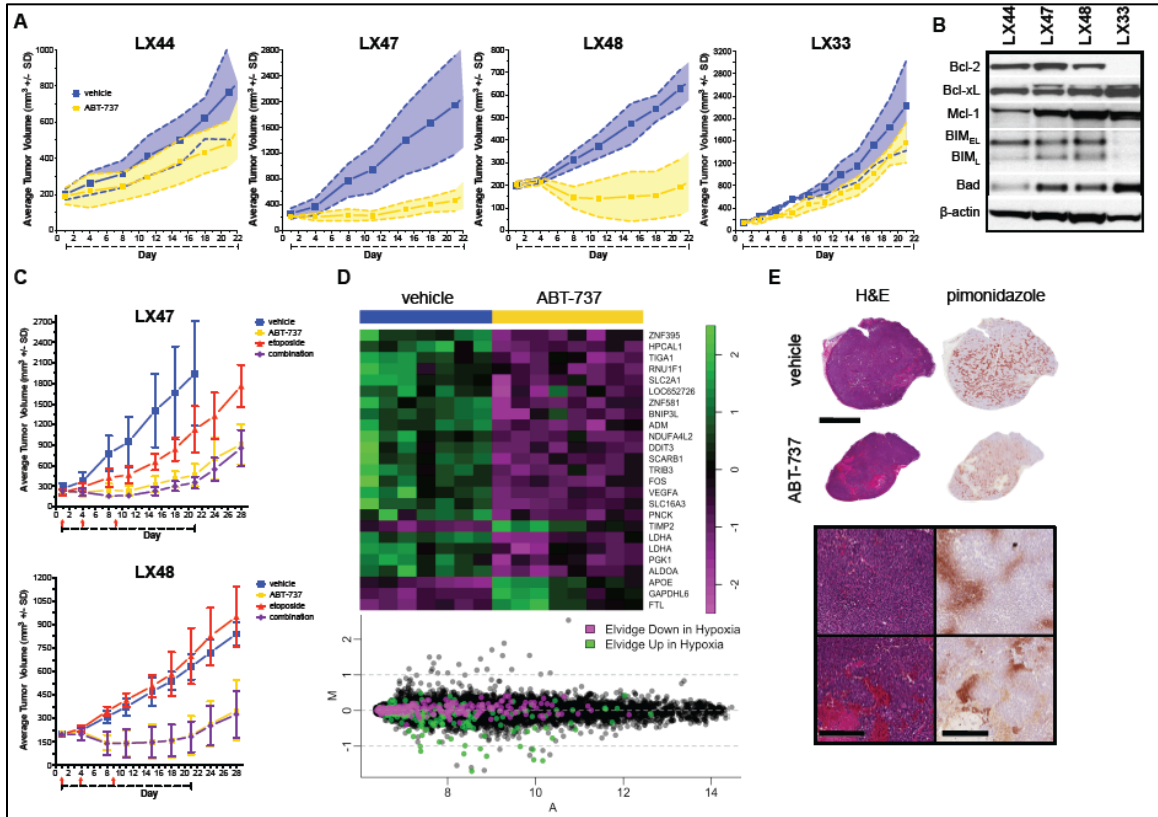


Figure 20. Responses to ABT-737 in PDX models of SCLC are short-lived and progression is preceded by a decrease in HIF-1 α transcripts.

(A) Tumor response curves in three Bcl-2 expressing (*left-to-right*; LX44, LX47 and LX48) and one Bcl-2 non-expressing (LX33) SCLC PDX models treated with ABT-737 or vehicle. Dashed line along x-axis indicates duration of treatment (21 days) with shaded area corresponding to standard deviation from the indicated averages; n=5-6 mice per arm.

(B) Western blot for protein expression of select Bcl-2 family members in PDX models used in this study. PDX tumor lysates were prepared from banked tumor tissue that had been propagated in untreated NOD scid mice without evidence of tumor necrosis. β -actin provided for loading control.

(C) Response of Bcl-2 expressing SCLC PDX models LX47 (*top*) and LX48 (*bottom*) to etoposide, ABT-737 or the combination of agents.

(D) Heatmap visualization of differentially expressed (log₂) genes between paired ABT-737 (*yellow*) and vehicle-treated (*blue*) tumors from LX47 and LX48 tumors at points at or before maximal response. Below, an MA plot for the distribution of select HIF-1 α responsive genes (e.g. "Elvidge Hypoxia" gene set) as a function of ABT-737 treatment in LX47 and LX48.

(E) Representative H&E and pimonidazole IHC of whole LX48 tumor capsules at the point of maximal response to ABT-737, paired with vehicle counterparts (n=3 tumors per arm); scale bar is 3 mm (*above*) or 200 μ m (*below*).

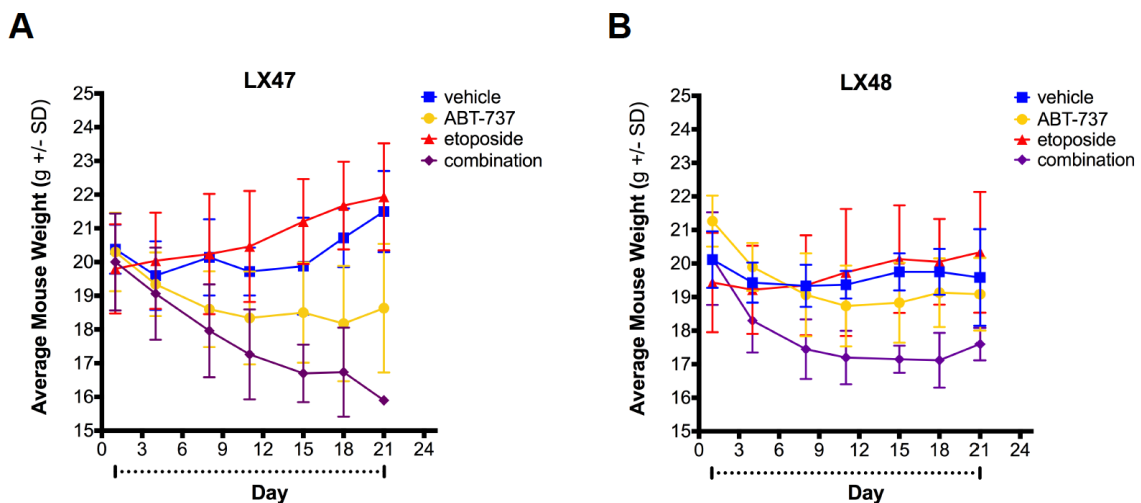


Figure 21. Combining ABT-737 with etoposide is not well tolerated *in vivo*.

Average mouse weights \pm standard deviation for (A) LX47 and (B) LX48 while on study treated with ABT-737, etoposide or the combination of ABT-737 and etoposide. Dashed lines indicate treatment period duration (21 days). Two of six mice in the combination arm that had lost weight in excess of 20% of starting body weight were euthanized at days 15 and 18 per protocol.

Table 6. Description of ABT-737 treatment collection time points in PDXs.

Mouse tag#	Age at engraftment	PDX Line	Treatment	Timepoint	Description
384	4-6wks	JHU-LX47	ABT-737	D4	Time of maximal response
368	4-6wks	JHU-LX47	ABT-737	D8	Time of maximal response
370	4-6wks	JHU-LX47	ABT-737	D8	Time of maximal response
377	4-6wks	JHU-LX47	ABT-737	D8	Time of maximal response
376	4-6wks	JHU-LX47	Control	D4	Matched control for D4 ABT-737 tumors
378	4-6wks	JHU-LX47	Control	D8	Matched control for D8 ABT-737 tumors
380	4-6wks	JHU-LX47	Control	D8	Matched control for D8 ABT-737 tumors
840	4-6wks	JHU-LX48	ABT-737	D12	Time of maximal response
844	4-6wks	JHU-LX48	ABT-737	D12	Time of maximal response
906	4-6wks	JHU-LX48	ABT-737	D12	Time of maximal response
914	4-6wks	JHU-LX48	ABT-737	D12	Time of maximal response
829	4-6wks	JHU-LX48	Control	D12	Matched control for D12 ABT-737-treated tumor
831	4-6wks	JHU-LX48	Control	D12	Matched control for D12 ABT-737-treated tumor
912	4-6wks	JHU-LX48	Control	D12	Matched control for D12 ABT-737-treated tumor
916	4-6wks	JHU-LX48	Control	D12	Matched control for D12 ABT-737-treated tumor

Table 7. Top 20 differentially expressed genes in ABT-737 treated tumors.

Gene ID	logFC	AveExpr	t	P.Value	adj.P.Val	Beta-statistic
<i>LDHA</i>	-0.692	11.820	-8.019	0.00000052	0.025	3.365
<i>VEGFA</i>	-0.729	7.220	-6.922	0.00000337	0.040	2.438
<i>ALDOA</i>	-0.719	10.634	-7.207	0.00000204	0.040	2.697
<i>ZNF581</i>	-0.428	8.331	-7.033	0.00000277	0.040	2.540
<i>PGK1</i>	-0.536	10.911	-6.651	0.00000547	0.043	2.179
<i>SLC16A3</i>	-0.518	6.820	-6.727	0.00000477	0.043	2.252
<i>ADM</i>	-1.283	8.886	-6.427	0.00000822	0.049	1.955
<i>TIGA1</i>	-0.720	9.294	-6.429	0.00000820	0.049	1.956
<i>HPCAL1</i>	-0.294	9.403	-6.228	0.00001188	0.062	1.748
<i>SCARB1</i>	-0.880	7.809	-6.074	0.00001585	0.068	1.584
<i>ZNF395</i>	-0.486	9.585	-6.078	0.00001575	0.068	1.588
<i>LDHA</i>	-0.768	11.510	-5.718	0.00003130	0.123	1.187
<i>BNIP3L</i>	-0.497	8.586	-5.629	0.00003719	0.135	1.085
<i>NDUFA4L2</i>	-1.541	8.208	-5.493	0.00004848	0.143	0.925
<i>TRIB3</i>	-0.628	7.610	-5.502	0.00004766	0.143	0.935
<i>TIMP2</i>	1.326	7.680	5.546	0.00004374	0.143	0.987
<i>SLC2A1</i>	-1.093	9.941	-5.362	0.00006273	0.148	0.768
<i>FOS</i>	-1.005	7.377	-5.388	0.00005964	0.148	0.799
<i>LOC652726</i>	-0.486	8.368	-5.365	0.00006239	0.148	0.771
<i>APOE</i>	2.536	10.748	5.376	0.00006105	0.148	0.785

Table 8. Gene Set Enrichment Analysis (GSEA) in ABT-737 treated tumors.

Gene Set	Size	ES	NES	FDR q-val	FWER p-val
GNF2_RAB7L1	32	-0.61147	-2.05170	0.00460	0.00400
WIERENGA_STAT5A_TARGET S_GROUP1	133	-0.58572	-1.64160	0.03489	0.66100
SHAFFER_IRF4_TARGETS_IN_ MYELOMA_VS_MATURE_B_LY MPHOCYTE	100	-0.56319	-1.64280	0.03502	0.65800
WINTER_HYPOXIA_METAGEN E	234	-0.61176	-1.65100	0.03515	0.62500
HELLER_HDAC_TARGETS_SIL ENCED_BY_METHYLATION_D N	268	-0.53805	-1.64360	0.03517	0.65700
KEGG_STEROID_BIOSYNTHES IS	16	-0.77407	-1.65180	0.03545	0.62500
BIOCARTA_NGF_PATHWAY	18	-0.66795	-1.64380	0.03567	0.65700
HEART_DEVELOPMENT	37	-0.49252	-1.65240	0.03587	0.62400
REACTOME_GLUCONEOGENE SIS	32	-0.66656	-1.64800	0.03589	0.63400
ELVIDGE_HYPOXIA_UP	166	-0.69536	-1.67320	0.03608	0.57100
GROSS_HYPOXIA_VIA_ELK3_ ONLY_UP	33	-0.66746	-1.65790	0.03621	0.60700
FLOTHO_PEDIATRIC_ALL_THE RAPY_RESPONSE_UP	53	-0.58118	-1.65450	0.03623	0.61400
BIOCARTA_IL6_PATHWAY	22	-0.64319	-1.64390	0.03625	0.65600
ELVIDGE_HYPOXIA_BY_DMOG _UP	126	-0.71961	-1.65560	0.03629	0.61000
QI_HYPOXIA	133	-0.65194	-1.65250	0.03656	0.62400
VARELA_ZMPSTE24_TARGETS _UP	40	-0.58802	-1.64460	0.03664	0.65300
THEODOROU_MAMMARY_TU MORIGENESIS	31	-0.47996	-1.67350	0.03683	0.57100
MOOHTA_GLUCONEOGENESI S	31	-0.68032	-1.65820	0.03690	0.60700
ADDYA_ERYTHROID_DIFFERE NTIATION_BY_HEMIN	71	-0.58878	-1.63600	0.03706	0.67800
ELVIDGE_HIF1A_AND_HIF2A_T ARGETS_DN	101	-0.75498	-1.65970	0.03708	0.60300

A rapamycin signature is predicted to connect with ABT-737 response and shows synergy with ABT-737 in vitro

To identify agents or pathways that are associated with responses to ABT-737 in BCL-2 expressing PDX models, we queried the Broad Institute's publicly-available Connectivity Map database (cMap build 2.0) using the most significantly differentially expressed genes between control and ABT-737-treated tumors (Table 7). The cMap database attempts to connect gene expression data to chemical perturbation by cataloging gene expression changes that result from exposures to bioactive compounds *in vitro* (Lamb et al., 2006). This approach is advantageous in the setting of data from whole genome profiling experiments where the contributions of individual transcripts may not hold clear significance to an overarching pathway or group of pathways being affected, and thus it provides more generalizable strategies to affect an observed profile. Several of the highest scoring bioactive compounds identified by our cMap query to align with an ABT-737 response were inhibitors of the PI3K/mTOR pathway (**Table 9**) – pathways known to regulate and interact with HIF-1 α (Laplante and Sabatini, 2012).

Taken together with literature supporting the combined effect of PI3K/mTOR and BCL-2 inhibition in other tumor types (Ackler et al., 2008; Muranen et al., 2012; Rahmani et al., 2013; Vaillant et al., 2013) and the mounting evidence for rationally co-targeting growth and survival pathways, we tested the combination of rapamycin and ABT-737 in two SCLC cell lines that express high levels of BCL-2 (NCI-H146 and NCI-H187) and two lines that do not express appreciable BCL-2 (NCI-H82 and NCI-H446) (Oltersdorf et al., 2005). As expected, treatment with ABT-737 resulted in dose-dependent decreases in viability in lines that express BCL-2 with little effect on lines that do not express BCL-2 (**Figure 22A**). BCL-2 expressing lines were also more sensitive than non-BCL-2 expressing lines to rapamycin. This effect was not dose-dependent after 72 hours of

exposure in the dose ranges studied (low nanomolar to micromolar) and we confirmed this trend in a larger set of SCLC cell lines (**Figure 23A**). Combining increasing doses of ABT-737 with 100 nM rapamycin had minimal effect on low expressing BCL-2 lines, but was at least additive in BCL-2 expressing lines. However, treating ABT-737-sensitive cell lines with 100 nM rapamycin for 24 or 72 hours prior to exposure to ABT-737 did not dramatically alter the sensitivity of these lines to ABT-737 (**Figure 22B**), suggesting that rapamycin does not acutely sensitize cell lines to ABT-737.

To demonstrate whether the combined effect of rapamycin and ABT-737 was synergistic, we focused on two cell lines that differed in their expression of BCL-2 (NCI-H146 and NCI-H82) and treated cells with ABT-737 and drugs targeting PI3K (wortmannin, LY294002), mTOR (rapamycin, everolimus, AZD8055) or both (BEZ235), selected based on our cMap results (**Figures 23B, C**). Using broad dose combinations we quantitatively calculated synergy for each drug combination across a range of doses using the method of Chou and Talalay and a non-constant ratio approach (Chou and Talalay, 1984). Representative dose-matrix outputs for the combination of ABT-737 and rapamycin in NCI-H82 (*above*) and NCI-H146 (*below*) are shown in **Figure 22C**. The agents studied had varying potency that generally segregated by inhibitor class (Figure 2D). Synergism in NCI-H146 is summarized in **Figure 22E** by plotting the combination index (CI) as a function of fraction affected (Fa) (Chou, 2010). For example, wortmannin showed no synergy at any dose, while all other compounds showed quantitative synergism. The mTOR inhibitors rapamycin and everolimus displayed strong synergism over a wide dose-response range. We felt that these data warranted testing rapamycin in combination with ABT-737 *in vivo*.

Table 9. Top 20 connectivity map (cMAP) hits for ABT-737 treatment signature.

rank	cMAP compound	mean	n	enrichment	p-value	specificity
1	monorden	0.212	22	0.572	0	0.0107
2	sirolimus	0.278	44	0.428	0	0.1145
3	LY-294002	0.267	61	0.423	0	0.094
4	quinisocaine	-0.601	4	-0.87	0.00058	0
5	dosulepin	-0.649	4	-0.85	0.00095	0
6	thapsigargin	-0.751	3	-0.913	0.00116	0.0774
7	apramycin	0.511	4	0.818	0.00195	0
8	clemizole	-0.539	5	-0.724	0.00344	0
9	pipemidic acid	0.49	3	0.871	0.00391	0.0159
10	diphepanil metilsulfate	-0.247	5	-0.712	0.00425	0.014
11	ionomycin	-0.577	3	-0.868	0.00453	0.0246
12	fluticasone	-0.607	4	-0.783	0.00454	0.0191
13	AR-A014418	0.438	3	0.849	0.00645	0.028
14	trihexyphenidyl	-0.621	3	-0.851	0.00651	0.015
15	16-phenyltetranorprostaglandin E2	0.31	4	0.75	0.0076	0
16	methoxamine	-0.436	4	-0.749	0.0079	0.0258
17	flumetasone	-0.31	6	-0.627	0.00842	0.0198
18	wortmannin	0.177	18	0.375	0.00859	0.3355
19	simvastatin	-0.469	4	-0.74	0.00891	0.0133
20	thiamazole	-0.425	6	-0.62	0.00963	0.0368

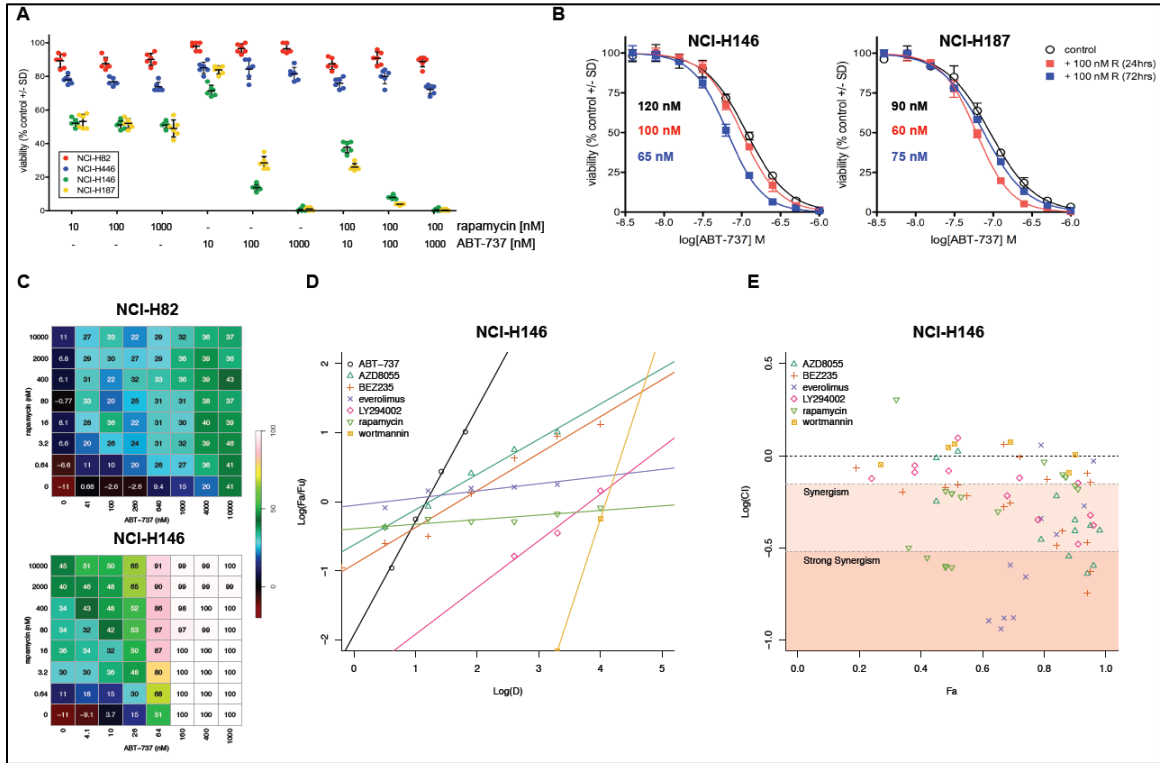


Figure 22. Rapamycin has potent *in vitro* synergy with ABT-737.

(A) Effect of single agent ABT-737 or rapamycin and fixed dose combinations on cell viability after a 72 h exposure in Bcl-2 high (NCI-H146 and NCI-H187) and Bcl-2 low (NCI-H82 and NCI-H446) SCLC cell lines; individual data points are shown +/- SD, n=6.

(B) Changes in ABT-737 sensitivity in NCI-H146 and NCI-H187 pre-treated with 100 nM rapamycin for 24 h (red) or 72 h (blue) before an overnight (~16 h) exposure to ABT-737; n=6 per data point. IC₅₀ values are shown for control (black) and rapamycin (24 h – red; 72 h – blue) pre-treatment traces.

(C) ABT-737 and rapamycin dose combination-response output matrices for the Bcl-2 low SCLC cell line NCI-H82 (above) and the Bcl-2 high SCLC cell line NCI-H146 (below). Color gradient of percent maximal possible response is shown on right.

(D) Fractional effect versus dose plot of ABT-737 and several mTOR (AZD8055, everolimus, rapamycin), PI3K (LY294002, wortmannin) and dual PI3K/mTOR (BEZ235) inhibitors in NCI-H146; data are representative of results obtained from multiple (>3) experiments.

(E) Combination Index (CI) versus fractional effect plot (“synergy plot”) for NCI-H146 treated with ABT-737 in combination with compounds described above. Levels of *in vitro* synergy are indicated using cutoffs described by others.

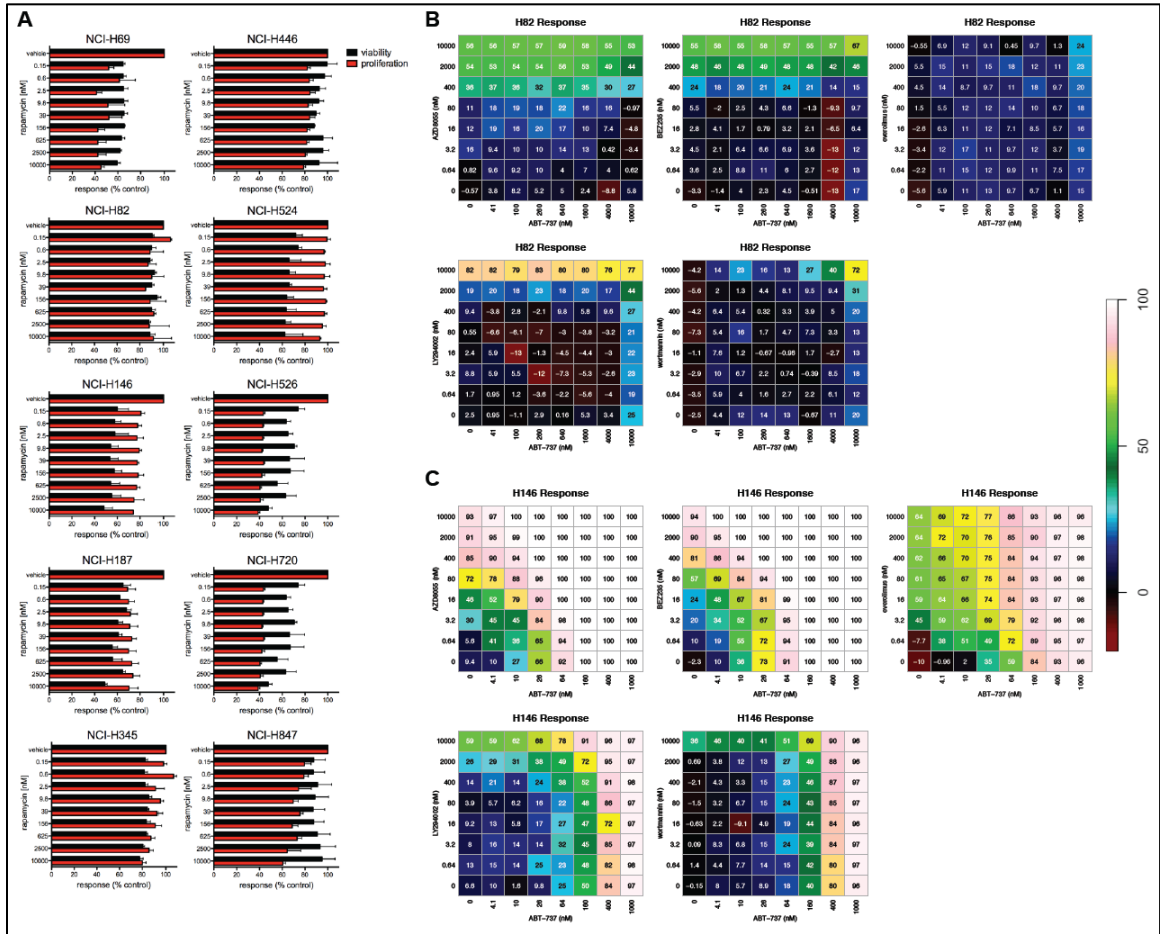


Figure 23. Rapamycin displays non-monotonic efficacy across a broad range of SCLC cell lines.

(A) Normalized responses in 10 SCLC cell lines exposed to rapamycin for 72 h as measured by viability (*black*) or proliferation (*red*); n=6 per data point with error bars showing standard deviation from the mean. Rapamycin concentrations were between ~150 picomolar and 10 micromolar. Synergy matrix outputs of proliferation measures in (B) NCI-H82 and (C) NCI-H146 exposed to dose combinations for 72 h. Top panels y-axes (left-to-right): AZD8055, BEZ235 and everolimus. Bottom panels y-axes (left-to-right): LY294002 and wortmannin. ABT-737 dilution series in NCI-H82 began at 10 uM (1 uM for NCI-H146) and was diluted 2.5-fold, covering a ~243-fold concentration range. All compounds tested in combination with ABT-737 began at 10 uM and were diluted 5-fold, covering a ~15,000-fold concentration range. Matrices of the paired 49 dose-combinations are scaled according to percent response, with a color gradient legend provided on the far right.

Rapamycin has combinatorial activity with ABT-737 in multiple SCLC PDX models

We next assessed the combination of ABT-737 and rapamycin in the same PDXs where we observed acute resistance to ABT-737 – LX47 and LX48 – as well as in a SCLC PDX that does not express appreciable BCL-2 protein (LX33) that we previously reported had little response to ABT-737 (Hann et al., 2008). All PDX models examined express PI3K/mTOR pathway components and exhibit pathway activation as demonstrated by basal levels of phospho-Akt (S473), phospho-4E-BP1 (T37/46) and phospho-ribosomal protein S6 (S235/6) (**Figure 24A**). In both BCL-2 expressing PDXs, treatment with either ABT-737 or rapamycin caused significant TGI and the combination of ABT-737 and rapamycin caused fairly rapid tumor regressions. Importantly, these responses were sustained well beyond the 14-day treatment period, with no detectable tumor masses in LX47 PDXs for several weeks after combination treatment was discontinued, though tumors eventually returned (*data not shown*). Consistent with our previous report, treatment of LX33 PDXs with ABT-737 did not affect tumor growth. Treatment of LX33 with rapamycin resulted in TGI and the addition of ABT-737 to rapamycin caused a modest increase in TGI over rapamycin alone (**Figure 25C**). While this combined effect lost statistical significance after one week of treatment, these data suggests there was some degree of combinatorial activity in the absence of high BCL-2 expression.

Mice tolerated the combination well, with no apparent weight loss across all 3 PDX models (**Figure 24B**). As both ABT-737 (Harper and Poole, 2012; Schoenwaelder et al., 2011) and rapamycin (Aslan et al., 2011) are known to affect platelets, we assessed hematologic measures in mice bearing LX47 after 7 days of treatment. Platelet counts in ABT-737 treated mice were significantly lower than those of vehicle-treated mice as expected; however, hematologic parameters from combination treated mice

were similar to vehicle and rapamycin alone (**Figure 25D**). All animals that received rapamycin were slightly anemic (**Figure 24C**). Histologically, tumors from mice treated with ABT-737 or combination exhibited greater necrosis than did vehicle or rapamycin treated tumors as evidenced by H&E sections showing increased eosinophilic regions throughout the tumor core (**Figure 25E**; *ABT-737 H&E section*). Pimonidazole staining of tumors from each treatment arm showed consistent, detectable hypoxic regions in all samples except tumors treated with combinatorial therapy. This striking difference was observed in multiple tumors treated with combination at early (after 3 days) and later (after 7 days) time points. Because this combination appeared to be well tolerated, we tested whether we could obtain similar tumor regressions in LX47 PDXs previously exposed to either ABT-737 or rapamycin. We observed tumor volume reductions of ~50% with two weeks of ABT-737 and rapamycin that were sustained after treatment discontinuation, adding strength to the potential utility of this combination (**Figure 25F**).

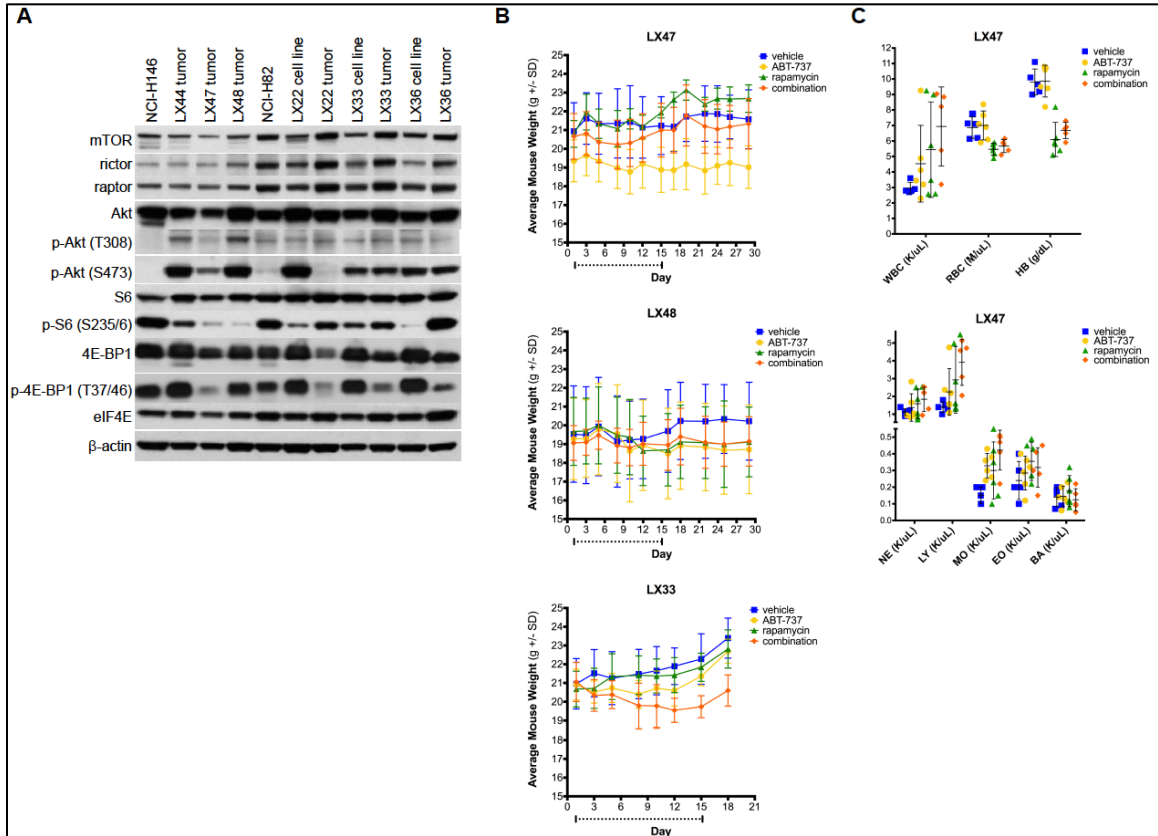


Figure 24. Combining rapamycin with ABT-737 (R+ABT) *in vivo* is well tolerated.

(A) Western blots for protein expression of several components of the mTOR signaling pathway in cell lines or PDX models used in this study or previous studies. Mouse weights monitored while on single agent and combination treatment for PDX models

(B) LX47, LX48 and LX33 as shown in Figure 22. Mice were weighed every 3 days before receiving treatment or more frequently if there were signs of distress. Treatment duration is indicated with a dashed line as in Figure 22; n=5-6 mice per arm. Effect of treatment arms on hematologic measures

(C) in C.B-17 scid mice with LX47 hind flank tumors and treated for one week with indicated arms; n=5-6 per arm. The following abbreviations were used: platelets (PLT), white blood cells (WBC), red blood cells (RBC), hemoglobin (HB), neutrophils (NE), lymphocytes (LY), monocytes (MO), eosinophils (EO).

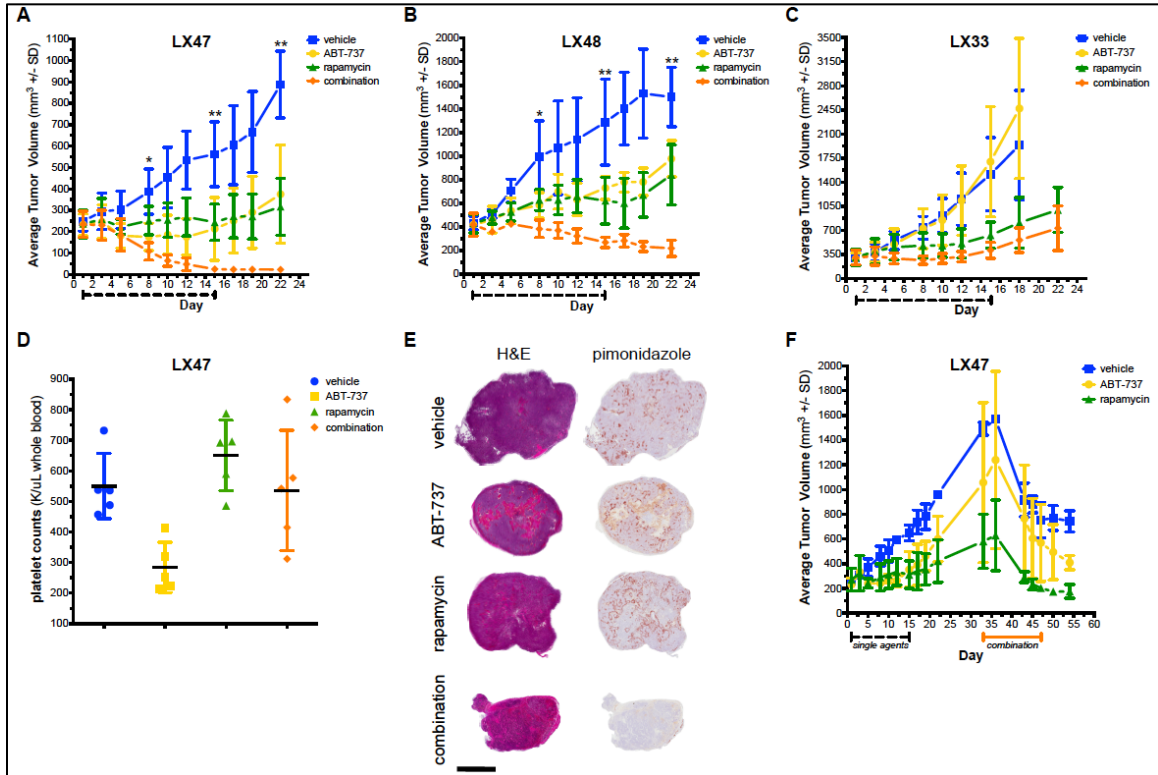


Figure 25. Combining rapamycin with ABT-737 (R+ABT) provides durable responses in SCLC PDXs that express BCL-2.

Tumor response curves to single agent ABT-737, rapamycin and combination in (A) LX47, (B) LX48, (C) and LX33 PDXs; n=5-6 mice per arm. Dashed lines indicate treatment periods (14 days). Statistical comparisons of tumor volumes in combination treatment groups versus all other arms were performed at days 8, 15 and 22; where indicated, *p<0.01, **p<0.001.

(D) Effect of treatment arm on platelets counts in whole blood obtained by cardiac puncture in C.B.-17 scid mice bearing LX47 hind flank tumors that were treated for one week with indicated arms; n=5 per arm. Blood was collected 24 hours after last dose.

(E) Representative paired H&E and pimonidazole IHC from whole LX48 tumor capsule sections treated with indicated arms (y-axes) for 7 days; n=3-4 tumors were analyzed per arm. Tumors were collected 24 hours after final dose; scale bar is set to 3 mm.

(F) Combination arm challenge in LX47 previously treated with single agent ABT-737 or rapamycin. LX47-bearing mice that were initially treated for 14 days with indicated single agents (*dashed line*) were subsequently treated at day 34; n=2 per previous treatment group. Combination treatments were performed for 14 days (*solid orange line*) and then tumor volumes were monitored for an additional week. Mice did not receive any treatment between days 15 and 32. Body weights were not significantly different while on combination treatment, nor did they differ by previous treatment arm.

Rapamycin induces expression of HIF-1 α targets in SCLC PDXs

To study the effects of rapamycin alone or in combination with ABT-737 on HIF-1 α targets, we compared protein and message expression in LX47 and LX33 PDXs after 7 days of treatment. In LX33, there was a notable decrease in tumor levels of HIF-1 α protein and several HIF-1 α targets such as CXCR4, Glut1 and VEGF-A in ABT-737-treated compared to vehicle-treated mice (**Figure 26A**). Treatment with rapamycin increased the protein levels of most targets examined; however, these changes were less evident in LX47. In LX47, but not LX33, combination treatment resulted in significant decreases in HIF-1 α , HIF-1b, LDHA and CXCR4 levels. One reason for these observations may relate to differences in tumor response: combination-treated LX47 tumors lose >70% of their starting volume by day 7, which may complicate analysis of protein samples.

Correlating these findings with transcriptional profiling data, we observed decreased levels of six HIF-1 α regulate genes in LX47 after treatment with ABT-737 (**Figure 26B**); this effect was less pronounced in LX33, but nonetheless, observed for most genes. Interestingly, rapamycin increased transcript levels of all highlighted genes. In the combination arm, levels of nearly all transcripts were less than vehicle controls, and in some cases (i.e. VEGF-A in LX33) lower than ABT-737 treated groups.

While this paired analysis of changes highlighted several similarities in the few targets examined, we sought to better understand whether there was a more general transcriptional response to ABT-737. This led us to examine the overall concordance between gene expression changes observed in LX33 and LX47 in response to ABT-737, as treatment influenced protein and transcript levels in these SCLC PDXs independent of BCL-2 expression. We generated a concordance at the top (CAT) plot to compare drug treatment effects in each model (Irizarry et al., 2005). This plot relates the

concordance between the top differentially expressed gene lists of n length for each model compared to what would be expected by chance. The ABT-737 treatment signature was more concordant than rapamycin alone, combination treatment, or what would be expected by chance (**Figure 26C**). These results were surprising, as we anticipated that there would have been a more pronounced concordance between models treated with rapamycin than ABT-737, as the effects on HIF-1 α regulated genes were similar in the rapamycin-treated groups as compared to the ABT-737-treated groups. One potential explanation could be that this ranked approach does not account for the magnitude of gene expression differences, nor does it weigh p values for each comparison.

The differences observed prompted further investigation into how the mTOR pathway was affected in these two models. In LX33, treatment with ABT-737 decreased protein levels of several mTOR components, including near complete loss of G β L by western blot (**Figure 26D**). This may reflect the extent to which the mTOR pathway is influenced by HIF-1 α in this PDX model, as we observed a similar loss of HIF-1 α and HIF-1 β /ARNT in LX33. In both PDXs, treatment with rapamycin – alone or in combination with ABT-737 – decreased levels of phospho-Akt (S473) versus the vehicle controls; this effect was most pronounced for the combination treatment in LX33. While we observed mTOR inhibition at the level of Akt, the levels of phospho-ribosomal protein S6 differed between rapamycin-treated groups, but were similar between combination treatment groups. This difference may reflect the degree of Akt feedback that is present when treating with rapamycin alone or in combination with ABT-737 (O'Reilly et al., 2006). Indeed, levels of phospho-Akt (T308) in LX47 treated with rapamycin appear to be elevated as compared to vehicle, but not in the context of the combination (**Figure 26D**).

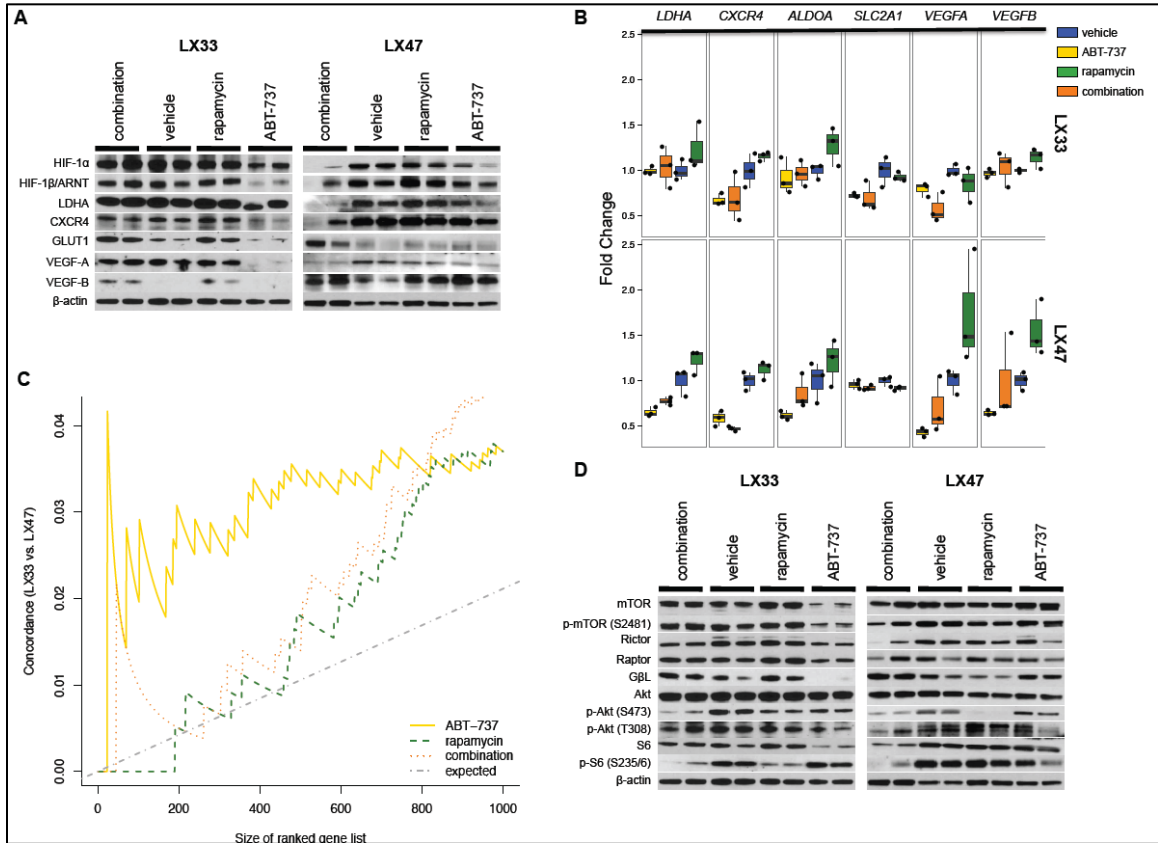


Figure 26. R+ABT differentially affects HIF-1 α regulated genes and the mTOR pathway in LX33 and LX47.

(A) Western blot for protein expression of select HIF-1 α regulated genes implicated from Figure 1 in PDX models LX33 and LX47 after one week of treatment; n=3-4 mice per arm with duplicates reflecting the extent of variability within a group. β -actin provided for loading control.

(B) Select gene expression fold changes (*y-axis*) between treatment arms in LX33 and LX47 treated as above; n=3 mice per arm.

(C) Concordance at the top (CAT) plot shows that a common set of genes are differentially expressed in LX33 and LX47 in response to ABT-737 after one week of treatment.

(D) Western blot for select protein expression in the PI3K/mTOR pathway in PDX models LX33 and LX47 after one week of treatment.

Rapamycin blocks ABT-737 induced decrease in BAX protein levels in SCLC

In parallel, we looked at protein expression of candidate BCL-2 family members in LX33 and LX47 PDXs at day 7 by western blot. We did not observe consistent changes in protein levels of previously reported determinants of ABT-737 sensitivity (MCL-1 or pro-apoptotic proteins Puma and Noxa) that correlated with response in our PDXs models. However, we did observe that the pro-apoptotic proteins BAX and BAK were increased in both PDXs treated with rapamycin alone or in combination with ABT-737 (**Figure 27A**).

As ABT-737 is known to cause programmed cell death in a BAX/BAK-dependent manner, and BAX is a key pro-apoptotic binding partner of BCL-2 (van Delft et al.), we assessed the effect of ABT-737 or rapamycin on BAX protein levels *in vivo*. For these analyses we selected LX33 that allowed for more control in size matching tumor volumes across treatment groups. We treated mice bearing LX33 for 7 days with vehicle, escalating doses of ABT-737 (5, 25 and 100 mg/kg), escalating doses of rapamycin (1, 5, and 20 mg/kg) or the combination of the highest doses of each agent. We observed a modest, but dose-dependent decrease in BAX protein from tumors treated with ABT-737 and an overall increase in BAX protein in tumors treated with rapamycin (**Figure 27B**). This change was also observed in heavy membranes isolated from tumors, enriching for mitochondria. Although we had small numbers of mice per dose-escalation group, we noted that all rapamycin doses caused TGI to a similar degree, consistent with our *in vitro* data (**Figure 28A**). We also observed an increase in the anti-apoptotic proteins Bcl-xL and Bcl-w with increasing doses of rapamycin (**Figure 27B**). Levels of MCL-1 protein were not significantly decreased by rapamycin *in vivo*, where MCL-1 levels were actually greater in combination-treated tumors (**Figure 28B**). Furthermore, ABT-737 caused a dose-dependent decrease in HIF-1 β /ARNT (**Figure 28C**). We also found that in SCLC

cell lines, exposure to rapamycin was associated with an increase in the amount of BAX present in the heavy membrane fraction of cells, most prominent in NCI-H146 (**Figure 27C**). This increase in BAX occurred without an apparent release of cytochrome C into the cytosol, suggesting that an increase in membrane-associated BAX in these lines was not by itself associated with greater programmed cell death, but that multiple mechanisms may be at play for the combined effect of rapamycin and ABT-737.

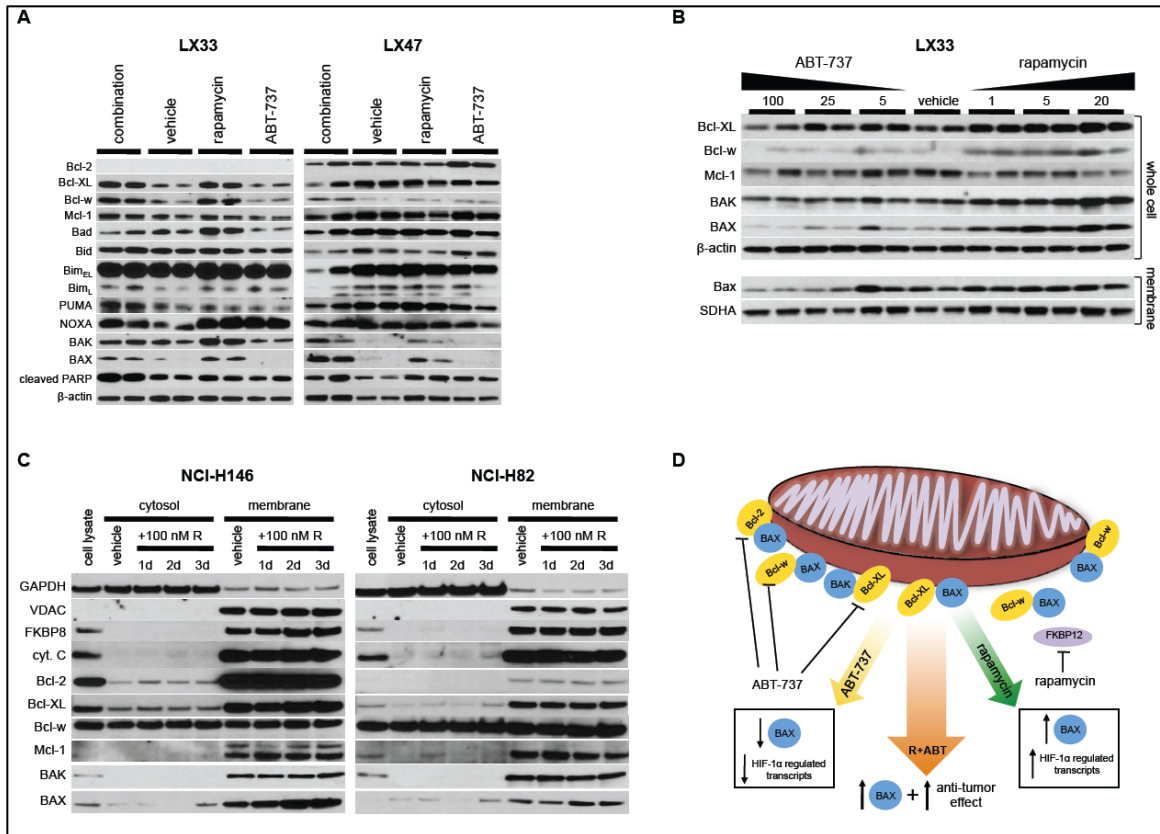


Figure 27. Rapamycin increases levels of BAX protein *in vitro* and *in vivo* in SCLC. (A) Protein expression of selected Bcl-2 family members in LX33 and LX47 in response to one week of treatment with respective arms; n=3-4 mice per arm with duplicates reflecting the extent of variability within a group. β-actin provided for loading control. (B) Dose-dependent effects of ABT-737 and rapamycin on candidate Bcl-2 family members in LX33 PDXs after one week of daily treatment; n=3-4 mice per dosing interval arm with duplicates reflecting variability as above; SDHA (complex ii) provided as a loading control for membrane-enriched fractions. (C) Cell fractionation experiments in NCI-H146 and NCI-H82 exposed to 100 nM rapamycin (+100 nM R) for 24 – 72 h (1d – 3d in Figure). Whole cell lysates and vehicle control lanes were exposed to vehicle (DMSO) for 72 h before collecting protein; 2.5 μg total protein was loaded per lane. (D) Schematic representation of combined rapamycin and ABT-737 effect in SCLC PDX and cell lines models.

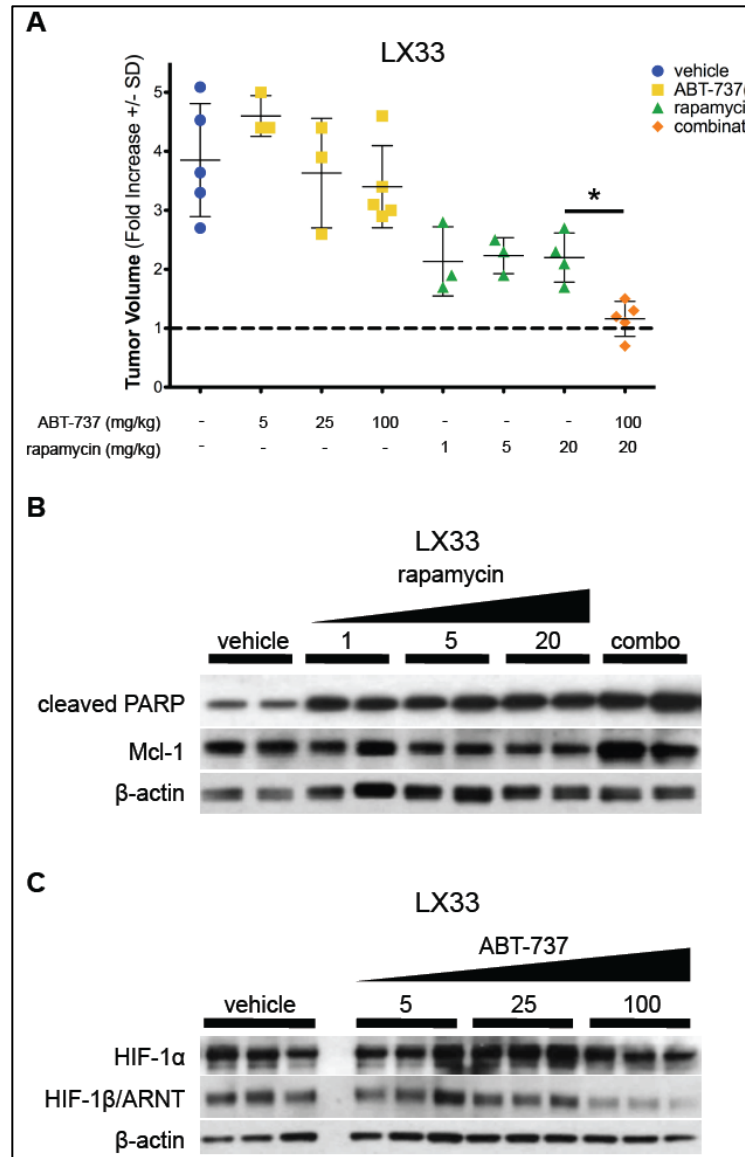


Figure 28. ABT-737 treatment *in vivo* leads to destruction of ARNT.

(A) Relative tumor volume fold increase by treatment arm after one week of treatment in LX33. Fold changes are shown because starting tumor volumes were variable (150-600 mm³); however, variability was represented in each group. Doses are indicated on the x-axis with n=3-5 per dose grouping; dashed line at y=1 provides a reference for tumor growth (+) or reduction (-) from starting volume.

(B) Change in cleaved PARP and MCL-1 protein levels as a function of rapamycin treatment dose and with combination of ABT-737 in LX33 after one week of treatment; β -actin shown as a loading control.

(C) Change in HIF-1 α and its cytosolic chaperone HIF-1 β /ARNT as a function of ABT-737 treatment dose in LX33.

Discussion

Here we report that the BH3 mimetic ABT-737 has limited single-agent efficacy in BCL-2 expressing SCLC PDXs, consistent with the modest clinical activity of ABT-263 observed in patients with recurrent SCLC. Using PDX models as a platform to study ABT-737 resistance, we found that acute treatment with ABT-737 was associated with a decrease in many HIF-1 α regulated transcripts. Rapamycin effectively blocked this decrease and increased message and protein levels of many of these genes. Combining rapamycin with ABT-737 was highly synergistic *in vitro* and provided durable tumor regressions in BCL-2 expressing PDX models *in vivo*. We observed a decrease in BAX protein levels upon exposure to ABT-737 that was prevented by rapamycin. As BAX protein levels are regulated by hypoxia through HIF-1 α dependent and independent mechanisms (Erler et al., 2004), we were surprised to see changes in BAX levels upon exposure to ABT-737 or rapamycin were not associated with observable changes in physiological hypoxia in tumors as compared to controls. This may in part be due to the basal levels of hypoxia in these SCLC PDX models, as heterogeneity within a given PDX may complicate mechanistic analysis.

Loss of BAX is a known mechanism of resistance to several classes of anti-cancer agents (Sarosiek et al., 2013; Zhang et al., 2000) and can promote tumorigenesis in certain models (Yin et al., 1997). In human cancers, loss of BAX through mutation (Rampino et al., 1997) or regulation of protein stability (Agrawal et al., 2008) is associated with events promoting tumor development and correlates with poor prognosis. Here, the observed changes in BAX protein after rapamycin exposure align well with known mechanisms by which ABT-737 induces apoptosis and with studies of genetic determinants of ABT-737 lethality (Carette et al., 2011; Oltersdorf et al., 2005). The most straightforward interpretation of these data is that acute treatment with ABT-

737 is self-limiting in nature, possibly through global decreases in critical HIF-1 α regulated transcripts and the pro-apoptotic protein BAX, both of which are effectively rescued or restored upon the addition of rapamycin (**Figure 27D**). However, multiple mechanisms are likely involved, warranting further investigation.

Of clinical relevance, the LX47 and LX48 PDXs were derived from chemotherapy-naïve and recurrent SCLC patient tumors, respectively; thus, the combination of ABT-737 and rapamycin was active independent of prior chemotherapy exposure and sensitivity to etoposide in our models. The observations made here have clear implications for clinical trials in patients with SCLC. The efficacy of single agent ABT-737 or its orally bioavailable derivative ABT-263 is limited, both in PDX models and in SCLC patients. Previous efforts to combine ABT-263 with cytotoxic chemotherapy in SCLC patients were stopped due to unacceptable levels of hematologic suppression. The combination of ABT-737 with rapamycin results in sustained anti-tumor activity in PDX models, without significant hematologic toxicity or weight loss, and in fact, the thrombocytopenia of single agent ABT-737 was abrogated in the presence of rapamycin. The mechanisms responsible for this potent combinatorial activity may include maintained tumor expression of BAX, a key regulator of apoptotic induction. These data strongly support assessment of combined targeted inhibition of BCL-2 and mTOR pathway in patients with SCLC.

Intended to be blank

Chapter 4. Allosteric or Kinase Inhibition of mTOR is Therapeutically Non-inferior When Combined with BCL-2/xL Inhibition in SCLC

Brevis

A recent report suggested that combining the BCL-2/xL inhibitor ABT-263 with the mTOR kinase inhibitor AZD8055 was capable of producing therapeutic responses in SCLC models, independent of BCL-2 status. These data furthered a hypothesis that we previously, directly rejected based on evidence presented combining ABT-737 with various classes of mTOR allosteric or kinase inhibitors *in vitro* (**Figure 29**). Moreover, as these therapeutic concepts approach clinical testing, it is important to define which SCLC patients are likely to benefit from such therapeutic approaches, as well as define appropriate treatment schedules, biomarkers of response, expected toxicities and mechanisms of acquired resistance to such combinatorial therapies. The experimental study that follows provides a comprehensive overview of the inferiority of selectively targeting BCL-2 alone (Venetoclax; ABT-199) in SCLC, as well as the non-inferiority of combining the dual BCL-2/xL inhibitor with an allosteric (“rapalog”) or kinase-directed mTOR inhibitor in preclinical models of SCLC, arguing that loss of *BAX* will confer resistance to single agent ABT-263 or in combination with mTOR inhibitors.

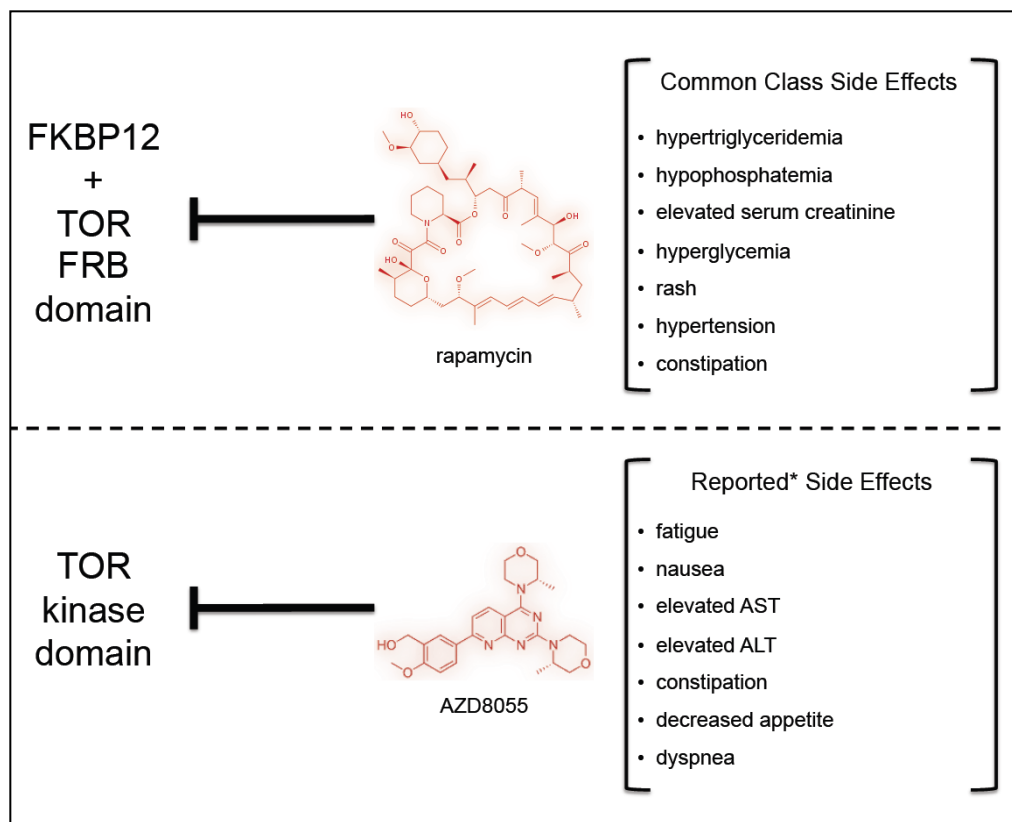


Figure 29. Allosteric versus kinase domain mTOR inhibitory small molecules.

The central difference between the rapalogs (*inset top*) and the first-in-class mTOR kinase inhibitors (*bottom*) is in their unique mechanism of action. Where the rapalogs bind to FKBP12, forming a complex that binds to the TOR FRB domain, the kinase domain targeting generation of mTOR inhibitors bind at the TOR kinase domain and compete with ATP or allosterically modulate the kinase function. Commonly reported side effects with the rapalogs are listed. While data are still emerging from on-going early phase clinical trials, reported toxicities for the mTOR kinase inhibitory AZD8055 are shown (Asahina et al., 2013; Naing et al., 2012).

The Mechanistic Target of Rapamycin (mTOR) Pathway and Therapeutic Targeting

The mechanistic target of rapamycin (mTOR) pathway has been one of the most extensively analyzed eukaryotic growth regulatory programs, and appears to function as a critical rheostat for anabolic and catabolic cellular processes. Rapamycin is a macrolide antibiotic that was discovered from *Streptomyces hygroscopicus* isolates from Rapa Nui (Easter Island) and was originally characterized as having broad antifungal activity (Sehgal et al., 1975; Vezina et al., 1975). The molecular targets of rapamycin in yeast, products of the yeast *TOR1* and *TOR2* genes, were initially identified through mutant screens for resistance (Cafferkey et al., 1993; Kunz et al., 1993; Sabatini et al., 1994). Subsequent work by multiple groups identified the homologous putative mammalian target, the atypical serine/threonine protein kinase mTOR. It is now known that rapamycin indirectly inhibits mTOR through physically binding to FK506 binding protein 12 (FKBP12), and that this complex associates with the FKBP12-rapamycin binding (FRB) domain of mTOR to inhibit its kinase function (Yang et al., 2013; Yip et al., 2010). Moreover, while there is only a single mammalian *TOR* gene, its protein product participates in two distinct complexes – termed mTORC1 and mTORC2 – with unique functions and differential sensitivity to inhibition by rapamycin.

The mTORC1 complex is perhaps best known for its ubiquitous roles in regulating growth and proliferation, integrating cellular environmental cues from at least five distinct classes of input, including amino acids, soluble growth factors, ATP levels, hypoxia, and stress pathway activation (Laplane and Sabatini, 2012). The tuberous sclerosis 1 and 2 (TSC1/2) protein complex negatively regulates mTORC1, serving as a GTPase-activating protein complex (GAP) for the Ras homolog enriched in brain (Rheb) GTPase. TSC1/2 stimulates the GTP hydrolysis activity of Rheb to decrease the kinase activity of mTOR (Inoki et al., 2003). Not surprisingly, germline mutations in *TSC1* or *TSC2* lead to tumor-prone syndromes (Inoki et al., 2005; Ma et al., 2005). Several

upstream kinases belonging to the phosphoinositide 3-kinase (PI3K) and Ras signaling pathways, such as protein kinase B (PKB/Akt) and extracellular-signal-regulated kinase (ERK1/2), respectively, negatively regulate the TSC1/2 complex through direct phosphorylation (Inoki et al., 2002; Manning et al., 2002). Interestingly, while TSC1/2 can function directly to integrate the majority of cellular cues described above, it cannot sense amino acid levels, and mTORC1 cannot be activated by any cues in the absence of certain amino acids (Hara et al., 1998; Smith et al., 2005). The sensing of amino acids is achieved at the level of the lysosomal surface where accumulating amino acids within the lumen of the lysosome affect the vacuolar H⁺-ATPase (v-ATPase) to then interact with a protein complex termed Ragulator. Ragulator provides a docking site for the family of Rag GTPases that serves to directly activate membrane localized Rheb and trafficked mTORC1 on the lysosomal surface (Kim et al., 2008; Sancak et al., 2010; Sancak et al., 2008; Zoncu et al., 2011). What emerges from such complex signaling interactions are controlled scenarios in which mTORC1 can only be activated when at the lysosomal surface in the presence of sufficient free amino acids. Moreover, various feedback loops are likely built into such a system as the expression of the v-ATPase appears to be under control of mTORC1-dependent signaling, and deletion of the v-ATPase inhibits mTORC1 signaling (Duvel et al., 2010; Pena-Llopis et al., 2011). Recently, molecular sensing of arginine was discovered to be a highly regulated process upstream of mTORC1 involving a protein complex termed the Cellular Arginine Sensor for mTORC1 (CASTOR1). CASTOR1 directly binds arginine and releases another bound protein complex termed GATOR2 to positively regulate mTORC1 activity (Saxton et al., 2016). Providing another level of control is Sestrin2 that functions downstream of AMPK to negatively regulate GATOR2 function, inhibiting mTORC1-dependent amino acid sensing (Chantranupong et al., 2014; Kim et al., 2015a; Parmigiani et al., 2014). While the interactions between GATOR1 and GATOR2 are still being worked out, it is

clear that GATOR1 functions as a GTPase activating protein (GAP) for the GTPases RagA and RagB, thus negatively regulating mTORC1 activity. Consistent with this observation, somatic mutations in GATOR1 in certain human cancers drive mTORC1 hyperactivity (Bar-Peled et al., 2013).

Upon activation, mTORC1 phosphorylates key regulators in protein synthesis, including the eukaryotic initiation factor 4E binding proteins (4E-BPs) and the p70 ribosomal S6 kinase 1 (S6K1), and it is the coordination of these events that lead to successful proliferation and growth (Dowling et al., 2010; Richter and Sonenberg, 2005). The translational program that activation of mTORC1 initiates appears to show preference for transcripts with 5' terminal oligopyrimidine (TOP) motifs (Thoreen et al., 2012). Akin to cancer reprogramming of basal metabolism, activation of mTORC1 leads to a similar metabolic focus on biomass accumulation.

Relative to mTORC1, the more recently described mTORC2 has fewer known functions, with early evidence focusing on Rho- and Rac-dependent remodeling of the cytoskeleton and regulation of certain members of the AGC family of kinases. In the acute setting, mTORC2 is not directly inhibited by the rapamycin-FKBP12 complex; however, it is now well established that long-term treatment with rapamycin will inhibit mTORC2 (Jacinto et al., 2004; Lamming et al., 2012; Sarbassov et al., 2004). Additionally, the function of mTORC2 in insulin signaling has been shown to act through a PI3K-dependent interaction with the ribosome, which may posit a critical role for mTORC2 in translational control (Zinzalla et al., 2011). Interestingly, no GTPase has been described to directly regulate mTORC2 activity (unlike Rheb for mTORC1), further limiting current understanding of mTORC2's role in the eukaryotic growth program. One of the direct targets of mTORC2 is the serine/threonine kinase Akt at position Ser473. As Akt is fully activated when phosphorylated at Thr308 and Ser473, it became apparent that one caveat to chronic rapamycin exposure, even in the presence of modest

mTORC2 inhibition, may be that the resulting activation of Akt can promote what initially appeared to be a paradoxical activation of available mTORC1 (Peterson et al., 2009; Sarbassov et al., 2005).

Within cancers, some of the most common oncogenic mutations and tumor suppressor losses converge to activate the mTOR pathway, directly and indirectly. For example, *PTEN* is commonly lost in solid tumors thereby removing some of the feedback regulation on PI3K signaling, leading to constitutively activated Akt (Vivanco and Sawyers, 2002). Focal amplifications of genes encoding PI3K and Akt as well as activating mutations within the p110 α catalytic domain of PI3K are also observed and confer similar growth advantages. Similarly, mutations within *STK11/LKB1* have been shown to occur in lung adenocarcinomas, resulting in a mutant Lkb1 that is no longer able to activate the family of adenosine monophosphate-activate protein kinases (AMPKs) that serve to negatively regulate the action of TSC1/2 on mTOR (Ji et al., 2007; Levine et al., 2005). Although influenced by multiple complex feedback loops, the role of mTOR in cancer is becoming clear – the ability for eukaryotic cells to respond and adapt to changes in bioenergetic stimuli involves many levels of regulation that ultimately converge on regulation of the mTOR signaling pathway.

As accumulating evidence pointed to mTOR as a critical integrator of cancer bioenergetics, multiple research groups began simultaneously developing small molecule inhibitors of this pathway. Rapamycin (also known as sirolimus) was first clinically approved as an inhibitor of transplant rejection due to its ability to suppress cytotoxic T cell proliferation, and serves as the founding member of a family of structurally related compounds collectively termed “rapalogs.” Sirolimus itself in fact does appear to have anticancer activity, but has been less extensively studied in cancer patients than its several derivatives, in part due to economic disincentives associated with its patent life, and in part due to low and variable oral bioavailability (Dabora et al.,

2011). Three rapalogs – temsirolimus, everolimus, and ridaforolimus – have been the primary focus of clinical drug development in oncology.

Temsirolimus was the first mTOR inhibitor to be FDA-approved for use in cancer, based on its superiority to a prior standard of care (interferon) in patients with advanced kidney cancer (Hudes et al., 2007). Everolimus approval followed shortly thereafter, initially also for metastatic kidney cancer, and subsequently for a subset of pediatric astrocytomas associated with mutations in TSC genes, and for pancreatic neuroendocrine tumors (Krueger et al., 2010; Motzer et al., 2008). Temsirolimus also gained a secondary approval in Europe for treatment of mantle cell lymphoma. Ridaforolimus, the newest of this class of drugs, while showing evidence of activity in soft tissue sarcoma and other diseases, has not yet gained regulatory approval (Chawla et al., 2012; Hess et al., 2009).

While demonstrating some clinically relevant anti-cancer efficacy, the magnitude of benefit provided by the rapalog agents is limited (e.g. for temsirolimus in renal cell carcinoma, 3.6 month improvement in median survival, and response rate 8.6%), and the initially hypothesized broad spectrum activity against most common cancers has not held up. There are several possible mechanisms of rapalog resistance, including but not limited to incomplete inhibition of the mTORC1 complex, and induction of the mTORC2 feedback loop activating Akt. These agents can be difficult to give in the clinic due to a spectrum of toxicities that appear largely as a class effect, including mucositis, maculopapular or acneform rash, nail changes, relatively rare, but sometimes severe pneumonitis, and metabolic derangements including hyperglycemia, hyperlipidemia, and hypophosphatemia (Soefje et al., 2011).

To address some of the perceived weaknesses of the rapalogs, notably the possibility of insufficient suppression of mTORC2-dependent feedback loops, a newer generation of ATP-competitive mTOR small molecule inhibitors is now in active clinical

development. By inhibiting the kinase activity of mTOR itself, these inhibitors have similar high potency against both mTORC1 and mTORC2; some also inhibit the homologous kinase domain of PIK3CA, the catalytic domain of PI3 Kinase responsible for Akt activation. This has rapidly become a crowded field, with at least eight dual mTOR/PI3K inhibitors and five pan-mTOR inhibitors from 11 pharmaceutical companies in active clinical trials, and several more in late preclinical testing. For most of these, definitive clinical reports on either toxicity or efficacy are not yet available.

For both the rapamycin derivatives and the mTOR kinase inhibitors, a particularly active area of clinical research now focuses on drug-drug combinations (Benjamin et al., 2011). Therapeutic strategies being actively investigated include concurrent inhibition of multiple levels of the mTOR signaling pathway, with the idea of interrupting feedback loops leading to resistance, concurrent inhibition of parallel critical pathways such as the PI3K/mTOR and RAS/RAF/ERK signaling cascades, and combinations with standard cytotoxic therapies.

Results

Changes in expression of core anti-apoptotic BCL-2 family members are not correlated with acquired resistance to cisplatin/etoposide in SCLC

To begin to address whether specific genomic amplifications or transcriptional increases in anti-apoptotic BCL-2 family members drive acquired resistance to cisplatin/etoposide, we compared RNA expression by from paired RNA sequencing data for several core BCL-2 family members, thought to be critical mediators of resistance to apoptosis in both hematologic and solid tumors (Beroukhim et al., 2010). From triplicate tumor samples in the chemosensitive setting across 10 unique PDX models, we found no correlation between best response of the tumor to cisplatin/etoposide and expression of *BCL2*, *BCL2L1*, *MCL1* or the pro-apoptotic effector *BCL2L11* (**Figures 30A-D**). Further, we analyzed paired chemosensitive and chemoresistant triplicates for these 10 models in aggregate and were unable to show statistically significant difference in the expression of these BCL-2 family members (**Figure 30E**). These data suggest that gene expression alone of BCL-2 (*BCL2*), BCL-xL (*BCL2L1*) and/or MCL-1 (*MCL1*), are not indicative of *de novo* chemoresistance as individual correlates in SCLC *in vivo*. While speculative, previous reports suggesting evidence that BCL-2 permits chemoresistance in SCLC may rather reflect artifact in cell lines and underpowered correlative studies, without functional interrogation. Moreover, while there is evidence that genes involved in the execution of programmed cell death are frequently silenced in NSCLC and SCLC, such as caspase-8 (*CASP8*) and TRAIL (Hopkins-Donaldson et al., 2003; Kaminsky et al., 2011; Shivapurkar et al., 2002; Venturelli et al., 2013), there is no reported evidence for these genes being inactivated in primary tumors by mutational events (**Figure 31**).

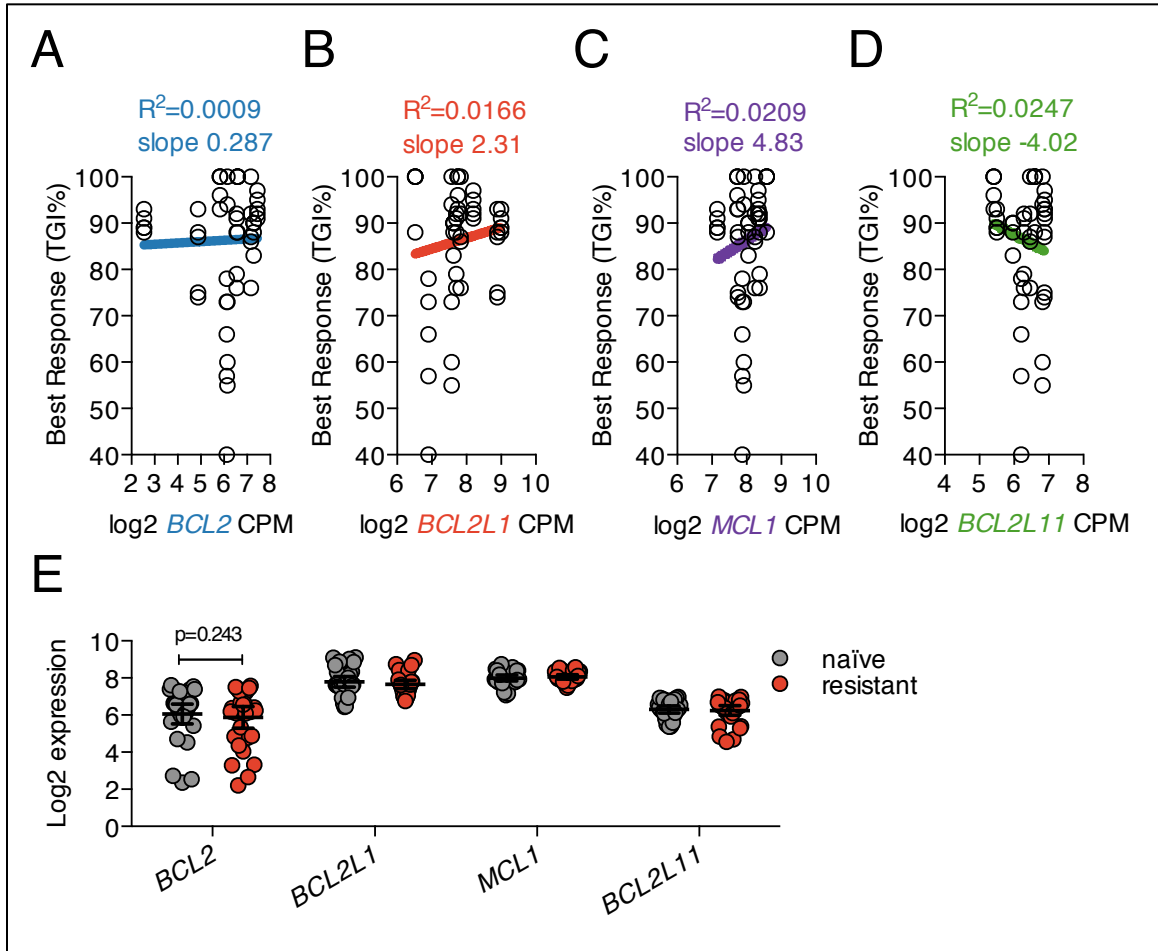


Figure 30. Expression of core anti-apoptotic BCL-2 family members does not correlate with response to cisplatin and etoposide.

(A) Response data for 5 animals per PDX were compared to vehicle controls at last available point on study (before vehicle hit endpoint of $\sim 1000\text{mm}^3$). 100% tumor growth inhibition (TGI) is considered a complete response of hind flank tumor. Treatment responses were compared to average log2 counts per million (CPM) transcript expression of various BCL-2 family members by RNAseq, including *BCL2* (B) *BCL2L1* (BCL-xL), (C) *MCL1*, (D) and pro-apoptotic *BCL2L11* (BIM). Linear regression best fit values for goodness of fit (R^2) and slope are reported for each transcript investigated. Averages of triplicate log2 CPM measures were used for 5 independent tumor responses per PDX.

(E) Changes in expression were compared between PDX models in the naïve and chemoresistant setting, as in Figure 4. Differences in aggregated between models were not significant; p -value reported for paired t-test comparison in *BCL2* expression between naïve and resistance groups.

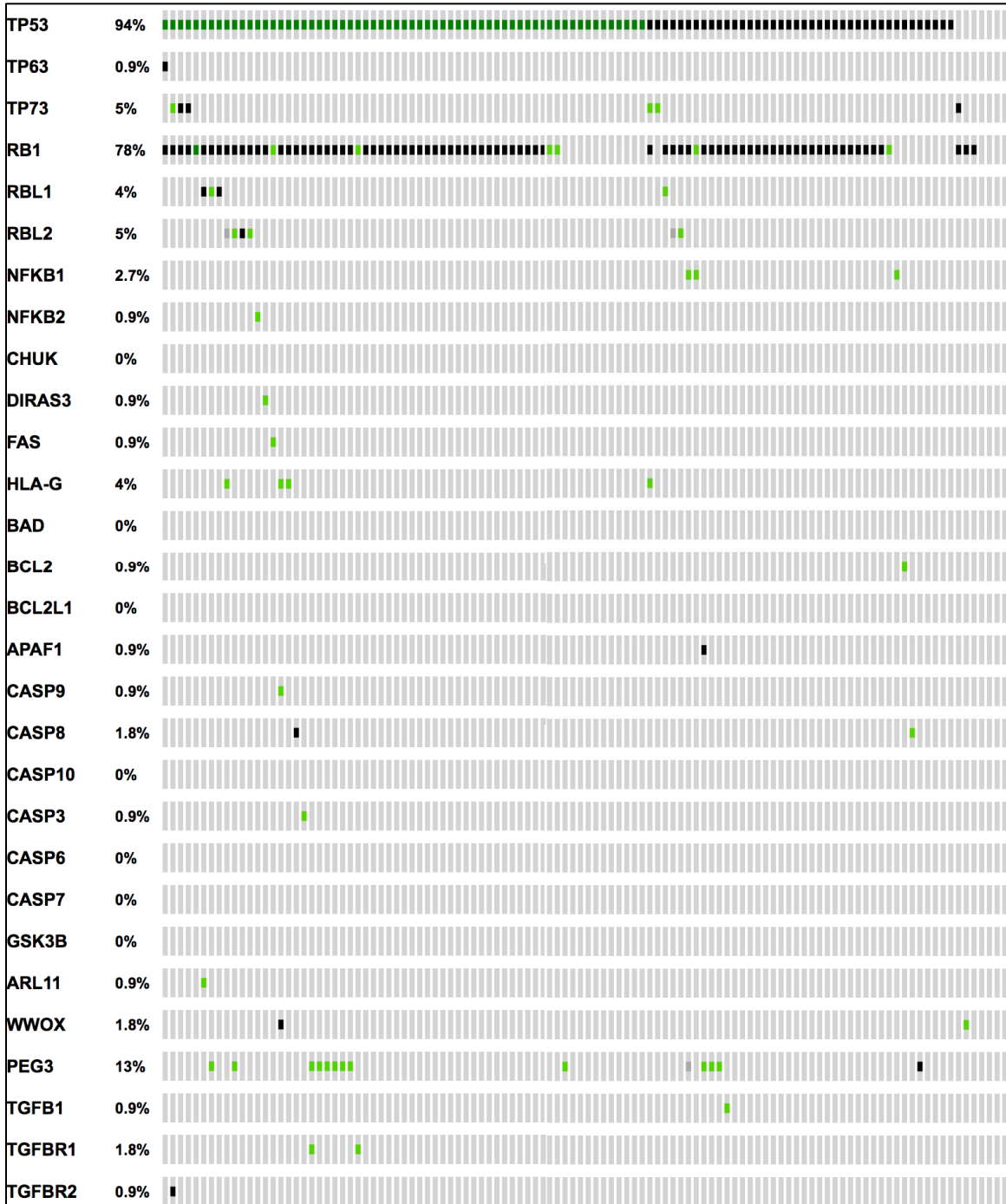


Figure 31. Genes involved in programmed cell death are not frequently mutated in primary SCLC.

Oncoprint mutational status of cell death and survival gene list in addition to core defining gene mutations (*TP53*, *TP63*, *TP73*, *RB1*, *RBL1* and *RBL2*) (cBioportal defined list) across 110 annotated primary SCLC cases. Frequency listed along left near gene name. Black-truncating mutation; dark green-missense mutation; dark grey-inframe mutation; neon green-missense (non-recurrent) mutation.

BCL-2 specific inhibition by ABT-199 is inferior to BCL-2/xL inhibition by ABT-263 as a single agent or in combination with mTOR inhibitor.

With ample evidence for a high frequency genomic amplification of BCL-2 in SCLC cell lines and high level protein expression in primary SCLC (Ben-Ezra et al., 1994; Breton et al., 1998; Byers et al., 2012; Ikegaki et al., 1994; Jiang et al., 1995; Sirzen et al., 1998; Takayama et al., 1996; Wang et al., 1998), it was reasonable to hypothesize that SCLC may be sensitive to BCL-2 specific inhibition by the small molecule ABT-199 (Souers et al., 2013). Further, emerging evidence suggested preclinical activity was not limited to hematologic malignancies alone (Vaillant et al., 2013). We determined the relative activity of ABT-199 versus ABT-263 in a panel of 15 SCLC cell lines, including those that had previously been characterized by other groups as being extremely sensitive to ABT-263/737 (Faber et al., 2015; Lin et al., 2007; Olejniczak et al., 2007; Shoemaker et al., 2008; Tahir et al., 2010). With the exception of one cell line – NCI-H889 known to have an amplification of BCL2 with an average copy number ~5 – all SCLC cell lines displayed an increased sensitivity to ABT-263 when compared to ABT-199 (**Figure 32A**). Moreover, when considering these agents are being proposed to be used in combination with other classes of mTOR inhibitors, we examined whether a pre-treatment period with a low dose of everolimus (1-10nM) was effectively sensitizing certain cell lines to BCL-2 or BCL-xL specific inhibition, through the use of the chemical tool WEHI-539, shown to be have ~1000X specificity for BCL-xL over other closely-related BCL-2 family members (Lessene et al., 2013). Interestingly, we observed differences in class specific sensitivity, such that one cell line (NCI-H146; **Figure 32B**) was more sensitive to BCL-xL inhibition versus BCL-2 inhibition, whereas another cell line (NCI-H187; **Figure 32C**) was more sensitive to BCL-2 versus BCL-xL-specific inhibition. This was independent of dramatic differences in expression of core

anti-apoptotic proteins (**Figure 32D**). These data are important because they suggest certain pro-apoptotic BCL-2 family members are being parsed or “shuttled” from different, restraining anti-apoptotic proteins under the stress cells experience from low level inhibition of mTOR (Levenson, 2016). Therefore, a class-specific inhibitor, even if better tolerated clinically, may lose efficacy over time by a tumor repositioning binding partners for pro-apoptotic proteins. This is clearly demonstrated by the amount of evidence suggesting that MCL-1, an anti-apoptotic protein not targeted by ABT-263, is a candidate acquired resistance mechanism (Brumatti and Ekert, 2013; Punnoose et al., 2016). We further show the superiority of combining ABT-263 with either an allosteric or catalytic inhibitor of mTOR as compared to combinations with ABT-199 (**Figure 33**).

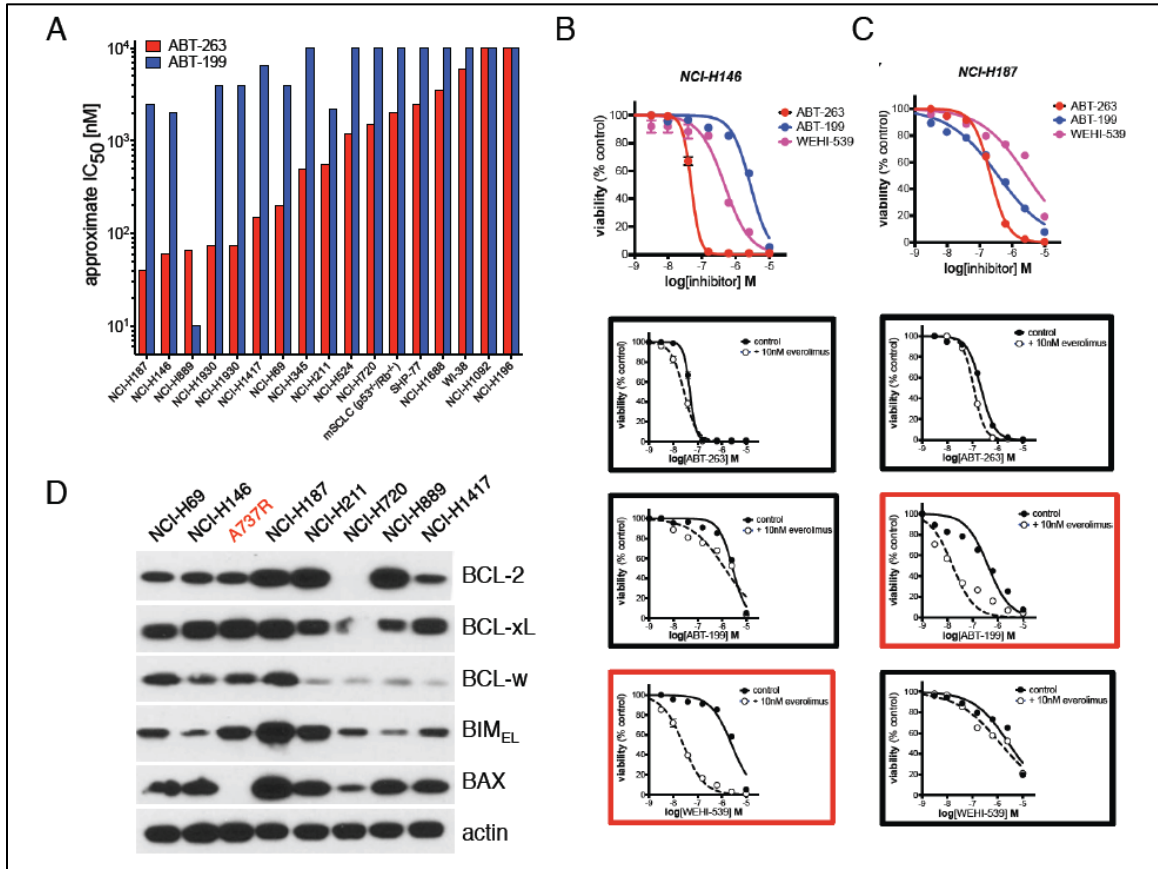


Figure 32. Combined inhibition of BCL-2/xL with ABT-263 is superior to ABT-199 in multiple *in vitro* models of SCLC.

(A) IC₅₀ values for ABT-199 and ABT-263 (red) reported from 72hr cell proliferation assays in multiple human or mouse SCLC cell lines. The human fibroblast WI-38 serves as a negative control and general indicator of compound pan-toxicity.

(B) SCLC cell lines expressing both BCL-2 and BCL-xL are differentially sensitive to specific inhibitors of BCL-2 or BCL-xL as compared to the dual inhibitor ABT-263. In the above panels, IC₅₀ cell viability curves for NCI-H146 (left)

(C) or NCI-H187 (right) for the dual inhibitor ABT-263 (red line), BCL-xL inhibitor WEHI-539 (magenta line) or BCL-2 inhibitor ABT-199 (blue line). Below: 72hrs pre-treatment with 10nM of the mTOR allosteric inhibitor everolimus differentially “primes” BCL-2 or BCL-xL, but is not easily observed with the dual inhibitor ABT-263. Largest individual effect highlighted by a red box.

(D) Protein expression by Western blot for various ABT-263 or ABT-199 protein targets across a select group of human SCLC cell lines. A737RS in red is the isogenic NCI-H146 cell line that has acquired resistance to ABT-737/263 via continuous *in vitro* exposure/dose escalation.

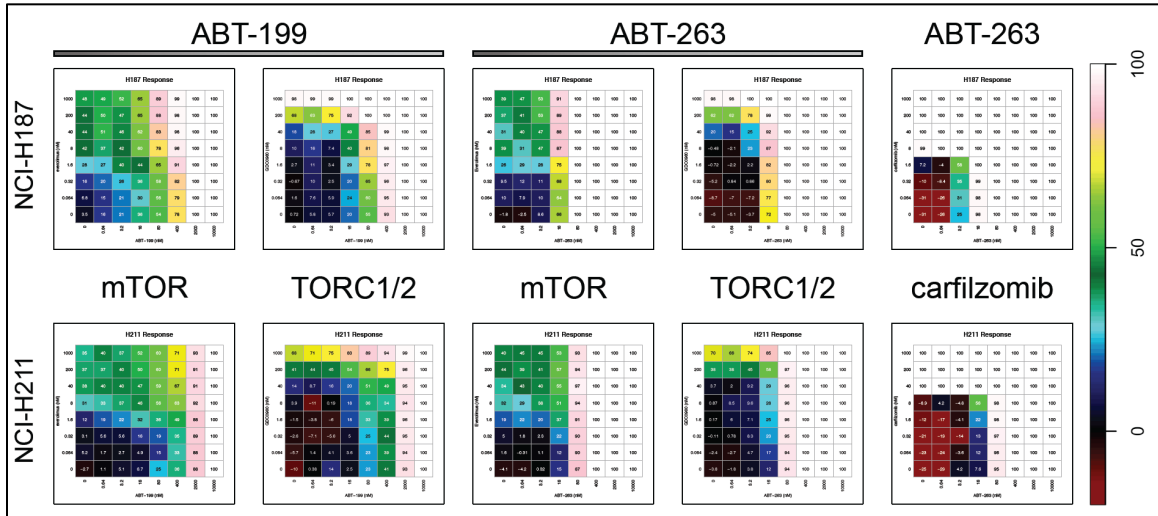


Figure 33. Inhibition of mTOR with an allosteric or kinase inhibitor is superior in combination with ABT-263 versus ABT-199 *in vitro*.

Combinatorial inhibition (synergy) plots versus highest single agent effect (HSA) for two BCL-2 expressing SCLC cell lines, NCI-H187 and NCI-H211. Dose range for the allosteric mTOR inhibitor everolimus and kinase inhibitor GDC-0980 ranges from 1000-0.064nM; dose range for the BCL-2 selective ABT-199 or BCL-2/xL inhibitor ABT-263 range from 10,000-0.64nM. On far right, synergy of BCL-2/xL inhibition with proteasome inhibition by carfilzomib. While highly active *in vitro*, the combination proved too toxic to explore preclinical efficacy (*data not shown*). Color-coded effect scale bar on right.

Loss of BAX permits resistance to BCL-2/xL inhibition as a single agent or in combination with mTOR inhibitors, but does not alter sensitivity to cytotoxic chemotherapy.

To address potential mechanisms of resistance to BCL-2/xL inhibition *in vitro* we chose to continuously culture one of the most sensitive SCLC cell lines, NCI-H146, under escalating doses of ABT-737. After approximately 6 month in culture, this isogenic cell line was robustly resistant to ABT-737 upon acute challenges (**Figure 34A**). When examining the protein expression of core pro- and anti-apoptotic proteins at the level of whole cell lysates and within mitochondrial membrane fractions, it was clear that although there were increases in MCL-1, BAX was completely lost in this cell line, which we confirmed by qPCR (**Figure 34B**; *data not shown*). This ABT-737 acquired resistant version of NCI-H146 (“A737R”) did not display differing growth kinetics in culture or *in vivo* when xenografted into the lungs or hind flanks of immunocompromised mice (**Figures 34C-E**), suggesting that a core phenotypic difference may be in programmed cell death response.

To determine the relative roles of the pro-apoptotic proteins BAK1 and BAX in affecting the sensitivity to ABT-737 in NCI-H146, we infected cell lines with lentiviruses expressing shRNAs against these genes, as well as a negative control. The stable cell lines were then challenged with ABT-737, and we noted that only complete suppression of BAX, but not BAK1, was capable of reducing the sensitivity of NCI-H146 to levels of that observed in the A737R line (**Figures 35A-B**). Further, when we compared the activity of a variety of combinations of mTOR inhibitors with ABT-263 versus that of cisplatin and etoposide, any drug combination containing the pro-apoptotic ABT-199 or ABT-263 was greatly reduced in the A737R cell line; however, the combined activity of cisplatin and etoposide was only marginally reduced in the A737R line (**Figures 35C-D**).

Taken together, these data suggest that loss of BAX can confer resistance to ABT-263 alone or in combination with mTOR inhibitors, but does not greatly affect sensitivity to cisplatin and etoposide.

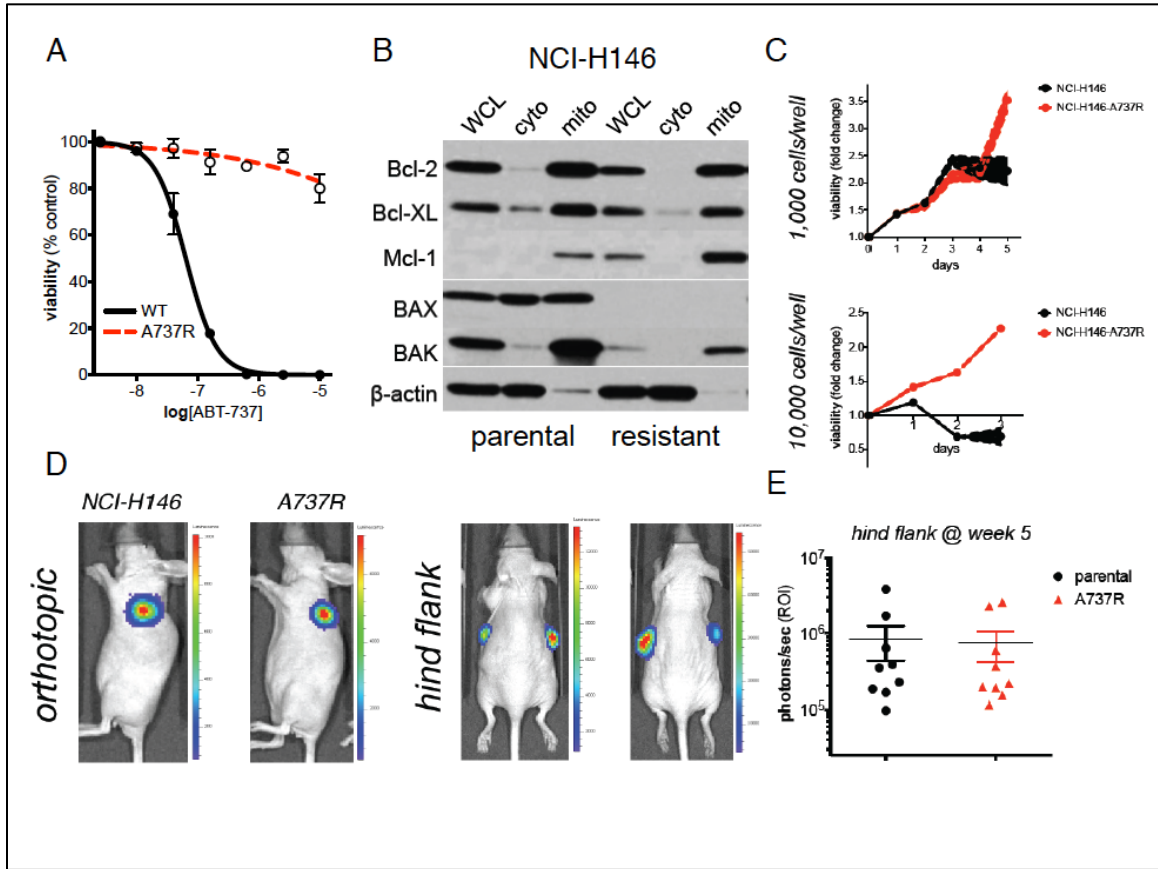


Figure 34. Acquired resistance to ABT-263/737 proceeds through the loss of BAX in SCLC.

(A) Isogenic NCI-H146-A737R (red trace) cell line is highly resistant to ABT-737 *in vitro*
 (B) Isolation of crude mitochondria in paired parental and ABT-737-resistant versions of NCI-H146. WCL=whole cell lysate, cyto=cytoplasmic fraction, mito=crude mitochondrial fraction using a QProteome™ mitochondria isolation kit (Qiagen)
 (C) Acquired resistance to ABT-737 *in vitro* does not alter proliferation kinetics, but does change response to media exhaustion; 96 well plates were inoculated with 1,000-10,000 cells per well and metabolic turnover of AlamarBlue was measured overtime
 (D) NCI-H146-A737R cell line does not show differences in growth kinetics *in vivo* when engrafted into the pleural space (*orthotopic*) or as a hind flank tumor in athymic mice.
 (E) Quantitation of luciferase signal flux from parental or A737R hind flank tumors at 5 weeks post-engraftment of equivalent cell number per mouse. 5 animals were engrafted with 1×10^6 cells per flank per cell line (10 data points per cell line); groups are not statistically different by paired *t*-test.

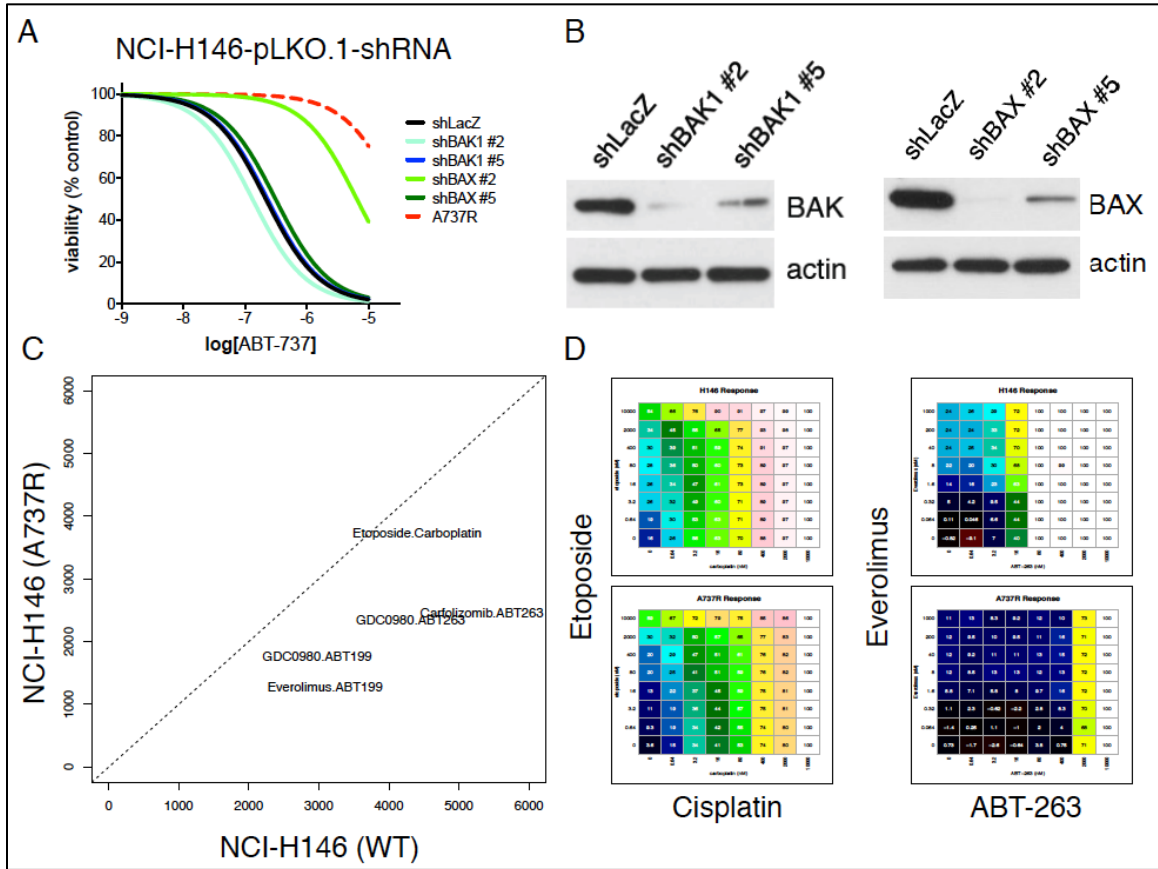


Figure 35. Suppression of BAX – but not BAK – is sufficient to confer resistance to BCL-2/xL inhibition, but not cisplatin+etoposide.

(A) Shift in IC_{50} cell viability curves for NCI-H146 with shRNAs against the pro-apoptotic proteins BAK1 or BAX, with an shRNA directed against LacZ as a negative control. Two independent shRNA sequences were used per target. A737R cell line included as a positive control/comparator.

(B) Protein expression by Western blot of BAK1 and BAX from shRNA knockdown cell lines used in A

(C) Combinatorial effect of ABT-199 or ABT-263 in combination with everolimus or GDC-0980 is altered in NCI-H146-A737R cell line. Data falling above the trend line (slope=1) would indicate greater activity in the A737R cell lines (y-axis), whereas data falling below the trend line indicates greater activity in the parental cell line NCI-H146 (x-axis).

(D) Example combinatorial response data sets for cisplatin+etoposide (*left*) or ABT-263+everolimus (*right*) in the parental (*top*) or A737R (*bottom*) cell line used to generate panel C.

Acute treatment with mTOR inhibitors does not strongly “prime” SCLC tumors for programmed cell death by ABT-263

One of the first observations for a differential apoptotic threshold in certain cell types came from the work of Anthony Letai in the lab of Stanley Korsmeyer. This work led to the development of methods focused on exploiting BH3 peptide binding affinities in *ex vivo* assays using whole cells or isolated mitochondria to determine relative ability to release cytochrome c upon manipulation of specific BCL-2 protein-protein interactions (Certo et al., 2006; Letai et al., 2002). Since then, these methods have progressed and been important in helping rationalize the relative sensitivity of certain tumor types, or populations of cells within a singular tumor type, to the activity of apoptotic stimuli (Chonghaile et al., 2014; Montero et al., 2015; Ni Chonghaile et al., 2011; Vo et al., 2012), and have been critical in the validation of certain pro-apoptotic compounds, such as ABT-737 (Oltersdorf et al., 2005).

An early observation in comparisons across tumor types was that certain SCLC cell lines were exquisitely sensitive to the pro-apoptotic effects of ABT-737, leading to clinical testing in a subset of relapsed SCLC. However, these efficacy data in SCLC were disappointing and safety was of a concern with all agent within this proposed class, leading our group to investigate why SCLC may not be as sensitive to ABT-737 *in vivo*, as was observed *in vitro* and in cell line xenografts (Gandhi et al., 2011; Hann et al., 2008; Rudin et al., 2012b). These results led to work describing feedback mechanisms at the level of the tumor important in the regulation of pro-apoptotic protein function, that could effectively be counteracted through mTOR inhibition (Gardner et al., 2014). One unanswered question from this work was whether the combined inhibition of mTOR and BCL-2/xL was due to independently additive effects, possibly displaying pre-clinical

synergy, or whether mTOR inhibition was “priming” tumors to a greater extent, effectively sensitizing SCLC to the activity of ABT-236/737.

Here we attempted to address these open questions through *in vivo* “run-in” experiments across 3 PDX models of SCLC that cover the hallmarks of gene/protein expression subtypes – including c-MYC and N-Myc expression, various levels of BCL-2, and varying levels of pro-apoptotic BIM (**Figure 36A**). Groups of size matched, tumor-bearing animals were treated with a single dose of an agent affecting various aspects of apoptotic sensitivity (e.g. birinipant as a cIAP1 inhibitor, silvestrol as a eIF4A/translation inhibitor, carfilzomib as a proteasome inhibitor) and then given a single oral dose of ABT-263, collecting tumors within 24hrs post-dosing. As an example in JHU-LX92, we found no evidence for a greater level of apoptosis within tumors acutely (“single dose”) conditioned with such agents, measuring apoptosis indirectly by the presence of a caspase cleaved motif and cleaved-PARP in tumor lysates (**Figure 36B**). Further, as various classes of mTOR inhibitors did not show strong pre-clinical single agent activity in multiple PDX models of SCLC when administered daily for 7d (**Figure 36C**), we asked whether tumors were now differentially sensitized to ABT-263, after a one week “run-in” period. Again, using JHU-LX92, we could find no evidence for a greater degree of apoptosis in tumors treated for 7d with different classes of mTOR inhibitors that were then treated with a single dose of ABT-263 (**Figure 36D**). Interestingly, it appeared that at least in JHU-LX92, levels of caspase cleaved motifs were higher in tumors pre-treated with rapamycin for one week than those treated with the mTOR kinase inhibitors AZD8055 or GDC-0980. While speculative, this may suggest that mTOR kinase inhibitors do have some influence on apoptotic threshold *in vivo*, as caspase cleaved motif levels were similar to tumors treated for 7d with ABT-263, where we suspect this is

reflective of a depletion in pro-apoptotic reserve over time (compare ABT*1 versus ABT*7 lanes for cleaved-PARP and caspase cleaved motifs).

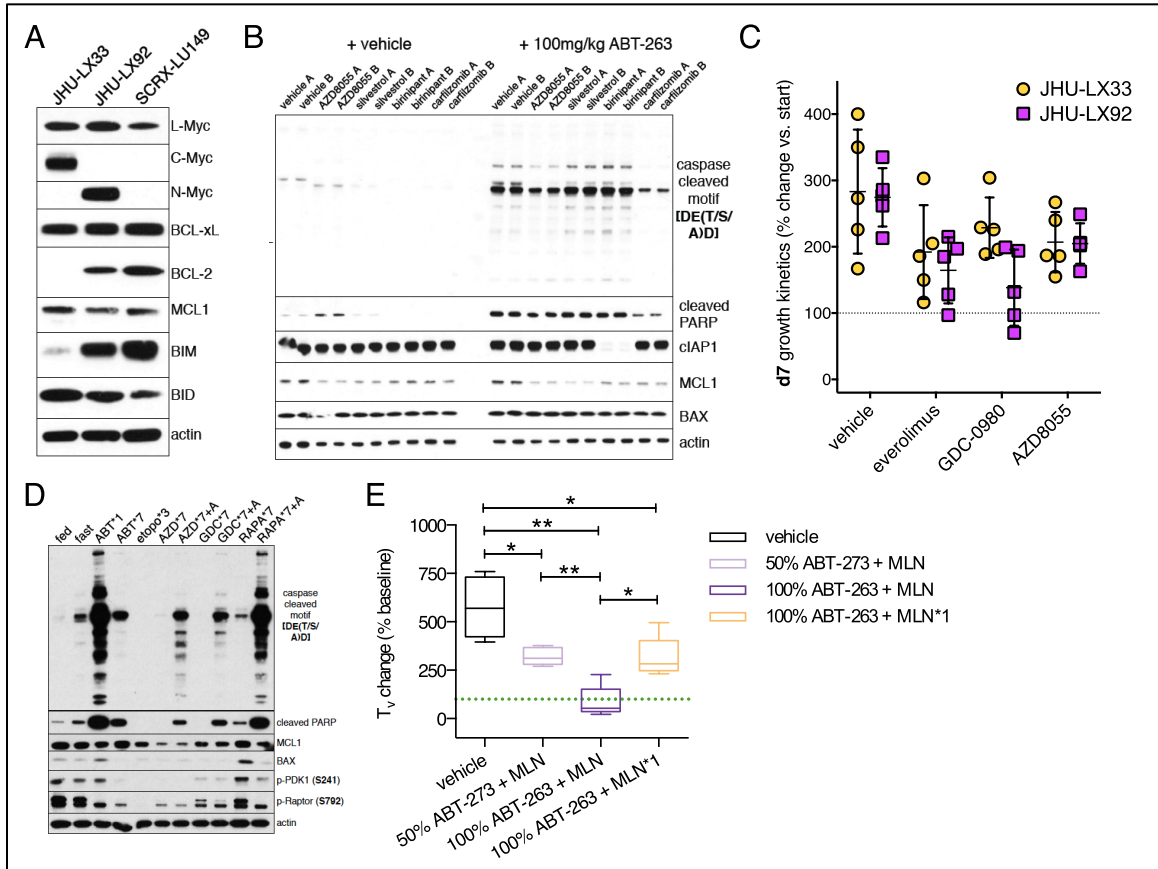


Figure 36. Acute conditioning of SCLC with different classes of mTOR inhibitors does not “prime” tumors for apoptosis with ABT-263.

(A) Protein expression of specific BCL-2 and MYC family members in SCLC PDX models used throughout this Chapter.

(B) Pre-administration of different classes of compounds shown to have synergy with ABT-263 *in vitro* does not acutely prime tumors for apoptosis *in vivo*. The N-Myc+/BCL-2+ PDX LX92 was engrafted into athymic mice and tumors were randomized near ~300mm³ to treatments groups of 4 animals bearing single, hind flank tumors. Mice were dosed with the listed agents (*below*) 4 hours before an oral dose of vehicle (*left*) or 100mg/kg ABT-263 (*right*): 10mg/kg AZD8055 PO, 1mg/kg silvestrol IP, 100mg/kg birinipant IP, or 2mg/kg carfilzomib IV. Tumors were flash frozen 16 hours after the dose of ABT-263 and analyzed for the substrates above by Western blot; biological replicate tumors are shown as A and B.

(C) Single agent allosteric or catalytic (kinase) mTOR inhibitors have limited efficacy as single agents in two MYC-amplified PDX models of SCLC. PDXs JHU-LX33 and JHU-LX92 were treated with 10mg/kg everolimus, GDC-0980, AZD8055 or vehicle daily for 7 days

(D) Individual animals from treatment groups were randomized to receive +/- a single oral dose of vehicle or 100mg/kg ABT-263 (+A) and then collected 16hrs later. Protein was extracted for Western blot. A single dose of ABT-263 or after 7d of daily ABT-263 and after 3d of daily etoposide (8mg/kg IP) are shown as +/- apoptotic controls, respectively.

(E) A single weekly dose of MLN0128 (MLN*1) is inferior to daily administration when in combination with ABT-263. Tumor volume changes (percent baseline; randomization ~100-150mm³) at d10 after 7d of treatment with indicated schedules (50% ABT-263 indicated 50mg/kg oral dose). All treatment arms produce statistically significant tumor growth inhibitor versus control; however, only the daily MLN0128 in combination with 100mg/kg ABT-263 dose produce tumor regression (data falling below green line); *p*-value levels of significance shown for paired *t*-tests.

Combining an mTOR allosteric or kinase inhibitor with ABT-263 is effective and non-inferior in SCLC

These observations of differences in apoptotic reserve between treatment groups challenged with a single dose of ABT-263 caused us to question whether combining an mTOR allosteric inhibitor (a “rapalog”) would have greater anti-tumor activity with ABT-263, as compared to an equivalent schedule of a kinase inhibitor in combination. The clinical development of AZD8055 has largely been abandoned due to limited activity and modest toxicity (Asahina et al., 2013; Naing et al., 2012), leading to a renewed focus on a similar compound MLN0128, recently reformulated as TAK-228, for clinical development (Ghobrial et al., 2016). We first determined that we were able to observe on-target efficacy of MLN0128 *in vivo* performing a time course experiment in animals bearing size matched JHU-LX92 tumors, and treated these mice with or without a single administration of ABT-263. The timing of separation of MLN0128 and the following dose of ABT-263 was approximately 2 hours and would be used in a similar spaced daily schedule for efficacy experiments. As both agents were being administered orally, there is some concern for one agent’s effect on the other, especially if formulations vary widely and compounds are administered simultaneously or within the expected window of gastric emptying in the mouse (~30 min). We did not observe significant differences in the suppression of p-4E-BP1 or decrease in MCL-1 between single agent or combination treated tumors (**Figure 37A**). However, we did note that the on-target activity of MLN0128 varied between tumors, where certain SCLC PDX models, when treated in a size-matched fashion, such as JHU-LX44, did not completely suppress p-4E-BP1 nor suppress cap-dependent translation, as measured by MCL-1 level (**Figure 37B**). These data argue that certain subtypes of SCLC, especially those that lose dependence on cap-dependent translation may not benefit from MLN0128 as a single agent or in

combination with ABT-263. Moreover, it is likely that both agents must be administered daily, as the rebound of p-4E-BP1 was within 24 hours (**Figure 37A**) post-MLN0128 administration, and the anti-tumor efficacy of daily administration was greater than weekly administration of MLN0128 in combination with daily ABT-263 (**Figure 36E**).

We extended these short-term comparative efficacy studies across those 3 SCLC PDX models previously introduced (**Figure 36A**) and were able to show that while highly active in JHU-LX92 and SCRX-Lu149, capable of producing tumor regressions, the combination of MLN0128 or everolimus with ABT-263 was not statistically different between treatment arms within individual PDX models, where the combinations were superior to single agent ABT-263. Moreover, the combination lacked efficacy in JHU-LX33, a model shown to not express BCL-2 and have no response to single agent ABT-263. Further, we chose to examine activity in two additional SCLC models where BCL-2 is differentially expressed (BCL-2^{LOW} JHU-LX22 and BCL-2^{HIGH} JHU-LX44), observing no activity in JHU-LX22 and modest anti-tumor activity in JHU-LX44, but not capable of producing regressions (**Figure 38B**). In terms of tolerability, both combination regimens were well tolerated and acute or chronic thrombocytopenia was largely due to ABT-263, with no greater reduction in circulating, mature platelets in combination arms on chronic treatment, whether in immunocompromised mice or mice with intact immune systems (**Figures 38C-E**).

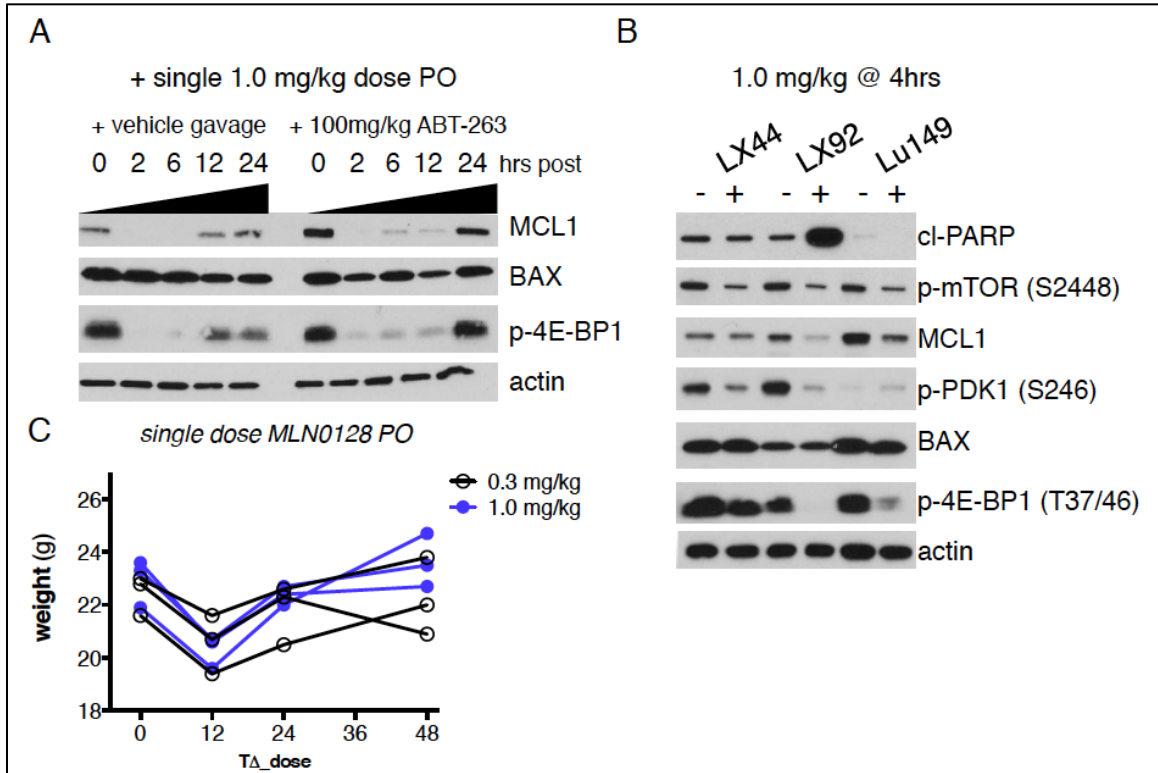


Figure 37. mTOR kinase inhibition by MLN0128 is variable across independent PDX models of SCLC.

(A) A single oral dose of MLN0128 suppressed cap-dependent translation for <24hrs *in vivo*. Size matched groups of JHU-LX92 tumor-bearing animals were orally administered a dose of vehicle or 100mg/kg ABT-263 four hours before an additional oral dose of 1mg/kg MLN0128, where tumor tissue was then collected at various time points (*in hours*) post-MLN dose and analyzed by Western blot for suppression of p-4E-BP1.

(B) Size matched tumor bearing animals (~300-400mm³) were administered an oral dose of vehicle or 1mg/kg MLN0128 and tumors tissue was collected 4hrs post-dose.

(C) Acute weight loss in non-tumor-bearing mice is resolved within 24hrs post-dose. Three 6-8 week old female NSG mice were administered a single dose of 0.3 (black trace) or 1.0 mg/kg (blue trace) MLN0128 and weights were monitored for acute drops over 48hrs.

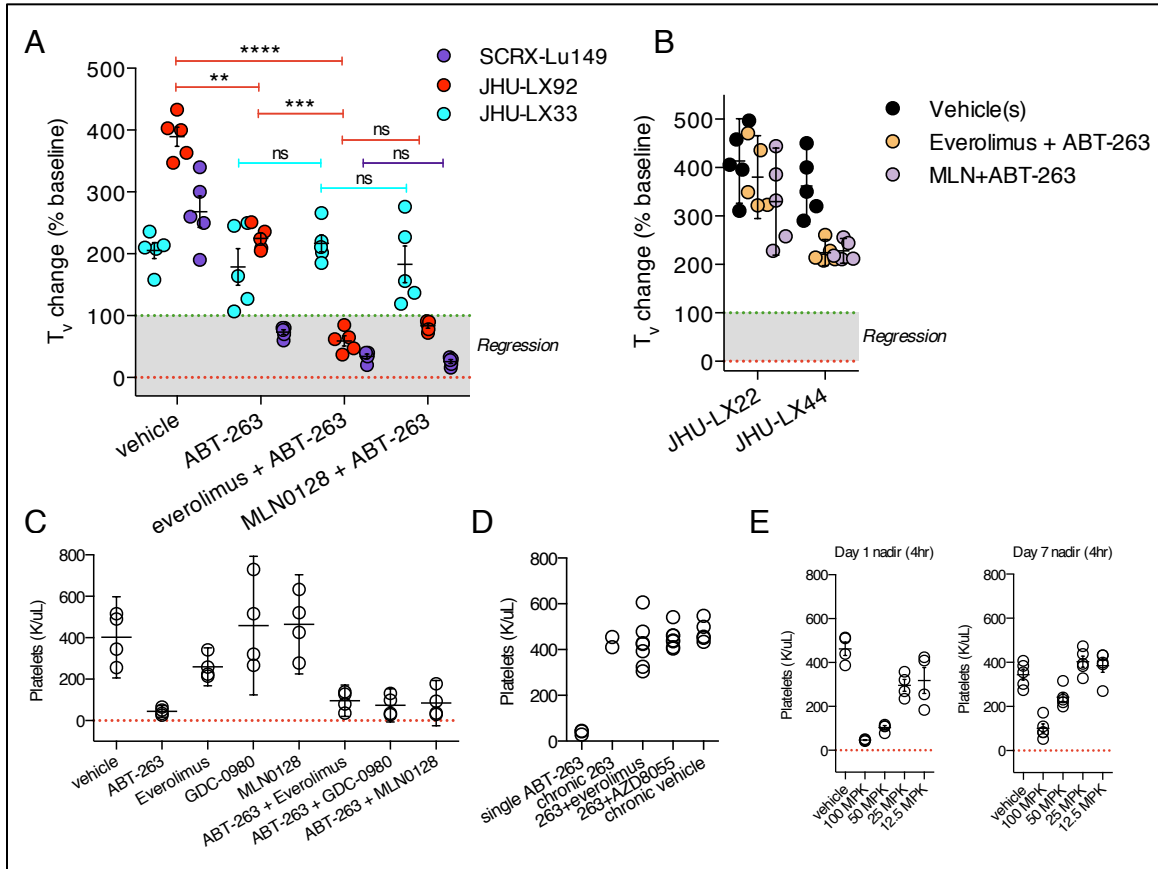


Figure 38. The combinations of ABT-263 with an mTOR allosteric or kinase domain inhibitor are non-inferior *in vivo* and ineffective in certain SCLC models.

(A) Tumor volume changes between 4 treatment arms across 3 PDX models of SCLC. Groups of tumor bearing animals were randomized to treatment arms when tumors approached $\sim 300\text{mm}^3$ (larger volume to allow for quantifiable regressions) to vehicle, daily 100mg/kg ABT-263 PO, or the combinations of 10mg/kg everolimus or AZD8055 PO with ABT-263. The rapalog and kinase inhibitor were administered two hours before the ABT-263 on a 24hr schedule for 7d. Response data are shown 24hrs after the final dose. *P*-values shown for paired *t*-tests between treatment groups within an individual PDX (color coded bars); n.s.=not significant.

(B) The combination of everolimus or MLN0128 with ABT-263 does not have broad anti-tumor activity in all models of SCLC. Groups of tumor bearing animals were randomized to treatment arms when tumors approached $\sim 300\text{mm}^3$ as above, and responses are compared 24hrs after the final dose. Tumor growth inhibition was observed in JHU-LX44 (BCL-2+ PDX), but no tumor regressions were noted, in contrast to SCRX-Lu149 or JHU-LX92.

(C) Acute treatment with various classes of mTOR inhibitors alone or in combination with ABT-263 does not worsen immediate platelet apoptosis (4hr nadir). Classes of mTOR inhibitor compounds (10mg/kg PO) were dosed 6hrs prior to tail bleed. When used in combination with 100mg/kg ABT-263, mTOR inhibitors were administered 2 hours before ABT-263. All platelet measures were performed on a Heska HemaTrue™ veterinary chemistry analyzer from tail bleeds ($\sim 100\mu\text{L}$) in EDTA-coated capillary tubes; n=5 non-tumor-bearing female NSG mice per acute treatment condition.

(D) Chronic administration of ABT-263 in combination with various classes of mTOR inhibitors does not worsen thrombocytopenia. Four hours after the day 7 dose of ABT-263 as a single agent or in combination with various mTOR inhibitors, mice were tail bled and platelets measured as above.

(E) Acute and chronic anti-platelet activity of ABT-263 in immune competent B6129SF1/J female mice (JAX strain #101043). Mice were tail bled and platelets assayed at 4hrs following a single dose or 7d of daily dosing of indicated tiers of ABT-263.

Acquired resistance to cisplatin and etoposide does not preclude activity of MLN0128 + ABT-263 in SCLC in vivo.

Once concern with moving a therapeutic strategy forward in SCLC is patient demographics. Virtually all patients with SCLC enrolled onto clinical trials of novel agents are being enrolled post-relapse with the randomization being at the level or 3rd or 4th line treatment. This yields a scenario where the patient's tumor has seen chemotherapy, relapsed at some interval of resistance (chemosensitive or chemorefractory) and is now largely considered resistant to standard of care cisplatin+etoposide. In examining the combined activity of cisplatin+etoposide versus ABT-263+everolimus, we did not note a linear trend in the data, suggesting that sensitivity or resistance to one combination did not preclude activity of the other (**Figure 39A**). Moreover, we had previously demonstrated the ability to model acquired resistance *in vivo* in a panel of chemosensitive PDX models of SCLC (Chapter 2 & **Figures 39B,C**).

In parallel, we had also explored generating isogenic resistant versions of NCI-H146, a SCLC cell line with *de novo* sensitivity to both the combinations of cisplatin+etoposide and ABT-263+everolimus. *In vitro* acquired resistance to etoposide or any class of mTOR inhibitor decrease the relative potency of etoposide in all isogenic versions tested, whereas these lines showed increased sensitivity to single agent ABT-263 (**Figure 39D**). These data help to suggest that resistance to etoposide, which is likely to be acquired in some way in all patients this combination will be tested in, is unlikely to directly promote resistance to ABT-263. Finally, we show that the *in vivo* activity of MLN0128 + ABT-263 is effectively preserved in one version of acquired resistance to cisplatin and etoposide in a paired chemosensitive and chemoresistant version of JHU-LX48, a BCL-2 expressing SCLC PDX. A weekly course of daily MLN0128 in combination with ABT-263 was capable to producing regressions in 5/5

animals on treatment in either the chemosensitive or chemoresistant setting (**Figures 39E,F**).

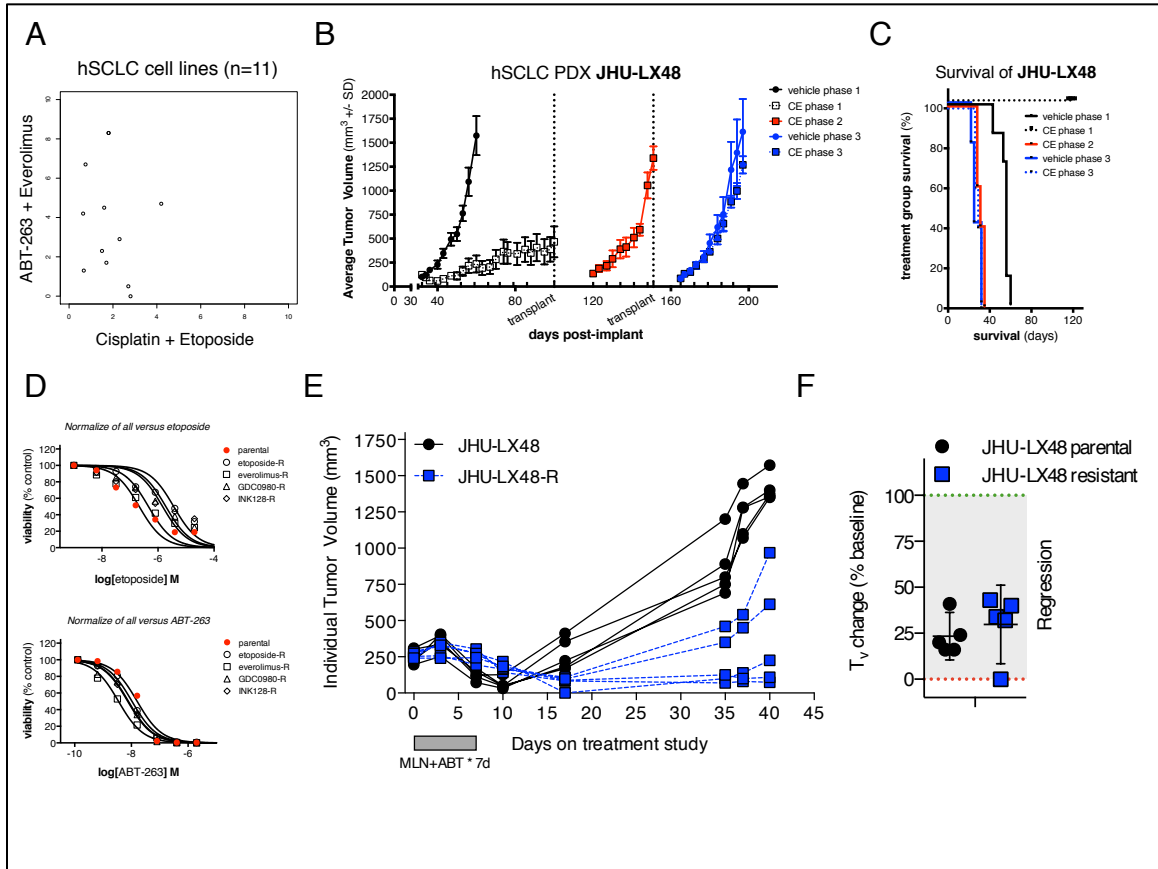


Figure 39. Acquired resistance to cisplatin/etoposide does not confer cross-resistance to ABT-263/MLN0128 *in vivo*.

(A) Effect size plot comparing the combinatorial activity of cisplatin+etoposide to everolimus+ABT-263 from a panel of SCLC cell lines (11 human SCLC cell lines). Data do not fit to a trend line

(B) Example *in vivo* tumor growth kinetic data from chemosensitive and chemoresistant versions of JHU-LX48 PDX model. Point of treatment tumors passage (“transplant”) indicated along x-axis with vertical dashed line.

(C) Survival differences between treatment arms in chemosensitive (CE phase 1; black dotted line) and chemoresistant (CE phase 3; blue dotted line) as a measure of time to reach 1000mm³. Tumors that did not reach endpoints (CE phase 1) are censored at the last point of measurement on protocol

(D) *In vitro* acquired resistance to multiple classes of mTOR targeted agents decreases the relative sensitivity to etoposide (*above*) while increases the sensitivity to ABT-263 (*below*). Data are shown for 72hrs cell proliferation assays (AlamarBlue). Cell lines were considered resistant when they were capable of doubling in at the same rate of the parental line under 100nM selection agent.

(E) The combination of MLN0128 and ABT-263 has activity *in vivo*, independent of sensitivity to cisplatin and etoposide. Paired chemosensitive and chemoresistant (“R”) BCL-2 expressing SCLC PDXs were engrafted into mice and treated for 7d with 100mg/kg ABT-263 + 1.0mg/kg MLN0128 daily for 7d.

(F) Best responses of parental or resistant JHU-LX48 tumors are non-inferior. Tumor volume changes (percent baseline volume) are not statistically different and both arms

show tumor regressions (data falling below green dotted line); p -value from paired t -test 0.452 (*not included on graph*).

Discussion

As agents targeting programmed cell death move towards late stage clinical testing, development and FDA-approval, it is critical to understand what subtypes of patients within a given tumor histology are likely to benefit. Moreover, it is becoming increasingly clear that targeting such vulnerabilities in tumors must be weighed against the expected toxicities – all of these agents, even if selective for BCL-2 over both BCL-2/xL, come with expectations of grade 3 or 4 hematologic toxicities (Konopleva et al., 2016; Levenson, 2016; Roberts et al., 2016). This creates a challenge for combinations with any cytotoxic agents or small molecular that induces cellular stress. Here we describe an effort to compare the relative activities of an allosteric mTOR inhibitor (everolimus) versus a catalytic mTOR (MLN0128) in combination with ABT-263 in multiple PDX models of SCLC. We were able to show that while *in vitro*, the catalytic mTOR inhibitor combination looked slightly more effective, *in vivo*, the comparison was non-inferior. Further, we established a daily schedule of each agent as most beneficial and show that acquired resistance to first line cisplatin/etoposide does not generate cross-resistance to ABT-263 + MLN0128, a central concern for moving these studies forward. Finally, we show that not all PDX models of SCLC will benefit from this therapeutic combination – notably, models that do not express BCL-2 or that have low baseline levels of pro-apoptotic BIM are anticipated to be resistant. Interestingly, in generating *in vitro* resistant models to BCL-2/xL inhibitors we show that loss of *BAX* permits resistance to any class of agent in combination with ABT-263, suggesting patients with genomic loss of inactivation of *BAX* will not benefit from this approach.

Loss of *BAX* is known to confer a greater resistance to chemotherapy and has been reported in several cancer types (Catasus et al., 1998; Rampino et al., 1997; Zhang et al., 2000). Several studies have shown that *BAX* levels can respond to various

insults including TRAIL (Liu et al., 2008), hypoxia (Erler et al., 2004), and p53-dependent apoptosis (Chipuk et al., 2004). Consensus in the literature has shown that *BAX* message levels do not change under these selective pressures. Interestingly, loss of *BAX* protein expression was observed in melanoma, another neural-crest-derived cancer, and this could be rescued with the proteasome inhibitor bortezomib (Chen et al., 2011; Miller et al., 2009). Several other publications have proposed a mechanism of ubiquitin-proteasome-mediated regulation of *BAX* levels (Benard et al., 2010; Fu et al., 2007; Li and Dou, 2000; Liu et al., 2008). While we have not explored the regulation of *BAX in vivo* to any exhaustive extent in SCLC, have been able to demonstrate acute down regulation at the protein level under treatment with the BCL-2/xL inhibitor ABT-737 (Gardner et al., 2014). Further, using shRNAs against BAK1 and *BAX*, we were able to show that it was suppression of *BAX*, and not BAK1, that permitted resistance to ABT-737 in our model systems. Importantly, suppression of either *BAX* or BAK1 did not greatly augment the responsiveness of multiple SCLC cell lines to cisplatin/etoposide, suggesting that the roles of these pro-apoptotic effector are likely to be cell intrinsic and should be examined thoroughly on the background of a given cell type.

Intended to be blank

Conclusions

SCLC remains a highly lethal disease with limited therapeutic options, outside of first line platinum+etoposide chemotherapy, second line topoisomerase I poisons, and third line enrollment onto a clinical trial. One of the challenges in advancing therapeutic development in this cancer has been a poor understanding of how tumors change from being exquisitely sensitive to chemotherapy, to a chemo refractory progressive disease. This work has substantially advanced this understand through the use of a set of genetically annotated chemoresponsive PDX models of SCLC, generating and annotating chemoresistant versions of each. The development of these tools helped to identify down-regulation of a *SLFN11*, a gene involved in DNA damage response. With recent knowledge of the epigenetic landscape of SCLC, we tied the down regulation of *SLFN11* to repressive histone methylation by the PRC2 component EZH2. Combining a clinical EZH2 inhibitor EPZ011989 with either first or second line chemotherapy in paired PDX models of chemosensitive or chemoresistant disease enabled complete disease control and prevented resistant outgrowth. This first part of this body of work has aided in uncovering one conserved mechanism of acquired resistance in vivo, with immediate clinical relevance.

The second half of this thesis has focused on targeting a resistance mechanism to programmed cell death, through the use of a small molecule BCL-2/xL inhibitor. The third chapter described an approach looking at the acute effects of single agent ABT-737 on responsive PDX models, trying to understand what the acute changes during response and immediately preceding resistant outgrowth looked like at the level of the transcriptome (**Figure 40**). This work was able to show that a loss in critical HIF-1 α transcripts and a down-regulation in protein levels of BAX were consistent changes observed across models. Combining an allosteric mTOR inhibitor with ABT-737 was

capable to reversing these gene expression changes, preserved BAX levels and led to durable tumor regressions in BCL-2 expressing PDX models.

The fourth chapter sought to address recent data from the Engelman group on broad activity of combining the BCL-2/xL inhibitor with AZD8055 in SCLC. These data slightly contradicted our findings in that they suggested ABT-263 would have activity in SCLC models with low levels of BCL-2 by the translational repression of AZD8055 on MCL-1 – effectively partnering pro-apoptotic effectors like BIM on BCL-xL, and sensitizing tumors to ABT-263. While their data were encouraging, we demonstrate that the combination of MLN0128 with ABT-263 is effectively non-inferior to combining ABT-263 with everolimus in multiple PDX models of SCLC. Further, there are likely to be scenarios where this combination is not effective, even in the presence of BCL-2 expression, as the ability of MLN0128 to suppress MCL-1 *in vivo* is variable across tumors due to variable use of cap-dependent translation. Unlike evidence in leukemia and lymphoma models where BCL-2 amplification or fusions are defining events, we show that SCLC does not exist in a “primed to die” state *in vivo* through sequential, time course analyses with or without various inhibitors of the mTOR pathway. The combined activity of an mTOR inhibitor with ABT-263 is something that required daily administration to achieve maximal anti-tumor effect, where loss of *BAX* was capable of promoting resistance to either single agent ABT-263 or the combination with various classes of mTOR inhibitors. Taken together, these studies demonstrate the utility of using SCLC PDX models in both a discovery mode, to determine mechanisms of acquired resistance to first line chemotherapy, and in an efficacy mode, to refine what subtypes of SCLC are likely to respond to combination therapies.

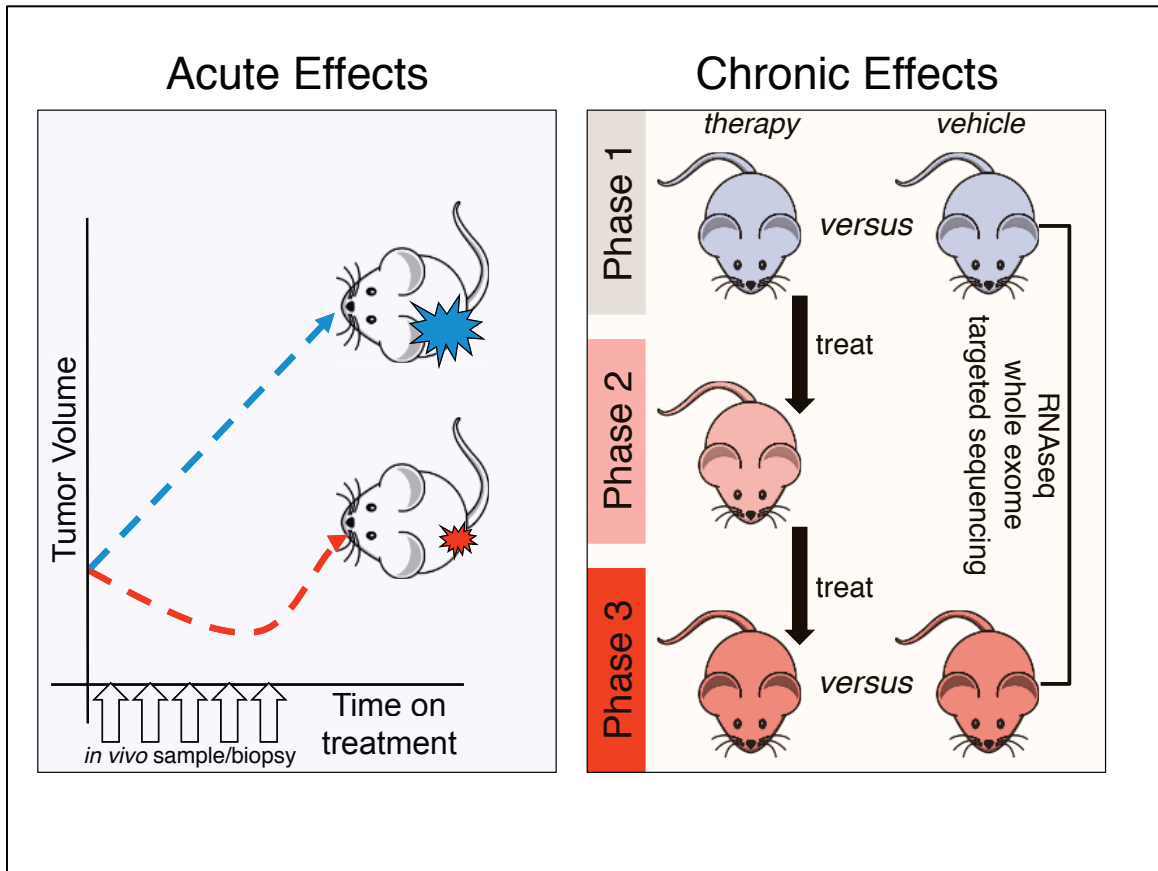


Figure 40. Approaches to studying mechanisms of acquired resistance *in vivo* using PDX models of SCLC.

When choosing phenotypic response data as a measure of acquisition of resistance or *de novo* sensitivity to a given therapeutic challenge, it is important to consider sampling times and establishment of acquired resistance *in vivo*. For example, on the **left** panel, acute effects can be thought of as the gene expression changes and events within the tumor that are occurring during the initial period of response or treatment challenge, such that they need to be surveyed within a defined time window in parallel to a contemporaneous vehicle group. In contrast, acquiring resistance to a therapeutic can be examined over time through multiple passages of a given PDX on or off therapy, such as on the **right** panel. In this example, re-enuftment of previously-treated PDX materials (survival fraction) to determine the extent the mechanism of acquired resistance (for example, gene expression changes) are conserved in the next generation of passage and phenotypically demonstrated.

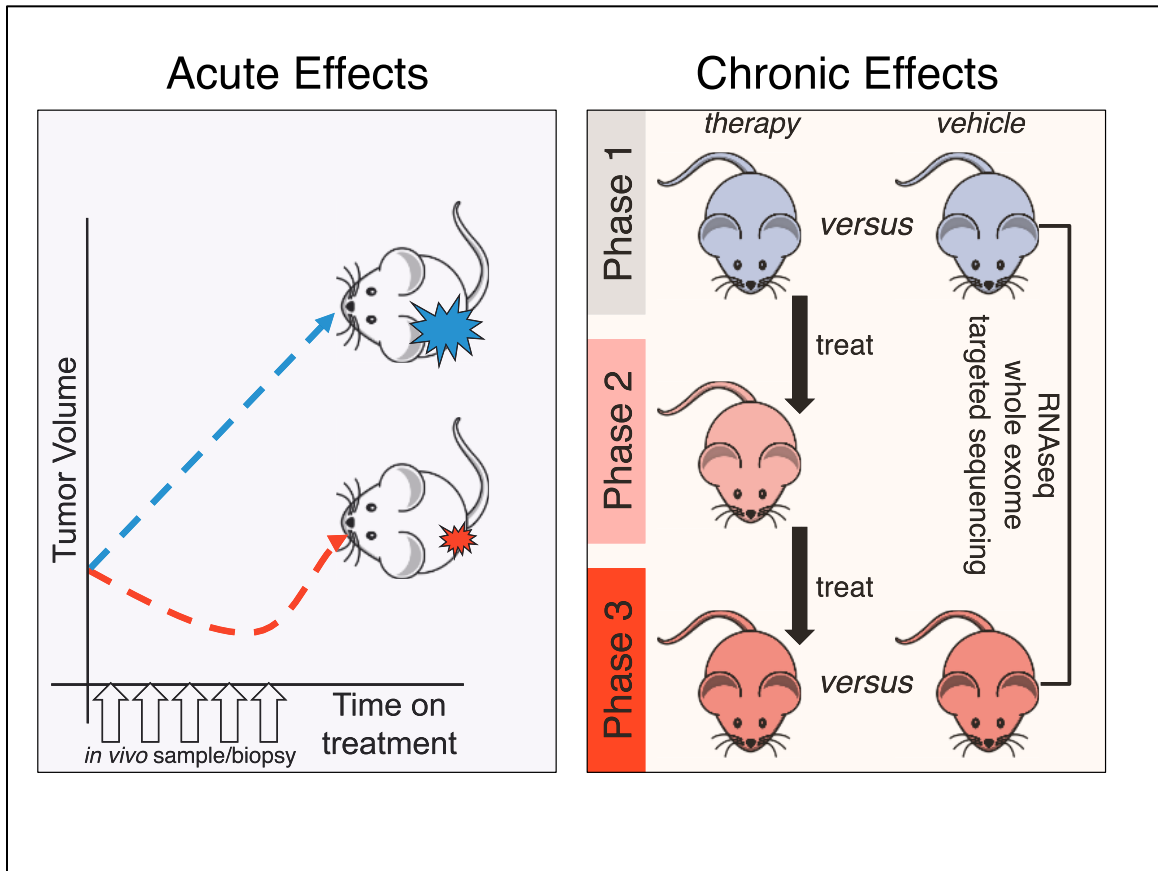


Figure 40. Approaches to studying mechanisms of acquired resistance *in vivo* using PDX models of SCLC.

When choosing phenotypic response data as a measure of acquisition of resistance or *de novo* sensitivity to a given therapeutic challenge, it is important to consider sampling times and establishment of acquired resistance *in vivo*. For example, on the **left** panel, acute effects can be thought of as the gene expression changes and events within the tumor that are occurring during the initial period of response or treatment challenge, such that they need to be surveyed within a defined time window in parallel to a contemporaneous vehicle group. In contrast, acquiring resistance to a therapeutic can be examined over time through multiple passages of a given PDX on or off therapy, such as on the **right** panel. In this example, re-enuftment of previously-treated PDX materials (survival fraction) to determine the extent the mechanism of acquired resistance (for example, gene expression changes) are conserved in the next generation of passage and phenotypically demonstrated.

Intended to be blank

References

- Abdelraouf, F., Smit, E., Hasan, B., Menis, J., Popat, S., van Meerbeeck, J. P., Surmont, V. F., Baas, P., and O'Brien, M. (2016). Sunitinib (SU11248) in patients with chemo naive extensive small cell lung cancer or who have a 'chemosensitive' relapse: A single-arm phase II study (EORTC-08061). *Eur J Cancer* 54, 35-39.
- Ackler, S., Xiao, Y., Mitten, M. J., Foster, K., Oleksijew, A., Refici, M., Schlessinger, S., Wang, B., Chemburkar, S. R., Bauch, J., *et al.* (2008). ABT-263 and rapamycin act cooperatively to kill lymphoma cells in vitro and in vivo. *Mol Cancer Ther* 7, 3265-3274.
- Agrawal, S. G., Liu, F. T., Wiseman, C., Shirali, S., Liu, H., Lillington, D., Du, M. Q., Syndercombe-Court, D., Newland, A. C., Gribben, J. G., and Jia, L. (2008). Increased proteasomal degradation of Bax is a common feature of poor prognosis chronic lymphocytic leukemia. *Blood* 111, 2790-2796.
- Asahina, H., Nokihara, H., Yamamoto, N., Yamada, Y., Tamura, Y., Honda, K., Seki, Y., Tanabe, Y., Shimada, H., Shi, X., and Tamura, T. (2013). Safety and tolerability of AZD8055 in Japanese patients with advanced solid tumors; a dose-finding phase I study. *Invest New Drugs* 31, 677-684.
- Aslan, J. E., Tormoen, G. W., Loren, C. P., Pang, J., and McCarty, O. J. (2011). S6K1 and mTOR regulate Rac1-driven platelet activation and aggregation. *Blood* 118, 3129-3136.
- Augsten, M. (2014). Cancer-associated fibroblasts as another polarized cell type of the tumor microenvironment. *Front Oncol* 4, 62.
- Bar-Peled, L., Chantranupong, L., Cherniack, A. D., Chen, W. W., Ottina, K. A., Grabiner, B. C., Spear, E. D., Carter, S. L., Meyerson, M., and Sabatini, D. M. (2013). A Tumor suppressor complex with GAP activity for the Rag GTPases that signal amino acid sufficiency to mTORC1. *Science* 340, 1100-1106.
- Barretina, J., Caponigro, G., Stransky, N., Venkatesan, K., Margolin, A. A., Kim, S., Wilson, C. J., Lehar, J., Kryukov, G. V., Sonkin, D., *et al.* (2012). The Cancer Cell Line Encyclopedia enables predictive modelling of anticancer drug sensitivity. *Nature* 483, 603-607.
- Beck, B., Lapouge, G., Rorive, S., Drogat, B., Desaedelaere, K., Delafaille, S., Dubois, C., Salmon, I., Willekens, K., Marine, J. C., and Blanpain, C. (2015). Different levels of Twist1 regulate skin tumor initiation, stemness, and progression. *Cell Stem Cell* 16, 67-79.
- Begley, C. G., and Ellis, L. M. (2012). Drug development: Raise standards for preclinical cancer research. *Nature* 483, 531-533.
- Behera, M., Ragin, C., Kim, S., Pillai, R. N., Chen, Z., Steuer, C. E., Saba, N. F., Belani, C. P., Khuri, F. R., Ramalingam, S. S., and Owonikoko, T. K. (2016). Trends, predictors, and impact of systemic chemotherapy in small cell lung cancer patients between 1985 and 2005. *Cancer* 122, 50-60.
- Belani, C. P., Dahlberg, S. E., Rudin, C. M., Fleisher, M., Chen, H. X., Takebe, N., Velasco, M. R., Jr., Tester, W. J., Sturtz, K., Hann, C. L., *et al.* (2016). Vismodegib or cixutumumab in combination with standard chemotherapy for patients with extensive-stage small cell lung cancer: A trial of the ECOG-ACRIN Cancer Research Group (E1508). *Cancer*.

- Ben-Ezra, J. M., Kornstein, M. J., Grimes, M. M., and Krystal, G. (1994). Small cell carcinomas of the lung express the Bcl-2 protein. *Am J Pathol* *145*, 1036-1040.
- Benard, G., Neutzner, A., Peng, G., Wang, C., Livak, F., Youle, R. J., and Karbowski, M. (2010). IBRDC2, an IBR-type E3 ubiquitin ligase, is a regulatory factor for Bax and apoptosis activation. *The EMBO journal* *29*, 1458-1471.
- Benjamin, D., Colombi, M., Moroni, C., and Hall, M. N. (2011). Rapamycin passes the torch: a new generation of mTOR inhibitors. *Nat Rev Drug Discov* *10*, 868-880.
- Beroukhi, R., Mermel, C. H., Porter, D., Wei, G., Raychaudhuri, S., Donovan, J., Barretina, J., Boehm, J. S., Dobson, J., Urashima, M., *et al.* (2010). The landscape of somatic copy-number alteration across human cancers. *Nature* *463*, 899-905.
- Bertotti, A., Papp, E., Jones, S., Adleff, V., Anagnostou, V., Lupo, B., Sausen, M., Phallen, J., Hruban, C. A., Tokheim, C., *et al.* (2015). The genomic landscape of response to EGFR blockade in colorectal cancer. *Nature* *526*, 263-267.
- Borromeo, M. D., Savage, T. K., Kollipara, R. K., He, M., Augustyn, A., Osborne, J. K., Girard, L., Minna, J. D., Gazdar, A. F., Cobb, M. H., and Johnson, J. E. (2016). ASCL1 and NEUROD1 Reveal Heterogeneity in Pulmonary Neuroendocrine Tumors and Regulate Distinct Genetic Programs. *Cell Rep* *16*, 1259-1272.
- Bracken, A. P., Pasini, D., Capra, M., Prosperini, E., Colli, E., and Helin, K. (2003). EZH2 is downstream of the pRB-E2F pathway, essential for proliferation and amplified in cancer. *EMBO J* *22*, 5323-5335.
- Breton, C., Story, M. D., and Meyn, R. E. (1998). Bcl-2 expression correlates with apoptosis induction but not loss of clonogenic survival in small cell lung cancer cell lines treated with etoposide. *Anticancer Drugs* *9*, 751-757.
- Brumatti, G., and Ekert, P. G. (2013). Seeking a MCL-1 inhibitor. *Cell Death Differ* *20*, 1440-1441.
- Bruna, A., Rueda, O. M., Greenwood, W., Batra, A. S., Callari, M., Batra, R. N., Pogrebniak, K., Sandoval, J., Cassidy, J. W., Tufegdzcic-Vidakovic, A., *et al.* (2016). A Biobank of Breast Cancer Explants with Preserved Intra-tumor Heterogeneity to Screen Anticancer Compounds. *Cell* *167*, 260-274 e222.
- Bunn, P. A., Jr., Minna, J. D., Augustyn, A., Gazdar, A. F., Ouadah, Y., Krasnow, M. A., Berns, A., Brambilla, E., Rekhman, N., Massion, P. P., *et al.* (2016). Small Cell Lung Cancer: Can Recent Advances in Biology and Molecular Biology Be Translated into Improved Outcomes? *J Thorac Oncol* *11*, 453-474.
- Byers, L. A., Wang, J., Nilsson, M. B., Fujimoto, J., Saintigny, P., Yordy, J., Giri, U., Peyton, M., Fan, Y. H., Diao, L., *et al.* (2012). Proteomic profiling identifies dysregulated pathways in small cell lung cancer and novel therapeutic targets including PARP1. *Cancer Discov* *2*, 798-811.
- Cafferkey, R., Young, P. R., McLaughlin, M. M., Bergsma, D. J., Koltin, Y., Sathe, G. M., Faucette, L., Eng, W. K., Johnson, R. K., and Livi, G. P. (1993). Dominant missense mutations in a novel yeast protein related to mammalian phosphatidylinositol 3-kinase and VPS34 abrogate rapamycin cytotoxicity. *Mol Cell Biol* *13*, 6012-6023.

- Calbo, J., van Montfort, E., Proost, N., van Drunen, E., Beverloo, H. B., Meuwissen, R., and Berns, A. (2011). A functional role for tumor cell heterogeneity in a mouse model of small cell lung cancer. *Cancer Cell* *19*, 244-256.
- Campbell, J. D., Alexandrov, A., Kim, J., Wala, J., Berger, A. H., Pedamallu, C. S., Shukla, S. A., Guo, G., Brooks, A. N., Murray, B. A., *et al.* (2016). Distinct patterns of somatic genome alterations in lung adenocarcinomas and squamous cell carcinomas. *Nat Genet* *48*, 607-616.
- Campbell, J. E., Kuntz, K. W., Knutson, S. K., Warholic, N. M., Keilhack, H., Wigle, T. J., Raimondi, A., Klaus, C. R., Rioux, N., Yokoi, A., *et al.* (2015). EPZ01989, A Potent, Orally-Available EZH2 Inhibitor with Robust in Vivo Activity. *ACS Med Chem Lett* *6*, 491-495.
- Carette, J. E., Guimaraes, C. P., Wuethrich, I., Blomen, V. A., Varadarajan, M., Sun, C., Bell, G., Yuan, B., Muellner, M. K., Nijman, S. M., *et al.* (2011). Global gene disruption in human cells to assign genes to phenotypes by deep sequencing. *Nat Biotechnol* *29*, 542-546.
- Carlisle, B., Demko, N., Freeman, G., Hakala, A., MacKinnon, N., Ramsay, T., Hey, S., London, A. J., and Kimmelman, J. (2016). Benefit, Risk, and Outcomes in Drug Development: A Systematic Review of Sunitinib. *J Natl Cancer Inst* *108*.
- Carney, D. N., Gazdar, A. F., Bepler, G., Guccion, J. G., Marangos, P. J., Moody, T. W., Zweig, M. H., and Minna, J. D. (1985). Establishment and identification of small cell lung cancer cell lines having classic and variant features. *Cancer research* *45*, 2913-2923.
- Catasus, L., Matias-Guiu, X., Machin, P., Munoz, J., and Prat, J. (1998). BAX somatic frameshift mutations in endometrioid adenocarcinomas of the endometrium: evidence for a tumor progression role in endometrial carcinomas with microsatellite instability. *Laboratory investigation; a journal of technical methods and pathology* *78*, 1439-1444.
- Certo, M., Del Gaizo Moore, V., Nishino, M., Wei, G., Korsmeyer, S., Armstrong, S. A., and Letai, A. (2006). Mitochondria primed by death signals determine cellular addiction to antiapoptotic BCL-2 family members. *Cancer Cell* *9*, 351-365.
- Chantranupong, L., Wolfson, R. L., Orozco, J. M., Saxton, R. A., Scaria, S. M., Bar-Peled, L., Spooner, E., Isasa, M., Gygi, S. P., and Sabatini, D. M. (2014). The Sestrins interact with GATOR2 to negatively regulate the amino-acid-sensing pathway upstream of mTORC1. *Cell Rep* *9*, 1-8.
- Chawla, S. P., Staddon, A. P., Baker, L. H., Schuetze, S. M., Tolcher, A. W., D'Amato, G. Z., Blay, J. Y., Mita, M. M., Sankhala, K. K., Berk, L., *et al.* (2012). Phase II study of the mammalian target of rapamycin inhibitor ridaforolimus in patients with advanced bone and soft tissue sarcomas. *J Clin Oncol* *30*, 78-84.
- Chen, H., Thiagalingam, A., Chopra, H., Borges, M. W., Feder, J. N., Nelkin, B. D., Baylin, S. B., and Ball, D. W. (1997). Conservation of the Drosophila lateral inhibition pathway in human lung cancer: a hairy-related protein (HES-1) directly represses achaete-scute homolog-1 expression. *Proc Natl Acad Sci U S A* *94*, 5355-5360.
- Chen, J., Jin, S., Abraham, V., Huang, X., Liu, B., Mitten, M. J., Nimmer, P., Lin, X., Smith, M., Shen, Y., *et al.* (2011). The Bcl-2/Bcl-X(L)/Bcl-w inhibitor, navitoclax, enhances the activity of chemotherapeutic agents in vitro and in vivo. *Mol Cancer Ther* *10*, 2340-2349.

- Cheng, D. T., Mitchell, T. N., Zehir, A., Shah, R. H., Benayed, R., Syed, A., Chandramohan, R., Liu, Z. Y., Won, H. H., Scott, S. N., *et al.* (2015). Memorial Sloan Kettering-Integrated Mutation Profiling of Actionable Cancer Targets (MSK-IMPACT): A Hybridization Capture-Based Next-Generation Sequencing Clinical Assay for Solid Tumor Molecular Oncology. *J Mol Diagn* 17, 251-264.
- Chipuk, J. E., Kuwana, T., Bouchier-Hayes, L., Droin, N. M., Newmeyer, D. D., Schuler, M., and Green, D. R. (2004). Direct activation of Bax by p53 mediates mitochondrial membrane permeabilization and apoptosis. *Science* 303, 1010-1014.
- Chonghaile, T. N., Roderick, J. E., Glenfield, C., Ryan, J., Sallan, S. E., Silverman, L. B., Loh, M. L., Hunger, S. P., Wood, B., DeAngelo, D. J., *et al.* (2014). Maturation stage of T-cell acute lymphoblastic leukemia determines BCL-2 versus BCL-XL dependence and sensitivity to ABT-199. *Cancer Discov* 4, 1074-1087.
- Chou, T. C. (2010). Drug combination studies and their synergy quantification using the Chou-Talalay method. *Cancer Res* 70, 440-446.
- Chou, T. C., and Talalay, P. (1984). Quantitative analysis of dose-effect relationships: the combined effects of multiple drugs or enzyme inhibitors. *Advances in enzyme regulation* 22, 27-55.
- Christensen, C. L., Kwiatkowski, N., Abraham, B. J., Carretero, J., Al-Shahrour, F., Zhang, T., Chipumuro, E., Herter-Sprie, G. S., Akbay, E. A., Altabef, A., *et al.* (2014). Targeting transcriptional addictions in small cell lung cancer with a covalent CDK7 inhibitor. *Cancer Cell* 26, 909-922.
- Crystal, A. S., Shaw, A. T., Sequist, L. V., Friboulet, L., Niederst, M. J., Lockerman, E. L., Frias, R. L., Gainor, J. F., Amzallag, A., Greninger, P., *et al.* (2014). Patient-derived models of acquired resistance can identify effective drug combinations for cancer. *Science* 346, 1480-1486.
- Cui, M., Augert, A., Rongione, M., Conkrite, K., Parazzoli, S., Nikitin, A. Y., Ingolia, N., and MacPherson, D. (2014). PTEN is a potent suppressor of small cell lung cancer. *Mol Cancer Res* 12, 654-659.
- Dabora, S. L., Franz, D. N., Ashwal, S., Sagalowsky, A., DiMario, F. J., Jr., Miles, D., Cutler, D., Krueger, D., Uppot, R. N., Rabenou, R., *et al.* (2011). Multicenter phase 2 trial of sirolimus for tuberous sclerosis: kidney angiomyolipomas and other tumors regress and VEGF- D levels decrease. *PLoS One* 6, e23379.
- Daniel, V. C., Marchionni, L., Hierman, J. S., Rhodes, J. T., Devereux, W. L., Rudin, C. M., Yung, R., Parmigiani, G., Dorsch, M., Peacock, C. D., and Watkins, D. N. (2009). A primary xenograft model of small-cell lung cancer reveals irreversible changes in gene expression imposed by culture in vitro. *Cancer Res* 69, 3364-3373.
- Day, C. P., Merlino, G., and Van Dyke, T. (2015). Preclinical Mouse Cancer Models: A Maze of Opportunities and Challenges. *Cell* 163, 39-53.
- De Smet, C., Lurquin, C., Lethe, B., Martelange, V., and Boon, T. (1999). DNA methylation is the primary silencing mechanism for a set of germ line- and tumor-specific genes with a CpG-rich promoter. *Mol Cell Biol* 19, 7327-7335.

- Denny, S. K., Yang, D., Chuang, C. H., Brady, J. J., Lim, J. S., Gruner, B. M., Chiou, S. H., Schep, A. N., Baral, J., Hamard, C., *et al.* (2016). Nfib Promotes Metastasis through a Widespread Increase in Chromatin Accessibility. *Cell* 166, 328-342.
- DePristo, M. A., Banks, E., Poplin, R., Garimella, K. V., Maguire, J. R., Hartl, C., Philippakis, A. A., del Angel, G., Rivas, M. A., Hanna, M., *et al.* (2011). A framework for variation discovery and genotyping using next-generation DNA sequencing data. *Nat Genet* 43, 491-498.
- DeRose, Y. S., Wang, G., Lin, Y. C., Bernard, P. S., Buys, S. S., Ebbert, M. T., Factor, R., Matsen, C., Milash, B. A., Nelson, E., *et al.* (2011). Tumor grafts derived from women with breast cancer authentically reflect tumor pathology, growth, metastasis and disease outcomes. *Nat Med* 17, 1514-1520.
- Di Maio, M., Bironzo, P., and Scagliotti, G. V. (2016). Raising the bar for enthusiasm when looking at results of randomized phase II trials-the case of sunitinib in small-cell lung cancer. *Transl Lung Cancer Res* 5, 89-91.
- Dobin, A., Davis, C. A., Schlesinger, F., Drenkow, J., Zaleski, C., Jha, S., Batut, P., Chaisson, M., and Gingeras, T. R. (2013). STAR: ultrafast universal RNA-seq aligner. *Bioinformatics* 29, 15-21.
- Dooley, A. L., Winslow, M. M., Chiang, D. Y., Banerji, S., Stransky, N., Dayton, T. L., Snyder, E. L., Senna, S., Whittaker, C. A., Bronson, R. T., *et al.* (2011). Nuclear factor I/B is an oncogene in small cell lung cancer. *Genes Dev* 25, 1470-1475.
- Dowling, R. J., Topisirovic, I., Alain, T., Bidinosti, M., Fonseca, B. D., Petroulakis, E., Wang, X., Larsson, O., Selvaraj, A., Liu, Y., *et al.* (2010). mTORC1-mediated cell proliferation, but not cell growth, controlled by the 4E-BPs. *Science* 328, 1172-1176.
- Duvel, K., Yecies, J. L., Menon, S., Raman, P., Lipovsky, A. I., Souza, A. L., Triantafellow, E., Ma, Q., Gorski, R., Cleaver, S., *et al.* (2010). Activation of a metabolic gene regulatory network downstream of mTOR complex 1. *Mol Cell* 39, 171-183.
- Elvidge, G. P., Glenny, L., Appelhoff, R. J., Ratcliffe, P. J., Ragoussis, J., and Gleadle, J. M. (2006). Concordant regulation of gene expression by hypoxia and 2-oxoglutarate-dependent dioxygenase inhibition: the role of HIF-1alpha, HIF-2alpha, and other pathways. *J Biol Chem* 281, 15215-15226.
- Erler, J. T., Cawthorne, C. J., Williams, K. J., Koritzinsky, M., Wouters, B. G., Wilson, C., Miller, C., Demonacos, C., Stratford, I. J., and Dive, C. (2004). Hypoxia-mediated down-regulation of Bid and Bax in tumors occurs via hypoxia-inducible factor 1-dependent and -independent mechanisms and contributes to drug resistance. *Molecular and cellular biology* 24, 2875-2889.
- Faber, A. C., Farago, A. F., Costa, C., Dastur, A., Gomez-Caraballo, M., Robbins, R., Wagner, B. L., Rideout, W. M., 3rd, Jakubik, C. T., Ham, J., *et al.* (2015). Assessment of ABT-263 activity across a cancer cell line collection leads to a potent combination therapy for small-cell lung cancer. *Proc Natl Acad Sci U S A* 112, E1288-1296.
- Faivre, S., Delbaldo, C., Vera, K., Robert, C., Lozahic, S., Lassau, N., Bello, C., Deprimo, S., Brega, N., Massimini, G., *et al.* (2006). Safety, pharmacokinetic, and antitumor activity of SU11248, a novel oral multitarget tyrosine kinase inhibitor, in patients with cancer. *J Clin Oncol* 24, 25-35.

- Fellmann, C., Hoffmann, T., Sridhar, V., Hopfgartner, B., Muhar, M., Roth, M., Lai, D. Y., Barbosa, I. A., Kwon, J. S., Guan, Y., *et al.* (2013). An optimized microRNA backbone for effective single-copy RNAi. *Cell Rep* 5, 1704-1713.
- Fillmore, C. M., Xu, C., Desai, P. T., Berry, J. M., Rowbotham, S. P., Lin, Y. J., Zhang, H., Marquez, V. E., Hammerman, P. S., Wong, K. K., and Kim, C. F. (2015). EZH2 inhibition sensitizes BRG1 and EGFR mutant lung tumours to Topoll inhibitors. *Nature* 520, 239-242.
- Fiorentino, F. P., Tokgun, E., Sole-Sanchez, S., Giampaolo, S., Tokgun, O., Jauset, T., Kohno, T., Perucho, M., Soucek, L., and Yokota, J. (2016). Growth suppression by MYC inhibition in small cell lung cancer cells with TP53 and RB1 inactivation. *Oncotarget* 7, 31014-31028.
- Fischer, K. R., Durrans, A., Lee, S., Sheng, J., Li, F., Wong, S. T., Choi, H., El Rayes, T., Ryu, S., Troeger, J., *et al.* (2015). Epithelial-to-mesenchymal transition is not required for lung metastasis but contributes to chemoresistance. *Nature* 527, 472-476.
- Forshe, T., Murtaza, M., Parkinson, C., Gale, D., Tsui, D. W., Kaper, F., Dawson, S. J., Piskorz, A. M., Jimenez-Linan, M., Bentley, D., *et al.* (2012). Noninvasive identification and monitoring of cancer mutations by targeted deep sequencing of plasma DNA. *Sci Transl Med* 4, 136ra168.
- Fu, N. Y., Sukumaran, S. K., and Yu, V. C. (2007). Inhibition of ubiquitin-mediated degradation of MOAP-1 by apoptotic stimuli promotes Bax function in mitochondria. *Proceedings of the National Academy of Sciences of the United States of America* 104, 10051-10056.
- Galluzzi, L., Buque, A., Kepp, O., Zitvogel, L., and Kroemer, G. (2015). Immunological Effects of Conventional Chemotherapy and Targeted Anticancer Agents. *Cancer Cell* 28, 690-714.
- Gandhi, L., Camidge, D. R., Ribeiro de Oliveira, M., Bonomi, P., Gandara, D., Khaira, D., Hann, C. L., McKeegan, E. M., Litvinovich, E., Hemken, P. M., *et al.* (2011). Phase I study of Navitoclax (ABT-263), a novel Bcl-2 family inhibitor, in patients with small-cell lung cancer and other solid tumors. *J Clin Oncol* 29, 909-916.
- Gao, D., Vela, I., Sboner, A., Iaquineta, P. J., Karthaus, W. R., Gopalan, A., Dowling, C., Wanjala, J. N., Undvall, E. A., Arora, V. K., *et al.* (2014). Organoid cultures derived from patients with advanced prostate cancer. *Cell* 159, 176-187.
- Gao, H., Korn, J. M., Ferretti, S., Monahan, J. E., Wang, Y., Singh, M., Zhang, C., Schnell, C., Yang, G., Zhang, Y., *et al.* (2015). High-throughput screening using patient-derived tumor xenografts to predict clinical trial drug response. *Nat Med* 21, 1318-1325.
- Gardner, E. E., Connis, N., Poirier, J. T., Cope, L., Dobromilskaya, I., Gallia, G. L., Rudin, C. M., and Hann, C. L. (2014). Rapamycin rescues ABT-737 efficacy in small cell lung cancer. *Cancer Res* 74, 2846-2856.
- Gentleman, R. C., Carey, V. J., Bates, D. M., Bolstad, B., Dettling, M., Dudoit, S., Ellis, B., Gautier, L., Ge, Y., Gentry, J., *et al.* (2004). Bioconductor: open software development for computational biology and bioinformatics. *Genome biology* 5, R80.
- George, J., Lim, J. S., Jang, S. J., Cun, Y., Ozretic, L., Kong, G., Leenders, F., Lu, X., Fernandez-Cuesta, L., Bosco, G., *et al.* (2015). Comprehensive genomic profiles of small cell lung cancer. *Nature* 524, 47-53.

- Gerstein, M. B., Kundaje, A., Hariharan, M., Landt, S. G., Yan, K. K., Cheng, C., Mu, X. J., Khurana, E., Rozowsky, J., Alexander, R., *et al.* (2012). Architecture of the human regulatory network derived from ENCODE data. *Nature* *489*, 91-100.
- Ghobrial, I. M., Siegel, D. S., Vij, R., Berdeja, J. G., Richardson, P. G., Neuwirth, R., Patel, C. G., Zohren, F., and Wolf, J. L. (2016). TAK-228 (formerly MLN0128), an investigational oral dual TORC1/2 inhibitor: A phase I dose escalation study in patients with relapsed or refractory multiple myeloma, non-Hodgkin lymphoma, or Waldenstrom's macroglobulinemia. *Am J Hematol* *91*, 400-405.
- Gould, S. E., Junttila, M. R., and de Sauvage, F. J. (2015). Translational value of mouse models in oncology drug development. *Nat Med* *21*, 431-439.
- Green, D. R. (2016). The cell's dilemma, or the story of cell death: an entertainment in three acts. *FEBS J* *283*, 2568-2576.
- Han, J. Y., Kim, H. Y., Lim, K. Y., Han, J. H., Lee, Y. J., Kwak, M. H., Kim, H. J., Yun, T., Kim, H. T., and Lee, J. S. (2013). A phase II study of sunitinib in patients with relapsed or refractory small cell lung cancer. *Lung Cancer* *79*, 137-142.
- Hanahan, D., and Weinberg, R. A. (2011). Hallmarks of cancer: the next generation. *Cell* *144*, 646-674.
- Hann, C. L., Daniel, V. C., Sugar, E. A., Dobromilskaya, I., Murphy, S. C., Cope, L., Lin, X., Hierman, J. S., Wilburn, D. L., Watkins, D. N., and Rudin, C. M. (2008). Therapeutic efficacy of ABT-737, a selective inhibitor of BCL-2, in small cell lung cancer. *Cancer Res* *68*, 2321-2328.
- Hara, K., Yonezawa, K., Weng, Q. P., Kozlowski, M. T., Belham, C., and Avruch, J. (1998). Amino acid sufficiency and mTOR regulate p70 S6 kinase and eIF-4E BP1 through a common effector mechanism. *J Biol Chem* *273*, 14484-14494.
- Harper, M. T., and Poole, A. W. (2012). Bcl-xL-inhibitory BH3 mimetic ABT-737 depletes platelet calcium stores. *Blood* *119*, 4337-4338.
- Harrison, L. R., Micha, D., Brandenburg, M., Simpson, K. L., Morrow, C. J., Denny, O., Hodgkinson, C., Yunus, Z., Dempsey, C., Roberts, D., *et al.* (2011). Hypoxic human cancer cells are sensitized to BH-3 mimetic-induced apoptosis via downregulation of the Bcl-2 protein Mcl-1. *J Clin Invest* *121*, 1075-1087.
- Henderson, V. C., Demko, N., Hakala, A., MacKinnon, N., Federico, C. A., Fergusson, D., and Kimmelman, J. (2015). A meta-analysis of threats to valid clinical inference in preclinical research of sunitinib. *Elife* *4*.
- Henderson, V. C., Kimmelman, J., Fergusson, D., Grimshaw, J. M., and Hackam, D. G. (2013). Threats to validity in the design and conduct of preclinical efficacy studies: a systematic review of guidelines for in vivo animal experiments. *PLoS Med* *10*, e1001489.
- Hess, G., Herbrecht, R., Romaguera, J., Verhoef, G., Crump, M., Gisselbrecht, C., Laurell, A., Offner, F., Strahs, A., Berkenblit, A., *et al.* (2009). Phase III study to evaluate temsirolimus compared with investigator's choice therapy for the treatment of relapsed or refractory mantle cell lymphoma. *J Clin Oncol* *27*, 3822-3829.

- Hidalgo, M., Amant, F., Biankin, A. V., Budinska, E., Byrne, A. T., Caldas, C., Clarke, R. B., de Jong, S., Jonkers, J., Maelandsmo, G. M., *et al.* (2014). Patient-derived xenograft models: an emerging platform for translational cancer research. *Cancer Discov* 4, 998-1013.
- Hidalgo, M., Bruckheimer, E., Rajeshkumar, N. V., Garrido-Laguna, I., De Oliveira, E., Rubio-Viqueira, B., Strawn, S., Wick, M. J., Martell, J., and Sidransky, D. (2011). A pilot clinical study of treatment guided by personalized tumorgrafts in patients with advanced cancer. *Mol Cancer Ther* 10, 1311-1316.
- Hopkins-Donaldson, S., Ziegler, A., Kurtz, S., Bigosch, C., Kandoler, D., Ludwig, C., Zangemeister-Wittke, U., and Stahel, R. (2003). Silencing of death receptor and caspase-8 expression in small cell lung carcinoma cell lines and tumors by DNA methylation. *Cell Death Differ* 10, 356-364.
- Horita, N., Yamamoto, M., Sato, T., Tsukahara, T., Nagakura, H., Tashiro, K., Shibata, Y., Watanabe, H., Nagai, K., Inoue, M., *et al.* (2015). Topotecan for Relapsed Small-cell Lung Cancer: Systematic Review and Meta-Analysis of 1347 Patients. *Sci Rep* 5, 15437.
- Hudes, G., Carducci, M., Tomczak, P., Dutcher, J., Figlin, R., Kapoor, A., Staroslawska, E., Sosman, J., McDermott, D., Bodrogi, I., *et al.* (2007). Temsirolimus, interferon alfa, or both for advanced renal-cell carcinoma. *N Engl J Med* 356, 2271-2281.
- Huijbers, I. J., Bin Ali, R., Pritchard, C., Cozijnsen, M., Kwon, M. C., Proost, N., Song, J. Y., de Vries, H., Badhai, J., Sutherland, K., *et al.* (2014). Rapid target gene validation in complex cancer mouse models using re-derived embryonic stem cells. *EMBO Mol Med* 6, 212-225.
- Ikegaki, N., Katsumata, M., Minna, J., and Tsujimoto, Y. (1994). Expression of bcl-2 in small cell lung carcinoma cells. *Cancer Res* 54, 6-8.
- Inoki, K., Corradetti, M. N., and Guan, K. L. (2005). Dysregulation of the TSC-mTOR pathway in human disease. *Nat Genet* 37, 19-24.
- Inoki, K., Li, Y., Zhu, T., Wu, J., and Guan, K. L. (2002). TSC2 is phosphorylated and inhibited by Akt and suppresses mTOR signalling. *Nat Cell Biol* 4, 648-657.
- Inoki, K., Zhu, T., and Guan, K. L. (2003). TSC2 mediates cellular energy response to control cell growth and survival. *Cell* 115, 577-590.
- Inuzuka, H., Shaik, S., Onoyama, I., Gao, D., Tseng, A., Maser, R. S., Zhai, B., Wan, L., Gutierrez, A., Lau, A. W., *et al.* (2011). SCF(FBW7) regulates cellular apoptosis by targeting MCL1 for ubiquitylation and destruction. *Nature* 471, 104-109.
- Irizarry, R. A., Warren, D., Spencer, F., Kim, I. F., Biswal, S., Frank, B. C., Gabrielson, E., Garcia, J. G., Geoghegan, J., Germino, G., *et al.* (2005). Multiple-laboratory comparison of microarray platforms. *Nature methods* 2, 345-350.
- Izumchenko, E., Meir, J., Bedi, A., Wysocki, P. T., Hoque, M. O., and Sidransky, D. (2016). Patient-derived xenografts as tools in pharmaceutical development. *Clin Pharmacol Ther* 99, 612-621.
- Jacinto, E., Loewith, R., Schmidt, A., Lin, S., Ruegg, M. A., Hall, A., and Hall, M. N. (2004). Mammalian TOR complex 2 controls the actin cytoskeleton and is rapamycin insensitive. *Nat Cell Biol* 6, 1122-1128.

- Jadhav, U., Nalapareddy, K., Saxena, M., O'Neill, N. K., Pinello, L., Yuan, G. C., Orkin, S. H., and Shivdasani, R. A. (2016). Acquired Tissue-Specific Promoter Bivalency Is a Basis for PRC2 Necessity in Adult Cells. *Cell* *165*, 1389-1400.
- Jahchan, N. S., Dudley, J. T., Mazur, P. K., Flores, N., Yang, D., Palmerton, A., Zmoos, A. F., Vaka, D., Tran, K. Q., Zhou, M., *et al.* (2013). A drug repositioning approach identifies tricyclic antidepressants as inhibitors of small cell lung cancer and other neuroendocrine tumors. *Cancer Discov* *3*, 1364-1377.
- Jahchan, N. S., Lim, J. S., Bola, B., Morris, K., Seitz, G., Tran, K. Q., Xu, L., Trapani, F., Morrow, C. J., Cristea, S., *et al.* (2016). Identification and Targeting of Long-Term Tumor-Propagating Cells in Small Cell Lung Cancer. *Cell Rep* *16*, 644-656.
- Ji, H., Ramsey, M. R., Hayes, D. N., Fan, C., McNamara, K., Kozlowski, P., Torrice, C., Wu, M. C., Shimamura, T., Perera, S. A., *et al.* (2007). LKB1 modulates lung cancer differentiation and metastasis. *Nature* *448*, 807-810.
- Jiang, S. X., Sato, Y., Kuwao, S., and Kameya, T. (1995). Expression of bcl-2 oncogene protein is prevalent in small cell lung carcinomas. *J Pathol* *177*, 135-138.
- Jiang, T., Collins, B. J., Jin, N., Watkins, D. N., Brock, M. V., Matsui, W., Nelkin, B. D., and Ball, D. W. (2009). Achaete-scute complex homologue 1 regulates tumor-initiating capacity in human small cell lung cancer. *Cancer Res* *69*, 845-854.
- Juin, P., Geneste, O., Gautier, F., Depil, S., and Campone, M. (2013). Decoding and unlocking the BCL-2 dependency of cancer cells. *Nature reviews Cancer* *13*, 455-465.
- Kalari, S., Jung, M., Kernstine, K. H., Takahashi, T., and Pfeifer, G. P. (2013). The DNA methylation landscape of small cell lung cancer suggests a differentiation defect of neuroendocrine cells. *Oncogene* *32*, 3559-3568.
- Kalemkerian, G. P., Akerley, W., Bogner, P., Borghaei, H., Chow, L. Q., Downey, R. J., Gandhi, L., Ganti, A. K., Govindan, R., Grecula, J. C., *et al.* Small cell lung cancer. *J Natl Compr Canc Netw* *11*, 78-98.
- Kalemkerian, G. P., Akerley, W., Bogner, P., Borghaei, H., Chow, L. Q., Downey, R. J., Gandhi, L., Ganti, A. K., Govindan, R., Grecula, J. C., *et al.* (2013). Small cell lung cancer. *J Natl Compr Canc Netw* *11*, 78-98.
- Kalluri, R. (2016). The biology and function of fibroblasts in cancer. *Nat Rev Cancer* *16*, 582-598.
- Kaminsky, V. O., Surova, O. V., Vaculova, A., and Zhivotovsky, B. (2011). Combined inhibition of DNA methyltransferase and histone deacetylase restores caspase-8 expression and sensitizes SCLC cells to TRAIL. *Carcinogenesis* *32*, 1450-1458.
- Karthaus, W. R., Iaquinta, P. J., Drost, J., Gracanin, A., van Boxtel, R., Wongvipat, J., Dowling, C. M., Gao, D., Begthel, H., Sachs, N., *et al.* (2014). Identification of multipotent luminal progenitor cells in human prostate organoid cultures. *Cell* *159*, 163-175.
- Kilkenny, C., Browne, W. J., Cuthill, I. C., Emerson, M., and Altman, D. G. (2010). Improving bioscience research reporting: the ARRIVE guidelines for reporting animal research. *PLoS Biol* *8*, e1000412.

- Kim, E., Goraksha-Hicks, P., Li, L., Neufeld, T. P., and Guan, K. L. (2008). Regulation of TORC1 by Rag GTPases in nutrient response. *Nat Cell Biol* 10, 935-945.
- Kim, J. S., Ro, S. H., Kim, M., Park, H. W., Semple, I. A., Park, H., Cho, U. S., Wang, W., Guan, K. L., Karin, M., and Lee, J. H. (2015a). Sestrin2 inhibits mTORC1 through modulation of GATOR complexes. *Sci Rep* 5, 9502.
- Kim, K. H., Kim, W., Howard, T. P., Vazquez, F., Tsherniak, A., Wu, J. N., Wang, W., Haswell, J. R., Walensky, L. D., Hahn, W. C., *et al.* (2015b). SWI/SNF-mutant cancers depend on catalytic and non-catalytic activity of EZH2. *Nat Med* 21, 1491-1496.
- Klymenko, T., Brandenburg, M., Morrow, C., Dive, C., and Makin, G. (2011). The novel Bcl-2 inhibitor ABT-737 is more effective in hypoxia and is able to reverse hypoxia-induced drug resistance in neuroblastoma cells. *Mol Cancer Ther* 10, 2373-2383.
- Knutson, S. K., Wigle, T. J., Warholic, N. M., Sneeringer, C. J., Allain, C. J., Klaus, C. R., Sacks, J. D., Raimondi, A., Majer, C. R., Song, J., *et al.* (2012). A selective inhibitor of EZH2 blocks H3K27 methylation and kills mutant lymphoma cells. *Nat Chem Biol* 8, 890-896.
- Kononen, J., Bubendorf, L., Kallioniemi, A., Barlund, M., Schraml, P., Leighton, S., Torhorst, J., Mihatsch, M. J., Sauter, G., and Kallioniemi, O. P. (1998). Tissue microarrays for high-throughput molecular profiling of tumor specimens. *Nat Med* 4, 844-847.
- Konopleva, M., Pollyea, D. A., Potluri, J., Chyla, B., Hogdal, L., Busman, T., McKeegan, E., Salem, A. H., Zhu, M., Ricker, J. L., *et al.* (2016). Efficacy and Biological Correlates of Response in a Phase II Study of Venetoclax Monotherapy in Patients with Acute Myelogenous Leukemia. *Cancer Discov*.
- Kosari, F., Ida, C. M., Aubry, M. C., Yang, L., Kovtun, I. V., Klein, J. L., Li, Y., Erdogan, S., Tomaszek, S. C., Murphy, S. J., *et al.* (2014). ASCL1 and RET expression defines a clinically relevant subgroup of lung adenocarcinoma characterized by neuroendocrine differentiation. *Oncogene* 33, 3776-3783.
- Kreso, A., O'Brien, C. A., van Galen, P., Gan, O. I., Notta, F., Brown, A. M., Ng, K., Ma, J., Wienholds, E., Dunant, C., *et al.* (2013). Variable clonal repopulation dynamics influence chemotherapy response in colorectal cancer. *Science* 339, 543-548.
- Krueger, D. A., Care, M. M., Holland, K., Agricola, K., Tudor, C., Mangeshkar, P., Wilson, K. A., Byars, A., Sahmoud, T., and Franz, D. N. (2010). Everolimus for subependymal giant-cell astrocytomas in tuberous sclerosis. *N Engl J Med* 363, 1801-1811.
- Krysko, O., Love Aaes, T., Bachert, C., Vandenabeele, P., and Krysko, D. V. (2013). Many faces of DAMPs in cancer therapy. *Cell Death Dis* 4, e631.
- Kunz, J., Henriquez, R., Schneider, U., Deuter-Reinhard, M., Movva, N. R., and Hall, M. N. (1993). Target of rapamycin in yeast, TOR2, is an essential phosphatidylinositol kinase homolog required for G1 progression. *Cell* 73, 585-596.
- LaFave, L. M., Beguelin, W., Koche, R., Teater, M., Spitzer, B., Chramiec, A., Papalex, E., Keller, M. D., Hricik, T., Konstantinoff, K., *et al.* (2015). Loss of BAP1 function leads to EZH2-dependent transformation. *Nat Med* 21, 1344-1349.

- Lamb, J., Crawford, E. D., Peck, D., Modell, J. W., Blat, I. C., Wrobel, M. J., Lerner, J., Brunet, J. P., Subramanian, A., Ross, K. N., *et al.* (2006). The Connectivity Map: using gene-expression signatures to connect small molecules, genes, and disease. *Science* 313, 1929-1935.
- Lamming, D. W., Ye, L., Katajisto, P., Goncalves, M. D., Saitoh, M., Stevens, D. M., Davis, J. G., Salmon, A. B., Richardson, A., Ahima, R. S., *et al.* (2012). Rapamycin-induced insulin resistance is mediated by mTORC2 loss and uncoupled from longevity. *Science* 335, 1638-1643.
- Landis, S. C., Amara, S. G., Asadullah, K., Austin, C. P., Blumenstein, R., Bradley, E. W., Crystal, R. G., Darnell, R. B., Ferrante, R. J., Fillit, H., *et al.* (2012). A call for transparent reporting to optimize the predictive value of preclinical research. *Nature* 490, 187-191.
- Laplante, M., and Sabatini, D. M. (2012). mTOR signaling in growth control and disease. *Cell* 149, 274-293.
- Lawrence, M. S., Stojanov, P., Polak, P., Kryukov, G. V., Cibulskis, K., Sivachenko, A., Carter, S. L., Stewart, C., Mermel, C. H., Roberts, S. A., *et al.* (2013). Mutational heterogeneity in cancer and the search for new cancer-associated genes. *Nature* 499, 214-218.
- Lehar, J., Krueger, A. S., Avery, W., Heilbut, A. M., Johansen, L. M., Price, E. R., Rickles, R. J., Short, G. F., 3rd, Staunton, J. E., Jin, X., *et al.* (2009). Synergistic drug combinations tend to improve therapeutically relevant selectivity. *Nat Biotechnol* 27, 659-666.
- Leong, T. L., Marini, K. D., Rossello, F. J., Jayasekara, S. N., Russell, P. A., Prodanovic, Z., Kumar, B., Ganju, V., Alamgeer, M., Irving, L. B., *et al.* (2014). Genomic characterisation of small cell lung cancer patient-derived xenografts generated from endobronchial ultrasound-guided transbronchial needle aspiration specimens. *PLoS One* 9, e106862.
- Lessene, G., Czabotar, P. E., Sleebs, B. E., Zobel, K., Lowes, K. N., Adams, J. M., Baell, J. B., Colman, P. M., Deshayes, K., Fairbrother, W. J., *et al.* (2013). Structure-guided design of a selective BCL-X(L) inhibitor. *Nat Chem Biol* 9, 390-397.
- Letai, A., Bassik, M. C., Walensky, L. D., Sorcinelli, M. D., Weiler, S., and Korsmeyer, S. J. (2002). Distinct BH3 domains either sensitize or activate mitochondrial apoptosis, serving as prototype cancer therapeutics. *Cancer Cell* 2, 183-192.
- Leverson, J. D. (2016). Chemical parsing: Dissecting cell dependencies with a toolkit of selective BCL-2 family inhibitors. *Mol Cell Oncol* 3, e1050155.
- Levine, D. A., Bogomolny, F., Yee, C. J., Lash, A., Barakat, R. R., Borgen, P. I., and Boyd, J. (2005). Frequent mutation of the PIK3CA gene in ovarian and breast cancers. *Clin Cancer Res* 11, 2875-2878.
- Li, B., and Dou, Q. P. (2000). Bax degradation by the ubiquitin/proteasome-dependent pathway: involvement in tumor survival and progression. *Proceedings of the National Academy of Sciences of the United States of America* 97, 3850-3855.
- Li, H., and Durbin, R. (2009). Fast and accurate short read alignment with Burrows-Wheeler transform. *Bioinformatics* 25, 1754-1760.
- Li, M., Kao, E., Gao, X., Sandig, H., Limmer, K., Pavon-Eternod, M., Jones, T. E., Landry, S., Pan, T., Weitzman, M. D., and David, M. (2012). Codon-usage-based inhibition of HIV protein synthesis by human schlafen 11. *Nature* 491, 125-128.

- Liao, Y., Smyth, G. K., and Shi, W. (2014). featureCounts: an efficient general purpose program for assigning sequence reads to genomic features. *Bioinformatics* *30*, 923-930.
- Lin, C. Y., Loven, J., Rahl, P. B., Paranal, R. M., Burge, C. B., Bradner, J. E., Lee, T. I., and Young, R. A. (2012). Transcriptional amplification in tumor cells with elevated c-Myc. *Cell* *151*, 56-67.
- Lin, X., Morgan-Lappe, S., Huang, X., Li, L., Zakula, D. M., Verneti, L. A., Fesik, S. W., and Shen, Y. (2007). 'Seed' analysis of off-target siRNAs reveals an essential role of Mcl-1 in resistance to the small-molecule Bcl-2/Bcl-XL inhibitor ABT-737. *Oncogene* *26*, 3972-3979.
- Little, C. D., Nau, M. M., Carney, D. N., Gazdar, A. F., and Minna, J. D. (1983). Amplification and expression of the c-myc oncogene in human lung cancer cell lines. *Nature* *306*, 194-196.
- Liu, F. T., Agrawal, S. G., Gribben, J. G., Ye, H., Du, M. Q., Newland, A. C., and Jia, L. (2008). Bortezomib blocks Bax degradation in malignant B cells during treatment with TRAIL. *Blood* *111*, 2797-2805.
- Lok, B. H., Gardner, E. E., Schneeberger, V. E., Ni, A., Desmeules, P., Rekhman, N., de Stanchina, E., Teicher, B. A., Riaz, N., Powell, S. N., *et al.* (2016). PARP Inhibitor Activity Correlates with SLFN11 Expression and Demonstrates Synergy with Temozolomide in Small Cell Lung Cancer. *Clin Cancer Res.*
- Loven, J., Hoke, H. A., Lin, C. Y., Lau, A., Orlando, D. A., Vakoc, C. R., Bradner, J. E., Lee, T. I., and Young, R. A. (2013). Selective inhibition of tumor oncogenes by disruption of super-enhancers. *Cell* *153*, 320-334.
- Ma, L., Chen, Z., Erdjument-Bromage, H., Tempst, P., and Pandolfi, P. P. (2005). Phosphorylation and functional inactivation of TSC2 by Erk implications for tuberous sclerosis and cancer pathogenesis. *Cell* *121*, 179-193.
- Maia, A. M., da Silva, J. H., Mencialha, A. L., Caffarena, E. R., and Abdelhay, E. (2012). Computational modeling of the bHLH domain of the transcription factor TWIST1 and R118C, S144R and K145E mutants. *BMC Bioinformatics* *13*, 184.
- Makela, T. P., Shiraishi, M., Borrello, M. G., Sekiya, T., and Alitalo, K. (1992). Rearrangement and co-amplification of L-myc and rlf in primary lung cancer. *Oncogene* *7*, 405-409.
- Manning, B. D., Tee, A. R., Logsdon, M. N., Blenis, J., and Cantley, L. C. (2002). Identification of the tuberous sclerosis complex-2 tumor suppressor gene product tuberlin as a target of the phosphoinositide 3-kinase/akt pathway. *Mol Cell* *10*, 151-162.
- McCabe, M. T., Ott, H. M., Ganji, G., Korenchuk, S., Thompson, C., Van Aller, G. S., Liu, Y., Graves, A. P., Della Pietra, A., 3rd, Diaz, E., *et al.* (2012). EZH2 inhibition as a therapeutic strategy for lymphoma with EZH2-activating mutations. *Nature* *492*, 108-112.
- McFadden, D. G., Papagiannakopoulos, T., Taylor-Weiner, A., Stewart, C., Carter, S. L., Cibulskis, K., Bhutkar, A., McKenna, A., Dooley, A., Vernon, A., *et al.* (2014). Genetic and clonal dissection of murine small cell lung carcinoma progression by genome sequencing. *Cell* *156*, 1298-1311.
- McKenna, A., Hanna, M., Banks, E., Sivachenko, A., Cibulskis, K., Kernysky, A., Garimella, K., Altshuler, D., Gabriel, S., Daly, M., and DePristo, M. A. (2010). The Genome Analysis Toolkit: a

MapReduce framework for analyzing next-generation DNA sequencing data. *Genome Res* 20, 1297-1303.

Meuwissen, R., Linn, S. C., Linnoila, R. I., Zevenhoven, J., Mooi, W. J., and Berns, A. (2003). Induction of small cell lung cancer by somatic inactivation of both Trp53 and Rb1 in a conditional mouse model. *Cancer Cell* 4, 181-189.

Miller, L. A., Goldstein, N. B., Johannes, W. U., Walton, C. H., Fujita, M., Norris, D. A., and Shellman, Y. G. (2009). BH3 mimetic ABT-737 and a proteasome inhibitor synergistically kill melanomas through Noxa-dependent apoptosis. *J Invest Dermatol* 129, 964-971.

Moffat, J., Grueneberg, D. A., Yang, X., Kim, S. Y., Kloepfer, A. M., Hinkle, G., Piqani, B., Eisenhaure, T. M., Luo, B., Grenier, J. K., *et al.* (2006). A lentiviral RNAi library for human and mouse genes applied to an arrayed viral high-content screen. *Cell* 124, 1283-1298.

Mohammad, H. P., Smitheman, K. N., Kamat, C. D., Soong, D., Federowicz, K. E., Van Aller, G. S., Schneck, J. L., Carson, J. D., Liu, Y., Buttice, M., *et al.* (2015). A DNA Hypomethylation Signature Predicts Antitumor Activity of LSD1 Inhibitors in SCLC. *Cancer Cell* 28, 57-69.

Montero, J., Sarosiek, K. A., DeAngelo, J. D., Maertens, O., Ryan, J., Ercan, D., Piao, H., Horowitz, N. S., Berkowitz, R. S., Matulonis, U., *et al.* (2015). Drug-induced death signaling strategy rapidly predicts cancer response to chemotherapy. *Cell* 160, 977-989.

Mootha, V. K., Lindgren, C. M., Eriksson, K. F., Subramanian, A., Sihag, S., Lehar, J., Puigserver, P., Carlsson, E., Ridderstrale, M., Laurila, E., *et al.* (2003). PGC-1alpha-responsive genes involved in oxidative phosphorylation are coordinately downregulated in human diabetes. *Nature genetics* 34, 267-273.

Morin, R. D., Johnson, N. A., Severson, T. M., Mungall, A. J., An, J., Goya, R., Paul, J. E., Boyle, M., Woolcock, B. W., Kuchenbauer, F., *et al.* (2010). Somatic mutations altering EZH2 (Tyr641) in follicular and diffuse large B-cell lymphomas of germinal-center origin. *Nat Genet* 42, 181-185.

Morton, J. J., Bird, G., Refaeli, Y., and Jimeno, A. (2016). Humanized mouse xenograft models: narrowing the tumor-microenvironment gap. *Cancer Res*.

Motzer, R. J., Escudier, B., Oudard, S., Hutson, T. E., Porta, C., Bracarda, S., Grunwald, V., Thompson, J. A., Figlin, R. A., Hollaender, N., *et al.* (2008). Efficacy of everolimus in advanced renal cell carcinoma: a double-blind, randomised, placebo-controlled phase III trial. *Lancet* 372, 449-456.

Mu, Y., Lou, J., Srivastava, M., Zhao, B., Feng, X. H., Liu, T., Chen, J., and Huang, J. (2016). SLFN11 inhibits checkpoint maintenance and homologous recombination repair. *EMBO Rep* 17, 94-109.

Muranen, T., Selfors, L. M., Worster, D. T., Iwanicki, M. P., Song, L., Morales, F. C., Gao, S., Mills, G. B., and Brugge, J. S. (2012). Inhibition of PI3K/mTOR leads to adaptive resistance in matrix-attached cancer cells. *Cancer Cell* 21, 227-239.

Murtaza, M., Dawson, S. J., Tsui, D. W., Gale, D., Forshew, T., Piskorz, A. M., Parkinson, C., Chin, S. F., Kingsbury, Z., Wong, A. S., *et al.* (2013). Non-invasive analysis of acquired resistance to cancer therapy by sequencing of plasma DNA. *Nature* 497, 108-112.

- Naing, A., Aghajanian, C., Raymond, E., Olmos, D., Schwartz, G., Oelmann, E., Grinsted, L., Burke, W., Taylor, R., Kaye, S., *et al.* (2012). Safety, tolerability, pharmacokinetics and pharmacodynamics of AZD8055 in advanced solid tumours and lymphoma. *Br J Cancer* *107*, 1093-1099.
- Nasgashio, R., Sato, Y., Matsumoto, T., Kageyama, T., Hattori, M., Iyoda, A., Satoh, Y., Ryuge, S., Masuda, N., Jiang, S. X., and Saegusa, M. (2011). The balance between the expressions of hASH1 and HES1 differs between large cell neuroendocrine carcinoma and small cell carcinoma of the lung. *Lung Cancer* *74*, 405-410.
- National Cancer Institute, T. (2014). 2014 Scientific Framework for Small Cell Lung Cancer. http://deainfocinihgov/advisory/ctac/workgroup/SCLC/SCLC_Congressional_Responsepdf.
- Nau, M. M., Brooks, B. J., Battey, J., Sausville, E., Gazdar, A. F., Kirsch, I. R., McBride, O. W., Bertness, V., Hollis, G. F., and Minna, J. D. (1985). L-myc, a new myc-related gene amplified and expressed in human small cell lung cancer. *Nature* *318*, 69-73.
- Nau, M. M., Brooks, B. J., Jr., Carney, D. N., Gazdar, A. F., Battey, J. F., Sausville, E. A., and Minna, J. D. (1986). Human small-cell lung cancers show amplification and expression of the N-myc gene. *Proc Natl Acad Sci U S A* *83*, 1092-1096.
- Ni Chonghaile, T., Sarosiek, K. A., Vo, T. T., Ryan, J. A., Tammareddi, A., Moore Vdel, G., Deng, J., Anderson, K. C., Richardson, P., Tai, Y. T., *et al.* (2011). Pretreatment mitochondrial priming correlates with clinical response to cytotoxic chemotherapy. *Science* *334*, 1129-1133.
- Nilsen, G., Liestol, K., Van Loo, P., Moen Vollan, H. K., Eide, M. B., Rueda, O. M., Chin, S. F., Russell, R., Baumbusch, L. O., Caldas, C., *et al.* (2012). Copynumber: Efficient algorithms for single- and multi-track copy number segmentation. *BMC Genomics* *13*, 591.
- Nogales, V., Reinhold, W. C., Varma, S., Martinez-Cardus, A., Moutinho, C., Moran, S., Heyn, H., Sebio, A., Barnadas, A., Pommier, Y., and Esteller, M. (2016). Epigenetic inactivation of the putative DNA/RNA helicase SLFN11 in human cancer confers resistance to platinum drugs. *Oncotarget* *7*, 3084-3097.
- O'Reilly, K. E., Rojo, F., She, Q. B., Solit, D., Mills, G. B., Smith, D., Lane, H., Hofmann, F., Hicklin, D. J., Ludwig, D. L., *et al.* (2006). mTOR inhibition induces upstream receptor tyrosine kinase signaling and activates Akt. *Cancer Res* *66*, 1500-1508.
- Ocak, S., Yamashita, H., Udyavar, A. R., Miller, A. N., Gonzalez, A. L., Zou, Y., Jiang, A., Yi, Y., Shyr, Y., Estrada, L., *et al.* (2010). DNA copy number aberrations in small-cell lung cancer reveal activation of the focal adhesion pathway. *Oncogene* *29*, 6331-6342.
- Ogiwara, H., Sasaki, M., Mitachi, T., Oike, T., Higuchi, S., Tominaga, Y., and Kohno, T. (2016). Targeting p300 Addiction in CBP-Deficient Cancers Causes Synthetic Lethality by Apoptotic Cell Death due to Abrogation of MYC Expression. *Cancer Discov* *6*, 430-445.
- Olejniczak, E. T., Van Sant, C., Anderson, M. G., Wang, G., Tahir, S. K., Sauter, G., Lesniewski, R., and Semizarov, D. (2007). Integrative genomic analysis of small-cell lung carcinoma reveals correlates of sensitivity to bcl-2 antagonists and uncovers novel chromosomal gains. *Mol Cancer Res* *5*, 331-339.

Oltersdorf, T., Elmore, S. W., Shoemaker, A. R., Armstrong, R. C., Augeri, D. J., Belli, B. A., Bruncko, M., Deckwerth, T. L., Dinges, J., Hajduk, P. J., *et al.* (2005). An inhibitor of Bcl-2 family proteins induces regression of solid tumours. *Nature* *435*, 677-681.

Orlando, D. A., Chen, M. W., Brown, V. E., Solanki, S., Choi, Y. J., Olson, E. R., Fritz, C. C., Bradner, J. E., and Guenther, M. G. (2014). Quantitative ChIP-Seq normalization reveals global modulation of the epigenome. *Cell Rep* *9*, 1163-1170.

Osborne, J. K., Guerra, M. L., Gonzales, J. X., McMillan, E. A., Minna, J. D., and Cobb, M. H. (2014). NeuroD1 mediates nicotine-induced migration and invasion via regulation of the nicotinic acetylcholine receptor subunits in a subset of neural and neuroendocrine carcinomas. *Mol Biol Cell* *25*, 1782-1792.

Oze, I., Hotta, K., Kiura, K., Ochi, N., Takigawa, N., Fujiwara, Y., Tabata, M., and Tanimoto, M. (2009). Twenty-seven years of phase III trials for patients with extensive disease small-cell lung cancer: disappointing results. *PLoS One* *4*, e7835.

Park, C. M., Bruncko, M., Adickes, J., Bauch, J., Ding, H., Kunzer, A., Marsh, K. C., Nimmer, P., Shoemaker, A. R., Song, X., *et al.* (2008). Discovery of an orally bioavailable small molecule inhibitor of prosurvival B-cell lymphoma 2 proteins. *Journal of medicinal chemistry* *51*, 6902-6915.

Park, K. S., Liang, M. C., Raiser, D. M., Zamponi, R., Roach, R. R., Curtis, S. J., Walton, Z., Schaffer, B. E., Roake, C. M., Zmoos, A. F., *et al.* (2011a). Characterization of the cell of origin for small cell lung cancer. *Cell Cycle* *10*, 2806-2815.

Park, K. S., Martelotto, L. G., Peifer, M., Sos, M. L., Karnezis, A. N., Mahjoub, M. R., Bernard, K., Conklin, J. F., Szczepny, A., Yuan, J., *et al.* (2011b). A crucial requirement for Hedgehog signaling in small cell lung cancer. *Nat Med* *17*, 1504-1508.

Parmigiani, A., Nourbakhsh, A., Ding, B., Wang, W., Kim, Y. C., Akopiants, K., Guan, K. L., Karin, M., and Budanov, A. V. (2014). Sestrins inhibit mTORC1 kinase activation through the GATOR complex. *Cell Rep* *9*, 1281-1291.

Peifer, M., Fernandez-Cuesta, L., Sos, M. L., George, J., Seidel, D., Kasper, L. H., Plenker, D., Leenders, F., Sun, R., Zander, T., *et al.* (2012). Integrative genome analyses identify key somatic driver mutations of small-cell lung cancer. *Nat Genet* *44*, 1104-1110.

Pelayo Alvarez, M., Westeel, V., Cortes-Jofre, M., and Bonfill Cosp, X. (2013). Chemotherapy versus best supportive care for extensive small cell lung cancer. *Cochrane Database Syst Rev*, CD001990.

Pena-Llopis, S., Vega-Rubin-de-Celis, S., Schwartz, J. C., Wolff, N. C., Tran, T. A., Zou, L., Xie, X. J., Corey, D. R., and Brugarolas, J. (2011). Regulation of TFEB and V-ATPases by mTORC1. *EMBO J* *30*, 3242-3258.

Peterson, T. R., Laplante, M., Thoreen, C. C., Sancak, Y., Kang, S. A., Kuehl, W. M., Gray, N. S., and Sabatini, D. M. (2009). DEPTOR is an mTOR inhibitor frequently overexpressed in multiple myeloma cells and required for their survival. *Cell* *137*, 873-886.

Poirier, J. T., Dobromilskaya, I., Moriarty, W. F., Peacock, C. D., Hann, C. L., and Rudin, C. M. (2013). Selective tropism of Seneca Valley virus for variant subtype small cell lung cancer. *J Natl Cancer Inst* *105*, 1059-1065.

- Poirier, J. T., Gardner, E. E., Connis, N., Moreira, A. L., de Stanchina, E., Hann, C. L., and Rudin, C. M. (2015). DNA methylation in small cell lung cancer defines distinct disease subtypes and correlates with high expression of EZH2. *Oncogene* *34*, 5869-5878.
- Polley, E., Kunkel, M., Evans, D., Silvers, T., Delosh, R., Laudeman, J., Ogle, C., Reinhart, R., Selby, M., Connelly, J., *et al.* (2016). Small Cell Lung Cancer Screen of Oncology Drugs, Investigational Agents, and Gene and microRNA Expression. *J Natl Cancer Inst* *108*.
- Pott, S., and Lieb, J. D. (2015). What are super-enhancers? *Nat Genet* *47*, 8-12.
- Punnoose, E. A., Levenson, J. D., Peale, F., Boghaert, E. R., Belmont, L. D., Tan, N., Young, A., Mitten, M., Ingalla, E., Darbonne, W. C., *et al.* (2016). Expression Profile of BCL-2, BCL-XL, and MCL-1 Predicts Pharmacological Response to the BCL-2 Selective Antagonist Venetoclax in Multiple Myeloma Models. *Mol Cancer Ther* *15*, 1132-1144.
- Rahmani, M., Aust, M. M., Attkisson, E., Williams, D. C., Jr., Ferreira-Gonzalez, A., and Grant, S. (2013). Dual inhibition of Bcl-2 and Bcl-xL strikingly enhances PI3K inhibition-induced apoptosis in human myeloid leukemia cells through a GSK3- and Bim-dependent mechanism. *Cancer Res* *73*, 1340-1351.
- Rampino, N., Yamamoto, H., Ionov, Y., Li, Y., Sawai, H., Reed, J. C., and Perucho, M. (1997). Somatic frameshift mutations in the BAX gene in colon cancers of the microsatellite mutator phenotype. *Science* *275*, 967-969.
- Richter, J. D., and Sonenberg, N. (2005). Regulation of cap-dependent translation by eIF4E inhibitory proteins. *Nature* *433*, 477-480.
- Ritchie, M. E., Diyagama, D., Neilson, J., van Laar, R., Dobrovic, A., Holloway, A., and Smyth, G. K. (2006). Empirical array quality weights in the analysis of microarray data. *BMC Bioinformatics* *7*, 261.
- Ritchie, M. E., Phipson, B., Wu, D., Hu, Y., Law, C. W., Shi, W., and Smyth, G. K. (2015). limma powers differential expression analyses for RNA-sequencing and microarray studies. *Nucleic Acids Res* *43*, e47.
- Roberts, A. W., Davids, M. S., Pagel, J. M., Kahl, B. S., Puvvada, S. D., Gerecitano, J. F., Kipps, T. J., Anderson, M. A., Brown, J. R., Gressick, L., *et al.* (2016). Targeting BCL2 with Venetoclax in Relapsed Chronic Lymphocytic Leukemia. *N Engl J Med* *374*, 311-322.
- Rongvaux, A., Willinger, T., Martinek, J., Strowig, T., Gearty, S. V., Teichmann, L. L., Saito, Y., Marches, F., Halene, S., Palucka, A. K., *et al.* (2014). Development and function of human innate immune cells in a humanized mouse model. *Nat Biotechnol* *32*, 364-372.
- Rudin, C. M., Durinck, S., Stawiski, E. W., Poirier, J. T., Modrusan, Z., Shames, D. S., Bergbower, E. A., Guan, Y., Shin, J., Guillory, J., *et al.* (2012a). Comprehensive genomic analysis identifies SOX2 as a frequently amplified gene in small-cell lung cancer. *Nat Genet* *44*, 1111-1116.
- Rudin, C. M., Hann, C. L., Garon, E. B., Ribeiro de Oliveira, M., Bonomi, P. D., Camidge, D. R., Chu, Q., Giaccone, G., Khaira, D., Ramalingam, S. S., *et al.* (2012b). Phase II study of single-agent navitoclax (ABT-263) and biomarker correlates in patients with relapsed small cell lung cancer. *Clin Cancer Res* *18*, 3163-3169.

- Sabatini, D. M., Erdjument-Bromage, H., Lui, M., Tempst, P., and Snyder, S. H. (1994). RAFT1: a mammalian protein that binds to FKBP12 in a rapamycin-dependent fashion and is homologous to yeast TORs. *Cell* 78, 35-43.
- Salama, J. K., Gu, L., Wang, X., Pang, H. H., Bogart, J. A., Crawford, J., Schild, S. E., Vokes, E. E., and Ready, N. E. (2016). Positive Interaction between Prophylactic Cranial Irradiation and Maintenance Sunitinib for Untreated Extensive-Stage Small Cell Lung Cancer Patients After Standard Chemotherapy: A Secondary Analysis of CALGB 30504 (ALLIANCE). *J Thorac Oncol* 11, 361-369.
- Sancak, Y., Bar-Peled, L., Zoncu, R., Markhard, A. L., Nada, S., and Sabatini, D. M. (2010). Ragulator-Rag complex targets mTORC1 to the lysosomal surface and is necessary for its activation by amino acids. *Cell* 141, 290-303.
- Sancak, Y., Peterson, T. R., Shaul, Y. D., Lindquist, R. A., Thoreen, C. C., Bar-Peled, L., and Sabatini, D. M. (2008). The Rag GTPases bind raptor and mediate amino acid signaling to mTORC1. *Science* 320, 1496-1501.
- Sarbassov, D. D., Ali, S. M., Kim, D. H., Guertin, D. A., Latek, R. R., Erdjument-Bromage, H., Tempst, P., and Sabatini, D. M. (2004). Rictor, a novel binding partner of mTOR, defines a rapamycin-insensitive and raptor-independent pathway that regulates the cytoskeleton. *Curr Biol* 14, 1296-1302.
- Sarbassov, D. D., Guertin, D. A., Ali, S. M., and Sabatini, D. M. (2005). Phosphorylation and regulation of Akt/PKB by the rictor-mTOR complex. *Science* 307, 1098-1101.
- Sarosiek, K. A., Chi, X., Bachman, J. A., Sims, J. J., Montero, J., Patel, L., Flanagan, A., Andrews, D. W., Sorger, P., and Letai, A. (2013). BID preferentially activates BAK while BIM preferentially activates BAX, affecting chemotherapy response. *Molecular cell* 51, 751-765.
- Sato, T., Kaneda, A., Tsuji, S., Isagawa, T., Yamamoto, S., Fujita, T., Yamanaka, R., Tanaka, Y., Nukiwa, T., Marquez, V. E., *et al.* (2013). PRC2 overexpression and PRC2-target gene repression relating to poorer prognosis in small cell lung cancer. *Sci Rep* 3, 1911.
- Saunders, L. R., Bankovich, A. J., Anderson, W. C., Aujay, M. A., Bheddah, S., Black, K., Desai, R., Escarpe, P. A., Hampl, J., Laysang, A., *et al.* (2015). A DLL3-targeted antibody-drug conjugate eradicates high-grade pulmonary neuroendocrine tumor-initiating cells in vivo. *Sci Transl Med* 7, 302ra136.
- Saxton, R. A., Chantranupong, L., Knockenhauer, K. E., Schwartz, T. U., and Sabatini, D. M. (2016). Mechanism of arginine sensing by CASTOR1 upstream of mTORC1. *Nature* 536, 229-233.
- Schaffer, B. E., Park, K. S., Yiu, G., Conklin, J. F., Lin, C., Burkhardt, D. L., Karnezis, A. N., Sweet-Cordero, E. A., and Sage, J. (2010). Loss of p130 accelerates tumor development in a mouse model for human small-cell lung carcinoma. *Cancer Res* 70, 3877-3883.
- Schmidt, J. M., Panzilius, E., Bartsch, H. S., Irmeler, M., Beckers, J., Kari, V., Linnemann, J. R., Dragoi, D., Hirschi, B., Kloos, U. J., *et al.* (2015). Stem-cell-like properties and epithelial plasticity arise as stable traits after transient Twist1 activation. *Cell Rep* 10, 131-139.

- Schneeberger, V. E., Allaj, V., Gardner, E. E., Poirier, J. T., and Rudin, C. M. (2016). Quantitation of Murine Stroma and Selective Purification of the Human Tumor Component of Patient-Derived Xenografts for Genomic Analysis. *PLoS One* *11*, e0160587.
- Schoenwaelder, S. M., Jarman, K. E., Gardiner, E. E., Hua, M., Qiao, J., White, M. J., Josefsson, E. C., Alwis, I., Ono, A., Willcox, A., *et al.* (2011). Bcl-xL-inhibitory BH3 mimetics can induce a transient thrombocytopenia that undermines the hemostatic function of platelets. *Blood* *118*, 1663-1674.
- Sehgal, S. N., Baker, H., and Vezina, C. (1975). Rapamycin (AY-22,989), a new antifungal antibiotic. II. Fermentation, isolation and characterization. *J Antibiot (Tokyo)* *28*, 727-732.
- Semenova, E. A., Kwon, M. C., Monkhorst, K., Song, J. Y., Bhaskaran, R., Krijgsman, O., Kuilman, T., Peters, D., Buikhuisen, W. A., Smit, E. F., *et al.* (2016). Transcription Factor NFIB Is a Driver of Small Cell Lung Cancer Progression in Mice and Marks Metastatic Disease in Patients. *Cell Rep* *16*, 631-643.
- Semenova, E. A., Nagel, R., and Berns, A. (2015). Origins, genetic landscape, and emerging therapies of small cell lung cancer. *Genes Dev* *29*, 1447-1462.
- Shepherd, F. A., Crowley, J., Van Houtte, P., Postmus, P. E., Carney, D., Chansky, K., Shaikh, Z., Goldstraw, P., International Association for the Study of Lung Cancer International Staging, C., and Participating, I. (2007). The International Association for the Study of Lung Cancer lung cancer staging project: proposals regarding the clinical staging of small cell lung cancer in the forthcoming (seventh) edition of the tumor, node, metastasis classification for lung cancer. *J Thorac Oncol* *2*, 1067-1077.
- Shivapurkar, N., Toyooka, S., Eby, M. T., Huang, C. X., Sathyanarayana, U. G., Cunningham, H. T., Reddy, J. L., Brambilla, E., Takahashi, T., Minna, J. D., *et al.* (2002). Differential inactivation of caspase-8 in lung cancers. *Cancer Biol Ther* *1*, 65-69.
- Shoemaker, A. R., Mitten, M. J., Adickes, J., Ackler, S., Refici, M., Ferguson, D., Oleksijew, A., O'Connor, J. M., Wang, B., Frost, D. J., *et al.* (2008). Activity of the Bcl-2 family inhibitor ABT-263 in a panel of small cell lung cancer xenograft models. *Clin Cancer Res* *14*, 3268-3277.
- Shultz, L. D., Brehm, M. A., Garcia-Martinez, J. V., and Greiner, D. L. (2012). Humanized mice for immune system investigation: progress, promise and challenges. *Nat Rev Immunol* *12*, 786-798.
- Siegel, R., Naishadham, D., and Jemal, A. Cancer statistics, 2013. *CA Cancer J Clin* *63*, 11-30.
- Siegel, R., Naishadham, D., and Jemal, A. (2013). Cancer statistics, 2013. *CA Cancer J Clin* *63*, 11-30.
- Sirzen, F., Zhivotovsky, B., Nilsson, A., Bergh, J., and Lewensohn, R. (1998). Higher spontaneous apoptotic index in small cell compared with non-small cell lung carcinoma cell lines; lack of correlation with Bcl-2/Bax. *Lung Cancer* *22*, 1-13.
- Slotman, B. J., and Senan, S. (2011). Radiotherapy in small-cell lung cancer: lessons learned and future directions. *Int J Radiat Oncol Biol Phys* *79*, 998-1003.
- Smith, E. M., Finn, S. G., Tee, A. R., Browne, G. J., and Proud, C. G. (2005). The tuberous sclerosis protein TSC2 is not required for the regulation of the mammalian target of rapamycin by amino acids and certain cellular stresses. *J Biol Chem* *280*, 18717-18727.

- Smyth, G. (2005). Limma: linear models for microarray data. In *Bioinformatics and Computational Biology Solutions using R and Bioconductor*, C.V. Gentleman R, Dudoit S, et al, ed. (New York: Springer), pp. 397-420.
- Soefje, S. A., Karnad, A., and Brenner, A. J. (2011). Common toxicities of mammalian target of rapamycin inhibitors. *Target Oncol* 6, 125-129.
- Souers, A. J., Levenson, J. D., Boghaert, E. R., Ackler, S. L., Catron, N. D., Chen, J., Dayton, B. D., Ding, H., Enschede, S. H., Fairbrother, W. J., *et al.* (2013). ABT-199, a potent and selective BCL-2 inhibitor, achieves antitumor activity while sparing platelets. *Nat Med* 19, 202-208.
- Souroullas, G. P., Jeck, W. R., Parker, J. S., Simon, J. M., Liu, J. Y., Paulk, J., Xiong, J., Clark, K. S., Fedorow, Y., Qi, J., *et al.* (2016). An oncogenic Ezh2 mutation induces tumors through global redistribution of histone 3 lysine 27 trimethylation. *Nat Med* 22, 632-640.
- Sousa, F. G., Matuo, R., Tang, S. W., Rajapakse, V. N., Luna, A., Sander, C., Varma, S., Simon, P. H., Doroshow, J. H., Reinhold, W. C., and Pommier, Y. (2015). Alterations of DNA repair genes in the NCI-60 cell lines and their predictive value for anticancer drug activity. *DNA Repair (Amst)* 28, 107-115.
- Stewart, E., Goshorn, R., Bradley, C., Griffiths, L. M., Benavente, C., Twarog, N. R., Miller, G. M., Caufield, W., Freeman, B. B., 3rd, Bahrami, A., *et al.* (2014). Targeting the DNA repair pathway in Ewing sarcoma. *Cell Rep* 9, 829-841.
- Straussman, R., Morikawa, T., Shee, K., Barzily-Rokni, M., Qian, Z. R., Du, J., Davis, A., Mongare, M. M., Gould, J., Frederick, D. T., *et al.* (2012). Tumour micro-environment elicits innate resistance to RAF inhibitors through HGF secretion. *Nature* 487, 500-504.
- Subramanian, A., Tamayo, P., Mootha, V. K., Mukherjee, S., Ebert, B. L., Gillette, M. A., Paulovich, A., Pomeroy, S. L., Golub, T. R., Lander, E. S., and Mesirov, J. P. (2005). Gene set enrichment analysis: a knowledge-based approach for interpreting genome-wide expression profiles. *Proc Natl Acad Sci U S A* 102, 15545-15550.
- Sutherland, K. D., Proost, N., Brouns, I., Adriaensen, D., Song, J. Y., and Berns, A. (2011). Cell of origin of small cell lung cancer: inactivation of Trp53 and Rb1 in distinct cell types of adult mouse lung. *Cancer Cell* 19, 754-764.
- Tahir, S. K., Wass, J., Joseph, M. K., Devanarayan, V., Hessler, P., Zhang, H., Elmore, S. W., Kroeger, P. E., Tse, C., Rosenberg, S. H., and Anderson, M. G. (2010). Identification of expression signatures predictive of sensitivity to the Bcl-2 family member inhibitor ABT-263 in small cell lung carcinoma and leukemia/lymphoma cell lines. *Mol Cancer Ther* 9, 545-557.
- Takahashi, T., Obata, Y., Sekido, Y., Hida, T., Ueda, R., Watanabe, H., Ariyoshi, Y., Sugiura, T., and Takahashi, T. (1989). Expression and amplification of myc gene family in small cell lung cancer and its relation to biological characteristics. *Cancer Res* 49, 2683-2688.
- Takayama, K., Ogata, K., Nakanishi, Y., Yatsunami, J., Kawasaki, M., and Hara, N. (1996). Bcl-2 expression as a predictor of chemosensitivities and survival in small cell lung cancer. *Cancer J Sci Am* 2, 212-216.
- Tan, W. L., Jain, A., Takano, A., Newell, E. W., Iyer, N. G., Lim, W. T., Tan, E. H., Zhai, W., Hillmer, A. M., Tam, W. L., and Tan, D. S. (2016). Novel therapeutic targets on the horizon for lung cancer. *Lancet Oncol* 17, e347-362.

- Tang, S. W., Bilke, S., Cao, L., Murai, J., Sousa, F. G., Yamade, M., Rajapakse, V., Varma, S., Helman, L. J., Khan, J., *et al.* (2015). SLFN11 Is a Transcriptional Target of EWS-FLI1 and a Determinant of Drug Response in Ewing Sarcoma. *Clin Cancer Res* 21, 4184-4193.
- Tentler, J. J., Tan, A. C., Weekes, C. D., Jimeno, A., Leong, S., Pitts, T. M., Arcaroli, J. J., Messersmith, W. A., and Eckhardt, S. G. (2012). Patient-derived tumour xenografts as models for oncology drug development. *Nat Rev Clin Oncol* 9, 338-350.
- Thomas, A., and Pommier, Y. (2016). Small cell lung cancer: Time to revisit DNA-damaging chemotherapy. *Sci Transl Med* 8, 346fs312.
- Thoreen, C. C., Chantranupong, L., Keys, H. R., Wang, T., Gray, N. S., and Sabatini, D. M. (2012). A unifying model for mTORC1-mediated regulation of mRNA translation. *Nature* 485, 109-113.
- Torre, L. A., Bray, F., Siegel, R. L., Ferlay, J., Lortet-Tieulent, J., and Jemal, A. (2015). Global cancer statistics, 2012. *CA Cancer J Clin* 65, 87-108.
- Townsend, E. C., Murakami, M. A., Christodoulou, A., Christie, A. L., Koster, J., DeSouza, T. A., Morgan, E. A., Kallgren, S. P., Liu, H., Wu, S. C., *et al.* (2016). The Public Repository of Xenografts Enables Discovery and Randomized Phase II-like Trials in Mice. *Cancer Cell* 29, 574-586.
- Vaillant, F., Merino, D., Lee, L., Breslin, K., Pal, B., Ritchie, M. E., Smyth, G. K., Christie, M., Phillipson, L. J., Burns, C. J., *et al.* (2013). Targeting BCL-2 with the BH3 mimetic ABT-199 in estrogen receptor-positive breast cancer. *Cancer Cell* 24, 120-129.
- van Delft, M. F., Wei, A. H., Mason, K. D., Vandenberg, C. J., Chen, L., Czabotar, P. E., Willis, S. N., Scott, C. L., Day, C. L., Cory, S., *et al.* (2006). The BH3 mimetic ABT-737 targets selective Bcl-2 proteins and efficiently induces apoptosis via Bak/Bax if Mcl-1 is neutralized. *Cancer cell* 10, 389-399.
- Venturelli, S., Berger, A., Weiland, T., Essmann, F., Waibel, M., Nuebling, T., Hacker, S., Schenk, M., Schulze-Osthoff, K., Salih, H. R., *et al.* (2013). Differential induction of apoptosis and senescence by the DNA methyltransferase inhibitors 5-azacytidine and 5-aza-2'-deoxycytidine in solid tumor cells. *Mol Cancer Ther* 12, 2226-2236.
- Vezina, C., Kudelski, A., and Sehgal, S. N. (1975). Rapamycin (AY-22,989), a new antifungal antibiotic. I. Taxonomy of the producing streptomycete and isolation of the active principle. *J Antibiot (Tokyo)* 28, 721-726.
- Vire, E., Brenner, C., Deplus, R., Blanchon, L., Fraga, M., Didelot, C., Morey, L., Van Eynde, A., Bernard, D., Vanderwinden, J. M., *et al.* (2006). The Polycomb group protein EZH2 directly controls DNA methylation. *Nature* 439, 871-874.
- Vivanco, I., and Sawyers, C. L. (2002). The phosphatidylinositol 3-Kinase AKT pathway in human cancer. *Nat Rev Cancer* 2, 489-501.
- Vo, T. T., Ryan, J., Carrasco, R., Neuberg, D., Rossi, D. J., Stone, R. M., Deangelo, D. J., Frattini, M. G., and Letai, A. (2012). Relative mitochondrial priming of myeloblasts and normal HSCs determines chemotherapeutic success in AML. *Cell* 151, 344-355.

- Wagle, N., Berger, M. F., Davis, M. J., Blumenstiel, B., Defelice, M., Pochanard, P., Ducar, M., Van Hummelen, P., Macconnaill, L. E., Hahn, W. C., *et al.* (2012). High-throughput detection of actionable genomic alterations in clinical tumor samples by targeted, massively parallel sequencing. *Cancer Discov* *2*, 82-93.
- Wallach, D., Kang, T. B., Dillon, C. P., and Green, D. R. (2016). Programmed necrosis in inflammation: Toward identification of the effector molecules. *Science* *352*, aaf2154.
- Wang, D. G., Johnston, C. F., Sloan, J. M., and Buchanan, K. D. (1998). Expression of Bcl-2 in lung neuroendocrine tumours: comparison with p53. *J Pathol* *184*, 247-251.
- Wang, J., Zhuang, J., Iyer, S., Lin, X. Y., Greven, M. C., Kim, B. H., Moore, J., Pierce, B. G., Dong, X., Virgil, D., *et al.* (2013). Factorbook.org: a Wiki-based database for transcription factor-binding data generated by the ENCODE consortium. *Nucleic Acids Res* *41*, D171-176.
- Wei, G., Margolin, A. A., Haery, L., Brown, E., Cucolo, L., Julian, B., Shehata, S., Kung, A. L., Beroukhim, R., and Golub, T. R. (2012). Chemical genomics identifies small-molecule MCL1 repressors and BCL-xL as a predictor of MCL1 dependency. *Cancer Cell* *21*, 547-562.
- Westerman, B. A., Neijenhuis, S., Poutsma, A., Steenbergen, R. D., Breuer, R. H., Egging, M., van Wijk, I. J., and Oudejans, C. B. (2002). Quantitative reverse transcription-polymerase chain reaction measurement of HASH1 (ASCL1), a marker for small cell lung carcinomas with neuroendocrine features. *Clin Cancer Res* *8*, 1082-1086.
- Wilson, B. G., Wang, X., Shen, X., McKenna, E. S., Lemieux, M. E., Cho, Y. J., Koellhoffer, E. C., Pomeroy, S. L., Orkin, S. H., and Roberts, C. W. (2010). Epigenetic antagonism between polycomb and SWI/SNF complexes during oncogenic transformation. *Cancer Cell* *18*, 316-328.
- Wilson, T. R., Fridlyand, J., Yan, Y., Penuel, E., Burton, L., Chan, E., Peng, J., Lin, E., Wang, Y., Sosman, J., *et al.* (2012). Widespread potential for growth-factor-driven resistance to anticancer kinase inhibitors. *Nature* *487*, 505-509.
- Witkiewicz, A. K., Balaji, U., Eslinger, C., McMillan, E., Conway, W., Posner, B., Mills, G. B., O'Reilly, E. M., and Knudsen, E. S. (2016). Integrated Patient-Derived Models Delineate Individualized Therapeutic Vulnerabilities of Pancreatic Cancer. *Cell Rep* *16*, 2017-2031.
- Wu, D., and Smyth, G. K. (2012). Camera: a competitive gene set test accounting for inter-gene correlation. *Nucleic acids research* *40*, e133.
- Wu, N., Jia, D., Ibrahim, A. H., Bachurski, C. J., Gronostajski, R. M., and MacPherson, D. (2016). NFIB overexpression cooperates with Rb/p53 deletion to promote small cell lung cancer. *Oncotarget*.
- Xu, H., and Krystal, G. W. (2010). Actinomycin D decreases Mcl-1 expression and acts synergistically with ABT-737 against small cell lung cancer cell lines. *Clin Cancer Res* *16*, 4392-4400.
- Yang, H., Rudge, D. G., Koos, J. D., Vaidialingam, B., Yang, H. J., and Pavletich, N. P. (2013). mTOR kinase structure, mechanism and regulation. *Nature* *497*, 217-223.
- Yang, J., Mani, S. A., Donaher, J. L., Ramaswamy, S., Itzykson, R. A., Come, C., Savagner, P., Gitelman, I., Richardson, A., and Weinberg, R. A. (2004). Twist, a master regulator of morphogenesis, plays an essential role in tumor metastasis. *Cell* *117*, 927-939.

- Yang, W. H., Lan, H. Y., Huang, C. H., Tai, S. K., Tzeng, C. H., Kao, S. Y., Wu, K. J., Hung, M. C., and Yang, M. H. (2012). RAC1 activation mediates Twist1-induced cancer cell migration. *Nat Cell Biol* 14, 366-374.
- Yap, D. B., Chu, J., Berg, T., Schapira, M., Cheng, S. W., Moradian, A., Morin, R. D., Mungall, A. J., Meissner, B., Boyle, M., *et al.* (2011). Somatic mutations at EZH2 Y641 act dominantly through a mechanism of selectively altered PRC2 catalytic activity, to increase H3K27 trimethylation. *Blood* 117, 2451-2459.
- Yin, C., Knudson, C. M., Korsmeyer, S. J., and Van Dyke, T. (1997). Bax suppresses tumorigenesis and stimulates apoptosis in vivo. *Nature* 385, 637-640.
- Yip, C. K., Murata, K., Walz, T., Sabatini, D. M., and Kang, S. A. (2010). Structure of the human mTOR complex I and its implications for rapamycin inhibition. *Mol Cell* 38, 768-774.
- Youden, W. J. (1950). Index for rating diagnostic tests. *Cancer* 3, 32-35.
- Zang, C., Schones, D. E., Zeng, C., Cui, K., Zhao, K., and Peng, W. (2009). A clustering approach for identification of enriched domains from histone modification ChIP-Seq data. *Bioinformatics* 25, 1952-1958.
- Zhang, L., Yu, J., Park, B. H., Kinzler, K. W., and Vogelstein, B. (2000). Role of BAX in the apoptotic response to anticancer agents. *Science* 290, 989-992.
- Zheng, X., Carstens, J. L., Kim, J., Scheible, M., Kaye, J., Sugimoto, H., Wu, C. C., LeBleu, V. S., and Kalluri, R. (2015). Epithelial-to-mesenchymal transition is dispensable for metastasis but induces chemoresistance in pancreatic cancer. *Nature* 527, 525-530.
- Zilliox, M. J., and Irizarry, R. A. (2007). A gene expression bar code for microarray data. *Nat Methods* 4, 911-913.
- Zinzalla, V., Stracka, D., Oppliger, W., and Hall, M. N. (2011). Activation of mTORC2 by association with the ribosome. *Cell* 144, 757-768.
- Zoncu, R., Bar-Peled, L., Efeyan, A., Wang, S., Sancak, Y., and Sabatini, D. M. (2011). mTORC1 senses lysosomal amino acids through an inside-out mechanism that requires the vacuolar H(+)-ATPase. *Science* 334, 678-683.
- Zoppoli, G., Regairaz, M., Leo, E., Reinhold, W. C., Varma, S., Ballestrero, A., Doroshow, J. H., and Pommier, Y. (2012). Putative DNA/RNA helicase Schlafen-11 (SLFN11) sensitizes cancer cells to DNA-damaging agents. *Proc Natl Acad Sci U S A* 109, 15030-15035.

Curriculum Vitae

The Johns Hopkins University School of Medicine

Eric Edison Gardner
Name

10/01/2016
Date of this version

Educational History:

PhD expected	2016	Pharmacology and Molecular Sciences Mentor: Charles M. Rudin, MD, PhD	Johns Hopkins School of Medicine
PharmD	2011	Doctor of Pharmacy <i>magna cum laude</i>	University of Pittsburgh School of Pharmacy
<i>DOB</i>	1986	October 25	Pittsburgh, PA

Other Professional Experience:

Research Rotation	2011	RF Ambinder, MD, PhD	Johns Hopkins SOM
APPE Elective Rotation	2011	HL McLeod, PharmD	UNC Chapel Hill SOM
POE Summer Fellow	2010	MV Relling, PharmD	St. Jude CRH
NINDS ARRA Fellow	2009	SM Poloyac, PharmD, PhD	U. Pittsburgh SOP
Carolina Summer Fellow	2008	RA Nicholas, PhD	UNC Chapel Hill SOM
RISE Summer Fellow	2007	RA Seifert, MD, PhD	Uni. Regensburg (de)
NSF Summer Fellow	2006	J Klein-Seetharaman, PhD	U. Pittsburgh SOM

Scholarships, Fellowships or Other External Funding:

June Beidler Award	2016	Scholar-in-Training	AACR
--------------------	------	---------------------	------

Awards and Honors:

Scheinberg Award	2014	Travel Grant	JHU SOM
------------------	------	--------------	---------

Publications:

Gardner EE, Lok BH, Schneeberger VE, Miles LA, Arnold PK, Desmeules P, Ni A, Khodos I, de Stanchina E, Rekhtman N, Nguyen T, Sage J, Ribich S, Dowlati A, Massion PP, Poirier JT, Rudin CM. Chemosensitive relapse in small cell lung cancer proceeds through an EZH2-SLFN11 axis. (*in revision*).

Bowman RL, Klemm F, Akkari L, Pyonteck SM, Sevenich L, Quail DF, Dhara S, Simpson K, **Gardner EE**, Iacobuzio-Donahue C, Brennan CW, Tabar V, Gutin PH, Joyce JA. Macrophage ontogeny underlies differences in tumor-specific education in brain malignancies. *Cell Reports* (accepted).

Miles LA, Burga L, **Gardner EE**, Bostina M, Poirier JT, Rudin CM. Anthrax toxin receptor 1 (ANTXR1) is the cellular receptor for Seneca Valley Virus in neuroendocrine cancers. (submitted).

Schneeberger VE, Allaj V, **Gardner EE**, Miles LA, Poirier JT, Rudin CM. Quantitation of murine stroma and selective purification of the human tumor component of patient-derived xenografts for genomic analysis. *PLoS One* (in press) 2016.

Lok BH, **Gardner EE**, Schneeberger VE, Ni A, Desmeules P, Rekhtman N, de Stanchina E, Teicher BA, Riaz R, Powell SN, Poirier JT, Rudin CM. PARP inhibitor activity correlates with SLFN11 expression and demonstrates synergy with temozolomide in small cell lung cancer. *Clinical Cancer Research* (in press) 2016.

Weiskopf K, Jahchan NS, Schnorr PJ, Cristea S, Ring AM, Maute RL, Volkmer AK, Volkmer JP, Liu J, Lim JS, Yang D, Seitz G, Nguyen T, Wu D, Jude K, Guerston H, Barkal A, Trapani F, George J, Poirier JT, **Gardner EE**, Miles LA, de Stanchina E, Lofgren SM, Vogel H, Winslow MM, Dive C, Thomas RK, Rudin CM, van de Rijn M, Majeti R, Garcia KC, Weissman IL, Sage J. CD47-blocking immunotherapies stimulate macrophage-mediated destruction of small-cell lung cancer. *Journal of Clinical Investigation* 2016;126(7):2610-20.

Shamay Y, Elkabets M, Li H, Shah J, Brook S, Wang F, Adler K, Baut E, Scaltriti M, Jena PV, **Gardner EE**, Poirier JT, Rudin CM, Baselga J, Haimovitz-Friedman A, Heller DA. P-selectin is a nanotherapeutic delivery target in the tumor microenvironment. *Science Translational Medicine* 2016;8(345):345ra87.

Poirier JT, **Gardner EE**, Connis N, Moreira AL, de Stanchina E, Hann CL, Rudin CM. DNA methylation in small cell lung cancer defines distinct disease subtypes and correlates with high expression of EZH2. *Oncogene* 2015;34:5869-78.

Dutta A, Altenbach C, Mangahas S, Yanamala N, **Gardner E**, Hubbell WL, Klein-Seetharaman J. Differential dynamics of extracellular and cytoplasmic domains in denatured States of rhodopsin. *Biochemistry* 2014;53:7160-9.

Gardner EE, Connis N, Poirier JT, Cope L, Dobromilskaya I, Gallia GL, Rudin CM, Hann CL. Rapamycin rescues ABT-737 efficacy in small cell lung cancer. *Cancer Research* 2014;74:2846-56.

***cover story**

Zinn RL, **Gardner EE**, Marchionni L, Murphy SC, Dobromilskaya I, Hann CL, Rudin CM. ERK phosphorylation is predictive of resistance to IGF-1R inhibition in small cell lung cancer. *Molecular Cancer Therapeutics* 2013;12:1131-9.

Zinn RL, **Gardner EE**, Dobromilskaya I, Murphy S, Marchionni L, Hann CL, Rudin CM. Combination treatment with ABT-737 and chloroquine in preclinical models of small cell lung cancer. *Molecular Cancer* 2013;2:12-6.

Relling MV, **Gardner EE**, Sandborn WJ, Schmiegelow K, Pui CH, Yee SW, Stein CM, Carrillo M, Evans WE, Hicks JK, Schwab M, Klein TE. Clinical pharmacogenetics implementation consortium guidelines for thiopurine methyltransferase genotype and thiopurine dosing: 2013 update. *Clinical Pharmacology and Therapeutics* 2013;93(4):324-5.

Yanamala N, **Gardner EE**, Riciutti A, and Klein-Seetharaman J. The cytoplasmic rhodopsin-protein interface: potential for drug discovery. *Current Drug Targets* 2012;3:3-14.

Scott SA, Sangkuhl K, **Gardner EE**, Stein CM, Hulot JS, Johnson JA, Roden DM, Klein TE. Clinical pharmacogenetics implementation consortium guidelines for cytochrome P450-2C19 (CYP2C19) genotype and clopidogrel therapy. *Clinical Pharmacology and Therapeutics* 2011;90(2):328-32.

Relling MV, **Gardner EE**, Sandborn WJ, Schmiegelow K, Pui CH, Yee SW, Stein CM, Carrillo M, Evans WE, Klein T. Clinical pharmacogenetics implementation consortium guidelines for thiopurine methyltransferase (TPMT) genotype and thiopurine dosing. *Clinical Pharmacology and Therapeutics* 2011;89:387-91.

Nickl K, **Gardner EE**, Geiger S, Heilmann J, and Seifert R. Differential coupling of the human cannabinoid receptors hCB1R and hCB2R to the G-protein Gai2 β 1 γ 2. *Neuroscience Letters* 2008;447:68-72.

Book Chapters

Gardner EE and Rudin CM. Cancer Metabolism. In Stadler (eds) *Cancer Biology Review: A Case-Based Approach*, Demos Medical Publishing, New York, NY 2014;117-38.

Editorials

Gardner EE and Rudin CM. News and Views: Preclinical oncology-reporting transparency needed. *Nature Reviews Clinical Oncology* 2016;13(1):8-9.

Service and Leadership

City Harvest Volunteer

2015

City Harvest, NYC